ProQuest LLC.
789 East Eisenhower Parkway
P.O. Box 1346
Ann Arbor, MI 48106 – 1346

THE ROLE OF MOLYBDENUM IN REDUCING TEMPER EMBRITTLEMENT IN STEELS

BY

MICHAEL MOTLEY BSc (HONS) MET.

A THESIS SUBMITTED TO THE COUNCIL FOR NATIONAL ACADEMIC AWARDS FOR THE DEGREE OF DOCTOR OF PHILOSOPHY

Sponsoring Establishment: Department of Metallurgy
Sheffield City Polytechnic

Collaborating Establishment: Atomic Energy Establishment,
Harwell

DATE OCTOBER 1984

PREFACE

This thesis is submitted to the Council for National Academic Awards for the degree of Doctor of Philosophy.

The research work was carried out during the period November 1978 to September 1981 at the Department of Metallurgy, Sheffield City Polytechnic. A number of post-graduate courses were attended at the Sheffield City Polytechnic during the above period and included:-

1. High-Strength Steels.
2. Statistics.

The author has attended a conference on "Hot Working and Forming Processes" held at Sheffield University July 1979.

The author would like to express his appreciation to the Atomic Energy Research Establishment, Harwell for the provision of financial support, supply of the alloys used in the investigation and the use of various pieces of instrumentation and equipment.

Grateful thanks are expressed to Dr. E.A. Wilson for his interest, guidance and constant encouragement throughout the course of this work. Also, grateful acknowledgement is made to Dr. B.C. Edwards, Industrial Supervisor and Dr. F.B. Pickering for numerous helpful discussions, and to the staff of the Electron Metallography section of the Applied Physics Department at the Polytechnic for provision of X-ray and Electron Microscopy facilities.

Thanks also to technicians, administrative staff and lecturing staff of the Department of Metallurgy, Sheffield City Polytechnic, especially Dr. G. Briggs, whose role as Research Tutor was invaluable.

I am also indebted to Major M. Wilkinson of Princess Marina College, Arborfield, who kindly gave up time to proof read the script.

Finally, I would like to pay tribute to my wife, Hilary, whose patience, support and constant encouragement played a large part in the production of the thesis. She also typed the text.

The results obtained and the theories developed are, to the best of my knowledge, original except where reference is made to the work of others. No part of this thesis has been submitted for a degree at any other university or college.

DEPARTMENT OF METALLURGY

SHEFFIELD CITY POLYTECHNIC

EMBRITTLEMENT IN FERRITIC ALLOYS

by

MICHAEL MOTLEY

Synopsis

The effect of two additions of molybdenum (2.5% and 5%) on the brittleness of an alloy based on Fe-8%Mn has been investigated. The intergranular brittleness exhibited by the as-quenched base alloy was eliminated by the addition of 2.5Mo possibly due to the interaction of molybdenum with embrittling agents Mn and N and the subsequent increase in solid solubility of these elements. A further addition of molybdenum did not significantly increase the toughness of the as-quenched Fe-8Mn-2.5Mo alloy in accordance with the theory of a limiting amount of molybdenum that may combat embrittlement.

Aging quenched alloys at 450°C gave rise to an increase in DBTT and a change in brittle fracture mode to intergranular. The effect was most severe in the alloy with higher molybdenum (5%) due to precipitation of second phase particles both increasing the hardness of the matrix dramatically and denuding the matrix of molybdenum that would otherwise be free to combat embrittlement. A build up of Mn and N at prior austenite grain boundaries was detected by AES, another factor contributing to embrittlement on aging.

Aging quenched alloys at 525°C led to a more rapid change from cleavage to intergranular fracture for both molybdenum additions but toughening of the alloy containing the lower molybdenum content (2.5%). Although grain boundary segregation in this alloy meant that the preferred crack path for brittle fracture changed from transgranular to intergranular on aging, the build up of reverted austenite at prior austenite grain boundaries acted as a crack blunter, slowing down crack

propagation and thus increasing overall toughness. Embrittlement in the alloy containing 5% Mo was very severe due to more rapid precipitation.

An investigation was also carried out on the aging of a commercial alloy based on 0.25C, 1.4Mn, 0.5Mo, 0.6Ni, 0.3Si doped with 0.4%Cu in one instance and 0.04%P in another. Phosphorus was seen to characteristically induce embrittlement on aging at 450°C and 525°C with an increase in the DBTT and a change in the brittle fracture mode from cleavage to intergranular. Aging of the base alloy at 450°C was also seen to be an embrittling treatment but the effects were not as severe as in the alloy containing phosphorus. The addition of copper is seen to retard this embrittlement on aging due to its grain refining ability.

CONTENTS

LIST OF PLATES

142	Fractographs of A217 after 10 hours aging at 450°C	455
143	" " A217 " 168 " " " 525°C	457
144	" " A317 " 10 " " " 450°C	459
145	" " A317 " 168 " " " 525°C	461
146	" " A317 " " " " " "	463
147	" " A417 " 10 " " " 450°C	465
148	" " A417 " 168 " " " 525°C	467
149	" " " " " " " " "	469
150	Micrographs showing propagation of cracks along austenite grain boundaries below the intergranular fracture surface in alloy K1526 after aging at 525°C for 480 hours.	471
151(a)	Interlath fracture shown on the intergranular	473
" (b)	facets of alloy K1527 after aging at 450°C for $193\frac{1}{2}$ hours.	475

1. Introduction

1.1 Identification of Problem, Cause and Effect

A difficulty faces the users of the high strength martensitic steels when the optimum combinations of strength, ductility and toughness are achieved by heat treatment. This problem is that the very heat treatment used to attain these superior qualities in the steel may cause embrittlement.

The embrittlement is seen to be a loss of toughness primarily as a result of either holding in or slow cooling through a temperature range 350°C - 550°C after tempering at a higher temperature, 600°C (classical temper embrittlement) or slow cooling as quenched alloy steels in the range 250°C - 450°C (tempered martensitic embrittlement).

The main cause of embrittlement is segregation of elements to the prior austenite grain boundaries with the effect of a reduction of grain boundary cohesive strength.

The embrittlement is manifest as an increase in the ductile/brittle transition temperature together with a change in the low temperature fracture mode from cleavage to intergranular.

1.2. Commercial Aspects

Pressure vessel and cryogenic facilities have for a long time now been two of the many fields of use for ferritic steels. While manganese is an accepted constituent of these steels, the problem it and other elements cause, due to the phenomenon of embrittlement, is well known.

This problem arises in pressure vessel steels by virtue of their high hardenability because,to attain through-section fracture toughness and high yield strength required for service,

they are often used in the quenched and tempered condition. These susceptible steels, when operated for long times at temperatures around 450°C, may severely embrittle, causing the temperature at which the material undergoes the ductile to brittle transition to increase dramatically. While this transition temperature is well below the material's operating temperature, in such applications it is possible that the embrittlement could be so severe that cooling to ambient would involve passing through the transition temperature. A load imposed on an embrittled pressure vessel, at or below this temperature, could be catastrophic.

The same problem has also faced the workers, in recent years, who have tried to devise a new cryogenic steel based on the iron-manganese system as an alternative to the more expensive but accepted iron-nickel system. Whether the iron-manganese system can lend itself as a basis for cryogenic high strength steels depends on the mechanical properties, in particular low temperature toughness, that can be achieved.

The advantages of the iron-manganese system in this application are economy, similar austenite → ferrite transformation products to the iron-nickel system, tensile properties and greater solid-solution strengthening. But, unfortunately, the iron-manganese systems have been shown to exhibit poor impact properties characterised by a low temperature intergranular fracture mode.[7]

The embrittlement behaviour is analogous to that of temper embrittled steels, with the fracture propagating along the prior austenite grain boundaries, and is enhanced on tempering within the temperature range 400°C - 500°C.

1.3 The Aims of the Programme

The characteristics of embrittlement in ferritic steels have been well documented over the past twenty years but still little is understood of its mechanisms. This programme of work sets out to investigate these embrittlement phenomena in ferritic steels, with particular reference to the cryogenic and pressure vessel applications.

The basis of the cryogenic alloy studied was the iron-8% manganese alloy developed in the department over the last few years.[8,9] Molybdenum has for a long time been known to inhibit embrittlement when it is present in steels in certain amounts. Therefore, its addition to the iron-8% manganese system would seem a useful if not obvious aspect for investigation.

Of particular interest to UKAEA Harwell, the sponsors of this work, was embrittlement of pressure vessel steels. The phase composition of the type of steel investigated here was 0. 25C, 1.4Mn, 0.5Mo, 0.57Ni, 0.3Si. The effects of embrittling elements Mn, P, and Cu and de-embrittlers C and Mo were to be studied separately and together on changes in mechanical properties and microstructure of the steels after various heat treatments.

Regarding the investigation of the pressure vessel types of alloys, the elements carbon, manganese, molybdenum, phosphorus and copper involved in the embrittlement problem form the basis of a series of permutations for alloys to be investigated.

Changes in mechanical properties, microstructure and internal chemistry are to be under investigation following a series of heat treatment conditions.

2. Review of Literature

2.1 The Embrittlement Phenomena in Steels

Embrittlement is confined mainly to tempered alloy steels, showing up most strongly when the steels are in the martensitic condition. The temperature range for the development of embrittlement is about 350°C-650°C [10,11]. At the low end of this range, the rates of the embrittlement processes are low but the maximum achievable amount of embrittlement is higher than at the higher temperatures when the rate is higher.

Embrittlement is manifest as an increase in ductile to brittle transition temperature [12], Fig. 20, and a change in brittle fracture mode from transgranular cleavage to intergranular, Fig. 21.

Work on chemical analysis of these intergranular fractures [13] using modern surface analysis techniques has shown embrittlement to be associated with segregation of elements to prior austenite grain boundaries, Fig. 22.

Ferrell [14] summarised temper embrittlement, as seen in Table 7. Although this does not cover all types of embrittlement, it shows the basic trends. Another type of embrittlement is tempered martensite embrittlement, which occurs when high temperature tempering, in certain alloys, has not been carried out [15] and is concurrent with inter-lath Fe_3C precipitation [16].

2.2 Physical and Chemical Factors Affecting Embrittlement

2.2.1. Chemical Considerations (Alloys and Residuals)

2.2.1.1. Residuals

A turning point in the understanding of embrittlement in steels was the demonstration that embrittlement in steels was only possible if certain impurities were present and so was only peculiar to commercial steels. [17,18] In this work, steels were made from high purity elements in combinations corresponding with well known alloy steel types that would normally be susceptible to temper embrittlement. The high purity steels were tested for embrittlement by slow cooling after tempering as well as by prolonged reheating at the temperature of maximum sensitivity. Transition temperatures remained unchanged and brittle fractures transgranular, Fig. 23.

The outcome of this work then was to associate the presence of residual impurities with susceptibility to temper embrittlement. Probably the most important of these impurities, not necessarily because of severity of effect but because of its ever prominent presence in low alloy steels, is phosphorus. It is a hard tramp element to eliminate wholly.

Work on a 1.5Mn-Mo steel with 0.06%P showed [19] that in both fully and partially hardened and tempered steels, rises in impact transition temperature were encountered with rises in phosphorus content of the steel. This may be compared to no effect in steels free from phosphorus.

How phosphorus has a major effect on embrittlement can be explained by the fact that surface analysis of fractures by auger electron spectroscopy has linked embrittlement with phosphorus segregation at austenite grain boundaries [20]. This segregation of

phosphorus is favoured by the phosphorus atom's poor fit in the iron based centred cubic lattice,[21] i.e. although the phosphorus atom is substitutional in the α-iron lattice[22] it is smaller than the substitutional site it is presumed to occupy. Hence, it would contract the parent lattice. This gives a driving force for phosphorus diffusion to grain boundaries. Also, phosphorus has a high diffusion mobility [23]. For example, this diffusion mobility is three times higher at annealing temperatures than that of alloys, giving rise to rapid phosphorus redistribution, Fig. 24 [24]. Figs. 25, 26 [25] show temperature dependence of diffusion coefficient of P for γ and α-iron respectively.

Phosphorus has been shown to reduce the surface energy of iron [26], Fig. 27. A monolayer of phosphorus on a grain boundary can lead to intergranular fracture paths because of greatly reduced surface energy requirements. For brittle materials, this is reflected as a decrease in the fracture stress, σ_f in the Griffiths equation [27]. The Gibbs adsorption theory [28] predicted that phosphorus would lower the surface energy of iron.

The segregation of phosphorus to surfaces of iron is seen to be equilibrium segregation, not precipitation [29,30].

The phosphorus segregation and increase in ductile to brittle transformation temperature are greater the lower the age temperature and the higher the bulk concentration of phosphorus, [31] another verification of the Gibbsean segregation model.

At what stage phosphorus segregates and causes this effect is a question that has been in some dispute. It is generally thought that phosphorus segregation occurs during solution treatment in the austenite range,[32,33] although some would challenge this [34]. The conclusion so far then is that phosphorus segregation in the γ range depends on certain factors such as solution treatment

temperature, quench rate, structure, composition and grain boundary area: phosphorus concentration ratio. Generally, phosphorus is seen only to segregate in the austenite region with large grain sizes. The majority of phosphorus segregation, then, is thought to occur during the ageing process.

The increase in intergranular grain boundary phosphorus concentration with ageing time and temperature is shown in Fig. 28. At high tempering temperatures, the acquisition of steady state is more rapid but total phosphorus build up is lower compared to lower ageing temperatures.

Some workers [35] have suggested that phosphorus promotes embrittlement by the formation of voids on grain boundaries during stress relaxation, thus reducing ductility. But the effect of phosphorus attracting the largest interest is the change induced on grain boundary energy. Grain boundary energy has been studied with respect to phosphorus segregation by observing triple points.[36] It was found that phosphorus segregation varies from one grain boundary to another. At coherent twin boundaries no phosphorus segregation was seen to occur; at incoherent twin boundaries, segregation of phosphorus was seen to occur. Therefore, phosphorus segregation does not just depend on grain boundary energy considerations per se but also on coherency or free volume. The atomic structure of the grain boundary is seen to be an important factor then in phosphorus segregation - the coherent boundary has associated free energy but no free volume which can accommodate misfitting atoms of solute.

Other impurities such as arsenic, tin and antimony also cause embrittlement but to a lesser effect [38] due to their much slower

rate of diffusion in the α-iron lattice.[37] Effects of other residuals depends on the amount of phosphorus present [39] and it has also been observed that the mechanism of segregation of phosphorus is very different to other impurities.[40]

2.2.1.2 Nitrogen

The tramp elements so far mentioned are seen as a problem but their amounts can be controlled in steel to a certain extent by the choice of materials for steelmaking. Nitrogen poses a different kind of problem in that pick up from the atmosphere during steelmaking is a real possibility.

As regards the embrittlement phenomenon, nitrogen has been seen to segregate during both austenitising and ageing treatments[32,40] causing one step temper embrittlement. In a tempered martensite structure, it has also been seen to segregate to dislocations.[32]

Usually, nitrogen is tied up within the matrix by elements such as Al. But in cases when sufficient nitrogen is released and untrapped at austenitising, it will segregate to grain boundaries without precipitation.[41]

2.2.1.3 Alloys and Alloy-Impurity Interaction

In plain carbon steels, with no major alloying additions, temper embrittlement due to the presence of metalloid elements does not occur.[42] The addition of alloying elements to these steels promotes rapid embrittlement.

The major alloys involved in embrittlement are Nickel, Chromium, Manganese and Molybdenum. These can be split into three categories; embrittlement enhancers, embrittlers, embrittlement retarders.

2.2.1.3.1 Embrittlement Enhancers

This category involves alloying elements which will promote embrittlement processes but in themselves are probably not embrittlers in their own right.

It has been reported that nickel [40,31] and chromium [41] segregate to prior austenite grain boundaries in the ferrite range during aging but not during solution treatment in the austenite phase field. Figures 29 and 30 show the build-up of nickel at grain boundaries during the aging of an En30A steel. Removal of nickel and chromium from alloy steels decreases the amount of shift in transformation temperatures produced by step cooling in the temper embrittlement range.[53] Work on Fe-C and Fe-C-P alloys produced no embrittlement on tempering, whereas Fe-Cr-C-P and Fe-Mn-C-P alloys were susceptible to temper embrittlement.[44]

The way in which alloying elements effect this phenomenon is a question under much debate. Chromium is known to increase matrix hardness, so enhancing hardenability and resistance to softening during tempering. This action would produce a tendency for steel containing chromium to temper embrittle.[31] Nickel is seen to increase

the segregation of phosphorus to grain boundaries by a factor of 10-100 when compared to an Fe-P alloy at 500°C.[46] Nickel has no solid solubility in carbides, so it would tend to build up at the carbide-ferrite interfaces, lowering the chemical potential of impurities in grain boundaries and so promoting impurity diffusion to grain boundaries.[46] Interfacial combinations of alloys and impurities, e.g. Sb-Ni [47], Sb-Mn [49], P-Ni [48] are seen to be stable in accordance with Gibbsean equilibrium segregation.

The reason that alloys segregate in the ferrite phase field is thought to be due to an alloy-impurity interaction. Double segregation was at one time thought to be involved [11] but has now been dismissed as a possibility.[51]

An example of this interaction is Sn-Ni which is expected from the effect of nickel in lowering the solubility of tin in α-iron.[50] This is due to a stronger mutual attraction and a tendency to form intermetallics between Ni-Sn than between Fe-Sn. Chromium also depresses the solubility of tin in α-iron.[50]

Low et al[53] obtained the earliest evidence for major element-impurity interaction and they suggested strong interactions of the Cr-P and Ni-Sn types but a weak one for Ni-P. The latter point was expanded on when it was found that phosphorus segregates whether nickel is present or not.[14]

Guttmann used a thermodynamic approach to assess the relative strength of any possible alloy-residual interaction by assuming equilibrium segregation of both types of solute in the α-phase. He used a ternary solution as a model and the matrix and the grain boundaries were treated as separate phases. His calculations reveal that interactions for the couples Ni-Sn, Ni-Sb and Ni-P should be strong in the forms Ni_3Sn_2, NiSb and Ni_3P respectively, amongst

many others. No direct evidence of these phases has been found as yet, although, indirectly from auger analysis for Sn < 6 atomic%, the Ni:Sn ratio at the boundary approximates to that of Ni_3Sn_2.[55]

2.2.1.3.2 Embrittlers

Generally, alloys are not seen as embrittlers in their own right but merely enhance the embrittling behaviour of metalloid elements. Manganese though is seen to be an exception to this rule.

An increase in the degree of temper embrittlement is seen with increase in manganese content of a steel [43] and manganese is seen to segregate to austenite grain boundaries in the ferrite phase. [41,56].

The first reports of manganese as an embrittling agent [18] met with a degree of sceptisism due to the fact that a Group VIIA element should act like a metal, not a metalloid, and being a γ stabilizer, manganese has effects on phase equilibria in iron different to any other embrittling agent. The other metalloid elements are all ferrite stabilizers or γ- loop formers. Hence, they are likely to be rejected from the austenite matrix during solution treatment and end up on the austenite grain boundaries.[58]

Manganese is not a γ- loop element and on this basis should be unlikely to segregate during austenizing. However, nickel is not a γ- loop element either, yet segregation of this element has been found at brittle intergranular surfaces.[59] It is therefore likely that when manganese is present in sufficient amount segregation to grain boundaries will occur. Indeed, manganese segregation per se has been blamed for temper embrittlement in a high purity Fe-Ni-Mn alloy [60] but nitrogen is present in the Auger signal.[130] It has also been stated that it is a more severe embrittler than tin, antimony or arsenic.[38]

As far as concentration of manganese in steel to cause

embrittlement is concerned, as little as 0.7% Mn has been found to induce temper embrittlement when added to Ni-Cr steel.[18]

It has also been suggested that manganese acts like chromium in enhancing the embrittling effect of phosphorus.[57] Manganese weakens the atomic bonds of phosphorus in ferrite [23] giving a drop in diffusion activation energy of phosphorus in ferrite. This would make the transfer of phosphorus in ferrite more favourable giving grain boundary enrichment of this impurity. Manganese has also been reported as an enhancer of the embrittling effects of tin, antimony and arsenic as well, due to some interaction, making these elements more effective at lower levels within the steel. Phosphorus has been seen to segregate to grain boundaries after manganese has segregated, presumably due to a Mn-P interaction.[61]

The kinetics of the build up of manganese and phosphorus on grain boundaries in Fe-8.0Mn alloys has been studied [62]. The conclusion of this work was that the diffusion coefficients of manganese and phosphorus are consistent with bulk lattice diffusion values of manganese and phosphorus in ferrite.

Some chemical interaction of manganese and phosphorus during austenitising may contribute to the driving force for manganese segregation in ferrite.[51]

2.2.1.3.3 Embrittlement Retarders

The addition of certain alloying elements to steels is seen to retard embrittlement. This action is thought to be caused by these elements somehow slowing down or halting the diffusion of the embrittling agent in the iron matrix.

The most widely reported in this class of alloying elements is the effect of molybdenum on phosphorus-induced embrittlement of steels.

The ductile to brittle transition temperature and the amount of intergranular fracture are seen to decrease with an increase in molybdenum content of a steel.[63] This is only true, though, up to a certain concentration of molybdenum. Too much of it is seen to actually be detrimental in that it will enhance embrittlement. Fig. 31 utilises a calculated temper embrittlement susceptibility factor to show the effect of molybdenum concentration. Fig. 32 measures the improvement in impact transition temperature with molybdenum concentration and shows an improvement only up to a critical molybdenum level, after which there is seen to be a deterioration in this property. Molybdenum also affects other mechanical properties in steel, as shown in Fig. 33.

It is generally believed that molybdenum retards embrittlement by its influence on solubility and consequently segregation of impurities.[65] With particular reference to the embrittling element phosphorus, molybdenum is seen to increase the activation energy for phosphorus diffusion and also the binding energy of phosphorus in the γ-iron lattice.[66] Evidence of this can be seen where molybdenum increases the activation energy for phosphorus diffusion in a Ni-Cr steel [23] which could lead to a slower diffusion and a lower concentration of embrittling elements at the grain boundaries.

Molybdenum increases the solubility of impurities, then, in steel but only as long as it is in solid solution. When it precipitates out, the solubility of impurities decreases and they can then diffuse to grain boundaries.[46]

Fig. 34 shows the excess solute, Γ, at grain boundaries as a function of temperature indicating how step cooling combines faster kinetics at higher temperatures with lower kinetics but

higher chemical driving forces at lower temperatures. If molybdenum shifts the Γ vs T curve to lower temperatures, the first stage of the step cooling process may not contribute significantly to the embrittling process, resulting in no apparent embrittlement.

Early workers [44] deduced that molybdenum decreased the equilibrium degree of embrittlement rather than the rate at which equilibrium is achieved.

Other elements, including tungsten, niobium and titanium [64] as well as some rare earths, [67] are seen to retard embrittlement.

Titanium has a particular effect on phosphorus by the formation of stable phosphides in the iron matrix thus lowering the phosphorus concentration in solution.[24] This is due to the higher affinity than iron that titanium has for phosphorus. The rare earths, lanthium and cerium also form stable microcompounds with phosphorus and have a higher affinity for it compared to iron, Fig. 35. In this way, then, they too retard embrittlement.

The retarding effect of these alloys mentioned is however affected by the level of carbon present in the steel. For instance, if molybdenum were to be precipitated in the steel by carbon, temper embrittlement would occur more readily. This effect is more pronounced with increasing age temperature and increasing carbon content. If the Mo:P ratio is high, molybdenum is not precipitated out by carbon and the molybdenum scavenges phosphorus. This is explained by Guttmann's analysis [54] dealing with the attraction of two solutes in a ternary system. He showed that in a ternary solution in which the attraction of the two solutes for each other is stronger than that of either for the solvent, then the solutes would tend to

segregate to the grain boundary. As the intensity of mutual attraction of the solutes increases, the tendency towards segregation should become stronger. However, at some point the attraction can become so strong that the solutes immobilize each other, either by precipitation or by the formation of some relatively immobile complex. Molybdenum is a strong carbide former negating the scavenging effect on phosphorus. So the ability of molybdenum to suppress phosphorus embrittlement depends on C:Mo and P:Mo ratios.[68]

As well as slowing down phosphorus diffusion in two phase $\alpha+\gamma$ regions, molybdenum also slows down the diffusion of this metalloid in Fe_3C.[23]

Manganese has also a response, as the metalloid embrittling agents have, to molybdenum additions.[57]

The effects of carbon on the retardation of embrittlement by titanium is similar to molybdenum, in that at high carbon contents titanium is competed for by carbon.[24]

2.2.1.3.4 Carbon

Carbon, especially in the form of carbides, has been seen to contribute quite an amount towards understanding the full picture of the embrittlement problem in commercial steels. Commercial steels inevitably contain carbon and, if tempered at some stage or other, will more than likely contain carbides.

These carbides are seen to contribute to embrittlement (a) mechanically and (b) chemically. (a) Mechanically they are seen as barriers of dislocation movement, so helping to initiate intergranular cracks.[32] A second factor is associated with the degree of carbon supersaturation produced on quenching from 650°C and its precipitation during subsequent ageing which will have an

effect on the flow stress. While age hardening that occurs within the temper embrittlement range does not by itself result in intergranular fracture it can make a significant contribution to the shift in DBTT.[52]

(b) Chemically, carbides can be rejectors of impurities, so enriching grain boundaries with them.

Changes in brittle fracture mode from transgranular to intergranular have been associated with the transformation of ϵ-carbide to fine, plate-like cementite.[70] But embrittlement was found not to occur in carbon steels of high purity i.e. containing no residual impurities.[33,71,72]

It has been postulated[58] that the reasons why the prior austenite grain boundaries are the preferred fracture paths are that they are the locus of the highest embrittling element concentration and they represent a continuous internal surface on which carbide precipitation has occurred. In the absence of embrittling elements, this carbide precipitation is of little consequence, but if the cohesive strength of the carbide-ferrite interface is lowered by impurity segregation, then an especially fragile situation develops. This is because the interface between a hard, brittle particle and a plastic matrix is much easier to separate (during shear in the matrix) than is the interface between two plastic grains. In the latter case accommodation by plastic flow is possible, in the former case it is not.

It has been shown[73] that if antimony is allowed to segregate, in a Ni-Cr steel, to carbide-ferrite interfaces in a high carbon ferrite, the interfaces can be made to split open in tension at low temperatures, whereas reheating to a higher (de-segregating)

temperature and quenching restores the normal high tenacity of these interfaces. This effect has also been shown in a Fe-C-Sb ferrite and other heats containing arsenic and tin. Figure 36.

It has been possible to obtain very large variations in intergranular strength in ferrite ($\sim$ 23ppm O_2, $\sim$ 46 ppm C) by varying the amount of segregated carbon through the selection of temperature from which the solution treated ferrite is quenched prior to low temperature testing.[74] Figure 37 shows this variation and its correlation with the amount of intergranular fracture. The lack of ductility to the right of the peak is due to carbon insufficiency at grain boundaries, caused by a low amount of equilibrium segregation of carbon at high temperatures. The low ductility to the left of the peak is caused by carbide-initiated cleavage fracture. The ductility maximum occurs when sufficient carbon has segregated to scavenge the residual oxygen, but when the formation of carbides larger than $\sim$ 1μm thickness has not yet occurred.

Because impurities segregation and carbide transformation have both coincided with the onset of temper embrittlement, a carbide-impurity interaction has long been postulated. Indeed, adjustments in carbide composition occur in alloy steels after precipitation has occurred[75] i.e. partitioning occurs such that, for example in a Cr-steel, the chromium content of the cementite increases with time[76] and it would be expected that other elements such as silicon and phosphorus would be expelled into the ferrite matrix where their chemical potential would be lower.

Rellick[77] used an Fe-C alloy doped with impurities to show these effects. The resultant splitting along carbide-ferrite interfaces is shown in figure 38. It was found that interfaces between large carbides

and the ferrite matrix were severely embrittled during a furnace cool to room temperature from 925°C for materials containing Sb, Sn or As, but not for one containing P. This mode of embrittlement could be reversed by reheating to 650°C for ½ hour and quenching but the original carbide-ferrite interfaces could not be re-embrittled by holding at 480°C for up to 74 days. Instead, a new mode of weakness accompanied the reprecipitation of fine cementite at ferrite grain boundaries at 480°C in all materials with embrittling elements added, including the P-doped alloy. None of these manifestations of interface weakness was found in similar Fe-C alloys free of added embrittling elements.

It is assumed that embrittling metalloid elements have negligible solubility in Fe_3C; a precipitating carbide would tend to reject such foreign atoms. Indeed, these elements and carbon are reported to have no measurable mutual solubility, and they do not form carbides.[78] The impurities would tend to build up in the ferrite alongside the carbide-ferrite interface. The subsequent series of events are shown diagramatically in figure 39.

Figure 40 shows that precipitate β can only grow as fast as the rejected solute diffuses away in the ferrite matrix resulting in a solute concentration gradient ahead of an advancing interface. A Zener analysis applied to this diffusion controlled growth gives figure 41 showing the carbide being cored with respect to impurity content.

Eventually, impurity concentration at carbide-ferrite interfaces is high enough to diffuse into the matrix giving a decrease in temper embrittlement or the phenomenon sometimes called overaging.[46]

This type of embrittlement is due to non-equilibrium segregation although it does not preclude equilibrium segregation, and the two types could exist together.

Grain boundary phosphorus decreases when carbon atoms dissolved in ferrite decreases,[79] supporting this idea of a non-equilibrium theory of segregation.

2.2.2 Effects of solution treatment temperature.

The main effect is the variation in grain size with temperature - the higher the austenitizing temperature before quenching, the larger the grain size. It has been well established that a small grain size can be utilised to strengthen a material and also improve the toughness.

Hall and Petch[83] gave the strength/grain size relationship of engineering materials as ;

$$\sigma_y = \sigma_i + d^{-\frac{1}{2}}Ky$$

where

σ_y = yield stress

σ_i = lattice friction stress

2d = grain diameter

Ky = constant - a measure of the difficulty of spreading yielding from grain to grain.

A decrease in grain size gives an increase in toughness and so a decrease in ductile to brittle transition temperature. In the case of brittle cleavage fracture, grain boundaries act as barriers to the propagation of brittle cracks and thus a finer grain size, giving more grain boundaries per unit area, produces greater toughness. Although austenite grain size is less effective than ferrite grain size on improving fracture toughness.[80] Therefore, solution treatment temperature is seen to indirectly affect temper embrittlement by the fact that increasing the austenitizing temperatures increases grain size giving an increase in ductile to brittle transition temperature.[21,67,69] This is seen to be a particular problem in the heat affected zones of welds in susceptible steels, where the grain size is often uncontrollably large.[38]

The grain size will affect the fracture path such that, with a large grain size, there are less frequent deflections in the fracture path so a

subsequent lower fracture energy associated with it.[21]

There is some question as to whether impurities segregate during austenitization or not.

Often, with very large grain sizes (250 - 500μm) evidence of phosphorus segregation to prior austenite grain boundaries has been obtained during solution treatment.[51,57] But the extent of enhanced concentration of phosphorus during austenitizing depends on a combination of parameters such as austenitizing temperature, quench rate, structure, composition and the ratio of phosphorus : grain boundary area. Without considering all of these some workers have concluded that no segregation occurs during austenitizing;[40] with increasing grain size (increasing austenitizing temperature) there is a small decrease in phosphorus concentration[32,36] hence giving a T^{-1} relationship; while others[41] have found phosphorus segregation to be unaffected by austenitizing treatment and grain size.

Mulford[31] graphically represented work by Capus[21], given in figure 42, to show the grain size effect on ductile to brittle transition temperature to be magnified by the addition of embrittling agents.

Guttmann[81] postulated that although there has been no segregation found (of Sb) to prior austenite grain boundaries on quenching after short austenitizing treatments near or well above A_{r_3}, it should be possible to obtain segregation after prolonged heat treatment. This is because a longer treatment at a lower temperature is more likely to induce a phenomenon supposedly controlled by a Langmuir-type isotherm. But, up to date, no segregation of Sb has been proven at these sort of temperatures.

Recently, studies of microcracking in plate martensite in Fe-C steels have been carried out. Microcracks are seen[82] to form on two sites

(a) Intergranularly at austenite grain boundaries.

(b) Intragranularly at points of impingement of martensite plates.

With a fine grained steel, the onset of one step temper embrittlement is seen to coincide with the formation of isolated intergranular microcracks acting as nuclei for cleavage cracks. With a coarse grained material, intergranular microcracks are larger and more readily connected. Therefore, the energy trough is produced and the whole energy curve is shifted downwards.

2.2.3 Effect of Tempering Temperature

The embrittlement problem arises when the material is slowly cooled through a critical temperature range (typically 350 - 600°C).[31] This is especially a problem for large components, for example heavy forgings, etc., which must, because of the masses involved, be cooled down very slowly from heat treatment temperatures.

Embrittlement has been found to occur up to the Ae_1 temperature[84] in nickel-chromium steels. Isothermal embrittlement was examined in SAE 3140 steel[85] and was found to occur in two separate regions. The lower nose or reversible embrittlement range extends downwards from 600°C being most rapid in the range 550 - 490°C and carries on to low temperatures where the rate of embrittlement is slow. The upper nose or irreversible embrittlement range starts at Ae_1 where it occurs rapidly and continues downwards, overlapping the lower range, the rate decreasing with decreasing temperature. These results were obtained by the use of the embrittlement diagram whose ordinate is temperature and abscissa is a plot of log time at temperature. The curves produced (e.g. figure 43) are then temperature against time resulting in the same ductile to brittle transformation temperature i.e. similar amounts of embrittlement.

Step cooling from around 590°C can produce as much embrittlement as much longer isothermal treatments at maximum embrittling temperatures.[86] This effect can be rationalised on the C-curve in that the initial embrittlement is the highest rate at high tempering temperatures whereas the actual maximum amount of embrittlement can only be achieved at lower temperatures. Step cooling treatments attempt to optimise the effects of the whole embrittlement range.

Figure 44 shows the typical toughness "trough" which exists during the tempering of a low alloy steel, the region of the trough being the

temper embrittlement region. Many suggestions for the trough have subsequently been put forward; the theory of Irani[87] suggests that the temperature range is both high enough for coarse carbide formation and yet too low for dislocation recovery.

Using the isoembrittlement curves, Seah[88] has taken vertical sections about one time (200h) to predict segregation of phosphorus at a function of isothermal holding temperature and compared it with the experimental data of Carr et al,[89] showing a good correlation in figure 45.

Historically, research into temper embrittlement has been divided into two. One type of embrittlement occurs in steels with very high yield strengths. Here, the martensite has been tempered for short times at low temperatures. Because this state of embrittlement has occurred after a single tempering treatment of the martensite, it has been referred to as one-step temper embrittlement.

The other type occurs in steels with a lower yield strength. This is the result of a high-temperature tempering of the martensite at $\sim 600^{o}C$ which may allow the martensite→ferrite + cementite reaction to near completion. The embrittlement occurs when the steel is subjected to an additional thermal age near $500^{o}C$, whether it be isothermal or slow cooling. This is two-step temper embrittlement. The schematic representation in figure 46 clearly demonstrates the basis on which these nomenclatures have been chosen.

2.2.4. Environmental Aspects

These must be briefly mentioned because the presence of an aggressive environment often induces intergranular brittleness in steels which may otherwise be ductile. The environment may be gaseous such as hydrogen or hydrogen sulphide, etc.[90], an aqueous solution such as NO_3^- or OH^-[91] or even a liquid metal e.g. Cadmium, mercury, etc.[92]

If the fracture is caused by hydrogen, then the process is often referred to as hydrogen embrittlement or hydrogen-assisted cracking. The fact that hydrogen induces intergranular failure in steel has been used in auger analysis to help measure segregation to grain boundaries in steels before they actually embrittle normally e.g. in the austenite field.[40] It is a useful tool in steels that would not normally fail by intergranular fracture.

If the fracture is caused by oxidation and dissolution of metal ions, it is called corrosion. If the corrosion failure is exacerbated by the simultaneous presence of a tensile stress (applied or residual) then it is regarded as stress corrosion cracking.

If liquid metal is involved then it is called liquid metal embrittlement.

Neutron irradiation may also be regarded as an aggressive environment causing intergranular embrittlement of steels.

2.3. Segregation - Theories and Effects

As mentioned earlier, the segregation of residuals and alloying elements in both austenite and ferrite phases plays an important part in the development of embrittlement in steels. Therefore, the following review attempts to outline theories which have been proposed to predict the amount of grain boundary segregation occurring.

The effect of this segregation on the strength of grain boundaries is then reviewed concentrating, on its effect on the ductile to brittle transition temperature and on the grain boundary brittle fracture stress.

2.3.1. Adsorption Theories Used in the Theoretical Understanding of Segregation

The initial development of these theories involves the fixing of a number of interacting sites. They then develop into an unlimited number of sites, mutual interactions and interactions between different species.

2.3.1.1. Dislocation Atmospheres

An early development of segregation theory was to consider solute/dislocation atmospheres. Strain energy is released when a solute atom segregates to a dislocation and this is a measure of the binding energy. If sufficient time is allowed for the necessary atomic migration to occur, the dislocation will become surrounded by solute atoms, whose composition at any point is given by the Maxwell-Boltzmann law;

$$C = Co \exp (Ed/RT)$$

where

Co = average composition

Ed = solute/dislocation binding energy.

High concentrations of carbon and nitrogen are thought to accumulate around dislocations in this way, causing them to be pinned, so increasing the yield stress.

The expression could be used for any interface but more accurate expressions are now available.

2.3.1.2. Langmuir Type Adsorption

This is the simplest type of adsorption theory obeyed. It employs a single layer, a single adsorbate and no site-to-site interaction; it is assumed that there is only one element segregating to the interface, and this interface has a fixed number of identical sites at which the segregating element will be preferentially located, and that filling any particular one does not alter the probability of filling the others. This theory was first evaluated by McLean for grain boundaries.[111]

2.3.1.3. The McLean Model[111]

For this model, the following are defined:-

N undistorted lattice sites, P solute atoms among them.

η distorted interface sites, p solute atoms among them.

Suppose; molar distortion energy of a solute atom in one of the N initially undistorted sites is E and one in one of the η initially distorted sites is e. The free energy,G, due to the solute atom is

$$G = pe + PE - RT \ln \omega$$

$RT \ln \omega$ is the configuration entropy caused by the solutes. The minimum G occurs when:-

$$\frac{p}{\eta - p} = \frac{P}{N - P} \exp \left[\frac{E - e}{RT} \right]$$

Re-expressed in the usual form:-

$$\frac{Xb}{Xbo - Xb} = \frac{Xc}{1 - Xc} \exp \left[\frac{E_1}{RT} \right]$$

Where

Xbo = saturation value of Xb

E_1 = free energy of adsorption at grain boundary.

This is the same relationship as described by the Langmuir adsorption theory of gas adsorption.

The last equation shows segregation rising as the solute content rises or as the temperature falls. Because there is a fixed number of adsorption sites, saturation at Xbo is reached (~ one monolayer).

A plot of log [Xb/(Xbo - Xb)] vs T^{-1} should give a straight line and many workers have found this.

The main difficulty of this theory is when it is needed to calculate or predict large free energies of segregation, as it is difficult to calculate E_1. To some extent, this is overcome by the use of an alternative Langmuir-type adsorption called the truncated Brunauer, Emmett, Teller (BET) theory.

2.3.1.4. The Truncated BET Model[113]

This uses the same boundary conditions as before. The result of the theory, using statistical mechanics, is;

$$\frac{Xb}{Xbo - Xb} = \frac{Xc}{Xco} \exp \left[\frac{E}{RT} \right]$$

where

E = energy term of segretation.

Xco = solute molar fraction at the solubility limit.

The introduction of Xco is important and

Xco = $\exp(-E_L/RT)$ for slightly soluble substances

where

E_L = free energy of solution.

This is similar to McLean's result but $E = (E_1 - E_L)$ which is the difference between free energy of adsorption of the first layer and free energy of condensation of successive layers.

It gives insight into the magnitude of E_1 and role of Xco.

2.3.1.5. Multilayer Adsorption: the BET Theory [113]

This theory uses many layers, a single adsorbate and no site-to-site interaction.

$$\frac{Xbo}{Xb}\quad\frac{Xc}{XCo - Xc} = \frac{1}{K} + \frac{K - 1}{K}\quad\frac{Xc}{XCo}$$

where

K = exp (E/RT)

Xbo = one monolayer.

It is assumed that atoms adsorbing in the first monatomic layer have a free energy of adsorption E, those in successive layers have E_L. No lateral interaction; one monolayer does not have to be completed before the next one is started.

At dilute levels;

$$\underbrace{\frac{Xb}{Xbo}\quad\frac{1}{Xc}} = \frac{\exp\ (E/RT)}{Xco}$$

enrichment ration, β_b

Figure 47 shows the relationship between enrichment ratio and atomic solid solubility from interfacial energy and AES approaches.

Generally $\beta_b = \frac{(1 \rightarrow 10)}{Xco}$

A modification of this theory [114] allowed for the free energy of adsorption of the second layer to be different from E_1 and E_L. In the dilute limit;

$$\beta_b = \exp\ (\Delta G_T/RT) = \exp\left\{ - [\Delta H - T\ (Svib + San + R \ln \alpha)]\ /RT \right\}$$

where

Svib = change in vibrational entropy of the system per mole of segregant.

San = entropy change produced by the anharmonicity arising from lack of perodicity at the interface.

α = site multiplicity term.

	Surface	Grain Boundary
Svib	3.5R	3.3R
San	0.0012RT	0.00085RT
α	1	2 (Substitional adsorbates can register with either of the two grains)

The temperature dependence of Δ G for segregation were calculated below 910°C;

$$\text{(grain boundary)} = -13100 - 4.0RT - 0.00085RT^2 \text{ J/mol}$$

Because of lack of numerical values for temperature dependent free energies, Δ G is often referred to in this case merely as heat of segregation.

2.3.1.6. Segregation in Multi-Component Systems [I]

This is a multilayer, multicomponent form of segregation, in which there is no site-to-site interaction. The only case of this type of system with strong site competition is the interaction of tin, sulphur and calcium at grain boundaries in iron.[115] At the free surface of iron, S has a high heat of adsorption and displaces Sn. With the preceding theories as a framework, the adsorption of S merely reduces Xbo for tin segregation. So, the observed level of tin segregation becomes;

$$Sn = Sneq\ (1-s) \qquad Sneq \leq 1$$

Adsorption of tin is inhibited in the second layer because of the presence of S in the first. After consideration of this the following expression

$$Sn = (1-s) + (Sneq - 1)\ (1 - 4.5s)$$

(Ref [116])

$$Sneq \geq 1,\ S \leq 0.222$$

is describing the competition for adsorption in the range $1 \leq Sneq \leq 2$.

2.3.1.7. The Fowler Theory

This theory employs a single layer, single adsorbate and site-to-site interaction.[115] In the Langmuir theory it is assumed that a filled site does not affect the probability of an adjoining site from being filled. In this theory, though, interaction energy, ω , is introduced. The equation is similar to McLean's;

$$\frac{Xb}{Xbo - Xb} = Xc \exp \left[\frac{E_1 - CW\,(Xb/Xbo)}{RT} \right]$$

where

C = coordination number in the filled layer.

With W = 0, no interation so the equation becomes the form given by McLean.

With W +ve, the adsorped atoms are mutually repulsive.

With W -ve, the temperature dependence of segregation deviates from that given by McLean by showing sharper rises in segregation as the temperature falls.

2.3.1.8. Segregation in Multicomponent Systems [11]

In these systems there is element-element interaction. The equation $\beta_b = {}^{(1 \text{ to } 10)}/Xco$ and Fig. 47 are valid for alloy steels as long as the correct solubility is known. The effect of alloying elements is merely to shift the point in Fig. 47 diagonally within the scatter band.

An alternative approach, though, develops a specific theory allowing for interaction energies of alloys and impurities instead of incorporating them in Xco. Such a theory has been developed by Guttmann.[54] The equation below deals with a ternary (e.g. Fe-alloy-impurity);

$$\frac{X_{bi}}{X^{o}_{bi}} = \frac{X_{ci} \exp\left(\Delta G_i / RT\right)}{1 + \sum_{j=1}^{2} X_{ci} \left\{ \exp\left(\Delta G_i / RT\right) - 1 \right\}}$$

with simplifying approximations

$$\Delta G_1 = \Delta G_1^\circ + \alpha'_{12} X_{b_2}$$

$$\Delta G_2 = \Delta G_2^\circ + \alpha'_{12} X_{b_1}$$

where

X_{b1} and X_{b2} = molar fractional monolayers segregated by the impurity and alloy at the grain boundary.

X_{bi}° = their saturation value.

X_{c1} and X_{c2} = bulk molar concentrations.

ΔG_1° and ΔG_2° = free energies of segregation of impurity and alloys separately in pure iron.

$\alpha'_{12} = \alpha_{12} - \alpha_{10} - \alpha_{20}$

α_{ij} = changes in nearest neighbour molar bond energies occurring during the formation of the relevant impurity-alloy atom bonds.

Guttmann assumes regular solutions:-

So $$\alpha_{ij} = - \frac{\Delta H_{ij}^\circ}{N_i N_j}$$

where

ΔH_{ij}° = enthalpy per gram atom

N_i and N_j = mole fractions of impurity and alloy elements in the compound.

Differential interaction coefficients for many alloy-impurity pairs are calculated for α iron (Table 8). Those alloys coupling strongly with an impurity will reduce its solubility in steel and have a high α_{ij} so increasing its segregation.

2.3.2. Segregation and the Strength of Grain Boundaries

Now that the theories concerning the amount of grain boundary segregation that may be present have been assessed, the effect of this segregation on the grain boundary strength must be reviewed.

Early theories promoted segregation as acting through a reduction of the grain boundary work of fracture. In the fracture of a brittle material, energy is required to propagate the crack. The energy change forms two new surfaces and if the fracture is intergranular, the excess energy associated with the grain boundary is released and offsets the energies required to form the fresh surfaces. Thus, work of fracture per unit area γ, for brittle fracture of a grain boundary is defined[117]

$$\gamma = 2\gamma_s - \gamma_b$$

where

γ_s and γ_b are the surface and grain boundary energies per unit area respectively.

The use of γ may be linked with the Griffith equation where

$$\sigma_F = (2E\gamma/\pi c)^{1/2}$$

where

σ_F = stress at which crack length C begins to propagate in a material with elastic modulus E.

In solute segregation γ_s and γ_b may be reduced to about the values of the pure host metal[118,119]. Therefore, it is assumed that γ is reduced to such an extent as to produce a segregation-induced brittle intergranular failure in a normally ductile material.[42,120] However, it has been shown[110] that for grain boundaries fractured at low temperatures the effect of segregation on γ_s and γ_b does not cause the work of fracture to be significantly altered at all.

The segregation involves the presence at a grain boundary of atoms whose size differs from those of the host crystal. When the atoms are larger than the host, atoms facing one another across the boundary are more separated than those for a "clean" boundary and the tensile stress to part them is less.

2.3.2.1. Effect of Segregation on Ductile to Brittle Transition Temperature and on the Grain Boundary Brittle Fracture Stress

The ductile-brittle transition temperature occurs at a temperature where ductility gives way to brittleness as shown in figure 55. In metals, as the temperature falls the yield stress rises until, at the transition temperature, it equals the brittle fracture stress and the material starts to exhibit brittleness.

If the brittle fracture stress of the grain boundary falls below that of the matrix, the transition temperature rises and many of the phenomena of temper brittleness follow.

The effect of segregation on the grain boundary brittle fracture stress may be evaluated by considering an interplanar potential across the boundary, similar to those used in discussing ideal strengths, as in figure 56. During segregation large atoms of size a_1 replace matrix atoms of size a_o substitutionally, so increasing the spacing of the atoms across the boundary. The linear scale of the interatomic stress with distance for the boundary must increase [figure 56 , from curve (i) to curve (ii)].

The equilibrium position shifts from a_o relevant to the matrix atoms at the grain boundary, to a_e , relevant to the average grain boundary atom after segregation,

where $$2a_e = (2 - X_b)a_o + X_b a_1 \qquad \text{——————} (1)$$

where X_b = solute molar fraction content at the grain boundary.

Since work done by fracture γ is equal to the area under the stress-distance curve and does not vary with segregation, the areas under curves (i) and (ii) must be equal.

Variation of grain boundary brittle fracture stress with segregation, σ_e, is given by;

$$\sigma_e = \sigma_o \, (a_o/a_e) \qquad \text{——————} (2)$$

σ_o = brittle fracture stress of the clean grain boundary.

Substituting a_e from equation ① gives

$$\sigma_e = \frac{\sigma_o}{1 + \frac{1}{2} X_b (a_1/a_o - 1)}$$

This equation shows the segregation dependence of grain boundary brittle fracture stress.

This equation allows the transition temperature shift to be calculated by measuring the value X_b by AES.[110]

2.4. Phenomenalogical Considerations

2.4.1. Kinetics and Thermodynamics

2.4.1.1. Binary Systems

The kinetics of segregating species were examined by McLean[111] who studied solute segregation in an ideal binary solution in which the grain boundary "phase" acts as a sink for the solute which diffuses in from the matrix. In this analysis, the specimen is imagined to have been equilibriated at a high temperature then suddenly cooled to a lower temperature, at which the grain boundary concentration is allowed to come to equilibrium.

Then the fractional grain boundary saturation can be expressed as a function of time:

$$\frac{C_t - C_o}{C_\infty - C_o} = 1 - \exp\left(\frac{4Dt}{\alpha^2 d^2}\right) \operatorname{erfc}\left(\frac{2\sqrt{D}\,t}{\alpha d}\right)$$

where

C_o = initial grain boundary concentration ($t = o$)

C_∞ = equilibrium grain boundary concentration ($t = \infty$)

C_t = grain boundary concentration at time, t

D = diffusion coefficient

d = grain boundary thickness

$\alpha = C_\infty / C_o$

In the above analysis, the grain size is assumed to be large compared with the thickness of the grain boundary, and local equilibrium is assumed at the "interface" between the grain boundary "phase" and the matrix such that the composition in the matrix at the interface at time t is a constant times the grain boundary composition. The enrichment factor, α, was assumed to remain constant.

Tyson[121] reanalysed the situation because he realised that a constant enrichment factor was only valid in limiting cases such as binary alloys with low equilibrium levels. He used a computer model to predict segregation kinetics and concluded that segregation in both binary and ternary systems occurs much more rapidly than predicted by McLean.

In fact, there is not a great deal of evidence to show that segregation kinetics follow McLean's analysis exactly. A lot of observations, though, are compatible with his work. The classic embrittlement data of Carr, Goldman, Jaffe, and Buffum[89] was analysed by Seah[88] who showed close correlation with McLean's work when predicting transition temperature.

2.4.1.2. Ternary Systems

The thermodynamic theory of Guttmann[54] also used the treatment of bulk grains and grain boundaries as separate phases, each of which approximates to a regular solution.

In his analysis, he showed that if two solutes have a stronger attraction for each other than either has for the solvent, then these solutes will tend to partition to the grain boundary "phase". As the intensity of mutual attraction of the solutes increases, the tendency towards segregation should become stronger. However, at some point the attraction can become so strong that the solutes immobilize each other, either by precipitation or by the formation of some relatively immobile complex.

This increase in segregation on interaction is thought to be caused by a decrease in solubility of the impurity on the addition of a ternary element to the binary solution of an impurity in a metal.[61] This was found to be the effect of nickel on solutions of Fe-Sb and Fe-Sn.[48]

It has also been found by Hondros[122] that if there exists a strong chemical attractive interaction between the substrate and the absorbed atoms, then the adsorption on the surface will be increased.

Guttmann tried to link the limited solubility and segregation potency in ternary systems because he felt that both these phenomena express the tendency of the solid solution to reject the impurity first as a segregate - then as a precipitate. Because of this they should have some parameter in common which he identified as the interaction coefficient, α_{MI}

2.5. Experimental Techniques Used to Study the Segregation Involved in Embrittlement

Numerous experimental techniques have been developed over the years in order to study segregation. In particular the past ten years have seen a phenomenal change in the advancement of already established techniques and development of new techniques.

The experimental techniques to study segregation can broadly be classified as indirect and direct methods. The indirect methods are based on measurement of one or more material property changes as influenced by segregation. They are numerous and generally simpler, but only provide a qualitative assessment of segregation and frequently require substantial amounts of supporting information from other measurements. The direct methods, on the other hand, generally identify the segregated species and provide a quantitative assessment.

2.5.1. Indirect Methods

These require little or no expensive equipment, involving the measurement of property changes associated with the segregation.

2.5.1.1. Metallographic Techniques

These techniques involve distinguishing the differences in reagent attack among segregated and solute free interfaces. This is achieved by a careful selection of reagent or electrochemical technique. These techniques show prior austenite grain boundaries being preferentially etched. One of the many examples of successful reagents used to give this effect is that developed by Krahe and Guttmann.[93] This was a special acqueous picric acid solution containing small amounts of teepol and hydrochloric acid to preferentially etch embrittled grain boundaries of a low carbon steel. The "channel-like" etching of the prior austenite boundaries in the embrittled specimens has been found to develop only when the alloying and impurity elements are segregated at the boundaries, as directly evidenced by Auger Electron Spectroscopy.

2.5.1.2. Fractographic Techniques

Fractographic studies can sometimes provide indirect evidence of segregation to interfaces. Segregation is the cause of grain boundary failure during embrittlement. An examination of the fracture mode can therefore provide an indication of segregation. Although it is possible that failures may occur along clean or solute free interfaces, solute segregation can greatly enhance the occurrence of interfacial failures under stress.

The direct evidence of segregation in specimens broken intergranularly was obtained from examination of Auger Electron Spectroscopy of in situ fracture surfaces and indicated that grain boundary fractures contain residual impurities of higher level than the matrix.

This is an example of how fractographic examination alone is useful and sometimes necessary, and further that the assistance from direct methods makes the investigation more conclusive.

2.5.1.3. X-Ray Techniques

Effects examined by X-ray analysis to detect grain boundary segregation include;

(a) changes in lattice parameter affected by solute segregation or transport of solute from bulk to the boundaries.[94]

(b) changes in the low angle scattering intensities due to solute segregated at boundaries.[95]

(c) changes in X-ray absorption resulting from non-uniform distribution of the solute.[96]

The success of these techniques depends on;

(i) volume of solute distributed at the boundaries.

(ii) differences in X-ray atomic scattering factors of solute and solvent atoms.

(iii) differences in absorption coefficients.

2.5.1.4. Surface and Grain Boundary Energy Measurements[119]

Since the reduction in interfacial energy is the driving force for segregation under equilibrium conditions, the measurement of interfacial energy can be used as a satisfactory method of detecting segregation. The common practice is to measure the surface and grain boundary tensions.

Surface tension is commonly measured at high temperatures by the zero-creep technique. The grain boundary tensions may then be calculated from measurements of equilibrium groove angles where a grain boundary meets a free surface. On measurement of interface energy, the solute enrichment at interfaces may be calculated using Gibb's isotherm, which, for grain boundary segregation in a dilute system (obeying Raoult's law), where the solute obeys Henry's law, is expressed as;

$$\frac{d\gamma_b}{dx_c} = -\left(\frac{RT}{x_c}\right)\Gamma_b$$

where γ_b = grain boundary energy.

Γ_b = excess solute at grain boundary in mole m^{-2}

x_c = solute molar fraction in the lattice.

Change in γ_b with x_c gives grain boundary enrichment of the solute.

Γ_b correlates with atomic solid solubility as shown in figure 47.

Also used is the measurement of solvent self-diffusion.[98] The grain boundary and lattice self-diffusion parameters D_b and D_I are measured using radioactive tracer penetration methods. The absolute grain boundary energy γ_b is then determined from;

$$\gamma_b = \rho RT \ln (D_b/D_I)$$

and $\rho = 4{\cdot}18 \times 10^7 / 2a^2 N_o$

2.5.1.5. Microhardness

Microhardness measurements made with 1 to 50g loads in the vicinity of grain boundaries on prepared metallographic specimens can provide semi-quantitative information on long range grain boundary segregation, which can cause boundary hardening. The boundary hardening extends several microns from the boundary line and is believed to be a non-equilibrium mode of segregation. Figure 48 is the classical piece of work showing this effect in aluminium.

Although microhardness measurements reveal grain boundary segregation, as a method it suffers from selectivity of solutes. Errors also arise during metallographic preparation when surface flow interferes with segregation induced hardening.

2.5.1.6. Electrical Properties

These include lattice and grain boundary resistivities, electrode potential of grain boundaries within an electrolyte and thermo emf which are affected by grain boundary segregation.

The choice of an indirect method to study segregation can encompass any measurable property that is sensitive to segregation. Surface segregation, for example, can be inferred from changes in surface electrical properties, absorption of selected gases, surface reactivity, adhesion, corrosion susceptibility, catalytic activity, etc. Similarly, interface segregation can be evaluated from a number of interface related properties such as embrittlement, for example the effect of time and temperature on reduction of area in a tensile test,[60] corrosion, liquid metal penetration, boundary hardening, grain growth, stacking fault widths and internal friction and from material behaviour during high and low strain rate testing. Caution should be taken, however, as these property changes may result from other intrinsic changes in the material.

2.5.2 Direct Methods

Traditionally chemical etching, autoradiography and electron microprobe methods have been used to study segregation. Recently developed are the AES, ESCA, ISS, RBS, SIMS and FIM surface analysis techniques which have high surface sensitivity.

AES = Auger Electron Spectroscopy

ESCA = X-ray photoelectron spectroscopy

ISS = Ion scattering spectroscopy

RBS = Ion scattering spectroscopy

SIMS = Secondary ion mass spectroscopy

FIM = Field ion microscopy.

2.5.2.1. Chemical Etching[102]

This involves etching away a selected surface and analysing the collected resulting solutions for elements of interest.

Although simple in principle it requires great care in selecting the reagents, performing the etching and calibrating the standards.

2.5.2.2. Autoradiography

The segregating element, doped in the form of a radioactive isotope, segregates to the interfaces in the normal fashion. The emissions from the segregated species (usually alpha or beta particles) are then used to expose a film that is brought into contact with the specimen.

The method is rather insensitive unless the range of the emitted particles is low and the concentration of the radioactive species at the grain boundary is two or three orders of magnitude greater than the average concentration of the grain.[100]

2.5.2.3. X-Ray Techniques

Various techniques such as X-ray fluorescence analysis (XFA), electron micropole analysis (EMA) and X-ray analysis of thin foil specimens within a scanning transmission electron microscope (STEM) fall under this category. The methods use the characteristic X-radiation, emitted by the specimen, for qualitative analysis.

XFA is largely impractical due to its depth of analysis.

EMA analyses the characteristic X-rays emitted by an excited sample by the use of wavelength dispersion crystal spectrometers or by solid state energy dispersive analysers (EDA) as usually preferred in the scanning electron microscope (SEM) systems.

Figure 49 shows a single event in an electron atom interaction.

Application of the electron probe technique to surface and interface segregation is limited by at least two factors: analysis depth and lateral resolution. The analysis depth is dictated by the electron-induced X-ray excitation depth and is usually in the 1-2 μm range. Lateral resolution is limited by the area from which X-rays are generated. The analysis volume is shown in figure 50. This large analysis volume restricts the utility of the technique only to specific cases of interface segregation, where it is long range or massive.

In thin foil X-ray analysis, a measure to increase lateral resolution has been to reduce the thickness of the specimen. Fluorescence, absorption and differential electron backscattering are also reduced. Thus STEM has been combined with EDA for characteristic X-ray analysis and with electron spectrometers for energy loss spectroscopy (ELS). The latter technique utilises the fact that when high energy electrons are transmitted through a thin foil specimen, some of them lose energy because of inelastic scattering processes.

2.5.3. Surface Analysis Techniques

These are also classed as direct techniques but deserve a section in their own right. Typically they give information on composition and sometimes chemical binding of atoms localized near the surface. Only the surface layer is analysed, sometimes as thin as only one atomic layer. The methods include Auger electron spectroscopy (AES), x-ray photoelectron spectroscopy (XPS or ESCA), secondary ion mass spectroscopy (SIMS) , electron stimulated desorption (ESD), ion scattering methods (ISS and RBS) and atom probe field ion microscopy (FIM). Each technique differs from others in a number of ways, including surface sensitivity, qualitative and quantitative capabilities, lateral resolution, amount of surface disruption and the type of chemical binding or molecular information that can be provided.

During the past ten years, the technique of Auger electron spectroscopy has emerged as the most widely used analytical technique for studying surface and in-depth chemical composition.

2.5.3.1. Auger Electron Spectroscopy

Progress has been rapid, in recent years, towards a better understanding of embrittlement in steels mainly due to the development of Auger electron spectroscopy in revealing and measuring grain boundary composition. This chemical analysis of surface layers is possible on very thin layers $\sim$ 5 - 10Å and about 0.1% (atomic) of an element is capable of being detected, making the technique very sensitive indeed.

Descriptions of the applications of Auger Spectroscopy to surface analysis were first introduced in 1968 by Palmberg and Rhodin[103] and Harris.[104,105] Harris[105] had attempted to analyse a fracture surface in air, but was troubled by carbon and oxygen contamination. Marcus[106] in 1969 analysed under a vacuum of 10^{-9} torr with much more success and the development of this technique took off from there.

2.5.3.1.1. The Physics of the Process

This has been covered comprehensively by Chang,[107] so a much simplified discussion is presented.

The Auger process is initiated when an outer shell electron falls into an inner shell vacancy. For elements with a high atomic number, the elimination of a K-shell vacancy, for example, would probably be followed by photon emission; but for atomic numbers below about 27, there is a higher probability of de-excitation through electron emission. The expelled electron is the Auger electron.

Consider the energy level diagram in figure 51. The process is known as $L_3M_{2,3}M_{4,5}$ Auger transition. The doubly ionised atom may now revert to the ground state by single or double electron jumps (with line emission), or by another Auger process. Chemical bonding can also be detected by the fact that Auger transitions often involve valence electrons and so the position and shape of the Auger feature will reflect changes in the valence bond due to this chemical bonding.

2.5.3.1.2. Auger Spectra

Excitation is by electron bombardment; the energy distribution of the emitted electrons is of the type in Fig. 52. The low energy peak results from primary electrons which lose energy due to scattering and also from knock-on electrons. The high energy peak is due to elastically reflected primaries. Between the two are the small characteristic Auger peaks. Due to the small secondary electron current under the Auger peaks, they are normally represented in the first derivative form of energy distribution $\frac{dN(E)}{dE}$.

2.5.3.1.3. Escape Depth of Auger Electrons

When an Auger electron collides within the matrix, evidence of its history is destroyed. So to detect its initial characteristic energy, the Auger electron must originate from a depth below the surface that does not exceed its mean free path. Determinations of escape depth for a range of materials with kinetic energy are shown in Fig. 53. In the 20-1000eV range (the most useful Auger transitions) the escape depth ~ 5-13Å. This narrow zone makes the Auger electron spectroscopy a surface analytical technique.

2.5.3.1.4. Composition Profiling

Composition variations in layers adjacent to a surface can be revealed by sequential inert-ion sputtering and Auger electron spectroscopy. The surface is eroded away in a controlled fashion by ion bombardment, and the composition of the freshly exposed surface determined by AES.

The technique presents some problems such as quantification of layers removed and preferential sputtering.

Typical sputtering profiles are shown in Fig. 54. Segregation modes can be distinguished by the profile produced. If a precipitate has caused the signal, material will be removed in a plane parallel to the boundary; the observed impurity signal should remain fairly constant until it disappears - Fig. 54(a).

With equilibrium segregation, to lower the free energy of a surface only a small amount of solute is needed to be transported to the surface - Fig. 54(b).

The non-equilibrium type of segregation involves the binding of solutes to vacancies and vacancy diffusion to grain boundaries creating a broader profile around the grain boundaries - Fig. 54(c).

2.6. Controlling Methods used to Combat Detrimental Effects of Grain Boundary Segregation on Embrittlement

The suppression of the detrimental effects of grain boundary segregation is an integral consideration in materials design. Certain detrimental residual elements in steel e.g. tin and copper, accumulate principally from the recovery of scrap. Since efforts to recycle scrap are currently increasing, the problem of increasing bulk levels of residuals becomes more important. Therefore, the need for suitable controls of the detrimental effects of residuals becomes more urgent.

In engineering steels, phosphorus is a major embrittling agent.[109] In general, permitted levels of phosphorus in commercial alloys are high, and in order to improve immunity to embrittlement, these tolerance levels must be reduced.

Other, indirect methods of improving this immunity are also at hand.

2.6.1. Fixation Reactions

The chemical potential of S, O and N in steel can be decreased by adding Mn. Surface-active elements such as P and Sn are less obviously immobilized by thermochemical treatments, although the possibility is still open. This is an attractive approach as normal material properties should not be greatly altered.[115]

2.6.2. Increasing the Solid Solubility of Embrittling Species

The inverse relationship between grain-boundary enrichment and solid solubility suggests that increasing the solid solubility of the embrittling species should reduce the amount at the grain boundary.[115]

2.6.3. Reducing the Kinetics of Embrittling Species

The beneficial effect of Mo in reducing temper brittleness is thought to be due to the appreciable reduction of phosphorus mobility during a typical embrittling heat treatment.[115] The problem here is that other useful additives in ferrous systems used to counteract the mobility of P, Sn, and Sb would probably significantly alter other material properties.

2.6.4. The Reduction of the Concentration of Embrittling Species Along Interfaces[115]

With small amounts of surface active species in an alloy with a small grain size, a larger area is provided for the species to segregate to and so it will not be as concentrated.

Also, if a large area of interphase boundary (e.g. carbide) is modelled into the system, and if the embrittling species adsorb on these interfaces, a spreading out effect may be achieved. Although these approaches will affect the mechanical properties, they may not be detrimental.

2.6.5. Slip Dispersal

Alloy designs altering local slip concentrations, i.e. which disperse slip, will tend to prevent grain boundary failure. Thus, reducing the grain size will reduce the length of the slip band and hence the magnitude of the stress concentration at the head of the band. Alternatively, non-shearable particles could be added to the alloy in order to encourage cross slip.[115]

2.6.6. Competitive Segregation

After Guttmann[54] it would appear possible that there is a class of segregants which repel each other from grain boundaries. Thus, it may be possible to find a fairly highly surface-active but safe segregant which has a repulsive interaction coefficient with the unwanted segregant.

2.6.7. Remedial Segregants

Seah's theory of embrittlement[110] predicts that small atoms segregating to grain boundaries will reduce the effect of large ones.

3. Experimental Details

3.1. Alloy Preparation

All of the alloys used, shown in tables 1 and 2 were prepared at BISRA, Sheffield by vacuum melting. Series I alloys (Table 1) were prepared as 9 kg melts using Japanese electrolytic iron and electrolytic manganese and molybdenum and were subsequently hot rolled to 80 mm x 16 mm plate. In order to reduce banding in the material, the bars were individually enclosed in mild steel boxes. The ends of the boxes were then welded up and the material homogenised at 1100°C for 50 hours. An atmosphere of argon was provided via mild steel tubes fabricated into the box. The sealed unit used for this homogenising treatment is shown in Figure 1. The alloys were then hot rolled down to their finished size of 85 mm x 16 mm plate.

Series II alloys were prepared as 10 kg melts and initially forged down to 45 x 25 x 700 mm bars. These alloys were homogenised by packing into a furnace and heating at 1250°C for 6 hours followed by furnace cooling. An inert atmosphere of argon was provided during homogenisation, Figure 2. These alloys were then further reduced by forging before hot rolling down to 15 mm x 10 mm, effectively providing charpy impact specimen blanks, thus reducing machining requirements for the finished impact specimen.

The plates produced for the former two series of alloys were of sufficient thickness to enable two layers of impact specimens to be machined from one 80 mm long plate.

3.2. Heat Treatment

Series I alloys were austenitized at different temperatures, as given in Table 4, to observe the effect of temperature on the amount of alloying elements going into solution. The treatments were carried out on 80 mm x 80mm x 16 mm plates providing a possible yield of 14 impact specimens per treatment. The significance of optimising on impact specimens was that to make sure of efficient usage of the material, which was in short supply, almost all other subsequent tests were carried out on samples machined from broken charpy impact specimens. The plates were coated in Berkatec before the solution treatments in order to reduce the degree of oxidation.

The tempering treatments were carried out after the solution treatment of one hour at 1000^{o}C followed by a water quench. The main reason for choosing this treatment was so that the effects of tempering could be directly compared to the base alloy, Fe-8Mn, K1525 which has already been tested within the department and which had received the same treatment as above.

Tempering was carried out on impact, hardness, tensile, auger, X-ray and electron microscope specimens from Series I alloys in neutral salt baths using the following salt mixtures for various temperature ranges:

Temperature range °C	Salt
150 - 530	Nitrate/Nitrite
300 - 600	Chlorite/Sulphate
560 - 920	Sodium Chlorite/Carbonate

Three salt baths were built, purely for this programme of work, within the Metallurgy Department at Sheffield City Polytechnic.

The tempering was carried out at various temperatures (Table 4) to provide not only compositional and time oriented effects, but also kinetic data relating to effect of temperature. Water was the quenching medium employed after each treatment.

Series II alloys, in 80 mm x 85 mm x 16 mm plate form, were coated in Berkatec and solution treated at 1000°C for one hour followed by a water quench. The plates were tempered at 650°C in a muffle furnace for one hour followed by a water quench. Individually machined specimens for different types of mechanical, metallographic and chemical analysis (as in Series I alloys) were then tempered in neutral salt baths at 450°C for different times.

3.3. Optical Metallographic Examination

Specimens after each heat treatment were examined metallographically, both in the unetched and etched condition. Mechanical polishing down to ¼ micron diamond paste was sufficient for this study. A point counting technique was used initially to assess the inclusion content of the steel. The results from this accurate but rather time consuming method were then used as a check against the department's new Optimax image analyser. This piece of apparatus was then subsequently used for all inclusion content analysis.

The total number of points laid down in both the manual and the automatic image analysis methods was ~ 13,000.

Different etching techniques were tried on the Series I alloys. A single etch was found to be sufficient in the as-quenched austenitized condition; the etchant being 2% Nital solution. In the tempered condition, only a light etch with 2% Nital was employed followed by an immersion in an aqueous solution of sodium metabisulphite/sodium thiosulphate. The two initial solutions were made up to 30% solutions and the mixture was 1:200 respectively. This immersion gave a staining effect and the method is due to Schumann.[1]

3.3.1 Grain Size Measurement

The mean linear intercept method was used to determine the grain sizes of the alloys after heat treatments. This method measures the chord length defined by the intersection of a random straight line by the grain boundaries in the plane section of the polish.

The mean linear intercept, m.l.i., sometimes called the Heyn intercept, is often given the symbol $\bar{d}$, where :-

$$\bar{d} = \frac{L}{n}$$

where

L = length of random line on a planar surface

n = number of grains occupying this line i.e. number of grain boundaries intersected by the line.

The m.l.i. is obviously smaller than the mean true grain diameter, $\bar{D}$. Thus $\bar{D} \simeq 1.75\bar{d}$.

3.4. Impact Toughness Testing

Ductile-brittle transition temperatures of the alloys were determined in various heat treated conditions using sub-standard 'v' notch charpy specimens (Figure 5).

Low temperature tests were carried out by immersing the impact specimens in thermos flasks of the following mixtures for their respective temperature ranges:

Solid carbon dioxide/methanol	$-10^{o}C$ to $-50^{o}C$
Solid carbon dioxide/acetone	$-50^{o}C$ to $-78^{o}C$
Liquid nitrogen/low boiling point Petroleum ether	$-78^{o}C$ to $-129^{o}C$
Liquid nitrogen/iso pentane	$-129^{o}C$ to $-159^{o}C$

Temperatures above room temperature were obtained by the use of a fluidised sand bath.

Due to a temperature variation between leaving the heating or cooling medium and the actual moment of impact, the temperature of thermocouple in the medium could not be taken as the temperature at impact. Therefore, the thermocouple was spot welded to a spare impact specimen and this duplicate was taken out of the heating/cooling medium at the instant the test piece was taken out. The thermocouple was attached to a constant read-out chart recorder and the moment of impact marked on the chart. The calibration of the chart had to be carried out and this is shown in Figure 17.

After fracture, the fracture surfaces were cleaned with acetone and dried and then protected with a plastic protective coating from a pressurized container. This coating could be removed, whenever the examination of the fracture surfaces was required, by ultrasonic cleaning in acetone.

3.5. Hardness Measurements

To optimise on material, broken charpy specimens were used to provide hardness specimens. Hardness measurements were made on a Vickers Hardness machine using a 30 kg. load. Ten impressions for each treatment were taken.

For aging experiments at one particular temperature, the same specimen was used, aged intermittently.

The variation of hardness with age time for Series I alloy was determined at 450^{o}C and 525^{o}C to obtain some idea of the kinetics of aging. The treatment was carried out into the "overaged" condition i.e. when softening occurs.

Polishing to the 1200 grade paper was found to be sufficient for hardness determinations.

3.6. Tensile Testing

The reduction in area of tensile specimens was used as a measure of the ductility of the alloys. The tensile specimens were designed and machined out of broken half charpy specimens of the dimensions shown in Figure 3.

The samples were tested at a strain rate of 0.5 min^{-1} at a temperature of $-78^{o}C$ using an Instron testing machine. The low temperature was attained by surrounding the testing jig with acetone and cardice contained in a vacuum flask, Figure 4.

3.7. X-Ray Diffraction Analysis

To determine phases present in the alloys after each treatment, X-ray analysis was employed on polished specimens.

The Philips Diffractometer was used with Cobalt radiation. The samples, again broken sub-standard charpies, if mechanically polished only could have contained mechanically-induced transformation products, so interfering with the results. Therefore, each sample was electropolished using a mixture of 94% glacial acetic acid and 6% perchloric acid in a Struers automatic electropolisher. Later, a manual electropolishing system, Figure 6, was developed to enable more of the sample to be polished than the automatic system facilitated.

The samples were 12 mm x 12 mm to enable them to fit into the X-ray holder. The settings finally standardised on the Struers were;

Polish initial adjustment	3
Current polishing	55
Time	20 secs.
Flow rate	6

3.7.1 Method for X-Ray Analysis and Quantification

In this method integrated intensities, on the X-ray spectra, of reflection planes (hkl) of martensite and austenite phases were compared.

The equation shown by Durnin and Ridal[3] was used to calculate the integrated intensity of a diffraction line.

$$I(hkl) = n^2 Vm(LP) e^{-2M} (F.f)^2$$

where $I(hkl)$ = Integrated intensity of (hkl) reflection

n = Number of cells in $1cm^3$

V = Volume exposed to X-ray beam in cm^3

LP = Lorentz-Polarisation factor

m = Multiplicity of (hkl) planes

e^{-2M} = Debye-Waller temperature factor

F = Structure factor

f = Atomic Scattering factor

For n^2V it is possible to substitute $\frac{V}{v^2}$

where v = volume of the unit cell.

$$I(hkl) = \frac{V}{v^2} m(LP) e^{-2M} (F.f.)$$

If α and γ are the two phases present, then

$$\frac{V\alpha}{V\gamma} = \frac{I\alpha}{R\alpha} \Big/ \frac{I\gamma}{R\gamma}$$

where Ri = Theoretical Intensity for phase i at a particular reflection angle.

And $$V\alpha + V\gamma = 1$$

$$\therefore \quad V\gamma = \frac{I\gamma / R\gamma}{\frac{I\gamma}{R\gamma} + \frac{I\alpha}{R\alpha}}$$

The theoretical intensity factor 'R' can be calculated from

$$R = \frac{1}{v^2} m(L.P.) e^{-2M} (F.f.)^z$$

where L.P. = $$\frac{1 + \cos^2 2\theta_c \cdot \cos^2 2\theta}{\sin\theta \cdot \sin 2\theta}$$

where θ = Bragg angle for particular reflection

θ_c = Bragg angle for monochromatising crystal.

The Debye- temperature has only been determined for ferrite and it is assumed that this value also applies to austenite and martensite. The multiplicity factor for hkl reflection is :-

Cubic System		Hexagonal System	
hOO	6	hO.θ	6
hhh	8	OO.l	2
hhO	12	hO.l	6
hkθ	24	10.l	6
hkl	48	hk.θ	6

The Structure Factor F is given for a α (B.C.C.) as F = 2f when (h + k + l) is even and for γ (F.C.C.) as F = 4f when h + k, k + l, h + l are even integers.

'f', the Atomic Scattering Factor, for different reflections (hkl) depends on composition of the alloys and taken from International Tables.

Calculated 'R' values for Series I alloys are given in Tables 5 and 6.

Figure 18 shows the atomic scattering factors for Fe, Mn and Mo (for different values of Sin θ/λ) using $Co\ K\alpha$ (1.790 Å) radiation used in the above calculations.

Figure 19 shows the temperature factor of iron at 20°C for different values of $Sin\theta/\lambda$ used in the above calculations for 'R'.

3.8. Electron Microscopy

For the Japanese Electron Optics electron microscope (JEM 100B) thin foils were prepared by the following method :-

3 mm discs were machined from rods of heat treated material by the use of a diamond cut-off wheel. The discs were then ground using a jig (Figure 7) on 600 grade paper down to a thickness of 250 μm. After experimentation with solutions and temperature for the Series I alloys, profiling with 25% perchloric acid in anhydrous methanol ($<$ 0.01% water) and perforating with a 10% perchloric acid in anhydrous methanol at -25^{o}C was finally decided on as the best method.

The apparatus used with the above solutions and temperatures initially was a manual Polaron set up (Figure 8) with an improvised, pressurised liquid nitrogen system feeding the apparatus to attain the low polishing temperatures.

Later, an automatic Struers electropolisher using what is known as the window technique was employed to produce the thin foils. The solution used in this case was 94% acetic acid 6% perchloric acid at -30^{o}C, attained by liquid nitrogen. The settings, after much experimentation, on the Struers were 14A, 56V and a flow rate of 6.

For the Philips 400C electron microscope at Harwell, slightly different foil preparation was necessary due to the completely different arrangement of holder. Although the foils were still 3 mm. diameter, initial grinding was down to 40 μm., much thinner than for the JEM. The profiling (Figure 9) and perforating (Figure 10) arrangements were also different using a 10% perchloric acid in methanol for profiling at 90V and 100mA.

Tantalum tipped tweezers were used because of the highly corrosive properties of perchloric acid. The profiling current was varied by a vertical movement of the specimen in relation to the negative terminal i.e. effectively increasing the length of the jet of solution emitted from the flask.

The perforating was carried out in a solution of 94% acetic acid 6% perchloric acid at a voltage of 15v at room temperature. The perforating current was around the 40mA mark. The time for perforating varied slightly but was usually of the order of 10 minutes for 0.25 mm removed.

3.9 Scanning Electron Microscopy

Impact and tensile fracture surfaces, longitudinal sections of fractures and etched and unetched polished sections are examples of the type of samples investigated by scanning electron microscopy using the Philips PSEM 500 and the Cambridge Stereoscan S4. The specimens were all ultrasonically cleaned before mounting on stubs and evacuating. Often, the samples would first be mounted in conductive bakelite, but more generally they would be directly mounted on the S.E.M. stub with silver or carbon base paint.

On the fractures, the percentage type of fracture was carried out using a systematic point counting method.

The EDAX energy dispersive X-ray analysis system mounted with the PSEM 500 was used to analyse particles on fracture and polished surfaces. X-ray mapping and line scanning were used to the same effect. A similar job was carried out by X-ray mapping on the Stereoscan S4.

3.10 Auger Electron Emission Analysis

To analyse changes in fracture surface chemistry with changes in fracture mode and heat treatment, an auger electron spectroscope was used at the Atomic Energy Research Establishment at Harwell. Specimens were machined, from broken sub-standard impact specimens, into the form shown in Figure 11 and the same figure shows the holder arrangement used to enable the samples to fit in the fracture stage of the machine.

After loading the fracture stage (Figure 12) with a maximum of twelve impact auger specimens, the whole system was baked at 200°C while being pumped down to ensure evaporation of atoms from internal surfaces so providing a greater vacuum. A vacuum of $\sim 10^{-10}$ Torr was obtainable with the vacuum system, shown systematically in Figure 13.

After impact in the fracture stage, while under vacuum at liquid nitrogen temperatures, one half of the fracture sample was transferred to the specimen chamber (Figure 14) via the specimen transfer system. (Figure 15)

A Vacuum Generator cylindrical mirror type analyser (CMA) of the type used and described by Bishop[4] was used for the AES analysis with an integral electron gun providing a spot size of $\sim 20\mu m$. The differential energy spectra were recorded at a modulation of 3v. peak to peak, a primary electron energy of 2.5 kV and a specimen current of $\sim 4\mu$A.

The electron multiplier voltage was chosen to produce a reasonable spectrum but was typically $\sim$ 1500v. The lock-in amplifier gain was constant but not well defined.

Argon-ion sputtering was used to remove progressive layers from the fracture surface in order to give some idea of composition profiling. This is particularly useful with intergranular fractures, then the profiling is actually that around a grain boundary.

The sputter gas pressure was 10^{-11} Torr with normal incidence on the fracture surface because of surface roughness. The current density corresponding to removal rate was

$\sim 10\mu A\ min^{-1} \equiv$ 5 Å removal at 3kv.

3.10.1 Quantification of Spectra

Weber[5] states that a good approximation is that the amplitude of an auger peak in the dN(E)/dE spectrum is proportional to the atomic concentration of the element giving rise to that peak.

The results can then be expressed as ratios of prominent peaks of alloying or impurity elements to a chosen prominent peak of the matrix, provided that the matrix element always dominates the surface composition. The peak heights were expressed as percentage ratios of one of the iron peaks. The alloy spectra were calibrated using AES spectra obtained from cleavage fracture surfaces, which were approximated to the bulk alloy compositions.

Conversion of peak ratios to approximate atomic percentages required information about relative elemental sensitivities. A widely used, simple approach to the conversion is to use the elemental spectra and scale factors in Reference (6).

4. EXPERIMENTAL RESULTS

4.1 Chemical Compositions

The alloys have been split up into two main types name Series I and Series II.

The three series I alloys were K1525 (after Nazim [8]) taken as the base Fe-8Mn alloy, K1526 which was nominally Fe-8Mn-2.5Mo and K1527 which was nominally Fe-8Mn-5Mo. Full analyses of these alloys may be found in Table I. The analyses show close similarity between the three alloys with the exception of carbon; K1525 was 0.004C, K1527 was 0.006C and K1526 was 0.014C.

The three series II alloys were closely related to a commercial pressure vessel type steel. The base alloy A217 was nominally Fe-0.25C-1.4Mn-0.5Mo-0.57Ni-0.3Si. Alloy A317 had a 0.4Cu addition and alloy A417 was composed of the base alloy plus an addition of 0.04P. Full analyses of these alloys are given in Table II.

4.2 Series I Alloys

4.2.1 Metallography and X-ray Examination of Alloys in the Solution Treated Condition

In previous work [8] alloy K1525 (Fe-8Mn) was solution treated at 1000°C for one hour followed by water quenching. Subsequently, alloys K1526 (Fe-8Mn-2.5Mo) and K1527 (Fe-8Mn-5Mo) were austenitized at various temperatures, including 1000°C, for one hour and water quenched. All alloys show a lath-martensite structure after all treatments as seen in the optical micrographs shown in Figs. 109 to 114. Fig. 114 also shows a delta-ferrite phase at the prior austenite grain boundaries. The alloy that gave this deviation from the fully martensitic structure, seen after all other treatments in both alloys, was K1527 containing 5% Molybdenum after a solution treatment of 1300°C for one hour followed by water quenching.

The prior austenite grain size was seen to vary with the type of solution treatment and with molybdenum content. These grain sizes are tabulated, together with the quantitative analysis of the steel for inclusion content, in Table XII.

The chemical analysis of the inclusions in alloys K1526 (Fe-8Mn-2.5Mo) and K1527 (Fe-8Mn-5Mo) was carried out on the microprobe at AERE Harwell. The results are shown in Table XIII and in Fig. 115 demonstrating that the inclusions are two-phase, a manganese oxide at the centre and a manganese sulphide surrounding it. The X-ray analysis of all of the alloys after every solution treatment showed that only α' lath type of martensite was present with no ϵ-martensite present.

In order to make a direct comparison with previous work on iron -8 manganese alloys, the solution treatment of 1000°C for one hour followed by water quenching was chosen as the initial austenitizing treatment prior to aging experiments.

4.2.2 Impact Toughness of the Solution Treated Alloys

The ductile-brittle transition curves of the alloys K1525 (Fe-8Mn), K1526 (Fe-8Mn-2.5Mo) and K1527 (Fe-8Mn-5Mo) in the various heat treated conditions are shown in Figs. 60 - 66. Table XIV summarises the impact transition temperature and the low temperature fracture mode together with Auger Electron Spectroscopy results. Figures 60 - 62 illustrate the effect of solution treatment on the impact transition curve for alloy K1526 (Fe-8Mn-2.5Mo). Figures 64-66 show the effect of solution treatment on the impact transition curve for alloy K1527 (Fe-8Mn-5Mo).

The effect of the addition of 2.5Mo to an Fe-8Mn alloy is to improve the toughness of the alloy in the as-quenched condition, as seen in Fig. 67. The ductile to brittle transition temperature is reduced from 116°C to 48°C. It is also noticed from Fig. 67 that the addition of 2.5Mo also

reduces the energy required to fracture the alloy by the ductile mode, above the ductile to brittle transition temperature, by 35 Joules.

The addition of 5% molybdenum to an Fe-8Mn alloy is again to improve the as-quenched toughness as illustrated in Fig. 72. The ductile to brittle transition temperature is reduced from 116°C to 58°C. This is not as good an improvement in toughness as that provided by the addition of 2.5% molybdenum to the alloy. The upper shelf energy was again reduced with the addition of 5% molybdenum to the Fe-8Mn alloy, though this time the reduction was only by about 10 Joules compared with a reduction of 35 Joules in the lower molybdenum alloy. This is illustrated in Fig. 77.

Figs. 78 - 82 show more clearly the comparison between the effects of the two additions of molybdenum on the impact transition curve of Fe-8Mn with different solution treatments. For every austenitizing treatment, the higher molybdenum alloy is seen to exhibit a higher upper shelf energy than the alloy containing 2.5% molybdenum.

4.2.3 Hardness Data for the Solution Treated Alloys

The hardness data for alloys K1525 (Fe-8Mn), K1526 (Fe-8M-2.5Mo) in different solution treated conditions is given in Table XIV. After a solution treatment at 1000°C for one hour followed by a water quench the hardness of K1526 was ~ 76 Hv30 higher than that for alloy K1525 after the same treatment. The hardness of alloy K1527 after the same treatment was ~ 26Hv30 higher than that for alloy K1525, making it ~ 50Hv30 lower than the hardness of alloy K1526.

4.2.4 Fracture Surface Examination of the Solution Treated Impact Specimens

The fracture surface of alloy K1525 (Fe-8Mn) showed completely intergranular fracture under impact testing at room temperature after being water quenched from the solution treatment temperature of 1000°C. The scanning electron micrograph showing this fracture surface is in Fig. 57. The ductile mode of fracture at temperatures above the ductile to brittle transition temperature was ductile dimpling.

The room temperature fracture mode of alloy K1526 (Fe-8Mn-2.5Mo) after the same solution treatment was a brittle cleavage/ductile dimpling mixture indicating tougher room temperature impact properties than the base alloy. The fracture mode below the ductile to brittle transition temperature is seen to be completely brittle cleavage and that above the ductile to brittle transition temperature is seen to be ductile dimpling. The appearance of these fracture surfaces is illustrated in the scanning electron micrographs in Fig. 68.

After the other three solution treatments of 1300°C for one hour then water quenching, 1300°C for one hour plus water quenching followed by a further hour at 1000°C followed by water quenching, and 1300°C for one hour plus water quenching followed by a further hour at 850°C plus water quenching, the brittle fracture mode in all cases was seen to be completely transgranular cleavage and the fracture surface of the alloy above the ductile to brittle transition temperature was seen to be by ductile dimpling. These fractures may be seen in Figs. 69 - 71. The room temperature fracture mode of alloy K1527 (Fe-8Mn-5Mo) after one hour at 1000°C followed by water quenching was again seen to be of a mixed brittle cleavage/ductile dimpling type indicating again a shift in the ductile to brittle transition temperature to a lower value by the addition of 5% Mo to the base Fe-8Mn alloy. This room temperature fracture was in the transition region

between fully brittle and fully ductile. Below the ductile to brittle transition temperature the mode of fracture was seen to be by brittle transgranular cleavage and above this temperature was by ductile dimpling as shown in Fig. 73.

After the other three solution treatments, described earlier, all brittle fractures were by transgranular cleavage with some evidence of faceting on the cleavage planes. The tougher mode of fracture above the ductile to brittle transition temperature was, in all cases, by ductile dimpling. These fracture surfaces are shown in Figs. 74 - 76.

In summary, both 2.5% and 5% additions of molybdenum are seen to increase the intergranular cohesive strength above that of the matrix brittle fracture strength (Fig. 54) such that the brittle fracture mode changed from intergranular to transgranular cleavage.

4.2.5 Hardness of Alloys on Isothermal Aging at 450°C and 525°C

Nazim reported[8] only a slight age hardening of alloy K1525 (Fe-8Mn) after isothermally holding at 450°C. The hardness first increased by 12Hv30 in ten minutes from 258Hv30 to 270Hv30 but the alloy then started to soften, the hardness dropping to 235Hv30 after 100 hours. His results of the variation of hardness with aging time, after the alloy was solution treated at 1000°C for one hour and then water quenched,are shown in Fig. 125 for aging temperatures 450°C, 350°C and 400°C.

The variation of hardness on isothermally holding alloy K1526 (Fe-8Mn-2.5Mo) at 450°C is shown in Fig.83. The prior austenitizing treatment was one hour at 1000°C followed by water quenching. The error bars shown are the 90% confidence limits. There is possibly an initial small hardening response after three minutes but a straight line is assumed as it falls within the errors of the hardness measurement. The alloy is seen to commence softening after 330 hours and the hardness value falls from 348 Hv30 to ~ 300Hv30 after 9000 hours.

The variation of hardness with aging time at 450°C for alloy K1527 (Fe-8Mn-5Mo), after being solution treated for one hour at 1000°C followed by water quenching, is shown in Fig. 83. An initial incubation period of ten hours occurred with no variation in hardness from ~ 280Hv30. After ten hours the hardness increased and reached ~ 480Hv30 after 3000 hours, an increase of 190Hv30. With a further holding time at 450°C, softening of the alloy occurred, the hardness level being reduced to ~ 410Hv30 after a total isothermal age of 9000 hours.

The variation of hardness with aging time at 525°C for alloy K1526 (Fe-8Mn-2.5Mo), after being solution treated for one hour at 1000°C followed by water quenching, is shown in Fig. 128. The hardness is seen to fall much quicker than the equivalent alloy aged at 450°C. The hardness level dropped immediately on aging unlike the same alloy at 450°C when the hardness was seen to remain constant for ~ 330 hours. At 525°C it fell from 340Hv30 to 318Hv30 after 100 minutes. A levelling of hardness is seen to occur after 17 hours with a value of 255Hv30 being maintained after 30 hours. After an equivalent holding time at 450°C the same alloy had a hardness of 330Hv30.

The variation of hardness on isothermally aging alloy K1527 (Fe- 8Mn-5Mo) at 525°C, after a solution treatment of 1000°C for one hour followed by water quenching, is shown in Fig. 128. An initial drop in hardness was observed from 280Hv30 to 264Hv30 after 68 minutes before the hardness increased steadily to 310Hv30 after a holding time of 28 hours. No incubation period was observed as with the 450°C age for the same alloy. The increase in hardness was not as dramatic as noted with the aging at 450°C.

4.2.6 X-Ray Diffraction Analysis of Aged Alloys

The set of constants calculated for use in the quantification of X-ray analysis for alloys K1526 (Fe-8Mn-2.5Mo) and K1527 (Fe-8Mn-5Mo) are tabulated in Tables V and VI.

The results of phase analysis during aging at 450°C and 525°C are summarised in Table XV for the above two alloys which had been solution treated (a) for one hour at 1000°C followed by water quenching, (b) for one hour at 1300°C followed by water quenching and (c) for one hour at 1300°C plus water quenching followed by a further hour at 1000°C followed by water quenching.

The aging was carried out for up to 9000 hours in order to not only investigate possible formation of reverted austenite but also to try and overage any precipitates formed so that they may be identified.

Nazim found that 1.5% reverted austenite formed in K1525 (Fe-8Mn) after 75 hours at 450°C [8] as shown in Table XVI. In alloy K1526 (Fe-8Mn-2.5Mo) an addition of 2.5% molybdenum is seen to suppress the formation of reverted austenite as none of the phase was detected even after 9000 hours at 450°C when comparing equivalent prior solution treatments. In the sample of K1526 with a larger grain size, a small amount of reverted austenite was detected only after 9000 hours at 450°C.

Reverted austenite was formed on aging alloy K1526 at 525°C. 0.2% austenite was detected after 30 hours holding time at this temperature. The level of austenite in the microstructure did not increase with holding time with still only 0.2% being detected after 670 hours.

The addition of 5% Molybdenum to the Fe-8Mn alloy fully represses the reintroduction of austenite into the matrix as none of the phase was detected on X-ray analysis of K1527 (Fe-8Mn-5Mo) after all aging times at both 450°C and 525°C.

In all the measurements for percentage phases, the combination of many peaks was used as a method of limiting the errors introduced due to any preferred orientation, etc. that may have occurred.

4.2.7 Metallographic Examination of Aged Alloys

Optical metallographic studies failed to show any difference in the microstructures of K1526 (Fe-8Mn-2.5Mo) and K1527 (Fe-8Mn-5Mo). Electron microscopy was used to study possible changes in lath structure and any precipitation that may have taken place on aging.

The lath structures of both alloys in the as-quenched state were very similar, as illustrated in Fig. 126.

The microstructure of alloy K1526 is seen to remain unchanged on aging for 193½ hours at 450°C, Fig. 127.

Electron micrographs of alloy K1527, with the higher molybdenum content of 5%, showed extensive precipitation after ten hours at 450°C. The precipitates were seen to be of a homogeneous distribution within the matrix with no preferred precipitation at the prior austenite grain boundaries or along martensite lath boundaries, Fig. 84(b).

For the analysis of the precipitates, the Philips 400 transmission electron microscope at Harwell was used using electron diffraction and microdiffraction techniques. The camera constant was not known but could be calculated using the diffraction pattern from the iron matrix. Although a bcc structure was assumed for the Fe-Mn-Mo alloy, the matrix was checked for tetragonality. This was achieved using the Japanese Electron Microscope at the Polytechnic which produced an electron diffraction pattern from the $\langle 110 \rangle$ zone axis of the iron matrix, as seen in Fig. 85. The resultant solving of the pattern produced the expected result of the matrix being bcc not bct.

The camera constant was then calculated using a diffraction pattern for the iron $\langle 111 \rangle$ zone axis. The pattern and the solution of the index is shown in Fig. 86 and the measurements used for the calculation are listed in Table X.

Once the camera constant was found, the diffraction pattern from the precipitates in Fig. 87, which produced the dark field image in Fig. 88, could be indexed.

The pattern was solved for both Fe-Mo σ phase, with a zone axis $0\bar{5}0$, which is a b.c.t. embrittling phase and for Fe_2Mo Laves phase, with a zone axis of $\bar{1}\bar{1}2$, a phase much reported as occurring in aged alloys of iron that contain molybdenum.[129]

Fig. 87 shows the ability of these precipitates to restrict the movement of dislocations within the matrix. Dislocations are seen to be strung inbetween precipitates unable to pass between them.

4.2.8. Impact Toughness Data for the Aged Alloys

The effect of isothermally aging at 450°C and 525°C on the shape and position of the impact transition curves for alloys K1526 (Fe-8Mn-2.5Mo) and K1527 (Fe-8Mn-5Mo) is shown in Figs. 90 and 91.

Three variables are seen to affect the ductile to brittle transition temperature. They are:-

(i) molybdenum content.

(ii) aging temperatures.

(iii) time at aging temperature.

The addition of 2.5% molybdenum is seen to retard the embrittling effect of aging Fe-8Mn at 450°C.

Although Nazim did not study the effect of aging K1525 (Fe-8Mn) at 450°C on ductile to brittle transition temperature, this aspect was studied in another alloy 181 (Fe-8Mn) at 450°C,[134] Fig. 58. The ductile to brittle transition temperature for this alloy is seen to shift from ~ 50°C to ~ 300°C after only 6 minutes at 450°C whereas the ductile to brittle transition temperature of K1526 showed only a shift from 48°C to 90°C after 17 hours at 450°C. Maximum embrittlement in Nickbaht's alloy (Fe-8Mn) occurs at 6 minutes.

After this time, the alloy is seen to improve in toughness with a corresponding shift in the ductile to brittle transition temperature to the left. Alloy K1526 (Fe-8Mn-2.5Mo), however, exhibited continued worsening of toughness properties with a shift to the right of the ductile to brittle transition temperature, to a value of $\sim$ 120°C after 480 hours at 450°C.

The effect of aging temperature on the impact toughness of alloy K1526 was seen to be quite dramatic. Whereas the alloy embrittled on aging at 450°C with a corresponding increase in the ductile to brittle transition temperature, on aging at 525°C, the reverse happened. The alloy continued to improve in toughness with age time with a shift in ductile to brittle transition temperature from 90°C in the as-quenched condition to 7°C after 17 hours at 525°C and down to $\sim$ -65°C after 480 hours at 525°C.

The ductile to brittle transition temperature was not the only factor to be altered on aging. Both upper and lower shelf energies showed some marked change from the as quenched alloy. In alloy K1526, the lower shelf energy dropped from 20 Joules to 3 Joules on aging at 450°C for 17 hours and the upper shelf energy increased from 40 Joules to 50 Joules. After 480 hours, however, no further increase in the upper shelf energy was observed and no change in the lower shelf energy.

At 525°C a similar effect on the upper and lower shelf energies was observed in alloy K1526. The lower shelf energy dropped as with the 450°C aging treatment. After 17 hours at 525°C the upper shelf energy increased from 40 Joules to 70 Joules. After 480 hours at 525°C the upper shelf energy dropped to 50 Joules which is the same value as that produced by the 450°C aging treatment.

On aging alloy K1527 (Fe-8Mn-5Mo) the effects of varying molybdenum

content, aging temperature and holding time at the aging temperature can once again be observed, though the effects are different than in K1526. The variation in ductile to brittle transition temperature and in upper and lower shelf energies with aging time and temperature for alloy K1527 is shown in Fig. 90. At 450°C, the effect of the 5% molybdenum addition, compared with the base Fe-8Mn alloy, is to cause embrittlement, initially, with a slight toughness loss of the matrix reflected in a slight shift to the right of the ductile to brittle transition temperature from 44°C in the as quenched condition to 50°C after aging for 17 hours at 450°C. The upper shelf energy stays the same as that for the as-quenched condition unlike alloy K1526 where the upper shelf energy increases after this aging treatment.

After a longer isothermal holding time of 480 hours at 450°C, alloy K1527 failed by brittle fracture right up to 364°C i.e. no transition to ductile fracture was observed.

At 525°C alloy K1527 shows more brittle characteristics than alloy K1526 with a shift in the ductile to brittle transition temperature from 50°C to 114°C after 17 hours. After 480 hours at 525°C the alloy is again fully brittle at all test temperatures.

Fig. 103 illustrates a relationship between age hardening and toughness for alloy K1527 on aging at 450°C. Both the hardness and the ductile to brittle transition temperature are initially unaffected by isothermally holding at 450°C, but after longer aging times both the hardness increases and the ductile to brittle transition temperature increases. Fig. 105 illustrates a relationship between age hardening and toughness in alloy K1527 on aging at 525°C. No incubation period was experienced in the hardness response and after 17 hours at temperature, both the hardness and the ductile to brittle transition temperature had increased.

Fig. 104 illustrates a relationship between softening in the matrix and toughness for alloy K1526 on aging at 525°C. The hardness is seen to decrease with increasing holding time as is the ductile to brittle transition temperature.

4.2.9. Fracture Surface Examination of Aged Alloys

On aging alloy K1526 (Fe-8Mn-2.5Mo) the low temperature fracture mode is seen to gradually change from completely cleavage to completely intergranular. In the as-quenched condition, after a solution treatment of one hour at 1000°C followed by a water quench, the fracture below the ductile to brittle transition temperature is seen to be by transgranular brittle cleavage, Fig. 68. After 17 hours at 450°C, the brittle fracture mode, seen in Fig. 92, is a mixture of cleavage and intergranular fracture. After 480 hours at 450°C the brittle fracture, as shown in Fig. 93, is seen to occur almost exclusively along prior austenite grain boundaries. Some cleavage fracture is present but only on a few isolated grains.

After 17 hours at 525°C the fracture mode below the ductile to brittle transition temperature for alloy K1526 (Fe-8Mn-2.5Mo) is shown in Fig. 94. The fracture appearance is again of mixed intergranular and cleavage fracture but the proportion of cleavage fracture is much less than that observed in this alloy after the same time at 450°C. The appearance of the brittle fracture in this alloy after 480 hours at 525°C is shown in Fig. 95. The fracture is still a mixture of cleavage and intergranular but the proportion of cleavage has increased with aging time.

Fracture above the ductile to brittle transition temperature for alloy K1526 was by ductile dimpling after every aging treatment.

The fracture surface of alloy K1527 (Fe-8Mn-5Mo) in the as-quenched condition after a solution treatment of one hour at 1000°C followed by water quenching is shown in Fig. 73. It is seen to be a completely transgranular cleavage type of fracture.

On aging at 450°C the brittle fracture mode of this alloy gradually transformed from a cleavage to an intergranular type of fracture.

Fig. 96 shows the fracture appearance after 17 hours at 450°C as a mixed intergranular/cleavage type. Above the ductile to brittle transition temperature fracture occurred by ductile dimpling.

After 480 hours at 450°C, the brittle fracture, shown in Fig. 97, is seen to occur completely by the intergranular mode. The high temperature fracture mode exhibited by this alloy after a 480 hour age at 450°C is also by 100% intergranular fracture as seen in Fig. 97, with no ductility exhibited on impact testing up to 364°C.

Fig. 98 illustrates the fracture surface appearance of alloy K1527 after aging for 17 hours at 525°C. The brittle fracture mode is seen to be of an almost 100% intergranular type with very little cleavage in contrast to alloy K1526 after the same heat treatment which did exhibit much cleavage fracture. Above the ductile to brittle transition temperature the fracture of K1527 was by ductile dimpling.

After the longer holding time of 480 hours at 525°C, alloy K1527 again failed by completely intergranular brittle fracture at all test temperatures up to 256°C, as shown in Fig. 99.

4.2.10. Auger Electron Emission Analysis of the as-Fractured Surfaces

The results of quantification of the Auger Electron Spectroscopy peak ratios for alloys K1526 (Fe-8Mn-2.5Mo) and K1527 (Fe-8Mn-5Mo) after aging at 450°C are given in Table XVII. Representative spectra of the alloys in the as-quenched condition are shown in Figs. 121 and 123 and in the aged and embrittled state in Figs. 122 and 124. The grain boundary concentration of manganese and molybdenum as a function of age time are shown in Fig. 120.

At the beginning of the aging sequence, a drop in the concentration of manganese, as measured on the spectra, occurred. The manganese level then increased on the fracture surface for both alloys. A concentration of 40 atomic percent was reached, after 193 hours at 450°C, on the fracture surface of alloy K1526. Thereafter, a dip in the concentration occurred between 193 and 800 hours before it again started to increase. The molybdenum content in this alloy was also seen to build up on the fracture surface. It increased from a level of 2 atomic percent in the as quenched state to 10 atomic percent after 193 hours at 450°C. Again a dip in the level occurred after this time before a higher concentration of 15 atomic percent was reached after 800 hours at 450°C.

On aging alloy K1527, after an initial drop, the manganese again built up on the fracture surface. With this higher molybdenum content alloy the rate of build up of manganese was slower and the final maximum level reached was higher than in the alloy with a lower molybdenum content. A maximum of 35 atomic percent of manganese was reached after 193 hours and then a decrease in concentration occurred thereafter.

The rate in which molybdenum built up on the fracture surface of alloy K1527 was very like that in alloy K1526. A maximum of 14 atomic percent was reached after 500 hours and thereafter the molybdenum content at the fracture surface was seen to decrease.

The grain boundary concentration of nitrogen in both alloys as a function of age time at 450°C is shown in Fig. 129. 1.3 atomic percent was detected, in alloy K1526 (Fe-8Mn-2.5Mo), on the fracture surface after 480 hours. 1% was detected in alloy K1527 (Fe-8Mn-5Mo) after only 17 hours at 450°C.

4.2.11. Auger Electron Emission Analysis after Ion Bombardment of the Fracture Surfaces

The concentration profiles of the elements manganese and molybdenum as a function of distance from the prior austenite grain boundary for alloy K1526 (Fe-8Mn-2.5Mo) after aging at 450°C for 480 hours is shown in Fig. 130. Table XVIII gives the data collected for this ion bombardment process.

Manganese is seen to drop from 37 atomic percent at the fracture surface along the prior austenite grain boundaries to 13 atomic percent at a distance of 5 atomic layers away from the fracture surface. After a further 10 atomic layers, the concentration of manganese does not drop any further.

The level of molybdenum is seen to be constant at 7 atomic percent over the 15 atomic layers sputtered away from the fracture surface indicating a much thicker segregate of molybdenum than manganese at the prior austenite grain boundaries.

As well as a brief look at manganese and molybdenum profiles around the prior austenite grain boundaries, ion bombardment was used to investigate the 120 eV peak on the spectra. The peak could either be from phosphorus or molybdenum. Indeed it is given as phosphorus in Table XVIII. On ion bombardment, it is known that phosphorus concentration falls away very rapidly indeed. The 120 eV did not diminish on sputtering and so it must be concluded that this peak belonged to the molybdenum spectrum.

It was very difficult to quantify the carbon peaks on the spectrum as there was a great deal of contamination from the electron gun.

4.2.12. Tensile Test Results

Due to poor manufacture most specimens failed at the shoulder. ∴ No reliable sets of results were obtained.

4.3. Series II Alloys

4.3.1. Metallography of the Quenched and Tempered Alloys

Alloys A217 (Fe-0.25C-1.4Mn-0.5Mo-0.57Ni-0.3Si), A317 (as A217 but with 0.4% Cu) and A417 (as A217 but with 0.04% P) were solution treated at 1000°C for one hour and water quenched. Tempering was then carried out at 650°C for one hour followed by water quenching.

Alloy A217 showed a martensite structure after water quenching from 1000°C, shown in Fig. 131, with a prior austenite grain size of 303 μm. The addition of 0.4% copper is seen to make the microstructure take a decidedly acicular form, when quenched from 1000°C, as shown in Fig. 132, with the grain size decreasing to 163 mm for this alloy A317. The grain size of alloy A417 (with the phosphorus addition) as seen to be almost the same as the base alloy when quenched from 1000°C. The microstructure of this alloy is lath martensite with a phase at the prior austenite grain boundaries as shown in Fig. 133. Figs. 131 to 133 also show the microstructures of the alloys after a one hour tempering treatment at 650°C followed by a water quench. The resulting microstructures exhibit a much lower level of acicularity with the most explicit example of this being alloy A317, which loses all of its acicular appearance.

4.3.2. Impact Toughness Data of the Quenched and Tempered Alloys

The fracture energy values at various temperatures are plotted in Fig. 134 to give the charpy impact transition curves for alloys A217, A317 and A417 both in the as-quenched from 1000°C state and the quenched and tempered at 650°C state. Table XX summarises the ductile to brittle transition temperature, the low temperature fracture mode and the hardness for all three alloys in both the heat treated conditions. The base alloy A217 after quenching from 1000°C is seen to have a ductile to brittle transition temperature of -23°C as does alloy A317 with the 0.4% Copper addition.

The alloy with the 0.04% phosphorus addition, A417, is seen to be slightly less tough in the as-quenched state with a ductile to brittle transition temperature of -15°C, an increase of 8°C from the base alloy. Both the additions of copper and phosphorus are seen to increase the lower shelf energy by a slight amount and increase the upper shelf energy relative to the base alloy.

Tempering at 650°C for one hour followed by water quenching is seen to toughen all the alloys, as expected. The respective ductile to brittle transition temperatures were -82°C for alloy A217, -90°C for alloy A317 and -70°C for alloy A417. In the tempered state, the copper alloy is seen to be the tougher of the three with also a much increased upper shelf energy. Again the alloy with the phosphorus addition was seen to be the least tough. The lower shelf energies in all three alloys after tempering were of the same value.

Generally, tempering at 650°C for one hour followed by water quenching has produced a shift to the left in the ductile to brittle transition temperature of $\sim$ 60°C and an increase in the upper shelf energy of $\sim$ 40 Joules.

4.3.3. Hardness Data of the Quenched and Tempered Alloys

Table XX records the hardness of alloys A217, A317 and A417 in the as-quenched from 1000°C and in quenched and tempered at 650°C conditions.

As expected, the hardness of the alloys in the as-quenched condition is much higher than that in the tempered condition.

The hardness of the alloy with the 0.4% copper addition is seen to be higher than the base alloy and the alloy with the phosphorus addition, both of which are of a similar hardness.

4.3.4. Fracture Surface Examination of Alloys after Charpy Impact Testing in the Quenched and Tempered States

All three alloys, A217, A317 and A417, exhibited brittle transgranular fracture below the ductile to brittle transition temperature and ductile dimpling above it after being solution treated for one hour at 1000°C followed by water quenching and then tempering for one hour at 650°C followed by water quenching. The scanning electron fractographs showing these fractures are in Figs. 135-137.

4.3.5. Age Hardening Characteristics on Aging at 450°C and 525°C

The variation in hardness with aging time at 450°C and 525°C for alloys A217 (base alloy), A317 (base + 0.4% Cu) and A417 (base + 0.04% P), after being solution treated and aged, is shown in Fig. 138 and Fig. 108. The error bars shown are the 90% confidence limits.

In the base alloy A217 (Fe-0.25C-1.4Mn-0.5Mo-0.57Ni-0.3Si) there was an initial hardening response on aging at 450°C with the hardness increasing from 164Hv30 to 170Hv30 after two minutes. There then followed a period of about 5 hours in which the hardness of the alloy remained constant. After 5 hours, the hardness increased to a maximum of 203 Hv30 after 25 hours. The alloy then softened after this maximum.

On aging alloy A317 (base alloy +0.4% Cu) at 450°C an initial softening was exhibited with a decrease in hardness from 175Hv30 to 165 Hv30 after only one minute. During the next hour of aging the hardness level remained constant. After one hour at 450°C the hardness of the alloy started to increase, 245Hv30 recorded after 1000 hours, and was still increasing after this time. Therefore, a much higher hardness was recorded on aging this alloy compared with the base alloy.

An initial drop in hardness was also recorded for alloy A417 (base alloy + 0.04% P) on aging at 450°C, falling from an initial level of 163HV30 down to 154Hv40 after only two minutes. There followed a period of five hours of isothermal aging at 450°C during which the hardness remained unchanged. After five hours, the alloy began to age-harden reaching a level of 206Hv30 after 1000 hours, lower than that in the alloy with the copper addition after the same time at 450°C. The shape of the graph indicates that a maximum hardness has almost been reached with alloy A417 after 1000 hours.

The hardness of all three alloys is seen to be unaffected by holding time at 525°C up to 1000 hours, as seen in Fig. 108.

4.3.6. Impact Toughness Data of the Alloys after Aging at 450°C and 525°C

The effect of isothermally aging alloys A217, A317 and A417 at 450°C and 525°C on the ductile to brittle transition temperature during charpy impact testing and on the energy required to produce low temperature brittle fracture and high temperature ductile fracutre is shown in Figs. 139, 140 and 141 respectively.

Aging alloy A217 (base alloy) for 10 hours at 450°C is seen to have no effect on the ductile to brittle transition temperature or on the shape of the impact transition curve as shown in Fig. 139. A further 70 hours at 450°C shows a small increase in toughness reflected in a slight decrease in the ductile to brittle transition temperature and an increase in the energy required to cause ductile fracture.

Aging for 289 hours at 450°C produced a decrease in toughness in the alloy A217 illustrated in Fig. 139 by an increase in the ductile to brittle transition temperature from -82°C to -44°C and a lowering of the upper shelf energy from 77 Joules to 70 Joules.

Aging at 525°C gave a more rapid response to embrittlement with an increase of 54°C in the ductile to brittle transition temperature from -82°C in the as-quenched condition to -28°C after 168 hours at 525°C. The upper shelf energy is also decreased from 77 Joules to 52 Joules after 168 hours.

The lower shelf energies for alloy A217 for all aging treatments were between 2 and 4 Joules.

Alloy A317 (base alloy + 0.4% Cu) did respond to an isothermal age for 10 hours in that although the ductile to brittle transition temperature remained unaltered, the upper shelf energy increased from 79 Joules to 87 Joules as seen in Fig. 140. A further 70 hours at this temperature increased this energy required for ductile fracture still further to 90 Joules

and the ductile to brittle transition temperature was shifted to the left to lower temperatures i.e. a toughening of the alloy. All of the points enabling the formation of the full transition curve could not be obtained due to the difficulty in obtaining and maintaining impact test temperatures below -120°C but if a similar shaped impact curve was assumed the ductile to brittle transition temperature of -180°C could be postulated for this 80 hour age at 450°C.

Aging alloy A317 at 450°C for 289 hours gave a decrease in toughness. The ductile to brittle transition temperature increased from -90°C to -60°C and the upper shelf energy decrease from 79 Joules to 65 Joules when compared with the as quenched condition.

A greater degree and rate of embrittlement was observed in alloy A317 when aged at 525°C. An increase in the ductile to brittle transition temperature from -90°C to -30°C and a decrease in upper shelf energy from 79 Joules to 45 Joules occurred after 168 hours at 525°C.

Little change in the lower shelf energy of alloy A317 was observed on aging at all of the treatments.

Fig. 141 shows the effect of aging at 450°C and 525°C on the ductile to brittle transition temperature and the shape of the charpy impact transition curve for alloy A417 (base alloy + 0.04% P).

Isothermally aging at 450°C for a duration of 10 hours and 80 hours only slightly decreased the ductile to brittle transition temperature from the as-quenched value. The upper shelf energy was reduced from 86 Joules to 77 Joules after 10 hours at 450°C. The value of this tough fracture energy after 80 hours was 81 Joules.

On further aging at 450°C to a total time of 289 hours, the toughness of the alloy decreased with an increase in the ductile to brittle transition temperature from -70°C to -6°C and a decrease in the upper shelf energy from 86 Joules to 56 Joules.

A faster rate and a greater degree of embrittlement occurred in alloy A417 on aging at 525°C. 168 hours at this temperature produced an increase in ductile to brittle transition temperature from -70°C in the as-quenched condition to +98°C in the aged condition and a decrease in the energy required to produce ductile fracture from 86 Joules to 48 Joules.

When comparing the effect of the copper additions on the impact toughness of the base alloy at 450°C it is seen that the 0.4% copper addition initially toughens the alloy but when embrittlement occurs i.e. after 289 hours, it is not at as high a level as in the base alloy, indicating a retarding effect on embrittlement, i.e. a shift to the right for the ductile to brittle transition temperature of 30°C for the alloy with copper addition compared with 38°C for the base alloy after the same age treatment. The 0.04% phosphorus addition is seen to accentuate the embrittlement with a shift to the right of the ductile to brittle transition temperature of 68°C after 289 hours at 450°C.

When comparing the effect of the copper and phosphorus additions on the impact toughness of the base alloy on aging at 525°C a different result is apparent. The shift to the right for the ductile to brittle transition temperature for alloy A317 with the copper addition after 168 hours at 525°C is seen to be 60°C, compared with 54°C for the base alloy after the same aging treatment, indicating a greater decrease in toughness for the alloy with added copper. The effect of the phosphorus addition is seen to be much more pronounced than in the other two alloys, with a greater decrease in toughness reflected in an increase in the ductile to brittle transition temperature of 168°C.

4.3.7. Fracture Surface Appearance of the Impact Tested Alloys after Aging at 450°C and 525°C

On aging alloy A217 (Fe-0.25C-1.4Mn-0.5Mo-0.57Ni-0.3Si) at 450°C and 525°C both the high and low temperature fracture modes remained unchanged after all isothermal holding times.

Fig. 142 shows the high and low temperature fracture appearances of alloy A217 after 10 hours at 450°C and Fig. 143 shows the same for alloy A217 after the most severe embrittling treatment of 168 hours at 525°C. The fracture mode below the ductile to brittle transition temperature in both cases is seen to be transgranular brittle cleavage, whereas that above this temperature is seen to be by ductile dimpling.

A 10 hour isothermal holding time at 450°C provided no change in the high and low temperature fracture appearance of alloy A317 (base alloy + 0.4% Cu addition) with brittle cleavage below the ductile to brittle transition temperature and ductile dimpling above it, as seen in Fig. 144.

Embrittlement in this alloy, however, did coincide with a change of fracture mode with the most severe recorded example, shown in Fig. 145, of a 168 hour aging treatment at 525°C. The brittle fracture mode was a mixture of intergranular facets appearing quite rough when looked at under high magnification. The fracture appearance of the alloy, fractured above the ductile to brittle transition temperature, changed from ductile dimpling in the as-quenched condition to intergranular ductile fracture as shown in Fig. 146. The high magnification micrograph of one of the intergranular facets shown in this figure shows a typical ductile dimpling appearance.

Aging alloy A417 (base alloy + 0.04% P) gradually changed the fracture mode to coincide with embrittlement. After 10 hours at 450°C no change in either the low or high temperature modes occurred as shown in Fig. 147.

The low temperature fracture mode was brittle cleavage and the high temperature fracture mode was ductile dimpling as in the as-quenched alloy.

On aging at 525°C for 168 hours, the most severe embrittlement treatment, the brittle fracture was by intergranular fracture as shown in Fig. 148, with the intergranular facets appearing very rough.

The fracture appearance of alloy A417 aged for 168 hours at 525°C and broken at a higher temperature is shown in Fig. 149 and is a mixture of ductile dimpling and intergranular brittle fracture indicating that the upper shelf energy had not been reached in the impact test at the highest test temperature.

5. Discussion of Results

5.1. Composition

The three series I alloy compositions were seen to be very similar, Table I. Alloy K1525 was the base Fe-8.0Mn alloy, K1526 was nominally Fe-8.0Mn-2.5Mo and K1527 was Fe-8.0Mn-5.0Mo. With these compositions it was possible to examine the effect of manganese and molybdenum on embrittlement. The only anomaly in similarity was the carbon; K1525 was 0.004C, K1526 was 0.006C and K1527 was 0.014C. This may have had some effect on the results as it has been reported[44] that an increase in carbon can enhance embrittlement under given conditions, but this is due to an overall change in the mechanical properties of the general bulk of the alloy. It has also been reported that carbides produce a preferential site for solute segregation, leading to carbide/ferrite interfacial cracking.[58]

In summary, series I alloys provide data on the effect of two levels of molybdenum on the as-quenched properties and the embrittlement characteristics of an Fe-8.0Mn alloy.

Series II alloys, Table II, are more closely related to commercial pressure vessel steels, Supertough G and JIS grade J SQV 2/3, the nominal compositions of which are shown in Table XXII. All three alloys had a base composition of 0.25C, 1.4Mn, 0.5Mo, 0.57Ni, 0.3Si - nominal. Alloy A217 was the base alloy, A317 had an addition of 0.39Cu and alloy A417 had an addition of 0.041P. The tempering treatment given to these alloys was, therefore, of the classical temper embrittlement type allied closely to the typical conditions under service. The effects of copper and phosphorus on tempering were thus monitored.

5.2. The Effect of Molybdenum Content on the Impact Transition of As-Quenched Fe-8.0Mn alloys

Previous work on the iron-8Mn system showed brittleness in the as-quenched condition with an impact transition of ~ 110°C and intergranular failure in the brittle fracture mode with ductile dimpling in the region of the upper shelf,[8] Fig. 57. The treatment given to the K1525 Fe-8Mn alloy was an austenitizing treatment at 1000°C for one hour followed by water quenching. This treatment was also given to the Series I alloys. It was possible that the solution treatment at 1000°C had not taken all the molybdenum into solid solution, so higher austenitizing temperatures were also carried out. It is apparent from the results that the treatment at 1000°C had in fact taken all the molybdenum into solution. This was confirmed by thin film electron microscopy which only revealed lath martensite and no second phase particles. Fig. 63 shows the impact transition curve for Fe-8Mn,alloy K1525, in the as-quenched condition. Figs. 60-62 show the impact transition curves for K1526 Fe-8Mn-2.5Mo after different solution treatments. Figs. 64-66 show the same for K1527 Fe-8Mn-5Mo. The effect of the addition of 2.5Mo to an Fe-8Mn alloy is to improve the as-quenched toughness, as seen in Fig. 67. The impact transition temperature is reduced from ~ 115°C to about 50°C. It is also noted from Fig. 67 that the upper shelf toughness is reduced by the addition of 2.5Mo by 35 Joules. This addition of molybdenum also has an effect on the mode of fracture, as seen in Figs. 68-71. The ductile mode of fracture, being ductile dimpling, is the same as in the base alloy. However, the molybdenum addition has improved the intergranular cohesive strength above that of the matrix brittle fracture strength, Fig. 55, such that brittle fracture occurred by brittle cleavage as opposed to intergranular brittle fracture as in the base alloy.

The addition of 5Mo to the Fe-8Mn alloy is seen to reduce the transition temperature from ~ 115°C to about 45°C, Fig. 72. Twice the amount of molybdenum has only produced a slightly better result in this respect. The upper shelf energy was again reduced when comparing with the base Fe-8Mn alloy, though the addition of 5Mo has increased the upper shelf energy compared with the 2.5Mo alloy, Fig. 77.

The effect of 5Mo on the fracture mode can be seen in Figs. 73-76. The result is the same as with the lower molybdenum alloy content - ductile dimpling above the transition temperature and brittle cleavage below.

Figs. 78-82 show more clearly the comparison between the two alloys with different molybdenum contents for the different austenitizing treatments, with respect to their impact energy characteristics. It may be noted that for every solution treatment, the alloy with the higher molybdenum content has a higher upper shelf energy and the alloy with the lower molybdenum has a higher lower shelf energy.

Bolton[9] found that the Fe-Mn alloys containing between 4-10% Mn in the lath-martensite condition exhibited brittleness in the as-quenched condition due to a weakness at prior-austenite grain boundaries. It was suggested that segregation of some impurities might have occurred during austenitization and led to the potential weakening of the grain boundaries in the as-quenched condition.

Nazim[8] also found this to be so in alloy K1525, Fe-8Mn, blaming nitrogen as the harmful impurity with some build up of phosphorus at the prior austenite grain boundaries. Therefore, for molybdenum to suppress intergranular fracture, as it is seen to do, it must have some effect on the segregation of these impurities. Some interaction between molybdenum and the impurities must occur in such a way as to increase

the solid solubility of the impurities in ferrite during quenching. If this happens, they are less likely to segregate to sites of lower strain e.g. grain boundaries. In this way, the driving force for segregation due to the misfit of atoms in the ferrite lattice is overcome and the impurities will remain in solution.

5.2.1. Optical Metallography of the As Quenched Alloys

All solution treatments gave a lath martensite structure in both alloys, as seen in Figs. 109-114. The grain sizes vary with austenitizing treatment and molybdenum content and are tabulated in Table 12 together with the quantitative analyses of the inclusion contents of the alloy. Figs. 116-119. A deviation from the fully martensite condition was observed in the higher molybdenum alloy after the highest solution treatment temperature of 1300^{o}C. Here, delta ferrite was seen to form at the prior austenite grain boundaries. This was due to molybdenum being a ferrite former and the high temperature favouring the formation of delta ferrite, Fig. 114.

The analysis of the inclusions found in the steel was carried out on the microprobe at Harwell. The results are shown in Table 13 and Figure 115 demonstrating how the inclusions are two phase, a manganese oxide at the centre and a manganese sulphide surrounding it.

5.2.2 General Discussion of the Effect of Molybdenum on the As Quenched Properties of the Fe-8Mn Alloy

The change of the brittle fracture mode from intergranular to transgranular cleavage with the addition of 2.5% molybdenum to the Fe-8Mn coincided with a lowering of the ductile to brittle transition temperature. This is in agreement with work by Squires, et al, on the effect of molybdenum additions on Fe-Ni-Mn alloys.[123] One explanation of this is to consider the effect of molybdenum on other elements in solid solution. Nazim concluded that manganese, phosphorus and nitrogen segregated to grain boundaries during austenitisation and nitrogen segregation occurred on cooling, when martensite was formed, to cause intergranular failure. Therefore, it may follow that molybdenum in the Fe-Mn-Mo alloys acts in some way to suppress these effects. The molybdenum immobilises the manganese, phosphorus and nitrogen. The mechanism of this immobilisation has not yet been determined but it has long been assumed to be a precipitation reaction such as the formation of Mo_3P or MoN. However, recently Wada has reported that molybdenum suppresses the grain boundary segregation of phosphorus[124] but the attractive interaction is not strong enough to form stable Mo-P pairs in ferrite. The tendency of these elements to stay in solid solution could then be due to the increase of the solubility of phosphorus, manganese and nitrogen in iron, although it has been reported that molybdenum lowers the solubility of phosphorus in iron.[125]

However, the former is more likely since molybdenum is a γ - loop element which increases solid solubility in ferrite.

Hondros and Seah[115] described the relationship between solid solubility and the interaction of solute and solvent. In empirical terms the lower the solid solubility, the smaller the amount of elements in the matrix. This gives rise to a strong solute/solvent interaction and

the elements are more likely to segregate. Conversely, the higher the solid solubility the larger the amount in the matrix. The solute/solvent interaction will be weaker and so the elements will be less likely to segregate.

It has also been reported that molybdenum can increase the activation energy for phosphorus diffusion in a Ni-Cr steel. So there may be possible similar interaction between molybdenum and manganese and between molybdenum and nitrogen. The increase in activation energy would result in a slower diffusion of these elements to grain boundaries.

Unlike the work done by Squires, the addition of a further 2.5% molybdenum to the alloy, making a total of 5%, does not decrease the ductile to brittle transition temperature still further. This is unusual, since the alloy containing 5% molybdenum is softer than the 2.5% alloy and the corresponding ductile to brittle transition temperature should then be lower. It is also seen that the 2.5% molybdenum alloy is harder than the base alloy but the ductile to brittle transition temperature is lower due to a change from intergranular to brittle cleavage fracture i.e. a suppression of embrittlement.

The existence of an optimum amount of molybdenum that can suppress embrittlement has been known about for a long time[86,128]. It may be that the optimum amount was reached in these alloys between 2.5% and 5% and so it will not increase the toughness further.

The hardness of the as-quenched alloys increases in the order K1525 (0% Molybdenum), K1527 (5% Molybdenum) K1526 (2.5% Molybdenum). Hardness depends on tensile strength rather than yield strength. Earlier work by Buick showed uniform increase in yield strength with molybdenum content from 0 - 3 - 5% in an Fe-Mo alloy whereas tensile strength increases in the order Fe - Fe5%Mo - Fe3%Mo.[126]

This effect could be due to a phenomenon known as alloy or solid solution softening.[127] This can be explained in two ways:-

1. The extrinsic theory in which the starting b.c.c. metal would be hardened by residual impurities and a scavenging of these impurities by substitutional atoms would induce softening e.g. clustering of nitrogen around molybdenum.

2. The intrinsic theory in which the low temperature yield stress of b.c.c. metals and alloys would be controlled by a lattice friction or Peierls stress on the screw dislocations and the softening would correspond to a decrease of the lattice friction strength in the dilute alloys.

As well as the effect on the ductile to brittle transition temperatures, additions of molybdenum are also seen to affect the upper and lower shelf energies. An addition of 2·5% molybdenum to the Fe-8Mn alloy lowers the upper shelf energy for ductile fracture from ~ 72J to ~ 42J. A further 2.5% molybdenum addition (5% total) increases the upper shelf to ~ 60J. Two further observations may be related to this effect. The first is that the inclusion content is higher in the alloy containing the lower level of molybdenum. The second is that the hardness increases in the order:-

Kl525 (0% Mo)	——	Kl527 (5% Mo)	——	Kl526 (2.5% Mo)
258 Hv 30		284 Hv 30		336 Hv 30

An increase in hardness means anincrease in yield stress and, therefore, a lower energy of fracture. Therefore, the 5% molybdenum alloy can be expected to have a lower energy for ductile fracture than the base alloy, as is observed, and the 2.5% molybdenum alloy a lower energy for ductile fracture than that observed in the alloy containing 5% molybdenum, again as observed.

The ductile dimple size is smaller ($\sim$ 10μm) in the 2.5% molybdenum alloy compared to $\sim$ 30μm in the alloy containing 5% molybdenum. A finer dimple size will give a higher upper shelf energy because a greater amount of tearing is involved and so more energy needed per unit area to propagate fracture.

The lower shelf energy increases in the order K1525 (base) - K1527 (5% Mo) - K1526 (2.5% Mo). This is more difficult to explain. The base alloy fails by intergranular fracture in the brittle fracture mode. The two other alloys, with additions of molybdenum fail by transgranular cleavage in the brittle fracture mode. The energy required for the latter can be expected to be higher. This does not explain the fact that an alloy with a higher addition of molybdenum has a lower value of brittle fracture energy than the alloy with the lower addition of molybdenum. It is noted here that the hardness of K1526 (2.5% molybdenum) has a higher hardness than the alloy containing 5% molybdenum. The same cause of this higher hardness may also inhibit cleavage crack propagation and have the effect of a higher energy needed for brittle fracture.

5.3. The Embrittlement of Fe-Mn-Mo Alloys on Aging

Iron-Manganese alloys exhibit a greater tendency towards embrittlement when tempered between 250°C and 450°C.[9,7] The conclusion, after many tensile ductility tests, was that this embrittlement was found to be a maximum at 450°C. Nazim[8] studied the embrittlement characteristics of Fe-8Mn, which showed a high degree of embrittlement on austenitizing which was seen to increase in potency on aging. He primarily used the aging temperature of 450°C. In the present investigation it was decided to examine the effect of aging at 450°C on the Fe-8Mn alloys with additions of molybdenum.

The two levels of molybdenum added to produce the alloys K1526 (2.5Mo alloy) and K1527 (5Mo) were introduced in an attempt to combat the embrittlement in the as-quenched condition and on aging.

An elevated aging temperature of 525°C was also used to investigate the kinetics of embrittlement in these alloys.

The experimental results will be first discussed individually and then related to the degree of embrittlement experienced on aging.

5.3.1. Hardness of the Alloys

In the quenched condition, the Fe-8Mn alloy had a hardness of ~258 Hv30, the Fe-8Mn-2.5Mo alloy a hardness of ~ 336 Hv30 and the Fe-8Mn-5Mo alloy a hardness of ~ 284 Hv30. The initial addition of 2.5Mo increased the hardness of the alloy by means of strain imposed on the lattice, the atomic radius of molybdenum being 136 pm compared to 123 pm for iron. A further addition of 2.5 Mo decreased the hardness. This does not correlate with the grain sizes measured which were ~ 62μm for the Fe-8Mn-2.5Mo alloy and ~50μm for the Fe-8Mn-5Mo alloy. A theory of solid solution softening, discussed earlier, could explain this effect.

During aging at 450°C, the initial hardening experienced with K1525 (Fe-8Mn) due to the precipitation of Manganese nitride was possibly observed in K1526 (Fe-8Mn-2.5Mo) after only three minutes aging, Fig. 83. However, it is also likely that the hardness of this alloy is unaffected by holding at this temperature until after 17 hours as the error bars on the graph will accommodate an undeviated straight, horizontal line. The absence of any noticeable precipitation hardening with this alloy may be due to the scavenging influence that molybdenum has on nitrogen. The decrease in hardness after 17 hours at 450°C for this alloy will be due to recovery and possibly recrystallisation of the lath martensite structure.

In K1527 (Fe-8Mn-5Mo), an initial incubation period of 10 hours occurred at 450°C when the hardness remained unaffected. After this time, the hardness of the alloy started to increase from ~ 290 Hv30 and reached a maximum of ~ 480 Hv30 after 3000 hours, Fig. 83. The initial incubation period can be attributed to the nucleation and growth of precipitates within the matrix of the alloy. At a critical precipitate size, the movement of dislocations within the heavily dislocated structure, Fig. 84a, became gradually more restricted so increasing the hardness of the alloy dramatically. A description of the precipitation is given in a later section of the text. The overaging or softening of the alloy that occurred after 3000 hours was due to the coarsening of these precipitates.

The effect of aging the two alloys at 525°C on hardness is seen in Fig. 128. The softening of alloy K1526 (2.5Mo) occurs very rapidly indicating a quicker onset of recovery and recrystallisation. K1527 (5Mo alloy) is seen to initially decrease in hardness after 2 hours aging at 525°C due to a release of strain from the heavily dislocated lath martensite structure.

After two hours, the hardening occurs in this alloy, as seen at 450°C, but without the initial long incubation period. The nucleation and growth of the precipitates must be accelerated at this elevated temperature and the critical precipitate size is reached earlier in the isothermal aging process. However, the hardness of this alloy does not increase as rapidly as that observed at 450°C. The reason for this is that recovery and recrystallisation will be occurring at a rapid rate within the matrix so counteracting the precipitation hardening process.

5.3.2. The Effect of Aging on the Impact Transition Behaviour of Alloys K1526 and K1527

The effect of aging on the toughness of these alloys, as exhibited in Figs. 90 and 91 showing the change in ductile to brittle transition temperature with isothermal aging time and temperature, is very dramatic.

Three variables may affect the transition temperature. These are the addition of molybdenum compared to the aging of the base Fe-8Mn alloy, the aging temperature and the isothermal aging time.

With an addition of 2.5Mo, an Fe-8Mn alloy is de-embrittled in the as-quenched condition. On aging for 17 hours at 450°C, the transition temperature is increased by ~ 20°C from ~ 40°C to ~60°C (Fig. 91), the lower shelf energy decreased because of the transition from a cleavage to an intergranular brittle fracture mode Fig. 92 i.e. a decrease in the brittle fracture stress. The upper shelf energy increases after 17 hours at 450°C compared to the as-quenched alloy from ~ 40J to ~ 50J. The ductile dimple size in both the as-quenched Fig. 68 and aged alloy Fig. 92 is seen to be approximately the same. The hardness is unaffected by aging at this temperature. The process causing grain boundaries to become weak must be impeding the propagation of ductile fracture across the matrix.

The factors affecting the change in grain boundary toughness, discussed later, therefore, contribute to a shift in the ductile to brittle transition temperature (embrittlement), a lowering of the lower shelf energy and an increase in the upper shelf energy. A further isothermal age at 450°C, cumulating in 480 hours, results in a further decrease in toughness reflected in an increase in ductile to brittle transition temperature of ~ 120°C, Fig. 91. The upper and lower shelf energies are at the same level as the test carried out on the alloy aged for 17 hours.

Generally, a 450°C aging treatment carried out on K1526 (Fe-8Mn-2.5Mo) is an embrittling treatment with an increase in the ductile to brittle transition temperature and a change in the fracture mode from cleavage to intergranular in the brittle regime. This may be compared to the base alloy K1525 (Fe-8Mn) which initially embrittles on aging at 450°C after only a few minutes to a level not experienced on aging alloy K1526. After one hour of isothermal aging,alloy K1525 begins to toughen with an associated decrease in the ductile to brittle transition temperature. This retoughening was not experienced with alloy K1526. Therefore, the effect of the addition of 2.5Mo on the impact toughness characteristics on aging a Fe-8Mn alloy is seen to be a beneficial one in that although the alloy with additional molybdenum embrittles on aging and this embrittlement increases with aging time, it does not embrittle to the extent of Fe-8Mn. Therefore, the addition of molybdenum is beneficial to the as-quenched toughness of the Fe-8Mn alloy and to some extent in the aged condition. Although it does not completely combat embrittlement it does retard it somewhat. It must be concluded that the ability of molybdenum to suppress segregation of elements in austenite which cause as-quenched embrittlement must be good whilst the tendency for molybdenum to affect the reactions in ferrite is less.

Aging alloy K1526 (Fe-8Mn-2.5Mo) at 525°C produced a different result. A 17 hour age at 525°C produced an increase in toughness in this alloy shown by a decrease in the ductile to brittle transition temperature from ~40°C in the as-quenched condition to ~-10°C in the aged condition. The lower shelf energy was again decreased on aging to the level of the alloys aged at 450°C. The upper shelf energy increased dramatically from ~ 40J in the quenched condition to ~ 70J after 17h at 525°C. Because ductile dimpling involves tearing along the sides of the "cups and cones" in the fracture as part of the crack

propogation, a tougher alloy would tend to impede the propagation of the ductile cracks, so increasing the energy required to cause ductile fracture.

A further cumulative age of 480 hours at 525°C produced more toughening in that the ductile to brittle transition temperature was moved to an even lower temperature (~ -70°C) but the upper shelf energy was decreased to ~ 50J.

The higher molybdenum alloy K1527 (Fe-8Mn-5Mo) exhibited different effects of aging on the impact toughness. A 17 hour age at 450°C decreased the toughness of the alloy as shown by an increase in the ductile to brittle transition temperature from ~40°C to ~50°C as shown in Fig. 90. Therefore, once again, a reaction in the ferrite, whether it be precipitation or segregation, caused a decrease in the toughness of the alloy. The upper shelf energy was not affected by the aging treatment.

A further isothermal age at 450°C, cumulating in a total of 480 hours, produced an alloy that was brittle at all temperatures up to 200°C, i.e. no transition temperature, an extreme of embrittlement.

Aging K1527 (Fe-8Mn-5Mo) at 525°C produced a greater degree of embrittlement than that produced by a 450°C age, Fig. 90. After 17 hours the ductile to brittle transition temperature was increased to ~ 100°C, a more rapid embrittling process than at 450°C with ~ 50°C for the transition temperature. The kinetics of the process causing this embrittlement must have increased for the higher aging temperature. After 480 hours at 525°C, the alloy is again fully brittle at all temperatures up to 200°C.

The initial age of 17 hours at 450°C on K1527 Fe-8Mn-5Mo was not as detrimental on DBTT (toughness) as with the lower molybdenum alloy K1526 Fe-8Mn-2.5Mo, although further aging of the alloy with more molybdenum drastically increased the DBTT. This would indicate that the higher level of molybdenum has an initial beneficial effect on the toughness on aging but a highly detrimental effect after longer age time.

5.3.3. The Effect of Aging Time, Temperature and Molybdenum Content on the Microstructure of the Aged Alloys K1526 and K1527

The microstructure of the alloys during aging was studied using transission electron microscopes. Initial work on the JEM electron microscope at the Polytechnic indicated that a heavily dislocated lath martensite type of structure was prevalent in both alloys in the as-quenched condition. Figs. 126, 84 and 85. No second phases or retained phases were obvious.

On aging at 450°C, no effect was observed on the microstructure of K1526 Fe-8Mn-2.5Mo except possibly some recovery, Fig. 127. This was in contrast to K1527 Fe-8Mn-5Mo, Fig. 84, which showed a precipitation reaction which was fairly homogenous within the matrix, i.e. no preference for grain boundaries. The precipitates in this alloy were analysed on the Philips 400C electron microscope at Harwell, Figs. 86, 87, 88, 89. The analysis of the diffraction patterns produced solutions for two phases, the Fe_2Mo laves phase (zone axis $\langle \bar{1}\bar{1}2 \rangle$) and the Fe-Mo σ phase (zone axis $\langle 0\bar{5}0 \rangle$).

The presence of such phases without any segregation effects would produce embrittlement by the strain induced in the lattice by the trapping of dislocations. It is clearly shown in Figure 87 that the precipitates immobilise the dislocation network, with dislocations strung out inbetween precipitates.

This is clearly the precipitation reaction which causes the increase in hardness of K1527 after 17 hours of aging. The incubation period before the hardening can be explained by previous work.[129] Before Fe_2Mo or σ precipitates, molybdenum must firstly cluster to form a nucleus for the precipitation reaction. Laves phases have been reported as precipitating discontinuously by a grain boundary reaction.

In the case of this alloy, though, Fe_2Mo or σ precipitates homogeneously within the matrix.

A precipitation reaction, then,can embrittle the alloy by increasing the strength of the matrix and lowering the toughness of the matrix. As the Fe_2Mo or σ particles grow the ductility decreases and a gradual transformation from cleavage to intergranular fracture can partly be attributed to the depletion of molybdenum in the matrix, which initially would have tied up the impurities. Also, if any Fe_2Mo or σ particles did happen to precipitate on grain boundaries, this would also promote intergranular fracture because of the lowering of the strength of the boundaries. A 2.5Mo addition is not enough to provide a precipitation reaction within the matrix of a Fe-8Mn alloy. This level must be below the critical level of molybdenum needed for cluster formation therefore no nuclei will be available for precipitation. The structure of the laths seems to be unaffected by the addition of molybdenum.

A further addition of molybdenum, producing alloy K1527 Fe-8Mn-5Mo, brings the level of molybdenum above the critical level of cluster formation and therefore, nucleation of precipitates is available within the matrix. The rate determining step is the segregation of molybdenum within the matrix to form these nuclei. Once formed, the nuclei grow relatively quickly to form a rapid precipitation hardening effect. The precipitates continue to grow with aging time until they become large enough for movement of dislocations to occur again and overaging or softening of the alloy occurs.

At 525°C, K1526 Fe-8Mn-2.5Mo again shows no precipitation within the microstructure. The precipitation within the K1527 (Fe-8Mn-5Mo) alloy occurs more rapidly at 525°C giving hardening due to the precipitation after only a few minutes aging.

The hardening response, thereafter, is not as rapid as at 450°C. The nucleation of the precipitates has occurred rapidly here due to the elevated aging temperature making the segregation of molybdenum easier to form the molybdenum clusters earlier in the aging process. The rate of increase in hardness is not as rapid because although the precipitates are growing at a faster rate, the effect they have on lattice strain is being counteracted by the high rate of recovery.

Also, because there is less supersaturation at this higher temperature there will be less volume fraction of precipitate and so the peak hardness will be less.

5.3.4. The Effect of Molybdenum Content, Age Time and Temperature on the Fracture Appearance of the Broken Impact Specimens

On aging alloy K1526 (Fe-8Mn-2.5Mo) at 450°C for 17 hours, the brittle fracture mode changed from cleavage in the as-quenched condition Fig. 68, to partially intergranular, Fig. 92. This would explain the decrease in toughness exhibited by the shift in ductile to brittle transition temperature. A further age, to give a total of 480 hours at 450°C,produced almost wholly intergranular fracture, Fig. 93, explaining the further embrittlement with age time shown in the impact tests.

Therefore, although the addition of molybdenum in the as-quenched condition increased the toughness of the alloy and consequently changed the brittle fracture mode from intergranular to cleavage; on aging the effect that molybdenum has on the segregation of elements to the grain boundaries is reduced such that embrittlement once more occurs. There is no precipitation in this alloy, so molybdenum is not tied up in the matrix in this way. Molybdenum must inhibit segregation in austenite so preventing intergranular fracture and also cause toughening in the austenitised condition but it does not have such a great effect on segregation in ferrite.

On aging alloy K1526 (Fe-8Mn-2.5Mo) at 525°C, the brittle fracture surface was seen to have a greater proportion of intergranular fracture than did the same alloy aged for the same time at 450°C, Fig. 94. The fact that more intergranular fracture is present after aging at 525°C than at 450°C would seem to indicate that the initial embrittlement in this alloy at 525°C is more rapid than at 450°C. However, this does not correlate with the decrease in the ductile to brittle transition temperature on aging at 525°C which would seem to indicate that the alloy is in a tougher condition even though the brittle fracture has changed from the cleavage to intergranular mode.

On further aging at 525°C, making a total of 480 hours at this temperature, the brittle fracture appearance is composed mainly of the cleavage mode, Fig. 95. This would indicate an increase in toughness and this is confirmed by a further decrease in the ductile to brittle transition temperature on impact testing.

The ductile fracture, above the transition temperature, is by ductile dimpling after all aging treatments for alloy K1526 (Fe-8Mn-2.5Mo).

An addition of 5%Mo to a Fe-8Mn alloy improved the as-quenched toughness and changed the brittle fracture mode from intergranular to transgranular cleavage, Fig. 73. Therefore, although it has been reported[69] that there is a limiting concentration that has a beneficial effect on embrittlement of ferritic alloys and thereafter addition of molybdenum is detrimental, in this alloy a 5% addition still inhibits embrittling reactions in the austenite regime.

On aging for 17 hours at 450°C, the brittle fracture mode is seen to change from fully cleavage to partially intergranular, partially cleavage, Fig. 96. Therefore, as with K1526, this 5% addition of molybdenum whilst having a beneficial effect on the as quenched toughness cannot combat reactions in the ferrite which cause embrittlement. In fact, compared to alloy K1526 Fe-8Mn-2.5Mo the extent of embrittlement on aging at 450°C is greater. With K1527, the metallographic evidence provides an explanation for this. As aging proceeds, molybdenum clusters and then precipitates as Fe_2Mo or σ . This will denude the matrix of molybdenum and therefore nullify any beneficial effect it has on segregation of embrittling species. However, the metallographic evidence does not explain the same effect of embrittlement in alloy K1526 Fe-8Mn-2.5Mo. Probably molybdenum is still clustering in this alloy, so denuding the matrix, but never reaches the concentration needed for precipitation either because of sluggish kinetics or the bulk concentration being too low.

The ductile fracture in K1527 (Fe-8Mn-5Mo) after 17 hours at 450°C occurred by ductile dimpling. After 480 hours at 450°C K1527 showed no signs of ductility at any of the test temperatures during the charpy impact test. The fracture mode was totally brittle intergranular at all test temperatures. This fracture appearance corresponded with a very low energy for fracture at all test temperatures.

With the growth of precipitates and corresponding increase in hardness after this aging time the part that molybdenum plays in inhibiting embrittlement becomes very small. At this stage the prior austenite grain boundaries have such a low cohesion that only a small amount of energy is needed to nucleate and propagate fracture along the γ grain boundaries and there is no transition to ductile fracture. Also, increasing precipitation hardening must add to the total embrittlement in the alloy by inducing lattice strain.

After 17 hours at 525°C, K1527 Fe-8Mn-5Mo is totally intergranular in the brittle fracture mode, Fig. 98, compared to alloy K1526 (Fe-8Mn-2.5Mo) which is only partially intergranular after the same treatment. More rapid embrittlement is due to the precipitation explained earlier. The charpy impact curve for this alloy demonstrates that more rapid embrittlement occurs at 525°C than at 450°C. This is due to the nucleation precipitates occurring more readily at 525°C, so the beneficial effect that molybdenum has on the embrittlement phenomena is nullified much more rapidly. The prior austenite grain boundaries are so weak after this treatment that fracture occurs at right angles to applied stress, as shown in Fig. 98.

Ductile dimpling occurs above the ductile to brittle transition temperature in K1527 (5Mo alloy) after 17 hours at 525°C.

After 480 hours at 525°C alloy K1527 (5Mo alloy) exhibited the same fracture characteristics as for the aging treatment of 480 hours at 450°C, i.e. completely brittle intergranular fracture at all test temperatures, Fig. 99.

The embrittlement on aging of K1527 Fe-8Mn-5Mo can be explained, as above, in terms of processes related to the precipitation of Fe_2Mo or σ within the matrix, as, to some extent, can the embrittlement of K1526 Fe-8Mn-2.5Mo.

The increase in toughness experienced with K1526 at 525°C needed further investigation which is explained below.

Compared to the base alloy K1525 Fe-8Mn, the extent of embrittlement on aging at 450°C is much less in alloys K1526 (2.5Mo alloy) and K1527 (5Mo alloy), as measured by the shift of ductile to brittle transition to higher temperatures. The Fe-8Mn alloy exhibited a shift from ~ 50°C to ~ 300°C after 6 minutes at 450°C, Fig. 58. The greatest shift in ductile to brittle transition temperature, for either of the two alloys with molybdenum additions, after aging at 450°C is only ~ 70°C and that is after 480 hours. Therefore, although the molybdenum additions do not prevent the embrittlement of Fe-8Mn on aging at 450°C, the extent of the embrittlement is seen to be suppressed.

5.3.5. X-Ray Diffraction of the Aged Alloys K1526 and K1527

The base alloy Fe-8Mn was initially seen to embrittle on aging at 450°C with a shift of the ductile to brittle transition temperature to higher temperatures. However, after only an hour, this shift was halted and the alloy increased in toughness with a corresponding decrease of the transition temperature. On X-Ray analysis, the microstructure of the aged alloy was seen to contain 2% to 7% reverted austenite compared with <2% in the as-quenched condition. This increase in the amount of austenite in the matrix may help to account for the increase in toughness together with the influence of any recovery within the microstructure that may be taking place.

The microstructure of the Fe-Mn-Mo alloys was also studied using X-Ray analysis.

The K1526 alloy Fe-8Mn-2.5Mo after a solution treatment at 1000°C did not show any reverted austenite on aging at 450°C. The level of molybdenum present in the alloy has suppressed the introduction of austenite into the alloy by the aging process. Molybdenum is a ferrite former and will suppress the formation of reverted austenite; in fact it prevents it forming at 450°C. At 525°C, 0.2% reverted austenite formed in K1526 (2.5Mo alloy) on aging after 35 hours. The driving force for its formation is greater at this temperature and the 2.5% molybdenum is not enough to suppress its formation. The presence of reverted austenite within the microstructure explains the increase in toughness after aging at 525°C, shown by a decrease in the ductile to brittle transition temperature. Although initial aging changed the brittle fracture of the alloy from cleavage to intergranular, the presence of reverted austenite counterbalanced what should be embrittlement to produce an increase in toughness. As aging progressed at 525°C, K1526 was seen to increase in

toughness and the brittle fracture was more of the cleavage type after 480 hours. Therefore, the reverted austenite not only increased the toughness but somehow increased the strength of the grain boundaries above that of the matrix.

Further metallographic examination of the aged alloy by the Phillips Scanning Electron Microscope is shown in Fig. 150. The micrograph is of a section taken at right angles to an intergranular fracture surface and follows a crack, at right angles to the fracture path and direction of applied stress, into the bulk of material following prior austenite grain boundaries. All the reverted austenite formed has nucleated and grown at prior austenite grain boundaries. When the crack has propogated, it has gone through the austenite rather than along the new austenite/ferrite interface. This will act as a crack blunting mechanism and with longer age times solutes will redistribute within the austenite away from the prior austenite grain boundaries. Eventually, the austenite increases the strength of the prior austenite grain boundary to a level above the matrix and at this stage the fracture will take place in a transgranular manner.

This process explains not only the increase in toughness of the alloy by crack blunting but also the subsequent further increase in toughness and change from fully intergranular fracture to a mixed intergranular/cleavage fracture by an elevation of grain boundary strength. All aging treatments carried out on K1527 Fe-8Mn-5Mo at 450°C and 525°C produced no reverted austenite within the microstructure as shown by X-ray analysis. The higher level of the ferrite-forming molybdenum was sufficient to prevent the formation of reverted austenite even at the elevated temperature of 525°C and so the alloy embrittled after both 450°C and 525°C aging treatments.

5.3.6. Effect of Aging on Grain Boundary Chemistry - AES

The build up of segregating elements at grain boundaries in the alloys can be observed for K1526 Fe-8Mn-2.5Mo in the spectra obtained from fracture surfaces Fig. 121 (bulk) and Fig. 122 (grain boundary fracture) and for K1527 Fe-8Mn-5Mo in Fig. 123 (bulk) and Fig. 124 (grain boundary fracture).

Analysis of these spectra shows a build up of manganese and molybdenum at the prior austenite grain boundaries, Fig. 120. The rise in grain boundary concentration of manganese in these alloys is a lot slower than in the Fe-8Mn base alloy covered in previous work by Nazim.[8] The higher molybdenum content of 5% has the effect of keeping the grain boundary manganese content below that of alloy K1526 (with only 2.5%Mo) at all times at 450°C. This would indicate that the presence of molybdenum suppresses the segregation of manganese to the prior austenite grain boundaries.

Nitrogen also builds up at the prior austenite grain boundaries on aging at 450°C, Fig. 129. As noted from Table XVIII, what was initially thought to be an increase in phosphorus concentration at the grain boundaries does not drop away with ion bombardment of the sample. This would indicate that the observed peak at 120 eV is not that of phosphorus as this element sputters away very quickly after 2 monolayers. Its peak is probably the 120 eV molybdenum peak.

A sputter profile of one of the embrittled alloys, Fig. 130, shows that manganese falls away rapidly with distance from the grain boundary whereas the molybdenum concentration stays the same up to the measured distance of 15 atomic layers away from the grain boundary. The segregation of manganese to prior austenite grain boundaries confirms other work reported.[130]

This element has been named as responsible for the lowering of grain boundary strength and subsequent embrittlement, as has nitrogen.[8] The build-up of these two elements at prior austenite grain boundaries would, therefore, be the cause of embrittlement on aging of these two alloys and the corresponding reduction of grain boundary strength below the matrix. The fact that molybdenum is closely associated with these elements, as shown by the build up of this element at grain boundaries, and the fact that the actual levels of the embrittling species are not as high at these sites as in the base Fe-8Mn alloy, shows that molybdenum suppresses the segregation of these two elements in ferrite. Increasing the level of molybdenum to 5% in the alloy decreases the manganese at the grain boundaries but the alloy with higher bulk levels of molybdenum has a higher susceptibility to embrittlement due to the effects of precipitation discussed earlier.

Further evidence of segregation within the ferrite during aging was uncovered during a fractographic study of the AES fracture surfaces Figs. 151 and 152. They show that many of the prior austenite grain boundaries, along which the brittle fracture occurred, were faceted. The distance between the facets was measured and compared to the width of the martensite laths from the transmission electron micrographs of the same alloy. The width of the facets was $\sim 2.5\mu m$, the size of the laths were $\sim 2.7\mu m$. Therefore the facets appearing on the fracture surface were in fact individual martensite laths. During aging, the lath/lath boundary strength has been decreased to a level below both the matrix and the prior austenite grain boundaries presumably due to segregation of embrittlement species to martensite lath interfaces.

The results from the AES analyses were used to investigate the kinetics of the build up of manganese and molybdenum on grain boundaries of alloys K1526 Fe-8Mn-2.5Mo and K1527 Fe-8Mn-5Mo on aging at 450°C, Figs. 152 and 153.

For manganese segregation the approximate equation derived by McLean[111] was used describing the grain boundary segregation of a solute as a function of time:-

$$\frac{C_{bt} - C_{bo}}{C_{b\infty} - C_{bo}} \sim \frac{4\sqrt{D}}{\sqrt{\pi}\,\alpha_2\, d} \cdot \sqrt{t}$$

where C_{bo} = the initial grain boundary concentration (t = o)

$C_{b\infty}$ = the equilibrium grain boundary concentration ($t = \infty$)

C_{bt} = the grain boundary concentration at time t.

D = the diffusion coefficient.

d = the grain boundary thickness

α_2 = the ratio of $C_{b\infty} / C_{bo}$

Further, if $C_{b\infty} \gg C_{bo}$

$$C_{bt} \sim \frac{4\sqrt{D}}{\sqrt{\pi}\, d} C_{bo} \sqrt{t}$$

Assuming the grain boundary thickness, d, to be 2.9Å and the value of $C_{b\infty}$ for Manganese to be 24 atomic percent, the equilibrium concentration of reverted austenite, the derived diffusion coefficient for manganese turns out to be 2.2×10^{-21} cm²/sec. This value is much less than the value of 2×10^{-18} cm²/sec obtained for the base alloy Fe-8Mn.[8] The presence of molybdenum has reduced the potential for manganese diffusion.

As a major driving force for manganese segregation is the formation of reverted austenite then a method by which molybdenum suppresses this segregation is in its ability to reduce the level of reverted austenite within the matrix, because it is a ferrite forming element.

5.3.7. Summary of the Embrittlement of Fe-Mn-Mo Alloys on Aging

Addition of 2.5% and 5% molybdenum to an Fe-8Mn alloy is seen to produce toughening in the as-quenched condition with a corresponding change from intergranular to cleavage fracture in the brittle fracture regime. The microstructure produced with these additions was lath martensite except for the alloy with 5% molybdenum after high austenitising temperatures, when delta ferrite formed. Molybdenum suppressed segregation of embrittling agents to grain boundaries in austenite such that the strength of prior austenite grain boundaries was not lowered below that of the matrix, as was the case in Fe-8Mn.

On aging at 450°C, alloys with 2.5% and 5% molybdenum embrittled but not to the extent shown with the base alloy. Molybdenum is seen to be influential on segregation in ferrite as well as in austenite. The limiting factor on this influence is the ability of molybdenum to form precipitates within the iron matrix. The alloy with the higher molybdenum addition exhibits a greater amount of embrittlement on aging than does the alloy with 2.5% molybdenum because precipitation takes place in the former alloy, taking molybdenum out of solution and reducing its effectiveness in combating embrittlement. The precipitates formed also contributed to the increase in embrittlement due to their effect on increasing hardness and so increasing strain within the matrix.

On aging at 525°C more rapid embrittlement was experienced in the alloy with 5% molybdenum due to precipitation occurring more readily. In the alloy with 2.5% molybdenum at 525°C, although a change in brittle fracture mode from cleavage to intergranular was exhibited, an increase in toughness was experienced. This was due to the presence of reverted austenite at the prior austenite grain boundaries.

Although segregation within the alloy has increased the potential of intergranular fracture the reverted austenite has acted as a crack arrester and therefore the energy needed for fracture has been raised.

Molybdenum in the Fe-8Mn alloy is seen to have an effect on three processes which affect the embrittlement of the alloy:-

(a) its effect on the segregation of embrittling species

(b) its effect on the formation of reverted austenite

(c) its ability to form precipitates within the matrix.

The beneficial effect of molybdenum only occurs up to a limiting percentage of it in solution; between $2\frac{1}{2}\%$ and 5%. Below this limit there is insufficient present to form precipitates or to prevent the formation of reverted austenite. Yet its presence in solution causes an increase in toughness in the quenched condition and a slowing down of the embrittlement phenomena on aging. Above the limiting percentage, precipitation occurs on aging, which itself is a cause of embrittlement while at the same time the process takes molybdenum out of solution so decreasing its potential effect on segregation. The higher level of molybdenum also prevents reverted austenite forming producing an inherently less tough alloy. Therefore, even though the presence of higher levels of molybdenum increases the toughness of the as-quenched alloy the aging process causes an increase in embrittlement compared to the alloy with less molybdenum in it.

5.4. Series II Alloys

5.4.1. Properties of the Quenched and Tempered Alloys

The higher hardness of the alloy with the addition of copper can be related to the microstructure. This alloy has the smaller prior austenite grain size of the three alloys, one factor which increases the hardness. During austenitisation, a fine dispersion of copper would restrict austenite grain growth. Also, Cu is known to depress the $\gamma \rightarrow \alpha$ transformation temperature.[131] Such a depression produces a refinement in the subsequent structure. The higher hardness may also be due to the solution hardening effect of copper and some dispersion hardening may also occur. The acicular ferrite observed in this alloy, Fig. 132, is probably bainite rather than martensite which will have an inherently higher hardness.

The three alloys show virtually no difference in their impact properties when in the as quenched condition. Fig. 134.

Tempering at 650°C produces the expected increase in toughness due to annealing out of the dislocations and the precipitating out of carbon which reduces solid solution hardening. Again, after tempering, all the impact transition temperatures for the three alloys are virtually the same.

The alloy containing Cu is slightly tougher than the base alloy and that containing P is slightly less tough than the base alloy.

5.4.2. Properties of the Aged Alloys

5.4.2.1. Hardness Aging at 450°C

The hardness of the base alloy A217 is seen to initially decrease on aging at 450°C, probably due to initial stages of precipitation taking alloy elements and carbon out of solution so decreasing the effects of solution hardening. But as the precipitates grow they begin to pin dislocations and so increase the hardness. Fig. 138.

An initial drop in hardness is again initially seen in alloy A317 (base + 0.4% Cu) probably due to the same reason as above. During the next hour, a plateau of hardness occurs probably due to steady growth of precipitates or zones up to a size when they will begin to pin dislocations effectively. After one hour aging at 450°C a much higher increase in hardness than that seen in the base alloy is observed. Fig. 138. Copper is known to associate with iron in the formation of precipitates Fe_3Cu or Cu responsible for precipitation hardening.[132] Similar age hardening characteristics shown by the base alloy A217 are exhibited in alloy A417 (with 0.04% P).

Aging at 525°C

Aging at 525°C is seen to not affect the hardness of the three alloys on isothermally holding for up to 1000 hours.

5.4.2.2. Ductile to Brittle Transition Temperature

Aging at 10 hours and 80 hours at 450°C is seen to have little effect on the ductile to brittle transition temperatures of the three alloys. (Figs. 139, 140, 141.) A longer age time of 289 hours, however, is seen to increase these transition temperatures by varying degrees i.e. embrittle the alloys. After this latter treatment, the base alloy's transition temperature is seen to increase by 50°C to -30°C; that of the alloy with the 0.4% Cu addition by only 20°C to -60°C; and highest in the phosphorus-doped alloy, a shift of 75°C to -5°C. 0.4% Copper suppresses embrittlement of this alloy and 0.04% Phosphorus increases the amount of embrittlement. The effect of phosphorus is discussed extensively in section 2.2.1.1.

The copper in this alloy has acted as a grain refiner, increasing the grain boundary area/unit volume so decreasing the concentration of any segregating species on the prior austenite grain boundaries. Also the stress to propogate the intergranular crack will be greater along an interface that will constantly change due to the smaller grain size.

Aging at 525°C for 168 hours is seen to increase the potency of embrittlement in all three alloys. The embrittlement after this treatment, as indicated by a movement of the ductile to brittle transition temperatures to higher temperatures, is more severe than 289 hours at 450°C. Comparing the ductile to brittle temperatures of the alloys after the 525°C age with the quenched and tempered alloys; the base alloy shows a shift of transition temperature of 70°C up to a level of -10°C, the alloy with 0.4% Cu shows an increase of 60°C reaching a level of -20°C and the alloy with 0.04% P again shows the highest increase of transition temperature by 160°C to +80°C.

At 525°C, the addition of copper again shows a beneficial effect on aged toughness and phosphorus shows the opposite effect, as expected. The level of embrittlement in all three alloys has increased more rapidly after a shorter time at this higher aging temperature indicating more rapid segregation of embrittling species, as was the case with series I alloys.

5.4.2.3. Fracture Appearance

The fracture appearances of alloys A217, A317 and A417 after the different aging treatments are shown in Figs. 135 - 149.

Although an increase in hardness and in embrittlement, as indicated by an increase in the ductile to brittle transition temperature, is recorded for the base alloy, the brittle fracture after charpy impact testing remains cleavage even after the most severely embrittling treatment of 168 hours at 525°C.

The expected change of brittle fracture mode from transgranular cleavage to intergranular is exhibited in alloy A417 (0.04% P) on aging for 168 hours at 525°C. This is due to the segregation of phosphorus to the prior austenite grain boundaries causing a decrease in the cohesive strength of these grain boundaries to a level below that of the rest of the matrix. This change in fracture mode does not occur in this alloy when there is no shift in ductile to brittle transition temperature i.e. 10 hours at 450°C. Fig. 147.

In alloy A317 (0.4% Cu) brittle intergranular fracture was not observable after 10 hours at 450°C but it was after 168 hours at 525°C when the alloy was seen to be embrittled. The facets of the intergranular fracture were not smooth Fig. 145 and the heavily marked fracture surfaces indicated that more energy was needed to create this fracture than for a "clean" intergranular facet. Above the ductile to brittle transition temperature, the ductile dimples were seen to be an intergranular facets, Fig. 146.

6. Conclusions

An investigation of grain boundary embrittlement has been carried out on alloys K1526 and K1527 based on Fe-8Mn-2.5Mo and Fe-8Mn-5Mo in comparison to previous work on Fe-8Mn alloys. The alloys had a lath martensite structure free of retained austenite at all cooling rates from the austenitising temperatures with the exception of the Fe-8Mn-5Mo alloy quenched from 1300°C which contained delta ferrite at the prior austenite grain boundaries.

An investigation of embrittling treatments was also carried out on an alloy similar to a commercial pressure steel of base composition 0.25C, 1.4Mn, 0.5Mo, 0.6Ni, 0.3Si. Alloy A217 was the base alloy, A317 was doped with 0.04P and A417 was doped with 0.4Cu.

The base alloy had a lath martensite structure on quenching from the austenitising temperature. Additions of 0.4%Cu produced a bainitic-type of structure on quenching. The alloy containing 0.04P was largely martensitic in the quenched condition with some ferrite at prior austenite grain boundaries.

1. An addition of 2.5Mo to an Fe-8Mn alloy produced brittle cleavage fracture in the quenched condition, compared to brittle intergranular fracture in the base alloy. It also lowered the ductile to brittle transition. Both of these results show that the addition of 2.5Mo has a de-embrittling effect on the as quenched alloy. It is suggested that the molybdenum interacted with segregating species increasing their solid solubility and so lowering the driving force for segregation on quenching.

2. A further addition of molybdenum, making a total of 5Mo, did not significantly improve the toughness from that of the alloy containing 2.5Mo. The de-embrittling effects of the addition of molybdenum on quenching are seen to be limited to just above 2.5% in this particular

alloy in accordance with an optimum amount of molybdenum that can suppress embrittlement.[86,128]

3. In the as-quenched state the commercial alloys A217, A317 and A417 show little variation in toughness as indicated by the charpy impact transition temperature.

4. Tempering at 650°C improves the toughness of alloys A217, A317 and A417. The alloy with addition of 0.4Cu is seen to be the toughest after tempering.

5. Aging the quenched alloy K1526 at 450°C resulted in the embrittlement of the alloy as detected by a rise in the ductile to brittle transition temperature and a change in the brittle fracture mode from cleavage to intergranular. The embrittlement on aging at 450°C in this alloy is much less than that in the base alloy on aging at the same temperature.

6. Aging the quenched alloy K1526 at 525°C resulted in a more rapid change from brittle cleavage to intergranular brittle fracture yet the alloy was seen to become tougher as indicated by the decrease in the ductile to brittle transition temperature. This was due to reverted austenite appearing at prior austenite grain boundaries, opposing the propagation of intergranular cracks. After longer aging times at 525°C the brittle fracture mode was seen to change back to transgranular cleavage due to the thin film of reverted austenite overcoming the embrittling effects of segregation to grain boundaries.

7. Aging the quenched alloy K1527 at 450°C produced a more rapid embrittlement than in the alloy containing less molybdenum although embrittlement occurred more slowly than in the base alloy. Extreme degrees of embrittlement after longer aging times was due to the precipitation of second phase particles of Fe_2Mo Laves or Fe-Mo σ'

within the matrix. This precipitation process took molybdenum out of solution thus decreasing its potency in de-embrittling and also the increase in strain lead to an increase in matrix hardness, itself contributing to embrittlement.

8. Aging the quenched alloy K1527 at 525°C produced more rapid embrittlement due to the precipitation processes occurring more rapidly.

9. AES results on both of the quenched K1526 and K1527 alloys shows an increase in the manganese, molybdenum and nitrogen contents at prior austenite grain boundaries on aging. This suggests a relationship between the amount of manganese and nitrogen at the grain boundaries and the embrittlement in these alloys and also shows the close association that molybdenum has with embrittling species.

10. Fractographic studies of the aged K1527 alloy has produced evidence of segregation in ferrite causing fracture along lath boundaries of the martensitic structure.

11. Aging the quenched alloy A217 is seen to be an embrittling treatment after long age times at 450°C as demonstrated by an increase in the ductile to brittle transition temperature although brittle fracture remains unchanged in the cleavage mode throughout the aging treatment.

12. Aging the quenched alloy A317 at 450°C is also seen to be an embrittling treatment as indicated by an increase in the ductile to brittle transition temperature but the embrittlement is not as severe as in the base alloy, due to the presence of copper.

13. Aging the quenched alloy A417 at 450°C is seen to produce more embrittlement than the base alloy due to the presence of phosphorus which will tend to segregate to prior austenite grain boundaries.

The ductile to brittle transition temperature is increased and brittle fracture changes from cleavage to intergranular as aging proceeds.

14. Aging at 525°C is seen to be more potent as an embrittling treatment for all three quenched alloys A217, A317 and A417.

7. Recommendations for Further Work

1. The aging of Fe-8Mn alloys produced a certain amount of reverted austenite within the structure of the martensite. Molybdenum acts as a de-embrittling agent but, as a ferrite former, retards the reversion of austenite as the concentration increases. It is seen that the combination of a small amount of molybdenum in the alloy and reverted austenite at the grain boundaries can be most beneficial in improving toughness on aging. Further work is needed to investigate more combinations of molybdenum and reverted austenite, probably induced by thermal cycling, in order that optimum effects on toughness can be determined.

2. It is obvious that one of the factors limiting the beneficial effects of molybdenum on embrittlement is the precipitation of second phase particles. It is therefore suggested that if de-embrittling elements, including molybdenum, are to be used to improve the toughness of an alloy then one of the considerations used in determining the amount of the element used should be the percentage required to induce precipitation reaction.

3. Much controversy has occurred in the past over whether or not embrittling elements segregate within ferrite. There is some fractographic evidence contained in this work to suggest that this segregation does occur but further work needs to be carried out to investigate this further.

4. Workers in the past have doubted the effect of the segregation of manganese on embrittlement. This work indicates that manganese segregation has a major effect but its true effect is masked by the presence of nitrogen. If the effect of manganese per se on embrittlement and subsequent effects of molybdenum are to be investigated, the

absence of nitrogen must be an overriding factor.

5. Preliminary investigations on the commercial alloys reinforced the effect of phosphorus as having detrimental effect on aged toughness. The 0.4% copper addition does seem to be beneficial in this respect. More work is required on these alloys to determine grain boundary chemistry by AES techniques. Tensile ductility tests also need to be carried out on these alloys to determine 'C' curve characteristics. Thin foil microscopy will also help to develop a clearer picture of microstructural changes in the alloys on aging.

Further Work of General Relevance

In order to develop manganese-based low carbon steels, with additions of molybdenum, as possible replacements for Fe-Ni steels in some applications it will be necessary to examine the performance of the alloys after fabrication and forming and the relationship of these to heat treatment conditions to produce optimum toughness.

A clearer picture of the beneficial effects of molybdenum on embrittlement caused by other elements such as P, Sn, Sb could be developed by simplifying the alloys to include as few interacting constituents as possible. This basis could then be used to "build up" the more complex picture of the commercial steel.

REFERENCES

1. Schumann H.
"Relation Between Structure and Other Properties of Low Carbon Manganese Steels"
Arch. Eisenhuttenwesen 38 (9) 1967 743-749

2. Bishop H.E.
"Operation of the HBA 200, a Combined Field Emission Scanning Microscope and Auger Electron Spectrometer"
AERE HARWELL Internal Report R-8953 1977

3. Durnin J., Ridal K.A.
"Determination of Retained Austenite in Steel by X-Ray Diffraction"
J.I.S.I. Jan. 1968 60-67

4. Bishop H.E.
"A Design for a Cylindrical Mirror Analyser for use in Auger Spectroscopy"
J. Electron Spectroscopy 1 1973 389-401

5. Weber R.E., Johnson A.L.
"Determination of Surface Structures using LEED and Energy Dispersive Analysis of Scattered Electrons"
J. Appl. Phys. 40 1969 314-318

6. Palmberg P.W., Riach G.E., Weber R.E., MacDonald N.C.
"Handbook of Auger Electron Spectroscopy"
Published by Physical Electronics Industries Inc., Feb. 1972

7. Bolton J.D., Petty E.R., Allen G.B.
"The Mechanical Properties of α-Phase Low-Carbon Fe-Mn Alloys"
Met. Trans. 2 1971 2915-2923

8. Nazim M.
"Brittleness in Ferritic Iron-Manganese Alloys"
Ph.D. Thesis. Sheffield City Polytechnic 1979

9. Bolton J.D.
"A Study of the Transformation Behaviour and Mechanical Propertis of Iron-Manganese Alloys"
Ph.D. Thesis. Sheffield City Polytechnic 1970

10. Olefjord I.
"Temper Embrittlement"
International Metals Review 4 (231) 1978 149-163

11. Capus J.M.
"The Mechanism of Temper Brittleness"
Temper Embrittlement in Steel ASTM STP 407 ASTM 1968 3-19

12. Jolivet H., Vidal G.
"Valeur de l'essai de resilience pour l'etude de la fragilite de revenue"
Revue de Metallurgie 41 1944 378-388

13. Palmberg P.W., Marcus H.L.
"An Auger Spectroscopic Analysis of the Extent of Grain Boundary Segregation"
Trans. ASM 62 1969 1016

14. Ferrell D.E.
"Creep and Temper Embrittlement of A-542 Steel"
Chrome Moly Steel in 1976 ASME Publications MPC-4.
Sponsored by Metals props. Council, Inc. Edited by:- G.V. Smith

15. Edwards B.C., Little E.A.
"Tempered Martensite Embrittlement in a 12% Cr Steel"
Int. Conf. on Ferritic Steel for Fast Reactor Steam Generators
BNES - London 6-10 June 1977 Paper 22

16 Horn R.M., Ritchie R.O.
"Mechanisms of Tempered Martensite Embrittlement in Low Alloy Steels"
Met. Trans. 9A 1978 1039-1053

17. Balajiva K., Cook R.M., Worn D.K.
"Effects of Trace Elements on Embrittlement of Steels"
Nature Aug. 25 1956 433

18. Steven W., Balajiva K.
"The Influence of Minor Elements on the Isothermal Embrittlement of Steels"
J.I.S.I. 193 1959 141-147

19. Allen N.P., Earley C.C.
"Effect of Phosphorus Content on Impact Value of Fully and Partially Hardened and Tempered Mn-Mo Steels"
J.I.S.I. 182 1956 375-386

20. Delage L., Galibors A., Krishnader M.R.
"An In Depth Study of Grain Boundary Phenomena in the Temper Embrittling Process of a Ni-Cr Commercial Steel"
Grain Boundaries in Engineering Materials. Proc. 4th Bolton Landing Conf. June 9-12 1974 Lake George N.Y. Edited by J.L. Walters, J.H. Westbrook, D.A. Woodford. 561-572

21. Capus J.M.
"Austenite Grain Size and Temper Brittleness"
J.I.S.I. 1962 922-927

22. Gale B.
"Lattice Parameters of Solid Solution of Phosphorus in Iron"
Acta Met 7 1959 420-421

23. Gruzin P.L., Mural V.V.
"Mechanisms Underlying the Effect of Molybdenum on the Reversible Temper Brittleness of Steel"
Metallovedenie i Term. Obrabot. Metallov. 3 March 1969 70-72

24. Graham W.R., Yen A.C.
"The Effect of Titanium on Phosphorus Solubility in a Ni-Cr Steel from a Study of Free-Surface Segregation"
Met. Trans. 9A 1978 1461-1465

25. Gruzin P.L., Minal V.V.
"Radiometric Study of Phosphorus Diffusion in Iron"
Fiz. metal. metalloved 16 (4) 1963 551-556

26. Hondros E.D.
"The Influence of Phosphorus in Dilute Solid Solution on the Absolute Surface and Grain Boundary Energies of Iron"
Proceedings of the Royal Society. A. 286 1965 479-498

27. Griffith A.A.
"The Phenomena of Rupture and Flow in Solids"
Phil. Trans. Roy. Soc. A 221 1920 163

28. Gibbs J.W.
"The Collected Works of J. Willard Gibbs"
Volume 1 Thermodynamics - Longmans 1928

29. Meyrick G.
"On the Segregation of Phosphorus at the Free Surface of an Iron-Phosphorus Alloy"
Acta. Met. 13 1965 691-693

30. Ramasubramanian P.V., Stein D.F.
"An Investigation of Grain Boundary Embrittlement in Fe-P, Fe-P-S, and Fe-Sb-S Alloys"
Met. Trans. 4 1973 1735-1742

31. Mulford R.A., McMahon C.J. Jr., Pope D.P., Feng H.C.
"Temper Embrittlement of Ni-Cr Steels by P"
Met. Trans. 7A 1976 1183-1195

32. Banerji S.K., McMahon C.J. Jr., Feng H.C.
"Intergranular Fracture in 4340-Type Steels : Effects of Impurities and Hydrogen"
Met. Trans. 9A 1978 237-247

33. Briant C.J., Banerji S.K.
"Phosphorus Induced 350°C Embrittlment in an Ultra High Strength Steel"
Met. Trans. 10A 1979 123-126

34. Doig P., Flewitt P.E.J.
"Microanalysis of Grain Boundary Segregation in Embrittled Iron-3 wt% Nickel Alloys using STEM"
Journal of Microscopy 112 (3) 1978 257-267

35. Brear J.M., King B.L.
"Stress Relief Embrittlement in Mn-Ni-Mo Pressure Vessel Steels"
Grain Boundaries. Institute of Metallurgists' Spring Residential Conference April 1976 Series 3 Number 5 901-76-Y

36. Ogura T., McMahon C.J. Jr., Feng H.C., Vitek V.
"Structure Dependent Intergranular Segregation of Phosphorus in Austenite in a Ni-Cr Steel"
Acta Met. 26 1978 1317-1330

37. Viswanathan R., Joshi A.
"Effect of Microstructure on Grain Boundary Segregation of P in a Cr-Mo-V Steel"
Scripta Met. 9 1975 475-478

38. Bonta J.E.
"Evaluation of 2-$\frac{1}{4}$Cr-1Mo Weld Metals : Notch Toughness and Temper Embrittlement Characteristics"
Chrome Moly Steel in 1976. ASME Publications MPC-4
Sponsored by Metals Props. Council, Inc. Edited by G.V. Smith

39. Kalmykov V.V.
"Temper Brittleness of Carbon Steels Containing Phosphorus and Arsenic"
Stal 2 1968 152-155

40. Edwards B.C., Bishop H.E., Riviere J.C., Eyre B.L.
"An AES Study of Temper Embrittlement in a Low Alloy Steel"
Acta Met. 24 1976 957-967

41. Inoue T.
"Grain Boundary Segregation of Impurity and Alloying Elements in Low Carbon Steels"
Grain Boundaries in Engineering Materials. Proc. 4th Bolton Landing Conference. June 9-12 1974 Lake George N.Y. Editor: J.L. Walter, J.H. Westbrook, D.A. Woodford 553-559

42. Joshi A., Stein D.F.
"Temper Embrittlement of Low Alloy Steels"
Temper Embrittlement of Alloy Steels. ASTM STP 499. ASTM 1972 59-89

43. Glikman Ye.E., Cherpakov Yu.I.
"Internal Friction Study of Grain Boundary Adsorption of Phosphorus Duringthe Temper Embrittlement of Alloyed Iron"
Fiz. Metal. Metalloved 34 1972 90-102

44. Preece A., Carter R.D.
"Temper Britleness in High Purity Iron-Base Alloys"
J.I.S.I. April 1953 387-398

45. Shimizu H., Ono M., Nakayama K., Yamada M.
"Surface and Grain Boundary Segregation of Steel Impurities"
Proc. 6th. International Vacuum Congress 1974 Japan. J.Appl.Phys. Suppl. 2 (1) 1974

46. Swift R.A.
"The Effects of Phosphorus on the Temper Embrittlement Susceptibility of 2$\frac{1}{4}$Cr-1 Mo Steel"
Chrome Moly Steel in 1976. ASME Publications MPC-4
Sponsored by Metals Props. Council, Inc. Edited by G.V. Smith

47. Guttmann M., Krahe P.R., Abel F., Amsel G., Bruneaux M., Cohen C.
"Temper Embrittlement and Intergranular Segregation of Antimony: a Quantitative Analysis Performed with the Backscattering of Energetic Ions"
Met. Trans. 5 1974 167-177

48. Ohtain H., Feng H.C., McMahon C.J.Jr., Mulford R.A.
"Temper Embrittlement of Ni-Cr Steel by Antimony: I. Embrittlement at Low Carbon Concentration"
Met. Trans. 7A 1976 87-101

49. Clayton J.Q., Knott J.F.,
"Effects of Ni and Sb on the Temper Embrittlemet in Alloy Steels"
Fracture 1977 (2) ICF4 Waterloo, Canada, June 19-24

50. Ciannelli A.K., Feng H.C., Ucisile A.H., McMahon C.J. Jr.
"Temper Embrittlement of a Ni-Cr Steel by Sn"
Met. Trans 8A 1977 1059-1061

51. Inoue T., Yamamoto K., Sekiguchi S.,
"Grain Boundary Segregation of Phosphorus and Manganese in Low Carbon Manganese Steels"
Trans. ISI Japan 14 1974 372-274

52. Edwards B.C., Eyre B.L., Gage G.
"Temper Embrittlement of Low Alloy Ni-Cr Steels"
AERE Harwell Internal Report

53. Low J.R., Stein D.F., Turkalo A.M., Laforce R.P.
"Alloy and Impurity Effects on Temper Brittleness of Steel"
Trans. Met. Soc. AIME 242 1968 14-24

54. Guttmann M.
"Equilibrium Segregation in a Ternary Solution: a Model for Temper Embrittlement"
Surface Science 53 1975 213-227

55. Viswanathan R., Sherlock T.P.
"Long-Time Isothermal Temper Embrittlement in Ni-Cr-Mo-V Steels"
Met. Trans. 3 1972 459-468

56. Joshi A., Palmbèrg P.W., Stein D.F.
"Role of Manganese and Silicon in Temper Embrittlement of Low Alloy Steels"
Met. Trans. 6A 1975 2160-2161

57. Schulz B.J., McMahon C.J. Jr.
"Alloy Effects in Temper Embrittlement"
Temper Embrittlement of Alloy Steels. ASTM STP 499. ASTM, 1972 104-135

58. McMahon C.J. Jr., Rellick J.R., Schulz B.J.
"Intergranular Embrittlement in Ferrous Alloys"
Fracture 1969. Proc. 2nd. International Conf. on Fracture. Brighton. April 1969. Editor P.L. Pratt - Chapman and Hall 278-287

59. Stein D.F., Joshi A., Laforce R.P.
"Studies Utilizing Auger Electron Emission Spectroscopy on Temper Embrittlement in Low Alloy Steels"
Trans. ASM. 62 1969 776-783

60. Squires D.R., Wilson E.A.
"Ageing and Brittleness in an Fe-Ni-Mn Alloy"
Met. Trans. 3 1972 575-581

61. Guttmann M.
"The Link Between Equilibrium Segregation and Precipitation in Ternary Solutions Exhibiting Temper Embrittlement"
Metal Science October 1976 337-341

62. Edwards B.C., Bishop H.E.
"An AES Study of Embrittlement in an Fe 8wt.% Mn Alloy"
Harwell AERE Internal Report R8516 September 1976

63. Katsumata M., Kinoshita S.
"Microfractographic Studies of Temper Embrittled Steels"
Trans. ISIJ 17 1977 693-700

64. Clauser C.D., Emmer L.G., Pense A.W., Stout R.D.
"A Phenomenological Study of the Susceptibility to Temper Embrittlement of 2.5% Cr - 1% Mo Steel"
Proceedings Div. of Refining : Am.Petroleum Inst. 1972. 37th Midyear Meeting 52 790-815

65. Floreen S.
"Producing a Tough, High Strength Cast Steel Free from Temper Embrittlement"
Trans. ASME 101 1979 90-103

66. Mural V.V., Gruzin P.L.
"Alloying as Affecting Phosphorus Diffusion in Austenite"
Fiz. Metal. Metalloved. 17 (5) 1964 792-795

67. Marcus H.L., Hackett L.H. Jr., Palmberg P.W.
"Effect of Solute Elements on Temper Embrittlements of Low Alloy Steels"
ASTM STP 499. 1972. 90-103

68. McMahon C.J. Jr., Cianelli A.K., Feng H.C.
"The Influence of Mo on P-Induced Temper Embrittlement in Ni-Cr Steel"
Met. Trans., 8A 1977 1055-1057

69. Knight R.F.
"Temper-Embrittlement Studies"
Dept. of Energy, Mines and Resources. Mines Branch. Ottowa Research Report R197. July 1968

70. Klinger L.J., Barnett W.J., Frohmberg R.P., Troiano A.R.
"The Embrittlement of Alloy Steel at High Strength Levels"
Trans. ASM 46 1954 p.1557

71. Banerjee B.R.
"Embrittlement of High Strength Tempered Alloy Martensites"
JISI 203 1965 p.166

72. Capus J.M., Mayer G.
"The Influence of Trace Elements on Embrittlement Phenomena in Low Alloy Steels"
Metallurgia. October 1960 133-138

73. Restaino P.A., McMahon C.J. Jr.
"The Role of Antimony in Temper Brittleness"
Trans. ASM 60 1967 699-706

74. McMahon C.J. Jr.
"Intergranular Brittleness in Iron"
Acta Met. 14 1966 839-845

75. Kula E.B.
"Tempered Martensite Embrittlement and Fracture Toughness"
J. Materials ASTM 4 1969 817

76. Kuo K.
"Carbides in Chromium, Molybdenum and Tungsten Steels"
JISI 173 1953 363-375

77. Rellick J.R., McMahon C.J. Jr.
"Intergranular Embrittlement of Iron-Carbide Alloys by Impurities"
Met. Trans. 5 1974 2439-2450

78. M. Hansen,K. Anderko
"The Constitution of Binary Alloys"
2nd Ed. - McGraw Hill. N.Y. 1958; R.P. Elliot, 1st Supplement, 1965; F.A. Shunk, 2nd. Supplement, 1969

79. Yamanaka K., Ohmori Y.
"Temper Embrittlement by P and Fracture Behaviour"
Trans. ISIJ 19 1979 339-346

80. Stonesifer F.R., Armstrong R.W.
"Effect of Prior Austenite Grain Size on the Fracture Toughness Properties of A533 B Steel"
Fracture 1977, ICF4 2 Waterloo Canada June 19-24 1977

81. Guttmann M., Krahe P.R., Abel F. Bruneaux M., Cohen C.
"Th Influence of the Austenitising Treatment on Temper Embrittlement"
Scripta Met 7 1973 93-96

82. Brobst R.P., Krauss G.
"The Effect of Austenite Grain Size on Microcracking in Martensite of an Fe - 1.22C Alloy"
Met. Trans. 5 1974 457-462

83. Petch N.J.
"The Ductile Fracture of Polycrystalline Alpha Iron"
Philosophical Magazine 1 1956 186-190

84. Woodfine B.C.
"Temper-Brittleness : a Critical Review of the Literature"
JISI March 1953 229-240

85. Jaffe L.D., Buffum D.C.
"Upper Nose Embrittlement of a Ni-Cr Steel"
J. of Met. (Jan. 1957); Trans AIMME 209 1957 8-16

86. Powers A.E.
"The Influence of Mo and W on Temper Embrittlement"
Trans. ASM 48 1956 149-164

87. Irani J.J., May M.J., Elliott D.
"Effect of Thermal and Thermochemical Treatments on the Temper Embrittlement of Low Alloy Steels"
Temper Embrittlement of Steel, ASTM STP 407 1968 168-202

88. Seah M.P.
"Grain Boundary Segregation and the T-t Dependence of Temper Brittleness"
Acta Met. 25 1977 345-357

89. Carr F.L., Goldman M., Jaffe L.D., Buffum D.C.
"The Isothermal Temper Embrittlement of SAE 3140 Steel"
Trans. AIME 197 1953 998 and
J. Metals 5 1953

90. Bernstein I.M.
"Role of Hydrogen in Embrittlement of Iron and Steel"
Materials Science and Engineering. 6 1970, 1

91. Henthorne M., Parkins R.N.
"Some Aspects of the Influence of Structure upon Stress-Corrosion Cracking and Grain Boundary Corrosion in Mild Steels"
Br. Corros. J.2 1967 186

92. Westwood A.R.C., Preece C.M., Kamdar M.H.
"Adsorption-Induced Brittle Fracture in Liquid Metal Environments"
in - "Fracture - an advanced treatise" (ed. H. Leibowitz)
Vol. 3 1971 p.589-645 New York - Academic Press

93. Krahe P.R., Guttmann M.
"Temper Brittleness and Grain Boundary Etching"
Metallography 7 1974 5-17

94. Arkharov V.I., Varskoy B.N., Skornyakov N.N.
"Causes of the Effect of Small Dissolved Admixtures on the Kinetics of the Aging of Alloys"
Doklady Akad. Nauk S.S.S.R. 89, 1953, 1003; NSF Translation No. 45.

95. Arkharov V.I., Borisov B.S., Vangengeim S.D.
"The Nature of Grain Boundaries as Revealed in the Scattering Patterns of X-Rays"
Physics of Metals and Metallography 10 (3) 1960 53-59

96. Arkharov B.I., Vangengeim S.D.
"X-Ray Study of Intercrystalline Adsorption in Silver Alloys"
Phys. Metals and Metallography 4 (3) 1957 41-47

97. Private Communication.

98. Gupta D.
"Influence of Solute Segregation on Grain Boundary Energy and Self Diffusion"
Met. Trans. 8A 1977 1431-1438

99. Hondros E.D.
"Grain Boundary Segregation. The Current Situation and Future Requirements"
Journal de Physique 36 1975 C4 - 117-134

100. Stein D.F.
"The Limitation of Autoradiography as a Technique to Measure Grain Boundary Segregation"
Trans. Met. Soc. AIME 239 1967 1721-1726

101. Aust K.T., Hanneman R.E., Niessen P., Westbrook J.H.
"Solute Induced Hardening near Grain Boundaries in Zone Refined Metals"
Acta. Met. 16 1968 291-302

102. Joshi A.
"Experimental Techniques to Study Segregation"
Interfacial Segregation. Seminar 1977 Mat. Sci. Div. of ASM
Edited by W.C. Johnson and J.M. Blakely. ASM 1979 39-109

103. Palmberg P.W., Rhodin T.N.
"Auger Electron Spectroscopy of f.c.c. Metal Surfaces"
J. Appl. Physics 39 (5) 1968 2425-2432

104. Harris L.A.
"Analysis of Materials by Electron-Excited Auger Electrons"
J. Appl. Physics 39 (3) 1968 1419-1427

105. Harris L.A.
"Some Observations of Surface Segregation by Auger Electron Emission"
J. Appl. Physics 39 (3) 1968 1428-1431

106. Marcus H.L., Palmberg P.W.
"Auger Fracture Surface Analysis of a Temper Embrittled 3340 Steel"
Trans. Met. Soc. of AIME 245 1969 1664-1667

107. Chang C.C.
"Analytical Auger Electron Spectroscopy"
from Characteristics of Solid Surfaces Editors:-
P.F. Kane, G.B. Larrabee. Plenum 1975 509-575

108. Riviére J.C.
"Auger Electron Spectroscopy"
Contemporary Physics 14 (6) 1973 513-539

109. Hondros E.D.
"Auger Electron Spectroscopy Reveals the Residuals in Steel"
Metals and Materials, January 1976 26-28

110. Seah M.P.
"Segregation and the Strength of Grain Boundaries"
Proc. Roy. Soc. London A. 349 1976 535-554

111. McLean D.
"Grain Boundaries in Metals"
Oxford Claredon Press. 1957

112. Floreen S., Speich G.R.
"Some Observations on Strength and Toughness of Maraging Steels"
Trans. A.S.M. 57 1964 714-726

113. Seah M.P., Hondros E.D.
"Grain Boundary Segregation"
Proc. Roy. Soc. London A. 335 1973 191-212

114. Seah M.P., Lea C.
"Surface Segregation and its Relation to Grain Boundary Segregation"
Phil. Mag. 31 (3) 1975 627-645

115. Hondros E.D., Seah M.P.
"Segregation to Interfaces"
Int. Metals Review. December 1977. Review 222 262-301

116. Lea, C., Seah M.P.
"Site Competition in Surface Segregation"
Surface Science 53 1975 272-285

117. Inman M.C., Tipler H.R.
"Interfacial Energy and Composition in Metals and Alloys"
Metallurgical Review. Inst. Metals 8 (3) 1963 105-166

118. Hondros E.D.
"Energetics of Solid-Solid Interfaces"
Interfaces Conference. Melbourne. 1969 Ed: R.C. Gifkins
Australian Inst. Metals. Butterworths 77-100

119. Hondros E.D., McLean D.
"Surface Energies of Solid Metal Alloys"
Surface Phenomena of Metals 1968. Symposium 1967. Soc. Chem. Ind. Monograph No. 28 39-56

120. Hondros E.D., McLean D.
"Cohesion Margin of Copper"
Phil. Mag. 29 (4) 1974 771-795

121. Tyson W.R.
"Kinetics of Temper Embrittlement"
Acta. Met. 26 1978 1471-1478

122. Hondros E.D., Seah M.P.
"Grain Boundary Activity Measurements by Auger Electron Spectroscopy"
Scripta Met. 6 1972 1007-1012

123. Squires D.R., Wilson F.G., Wilson E.A.
"The Influence of Mo and Co on the Embrittlement of an Fe-Ni-Mn Alloy"
Met. Trans. 5 1974 2569-2578

124. Wada M., Fukase S., Nishikawa O.
"Role of Carbides in Grain Boundary Segregation of Phosphorus in a 2.25 Cr - 1 Mo Steel"
Scr. Met 16 (12) 1982 1373-1378

125. Kaneko H. et. al.
J. Japan. Inst. Met. (in Japanese)
29 1965 p.166

126. Burck L.H. and Weertman J.
"Fatigue Crack Propogation in Iron and Fe-Mo Solid Solution Alloys (77 to 296k)"
Met. Trans. 7A 1976 257-264

127. Astie P. et. al.
"Dislocation Relaxation Peaks and Solid Solution Softening in Substitutional Alloys"
Scr. Met. 16 (8) 1982 977-980

128. Powers A.E.
"A Study of Temper Brittleness in Cr-Mn Steel Containing Large Amounts of Mo, W and V"
J.I.S.I. July 1957 323-328

129. Yodogawa M., Suzuki T., Tanaka M.
"Effect of Mo on age-hardening Behaviours and Mechanical Properties on Fe-9% Ni-4.5% Mn Martensitic Alloy"
Trans. ISIU 18 1978 295-303

130. Feng H.C., Wilson E.A., McMahon C.J. (Jr)
"On the Mechanism of Embrittlement During the Aging of an Fe-Ni-Mn Alloy"
Proceedings of the 3rd International conference on Strength of Metals and Alloys. Sponsored by IM and ISI England 1973 Paper 26

131. Andrews K.W.
"Empirical Formulae for the Calculations of Some Transformation Temperatures"
JISI 203 July 1965 p. 721

132. Tupholme K.W., Bisby R.K., Wilson F.G.
"The Effect of Aging on the Mechanical Properties of Fe-Cu Alloys"
BSC Internal Report PROD/MP/6155/-/71/A

133. Seah M.P., Spencer P.J., Handros E.D.
"Additive Remedy for Temper Brittleness"
Metal Science. May 1979 307 - 314

134. Nickbaht F.
"Embrittlement in Fe-8Mn Alloys"
M.Sc. Thesis (CNAA). Sheffield City Polytechnic 1978

TABLE 1

CHEMICAL COMPOSITION OF SERIES I ALLOYS

CAST NO.	N	C	Si	S	P	Ni	Cr	Sn	Ti	Al	Mo	Mn
K1525	0.003	0.004	0.011	0.010	0.006	0.0027	0.002	0.005	-	-	-	8.1
K1526	0.0092	0.014	-	0.010	v/low	-	-	-	1.1ppm	2.5ppm	2.35	7.95
K1527	0.0073	0.006	-	0.011	v/low	-	-	-	1.8ppm	2.5ppm	4.65	8.0

TABLE II

CHEMICAL COMPOSITION OF SERIES II ALLOYS

CAST NO.	C	Mn	Mo	Ni	Si	P	S	Cr	Cu	V	Nb	W	Sn	Sb	As	O	N
A217	0.225	1.4	0.48	0.57	0.32	.002	.006	.01	.01	.01	.006	.08	.01	.01	.01	.002	.00
A317	0.25	1.37	0.49	0.57	0.30	.002	.004	.01	0.39	.01	.01	.01	.01	.01	.02	.005	.00
A417	0.235	1.43	0.485	0.57	0.31	.041	.006	.01	.01	.01	.01	.01	.01	.01	.02	.013	.00

TABLE III

Salt-bath mixtures used for different tempering temperature ranges.

Temperature Range °C	Salt
150 - 530	Nitrate/Nitrite
300 - 600	Chlorite/Sulphate
560 - 920	Sodium Chlorite/Carbonate

TABLE IV

SUMMARY OF HEAT TREATMENTS CARRIED OUT ON SERIES I ALLOYS

ALLOY	HOMOGENISATION		AUSTENITIZING			TEMPERING	
	TEMPERATURE (°C)	TIME (HRS)	TEMPERATURE (°C)	TIME (HRS)	QUENCH MEDIUM	TEMPERATURE (°C)	QUENCH MEDIUM
K1526	1100	50	1000 1300 (1300 ((+1000	1 1 1 1	Water Iced brine (Water) (Water)	450 525	Water Water
K1527	1100	50	1000 1300 (1300 ((+1000	1 1 1 1	Water Iced brine (Water) (Water)	450 525	Water

TABLE V

CALCULATION OF "R" FOR ALLOY K1526

RADIATION $\lambda Co\ K\alpha$ = 1.790Å

Reflection	θ°	Sin θ	d	V (m^3)	m	L.P	e^{-2m}	$\frac{\sin\theta}{\lambda}$	f	F	R
$(110)_\alpha$	27	.4540	2.027	23.54×10^{-30}	12	7.327	0.95	.452	13.94	27.88	118.78
$(200)_\alpha$	38.65	.6246	1.433	23.54×10^{-30}	6	3.440	0.91	.545	10.59	21.18	15.41
$(211)_\alpha$	49.9	.7649	1.170	23.54×10^{-30}	24	2.730	0.875	.551	8.89	17.78	33.16
$(220)_\alpha$	62.05	.8834	1.013	23.54×10^{-30}	12	3.594	0.845	.463	7.88	15.76	16.56
$(200)_\gamma$	30.01	.5015	1.793	46.1×10^{-30}	6	5.731	0.938	.485	12.29	49.16	36.68
$(220)_\gamma$	45.15	.7090	1.268	46.1×10^{-30}	12	2.822	0.890	.559	11.39	45.56	29.44
$(311)_\gamma$	56.24	.8313	1.081	46.1×10^{-30}	24	2.984	0.860	.516	8.38	33.52	32.56

TABLE VI

CALCULATION OF "R" FOR ALLOY K1527

Reflection	$\theta°$	Sin θ	d	V	m	L.P.	e^{-2m}	$\frac{\sin\theta}{\lambda}$	f	F	R
$(110)_\alpha$	27	.4540	2.027	23.54×10^{-30}	12	7.327	0.95	0.452	13.41	26.82	109.92
$(200)_\alpha$	38.65	.6246	1.433	23.54×10^{-30}	6	3.440	0.91	0.545	10.74	21.48	15.85
$(211)_\alpha$	49.9	.7649	1.170	23.54×10^{-30}	24	2.730	0.875	0.551	9.62	19.24	38.84
$(220)_\alpha$	62.05	.8834	1.013	23.54×10^{-30}	12	3.594	0.938	0.463	8.00	16.00	17.07
$(200)_\gamma$	30.1	.5015	1.793	46.1×10^{-30}	6	5.731	0.898	0.485	12.35	49.40	35.46
$(220)_\gamma$	45.15	.7090	1.268	46.1×10^{-30}	12	2.822	0.890	0.559	9.53	38.12	20.61
$(311)_\gamma$	56.24	.8313	1.081	46.1×10^{-30}	24	2.984	0.860	0.516	8.50	34.00	33.50

TABLE VII

CHARACTERISTICS OF TEMPER EMBRITTLEMENT.[14]

1.	Embrittlement can occur in alloy steels having ferrite + carbide microstructures when held in the temperature range 343-593°C. Embrittlement exhibits C curve time-temperature relationships within this range.
2.	Even embrittled material is so tough that except at very low temperatures or for large specimens thickness, an impact test is needed to measure the progress of embrittlement with time. Charpy shelf energies are unaffected by temper embrittlement.
3.	Decohesion occurs in ferrite-ferrite and ferrite-carbide grain boundaries, but is restricted almost entirely to those which lie along prior austenite grain boundaries.
4.	Embrittlement occurs only in the presence of specific impurity elements. The ones primarily of interest are P, Sb, Sn and As.
5.	Both impurity elements and alloying elements segregate to prior austenite grain boundaries during the embrittlement process.
6.	Embrittlement is reversible, and may be completely removed by heating for short times above the embrittling temperature range.
7.	Plastic deformation during embrittlement (creep strain) appears to delay the development of embrittlement, although this is not perfectly clear.

TABLE VIII

VALUES OF DIFFERENTIAL INTERACTION COEFFICIENTS α'_{12} KJ/mol

Alloy-impurity Pair	Compound	α'_{12} (Ref.54)	α'_{12} (Ref.61)
Mn-Sb	MnSb	81.9	-
Ni-Sb	NiSb	113.7	56.9
Ni-Se	NiSe	-66.9	-
Ni-Te	NiTe	-59.4	-
Ni-P	Ni_3P	75.2	30.1
Mn-S	MnS	221.9	-
Mn-P	Mn_3P	-	67.0
Cr-P	Cr_3P	-	102.6
Mo-P	Mo_3P	-	180.5
Cr-Sb	CrSb	-	33.5

TABLE IX

Measurements taken from the Diffraction Pattern in Fig. 85 to enable Indexing of the Pattern.

$$Dd = 2\lambda L$$

Camera Constant ($2\lambda L$) = 23.65 Åmm

Lattice Parameters a, b, c = 2.866 Å

D(mm)	d(Å)	hkl
20.5	0.867	$\bar{2}11$
11.75	0.497	011
20.25	0.856	211
16.625	0.703	200
20.5	0.867	$2\bar{1}\bar{1}$

TABLE X

Measurements used in the Calculation of Camera Constant for the Philips 400C using the Diffraction Pattern shown in Fig. 86

hkl	d(Å)	D(mm)	Camera Constant $2\lambda L$(Å mm)
[110]	2.027	20.2	40.945
[112]	1.170	34.975	40.92
[200]	1.013	40.4	40.925

The average camera constant = 40.93 Åmm

TABLE XI

Measurements Used for the Indexing of the Electron Diffraction Pattern Shown in Fig. 89

$2\lambda l = 40.93\ \text{Å mm}$

D(mm)	d(Å)	hkl (Fe_2Mo)	hkl (Fe-Mo σ)
21.20	1.940	021	302
9.80	4.241	110	101
21.80	1.887	201	500
19.10	2.154	111	401
21.30	1.940	021	302

For Laves phase, Fe_2Mo hcp — $a = 4.73$Å, $c = 7.72$Å — lattice parameters for the laves hexagonal structure

Zone axis $\bar{2}\bar{2}4$

For the sigma phase, FeMo bct — $a = 9.188$, $c = 4.812$ — lattice parameters for the sigma bct structure

Zone axis = $0\bar{5}0$

TABLE XII

Solution Treatment	K1526		K1527	
	Grain Size (μm)	Quantitative Analysis (inclusion content) (Vf) %	Grain Size (μm)	Inclusion Content (Vf) %
1000°C 1hr + WQ	62	.004	50	.002
1300°C 1hr + WQ	260	-	124	-
1300°C 1hr + WQ + 1000°C 1hr + WQ	132	.004	54	.002

TABLE XIII

Analysis of the Inclusions Present in the as Quenched K1526 and K1527 Alloys

Specimen	Position	O	Si	Mo	S	Mn	Fe
		wt%					
A. K1526 1h 1300 IBQ	1	23.24	0.12	-	-	73.58	2.09
	2	20.59	0.24	-	-	69.84	1.87
	3	16.70	3.92	1.77	19.82	56.39	3.03
	4	23.70	4.75	1.91	11.48	55.64	4.43
C. K1526 1h 1100°C WQ	1	23.74	0.14	-	-	75.34	1.07
	2	23.40	0.05	-	-	76.27	1.99
	3	22.33	0.05	-	-	76.12	1.99
	4	23.15	0.21	-	-	77.13	0.67
	5	4.97	0.07	-	21.49	44.25	29.33
D. K1527 1h 1300 IBQ	1	13.60	1.13	-	13.94	55.32	5.48

TABLE XIV

Summary of Impact, Tensile, Fractographic and Auger Results

Alloy	Heat Treatment	Hardness HV30	DBTT	Reduction of Area at -78°C and a Strain Rate of 0.5 min^{-1}	Low Temperature Fracture Mode	A E S	
						Mn (At%)	Mo (At%)
K1525	ST 1000°C/1h - WQ	258 ± 2	+115°C	60%	IG	7.6 1.4	0
	ST 1000°C/1h - WQ + 1.5 min 450°C-WQ	261 ± 2	-	55%	IG	14.2 1.2	0
	ST 1000°C/1h - WQ + 3 min 450°C-WQ	263 ± 2	-	52%	IG	14.9 1.6	0
	ST 1000°C/1h - WQ + 6 min 450°C-WQ	267 ± 2	-	0%	IG	18.5 2.8	0
	ST 1000°C/1h - WQ + 12 min/450°C-WQ	272 ± 2	-	0%	IG	17.8 2.0	0
K1526	ST 100°C/1h - WQ	336 ± 1	+48°C	60%	Brittle Cleavage. 100%	5.4 1.3	6.2 1.2
	ST 1000°C/1h - WQ + 1 min 450°C-WQ	343 ± 19	-	60%	Brittle Cleavage.5% IG	5.6 1.3	6.2 1.2
	ST 1000°C/1h - WQ + 4 min 450°C-WQ	350 ± 19	-	47%	10% IG Brittle Cleavage	6.0 1.4	6.3 1.3
	ST 1000°C/1h - WQ +16 min 450°C-WQ	332 ± 17	-	10%	50% IG/Brittle Cleavage	6.4 1.3	6.3 1.4
	ST 1000°C/1h - WQ +17h 450°C-WQ	340 ± 15	80°C	0%	100% IG	25 2.2	9.3 1.7
	ST 100°C/1h - WQ + 480h 450°C-WQ	330 ± 12	120°C	0%	100% IG	35.2 3.1	13.2 1.9

TABLE XIV (Continued/...)

K1527	ST 100°C 1h WQ	284 ± 2	+50°C	40%	100% Brittle Cleavage	7.6 1.7	5.8 1.5
	ST 1000°C 1h WQ + 1min 450°C-WQ	289 ± 3	-	47%	5% IG 95% Brittle Cleavage	7.7 2.0	5.9 1.6
	ST 1000°C 1h WQ + 4 min 450°C-WQ	296 ± 6	-	37%	10% IG 90% Brittle Cleavage	7.8 1.9	5.9 1.5
	ST 1000°C 1h WQ + 17h 450°C-WQ	305 ± 3	+60°C	0%	100% IG	12.4 2.4	10.3 2.1
	ST 1000°C 1h WQ + 480h 450°C-WQ	434 ± 16	Totally Brittle at all Temperatures	0%	100% IG	30.5 5.3	24.7 2.8

TABLE XV

X-Ray Diffraction Analysis

ALLOY K1526

Heat Treatment	%age γ with different peak combinations						%age Phases	
	$(200)_\alpha - (200)_\gamma$	$(110)_\alpha - (200)_\gamma$	$(211)_\alpha - (200)_\gamma$	$(211)_\alpha - (220)_\gamma$	$(200)_\alpha - (220)_\gamma$	$(110)_\alpha - (220)_\gamma$	% γ	%
ST 1000°C 1h - WQ	-	-	-	-	-	-	-	10
ST 1000°C 1h-WQ 300 hours 450°C WQ	-	-	-	-	-	-	-	10
ST 1000°C 1h-WQ 9078 hours 450°C WQ	0.0	0.06	0.01	0.08	0.06	0.28	0.08	9
ST 1000°C 1h-WQ 17h 525°C WQ	-	-	-	-	-	-	-	10
ST 1000°C 1h WQ 34½h 525°C WQ	0.13	0.28	-	-	0.10	0.22	0.18	9
ST1000°C 1h WQ 193½h 525°C WQ	0.07	-	-	-	-	-	0.07	9
ST 1000°C 1h WQ 670h 525°C WQ	0.18	-	0.22	0.14	0.12	-	0.17	9

ALLOY K1527 fully ferritic in the solution treated and as quenched state and also in the aged condition after 9000 hours at 450°C and 525°C.

TABLE XVI

X-RAY DIFFRACTION ANALYSIS

ALLOY K1525 - ST 1000°C/1h Water Quenched - Aged at 450°C

Heat Treatment	%age Phases with different Peak Combinations						Average %age Phases	
	$(200)_\alpha - (200)_\gamma$	$(200)_\alpha - (220)_\gamma$	$(200_\alpha - (311)_\gamma$	$(211)_\alpha - (200)_\gamma$	$(211)_\alpha - (220)_\gamma$	$(211)_\alpha - (311)_\gamma$	% γ	% α
ST 1000°C 1h WQ	-	-	-	-	-	-	-	100%
ST - WQ - 25h 450°C	-	-	-	-	-	-	-	100%
ST - WQ - 50h 450°C	-	-	-	-	-	-	-	100%
ST - WQ - 75h 450°C	1.5	-	-	-	-	-	1.5	98.5
ST - WQ - 100h 450°C	1.8	1.8	-	-	-	-	1.8	98.2

TABLE XVII

Auger Electron Emission Analysis

Solution treatment for both alloys - One hour at 1000°C followed by a water quench.

K1526 (Fe-8Mn-2.5M0)	percentage of Fe (703ev) peak					atomic percentage				
	Mn	Mo	P	N	C	Mn	Mo	P	N	C
As quenched	5.25	1.78	-	1.1	13.3	8.10	1.38	-	0.69	-
30 mins. at 450°C	3.65	4.43	0.25	-	18.9	5.63	3.73	0.12	-	-
17 hrs. at 450°C	16.64	6.45	0.53	0.82	28.6	25.69	5.42	0.26	0.51	-
193½ hrs. at 450°C	26.90	12.05	2.17	2.05	31.5	41.55	10.18	1.05	1.28	-
480 hrs. at 450°C	23.38	9.12	1.26	2.09	23.5	36.14	7.67	0.61	1.31	-
858 hrs. at 450°C	24.26	17.9	3.25	1.77	28.5	37.53	15.06	0.86	1.11	-
K1527 (Fe-8Mn-5Mo) Heat Treatment										
As quenched	5.38	2.98	-	0.32	-	8.30	2.76	-	0.20	-
30 mins. at 450°C	5.06	4.60	-	0.54	12.34	7.89	3.50	-	0 34	-
17 hrs. at 450°C	8.50	7.90	1.93	1.79	17.70	13.25	6.10	0.93	1.12	-
193½ hrs. at450°C	15.98	14.15	2.03	1.82	25.70	24 84	12.01	0.98	1.14	-
480 hrs. at 450°C	22.58	17.31	1.35	1.88	23.60	35.22	14.69	0 65	1.18	-
858 hrs. at 450°C	20.16	13.83	1.74	1.79	20.40	31.43	11.74	0.84	1.12	-

Atomic percentages of Mn and Mo calibrated from normalised peaks by taking the as-quenched peaks to represent bulk concentrations. Elemental sensitivities for N = 1.60 P = 2.07

TABLE XVIII

Details of Ion Bombardment on the Fracture Surface of Alloy K1526 (Fe-8Mn-2.5Mo) after a solution treatment of one hour at 1000°C + a water quench followed by an aging treatment of 480 hours at 450°C followed by a water quench

	Percentage of Fe(703ev) Peak					Atomic Percentage				
	Mn	Mo	P	C	N	Mn	Mo	P	C	N
As Fractured	23.38	12.89	1.26	23.50	2.58	36.14	7.67	0.61	-	1.31
1st. Ion Bombardment ~ 5 atomic layers	7.48	11.94	2.14	60.33	-	11.55	7.11	1.04	-	-
2nd. Ion Bombardment ~ 15 atomic layers	7.85	10.52	2.11	71.99	-	12.12	6.26	1.02	-	-

TABLE XIX

Data from Charpy Impact Tests for Solution Treated And aged Series I Alloys

Testing Temperature °C	K1525 Soln. T	K1526 Soln. Treatment			K1527 Soln. Treatment			Soln. Treated 1000°C 1h WQ							
								K1526 Age Treatment				K1527 Age Treatment			
	1000°C 1h WQ	1000°C 1h WQ	1300°C 1h WQ	1300/h + WQ 1000°C 1h WQ	1000°C 1h WQ	1300°C 1h WQ	1300°C 1h WQ + 1000°C 1h WQ	17h @ 450°C	480h @ 450°C	17h @ 525°C	480h @ 525°C	17h @ 450°C	480h @ 450°C	17h @ 525°C	480h @ 525°C
-135										2		3			
- 90												2			
- 80									1		17				
- 75			6			2									
- 65											35				
- 60								2							
- 50		19		16	5.5		6								
- 40												2			
- 37										3	42				
- 26			6												
- 25						3									
- 23					11						52				
- 19		17.5												5	
- 15				18											
- 13							8								
0		21.5			9.5										
18	5.5	21.5			16.2										
19				19											
20			20			7	10								
23								3	2	63		26	5	6	1
34		34			7										
40							39								
43			31												
47					26										
50						21									
58				11	57		59								
59				32											
66				43											
70	20		42			44									
73					55.5										
74		39													
83				48											
84								25	1	70	53	47	2	14	0
100	21.5	43			64										
105				42			61								
110	20														
118			40			63									
120	76														
140	73														
142								51	51			60	1	47	2
150					58										
152		43.5		42											
157	68														
172		39													
177			39			50									
187										57					
256								54				63	2	56	2
266									53						
320								55							
364													2		

TABLE XX

The As Quenched Properties of Alloys A217 (Fe-0.2C-1.4Mn-0.5Mo-0.6Ni-0.3Si), A317 (base alloy + 0.4%Cu) and A417 (base alloy + 0.04%P) after an hour at 1000°C (tempering carried out for one hour at 650°C followed by water quenching).

	Prior Austenite Grain Size (μm)		Hardness (Hv30)		Ductile to Brittle Transition Temperature	
	Q	Q + T	Q	Q + T	Q	Q + T
A 217	221	242	437	164	-23°C	-82°C
A 317	457	429	469	175	-23°C	-90°C
A417	266	247	430	163	-15°C	-70°C

Q = as quenched from 1000°C

Q + T = quenched and tempered

TABLE XXI

Properties of Alloys A217, A317 and A417

After Various Heat Treatments

ALLOY	Heat Treated Condition	Hardness HV30	Ductile to Brittle Transition Temperature	Low Temperature Fracture Mode
A217	Q	437	-23°C	BRITTLE CLEAVAGE
	Q + T	164	-82°C	
	10h @ 450°C	172	-78°C	
	80h @ 450°C	188	-80°C	
	189h @ 450°C	201	-44°C	
	168h @ 525°C	158	-28°C	
A317	Q	469	-23°C	BRITTLE CLEAVAGE
	Q + T	175	-90°C	
	10h @ 450°C	170	-80°C	
	80h @ 450°C	198	-180°C	
	189h @ 450°C	195	-60°C	
	168h @ 525°C	170	-30°C	IG/CLEAVAGE
A417	Q	430	-15°C	BRITTLE CLEAVAGE
	Q + T	163	-70°C	
	10h @ 450°C	162	-80°C	
	80h @ 450°C	186	-88°C	
	189h @ 450°C	198	- 6°C	IG
	168h @ 525°C	160	+98°C	IG

KEY: IG = Intergranular

TABLE XXII

Nominal Compositions of two Commercial

Steels Similar to Series II Alloys

Supertough G

C	Si	Mn	P and S	Cr	Mo	Ni
0.15/ 0.23	0.35 max.	0.75/ 1.25	0.25 max.	0.75/ 1.25	0.40/ 0.60	0.50/ 1.00

JIS grade J SQV 2/3

C	Si	Mn	Mo	Ni
0.25 max.	0.15/ 0.30	1.15/ 1.50	0.45/ 0.60	0.40/ 0.70

FIGURE 1

Schematic Diagram Showing Arrangement Used to Ensure Homogenisation in an Inert Atmosphere. (Series I Alloys)

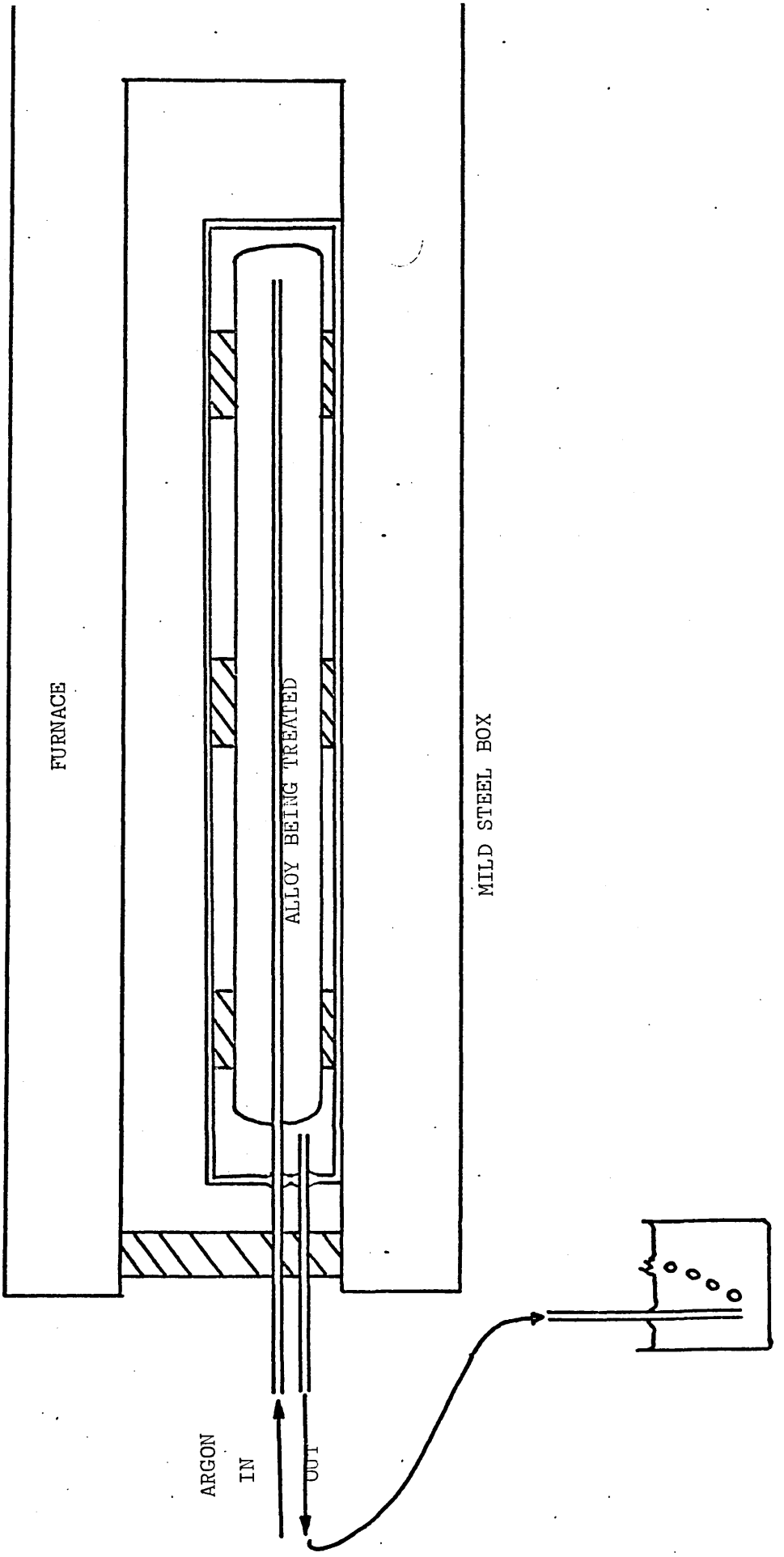
FURNACE
ALLOY BEING TREATED
MILD STEEL BOX
ARGON
IN
OUT

FIGURE 2

Schematic Diagram Showing Furnace Arrangement Used to Ensure Homogenisation in an Inert Atmosphere. (Series II Alloys)

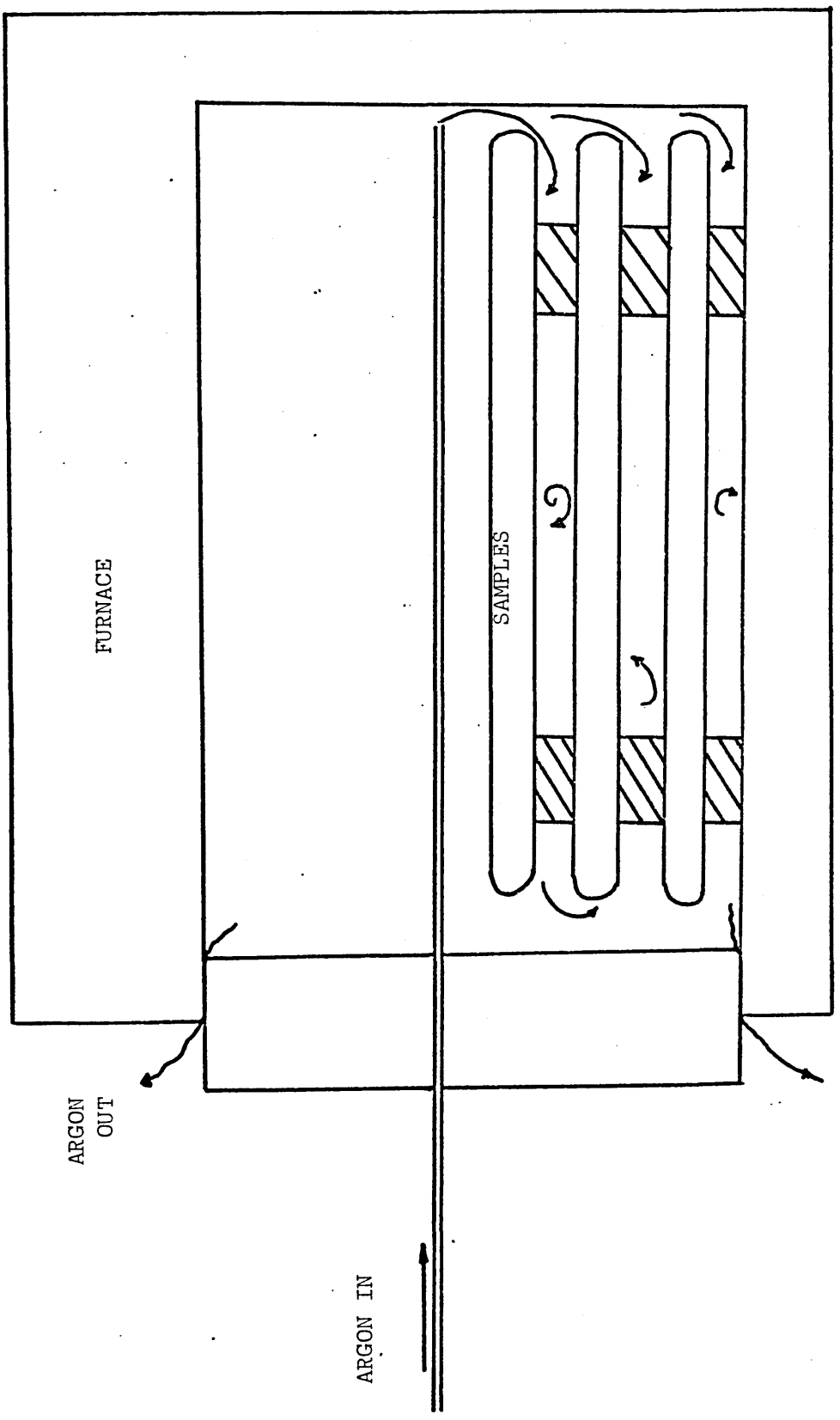
FURNACE
SAMPLES
ARGON OUT
ARGON IN

FIGURE 3

Tensile Sample for the Instron Machine Designed from Broken Sub-Standard Charpy Specimens

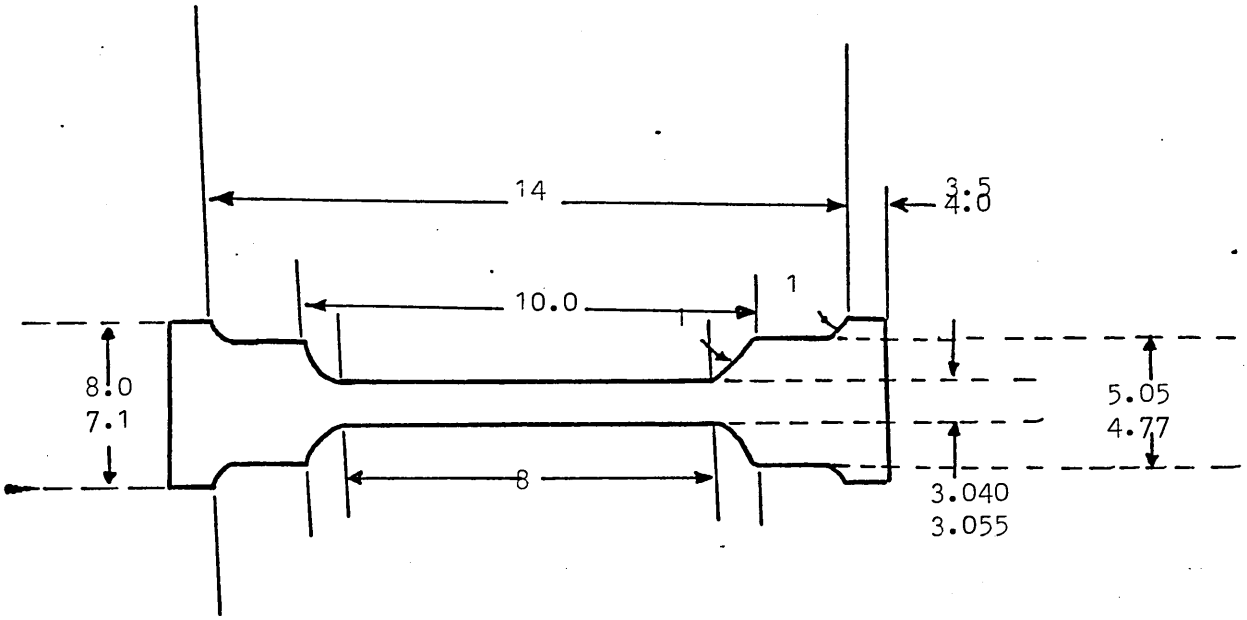

DIMENSIONS IN mm.

FIGURE 4

Low Temperature Arrangement for

Tensile Testing on the Instron

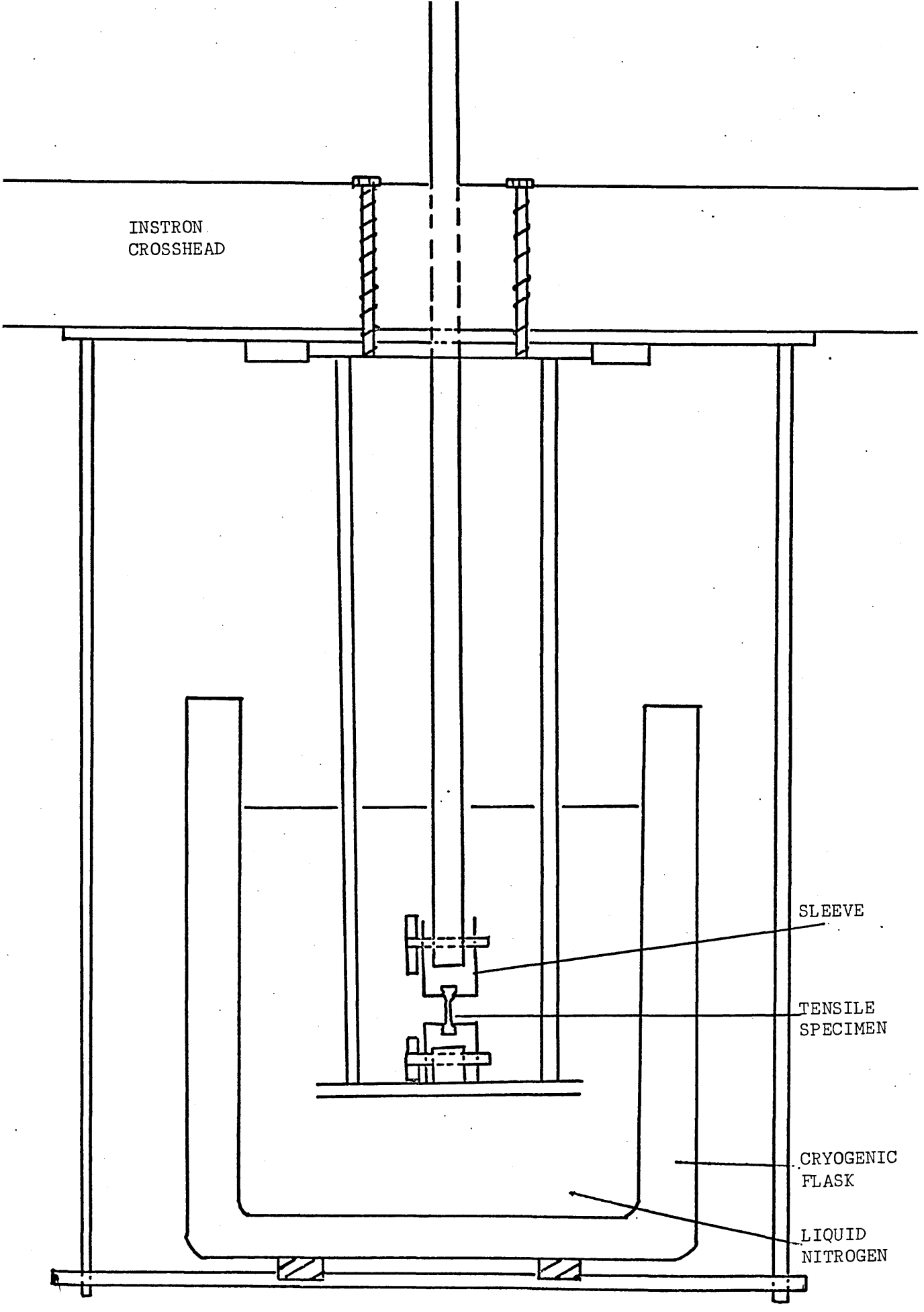
INSTRON
CROSSHEAD
SLEEVE
TENSILE
SPECIMEN
CRYOGENIC
FLASK
LIQUID
NITROGEN

FIGURE 5

Dimensions of Sub Standard Charpy Impact Specimen

Dimensions in mm

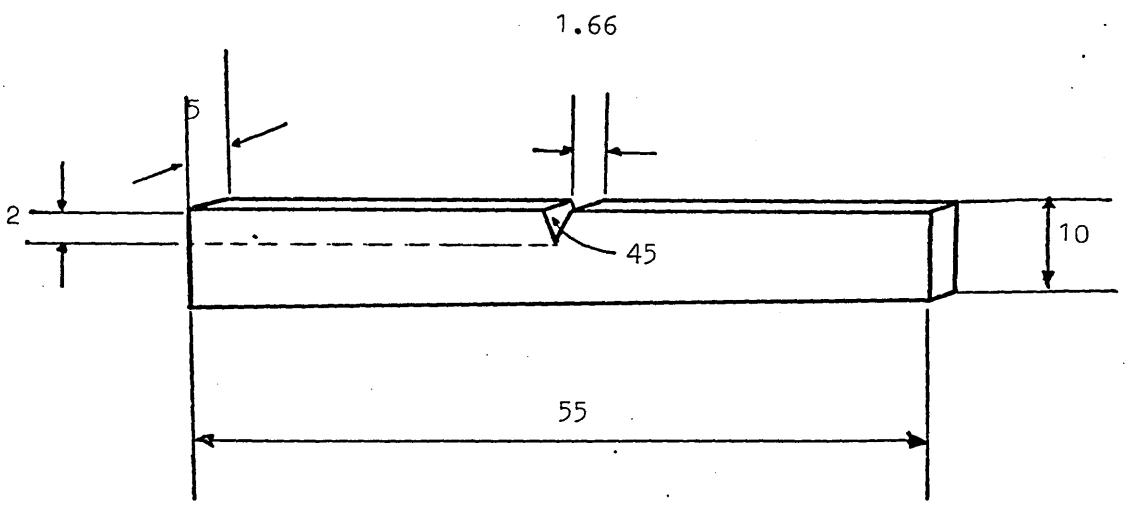
1.66
5
2
45
10
55

FIGURE 6

Schematic Diagram of Manual Electro-

Polishing Arrangement for X-ray Samples

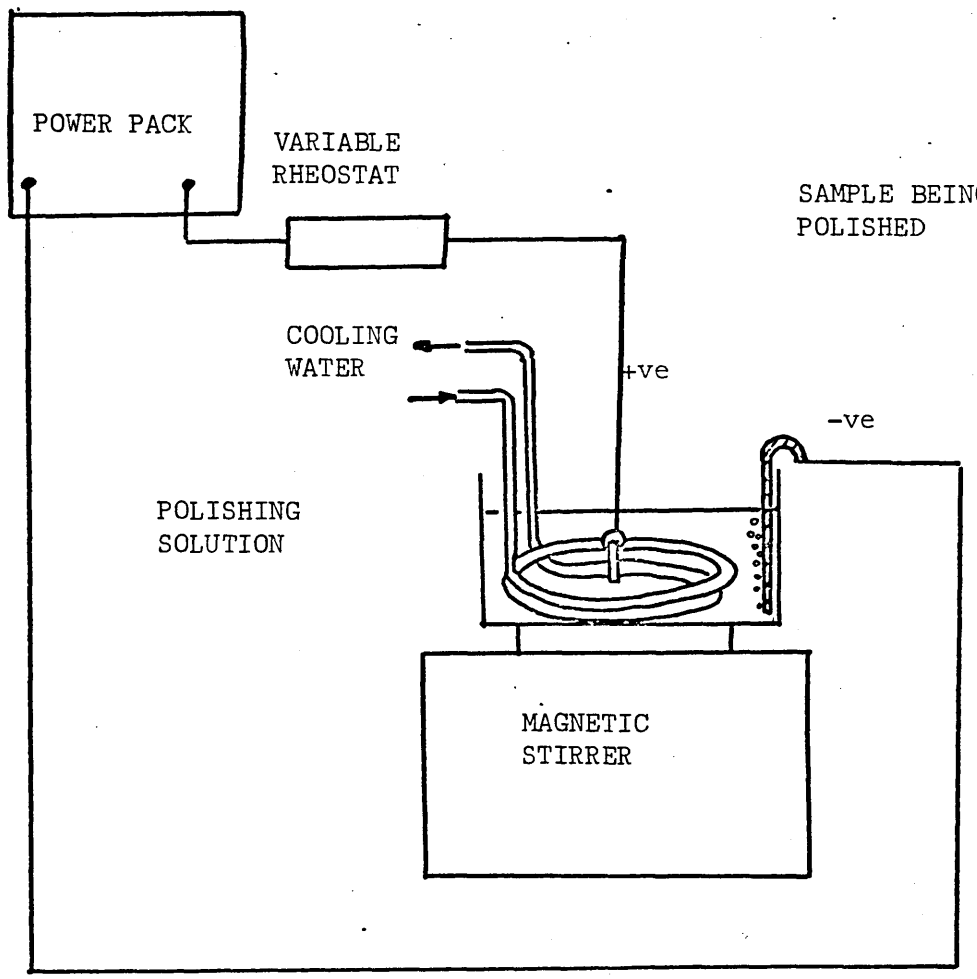
POWER PACK
VARIABLE
RHEOSTAT
SAMPLE BEING
POLISHED
COOLING
WATER
+ve
-ve
POLISHING
SOLUTION
MAGNETIC
STIRRER

FIGURE 7

Jig Used to Grind 3mm Discs for Thin Foil Preparation

FIGURE 8

Schematic Diagram of Profiling and Perforating Apparatus (Manual) for Thin Foil Preparation at Sheffield

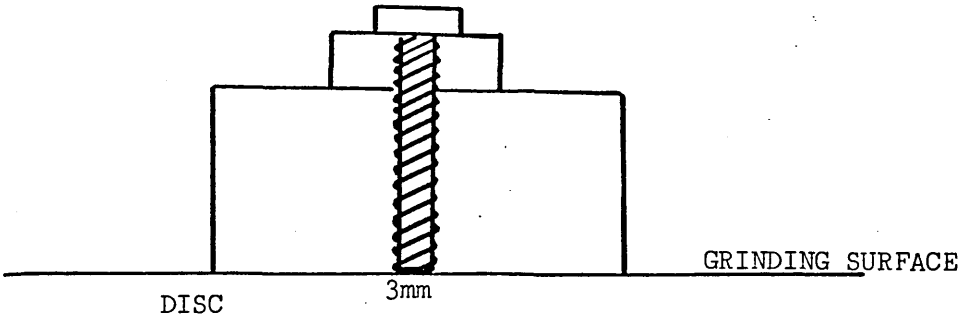

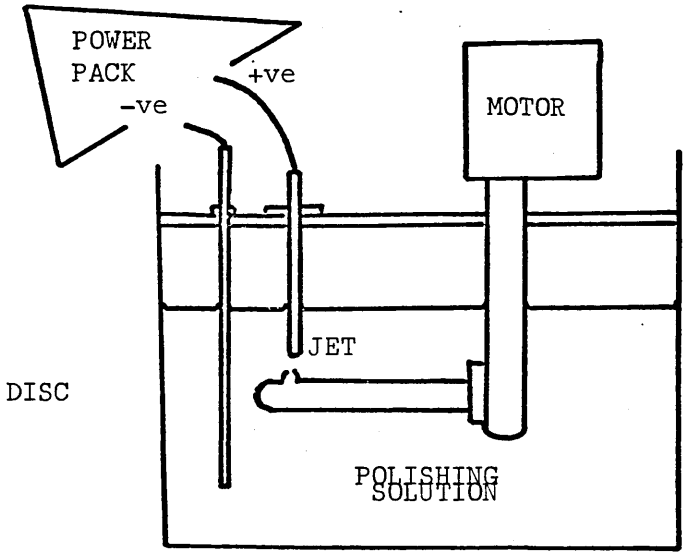

PROFILING

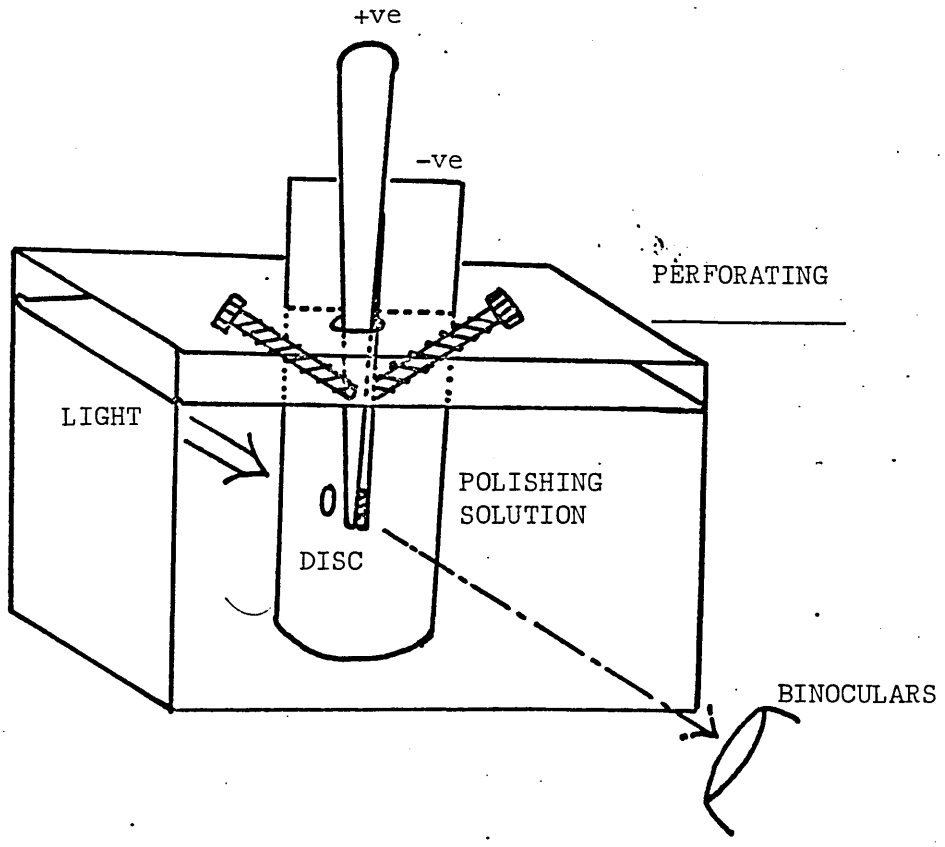

PERFORATING

FIGURE 9

Schematic Diagram of Manual Disc Profiling Arrangement Used at Harwell

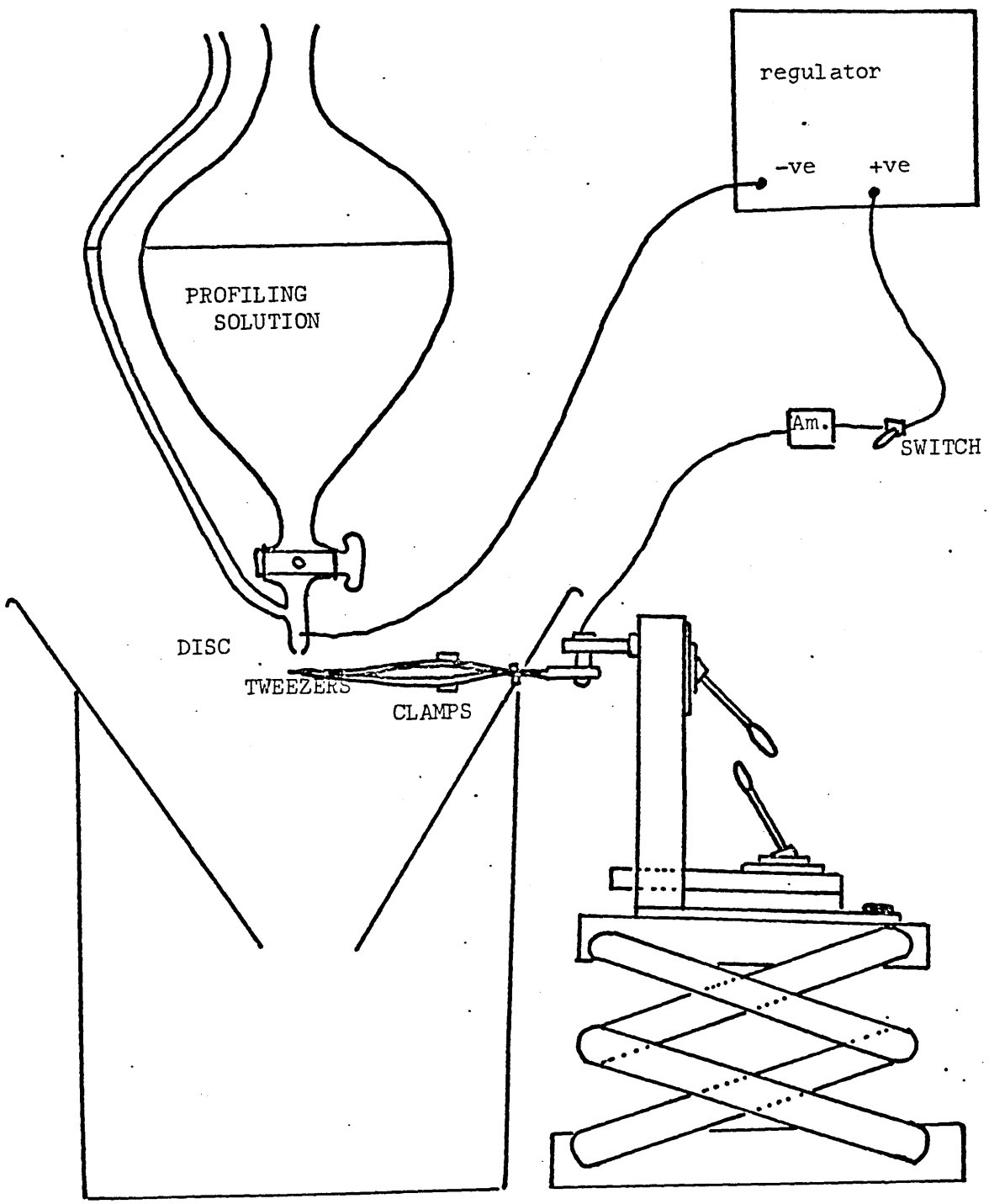
regulator
-ve
+ve
PROFILING
SOLUTION
Am.
SWITCH
DISC
TWEEZERS
CLAMPS

FIGURE 10

Schematic Diagram of Manual Disc Perforating Technique Used at A.E.R.E., Harwell

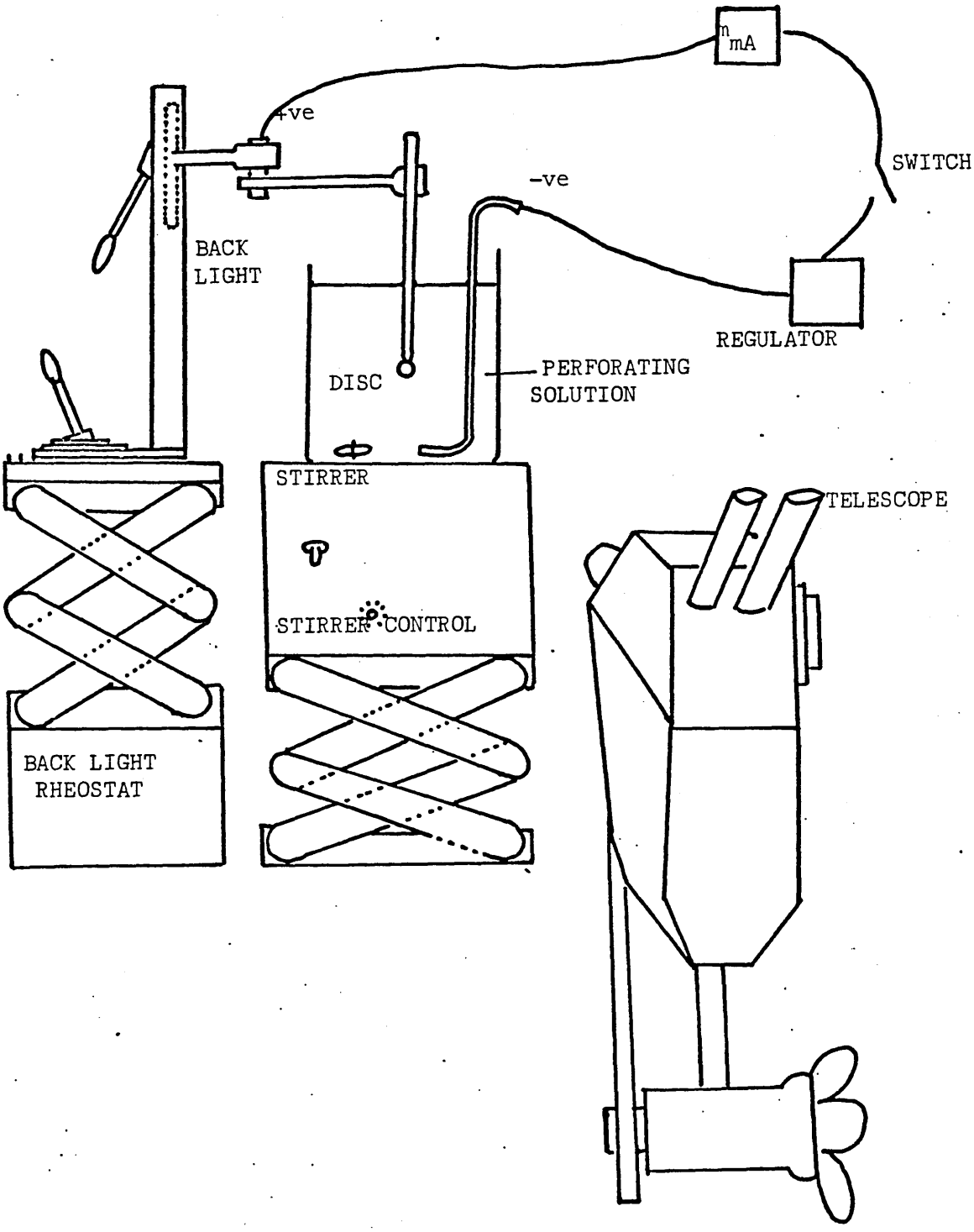
mA
+ve
-ve
SWITCH
BACK
LIGHT
REGULATOR
DISC
PERFORATING
SOLUTION
STIRRER
STIRRER CONTROL
TELESCOPE
BACK LIGHT
RHEOSTAT

FIGURE 11

(a) Auger Sample Design for Harwell Stage

(b) Sample in Position in Holder Sleeve

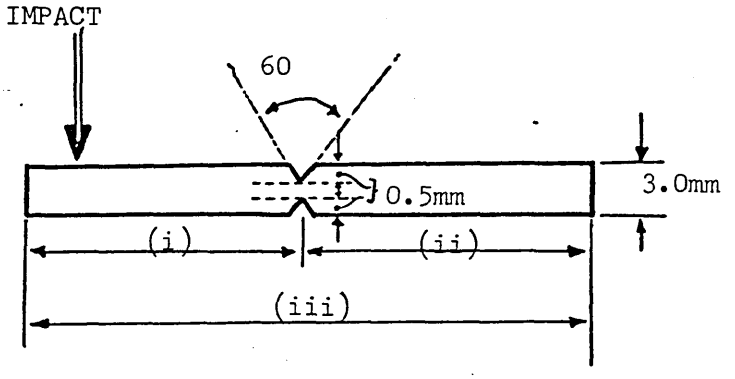
IMPACT
60
0.5mm
3.0mm
(i)
(ii)
(iii)

(a)

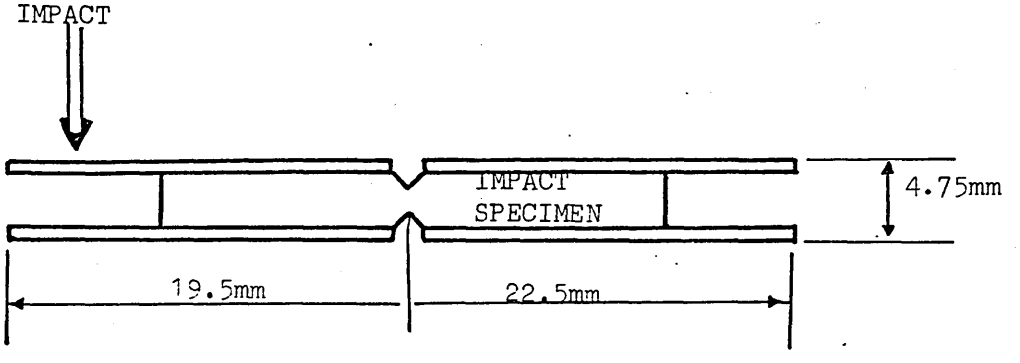
IMPACT
IMPACT
SPECIMEN
4.75mm
19.5mm
22.5mm

(b)

FIGURE 12

The Harwell In-Situ Fracture Stage Used to Fracture Specimens Before Being Analysed in the Auger Electron Spectrometer.

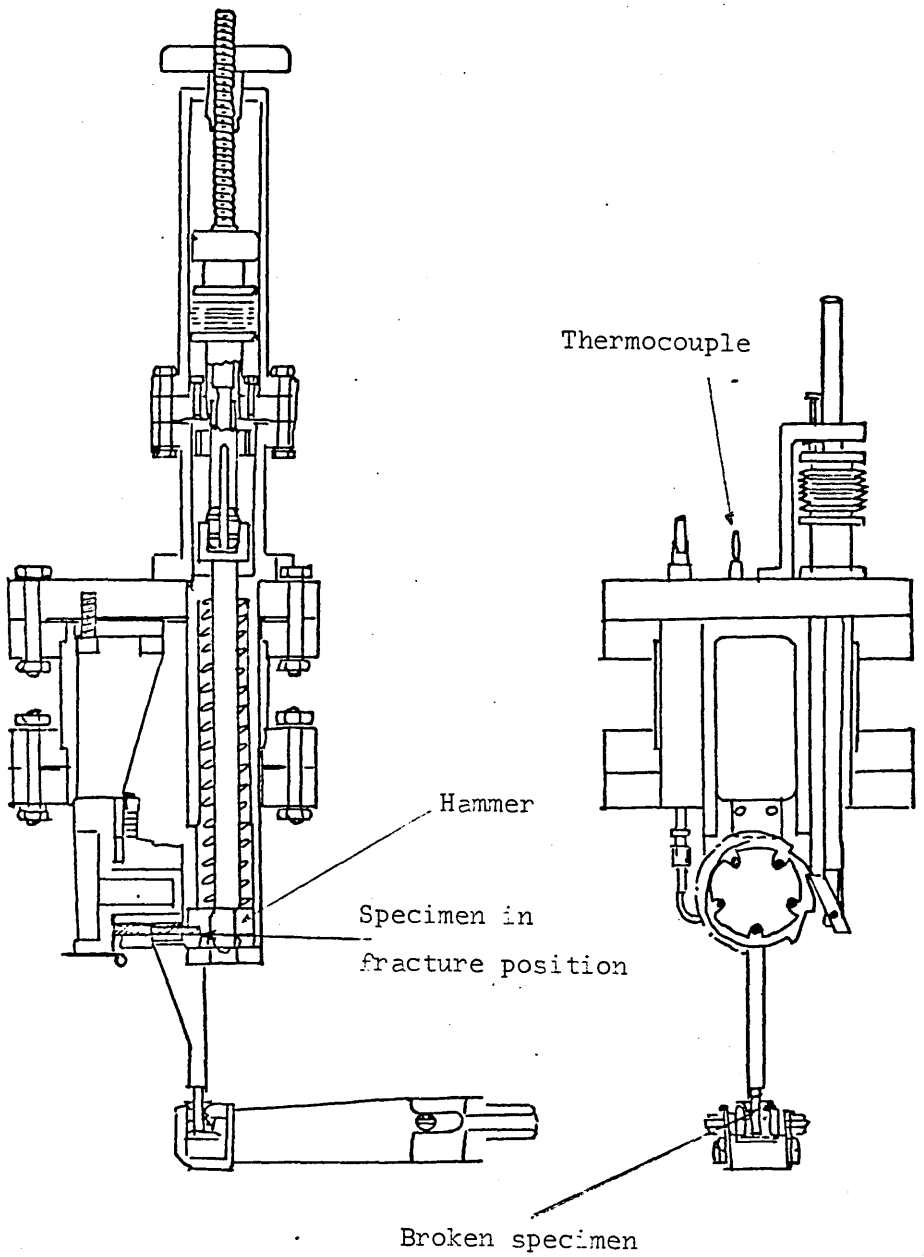
Thermocouple
Hammer
Specimen in
fracture position
Broken specimen

FIGURE 13

Schematic Diagram of the Vacuum System for the Auger Electron Spectrometer Used at Harwell.

Key

1. Field Emitter Gun.
2. Isolation Valve.
3. Specimen Manipulator.
4. Isolation Valve.
5. Fracture Stage.
6. Specimen Transfer Mechanism.
7. Diffusion Pump Stack.
8. Isolation Valve.
9. Separation Sublimation Ion Pump Combinations for Specimen and Gun Chambers.

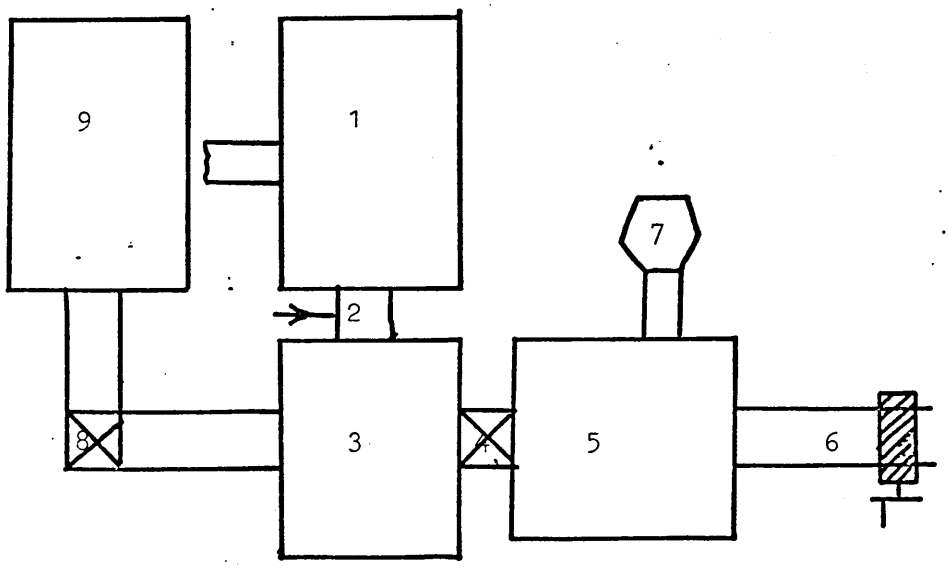
9
1
7
2
8
3
4
5
6

FIGURE 14

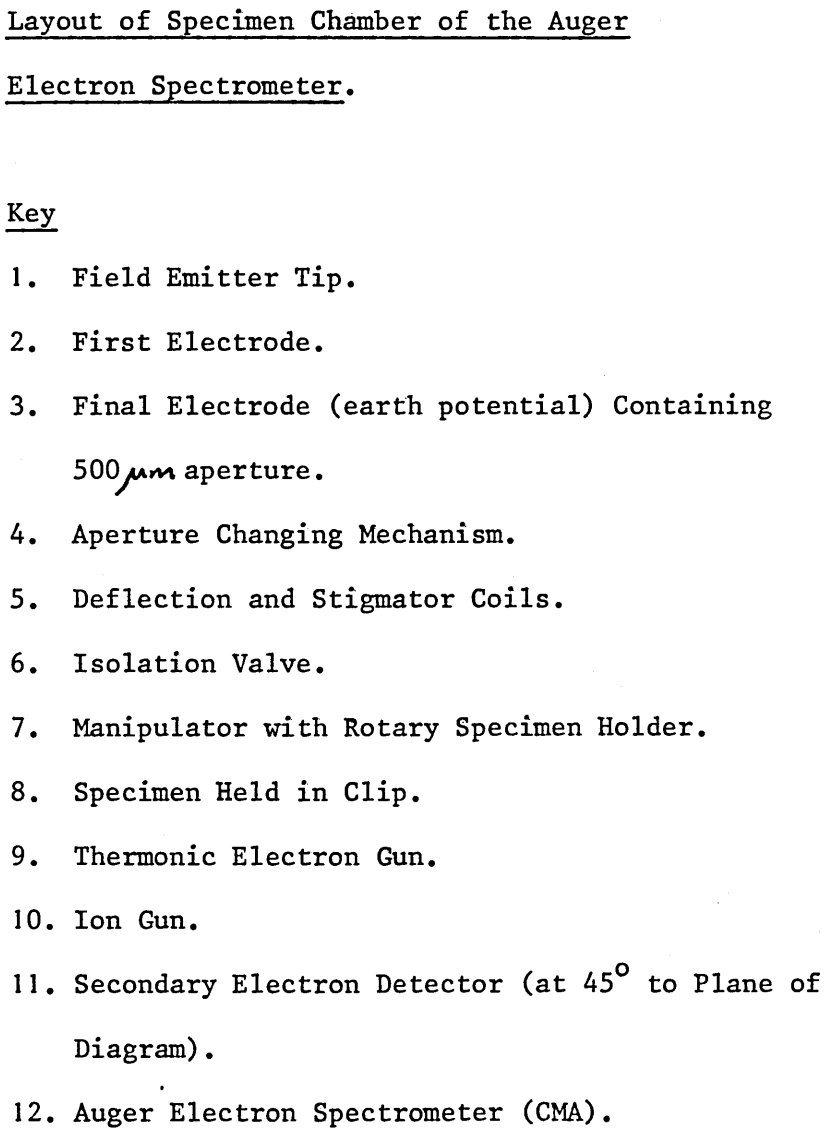

Layout of Specimen Chamber of the Auger Electron Spectrometer.

Key

1. Field Emitter Tip.
2. First Electrode.
3. Final Electrode (earth potential) Containing 500 μm aperture.
4. Aperture Changing Mechanism.
5. Deflection and Stigmator Coils.
6. Isolation Valve.
7. Manipulator with Rotary Specimen Holder.
8. Specimen Held in Clip.
9. Thermonic Electron Gun.
10. Ion Gun.
11. Secondary Electron Detector (at 45° to Plane of Diagram).
12. Auger Electron Spectrometer (CMA).

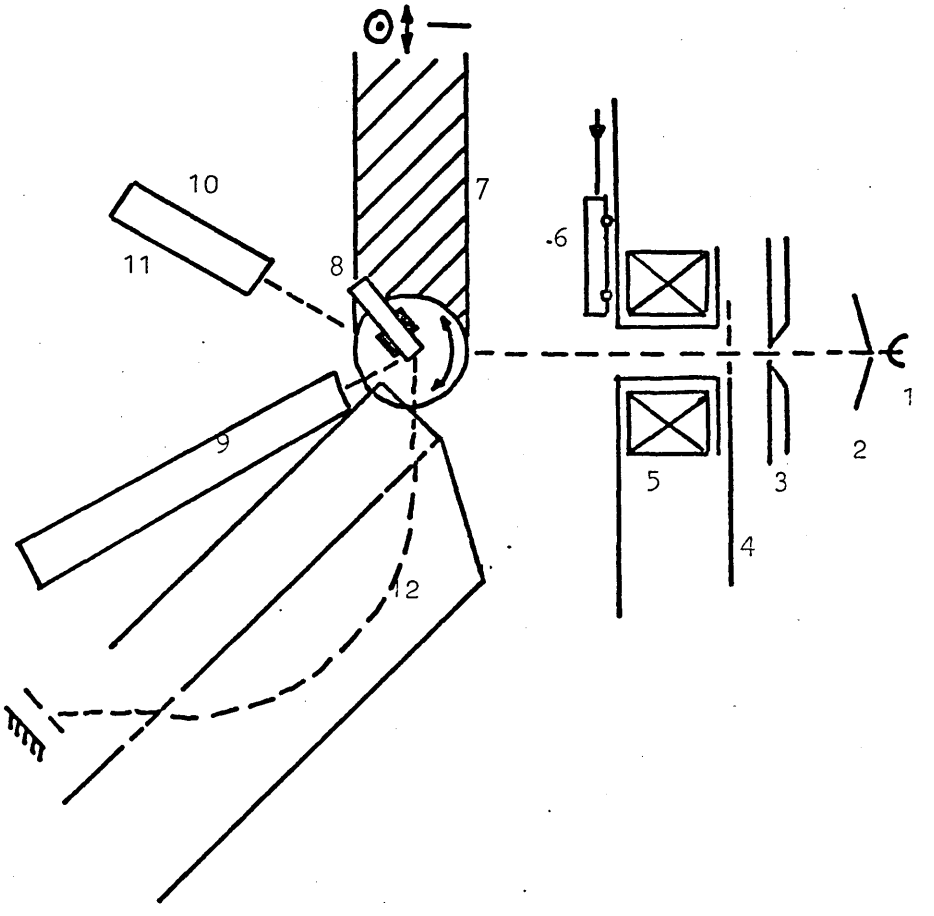
10
11
8
7
6
9
12
5
4
3
2
1

FIGURE 15

Specimen Transfer Mechanism for the Auger Electron Spectrometer.

Key

1. Jaw Mechanism.
2. Split Guide Tube.
3. Clamping Recess.
4. Chute from Fracture Stage.
5. Position of Specimens Immediately After Fracture.
6. Catching Table.
7. Isolation Valve.
8. Specimen Stage.
9. Pulley Mechanism for Rotating the Specimen.
10. Specimen Clip.
11. Specimen in Position on Stage.
12. Driving Rod for Transfer Mechanism.
13. Bellows.
14. Actuating Rod for Jaws.

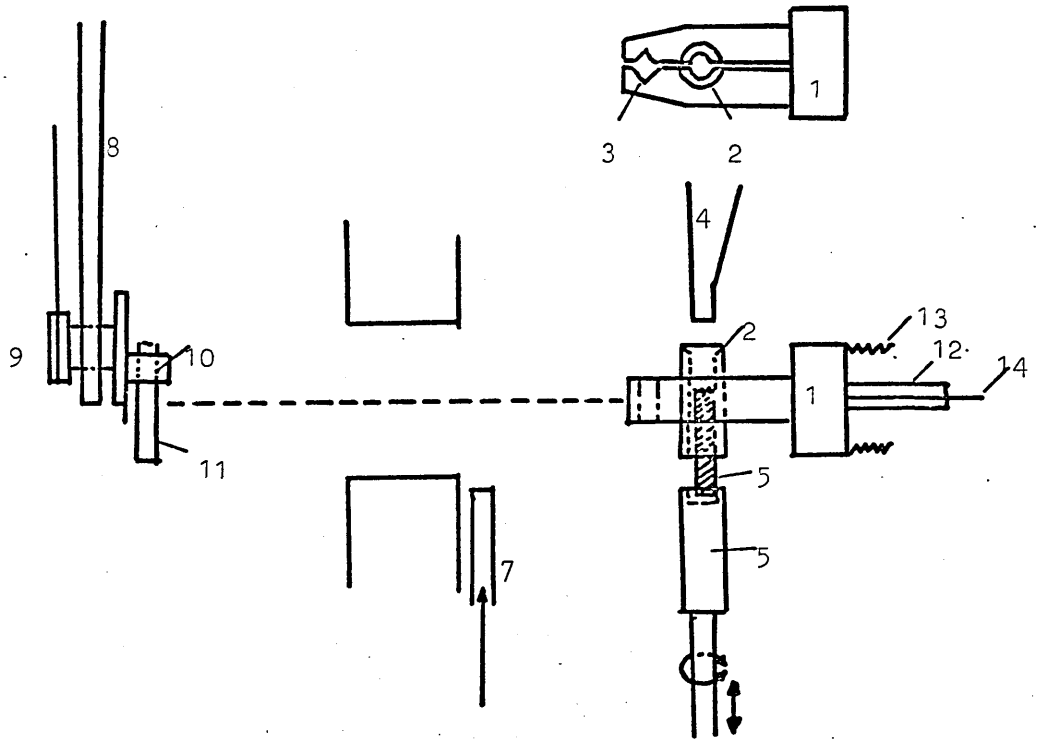
1
3
2
8
4
9
10
2
13
12
14
1
11
5
5
7

FIGURE 16

The Collection of Auger Electrons in the Auger Electron Spectrometer.

The angle Θ and therefore the lock-in amplifier gain, although constant, was not well defined.

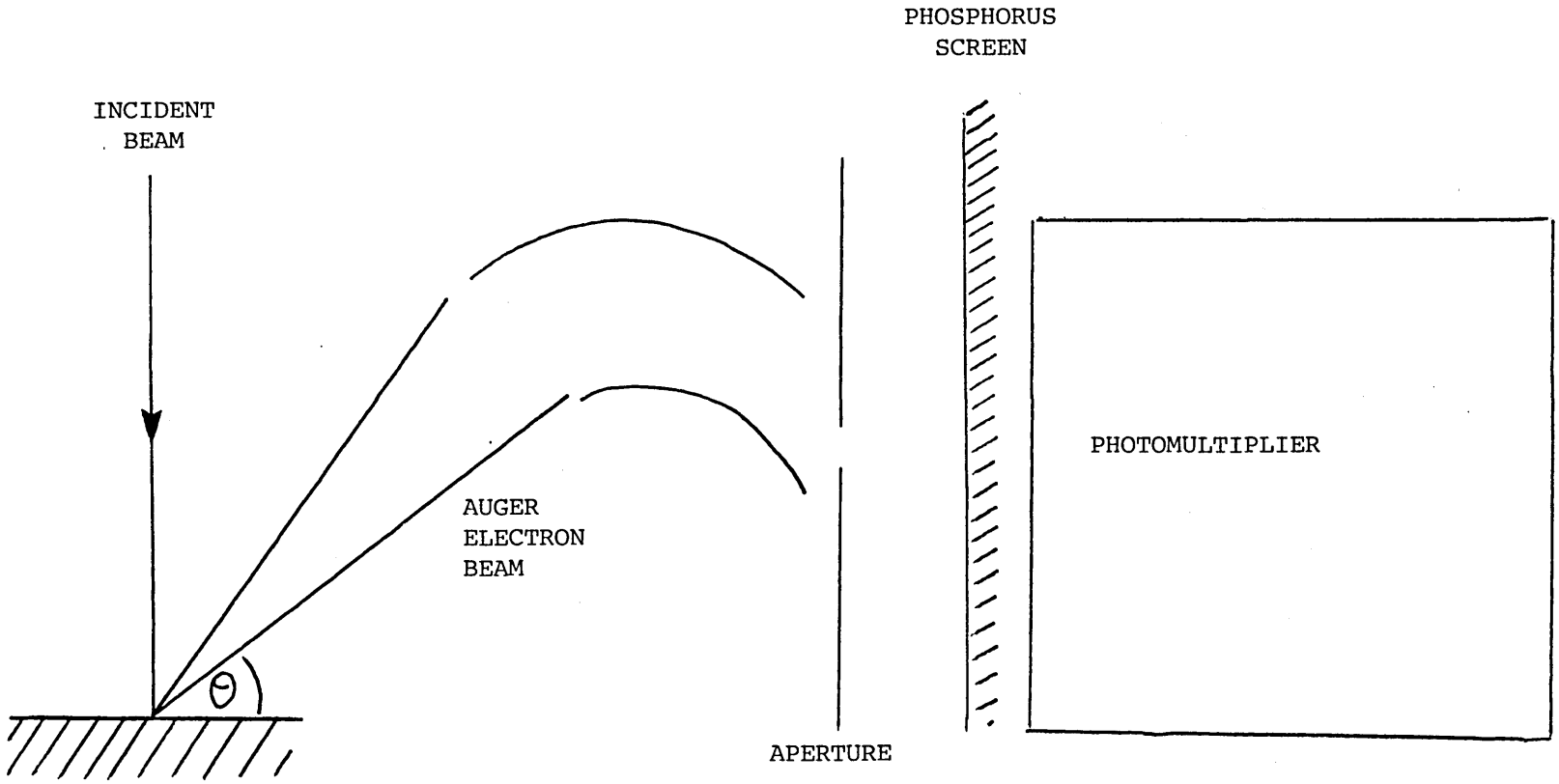
PHOSPHORUS
SCREEN
INCIDENT
BEAM
AUGER
ELECTRON
BEAM
θ
APERTURE
PHOTOMULTIPLIER

FIGURE 17

Calibration for Thermocouple-Chart Used

in the Charpy Impact Test

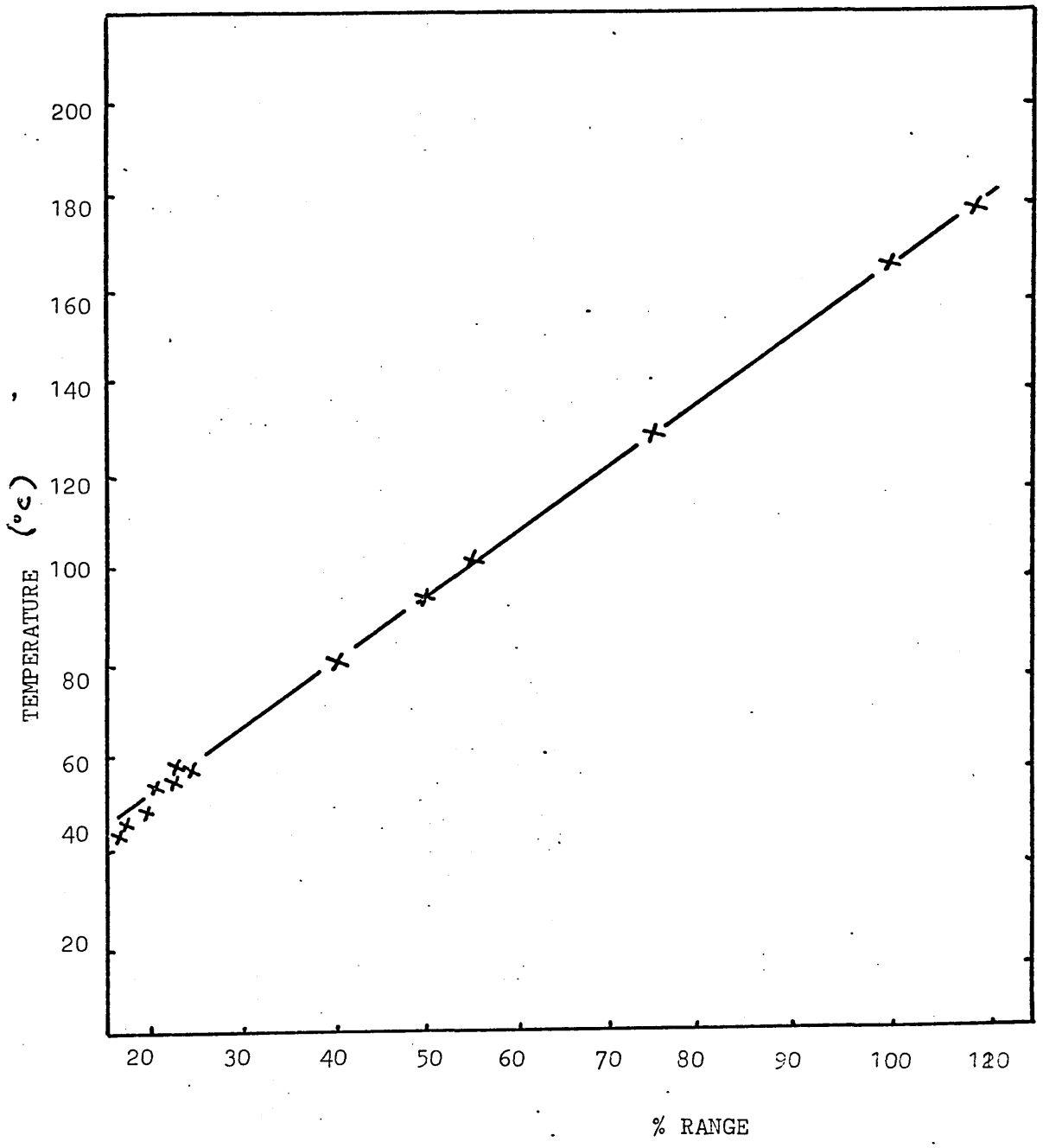
200
180
160
140
120
100
80
60
40
20
TEMPERATURE (°c)
20
30
40
50
60
70
80
90
100
120
% RANGE

FIGURE 18

Atomic Scattering Factors for Fe, Mn, Mo

Using CO $K\alpha$ (1.790 Å) Radiation

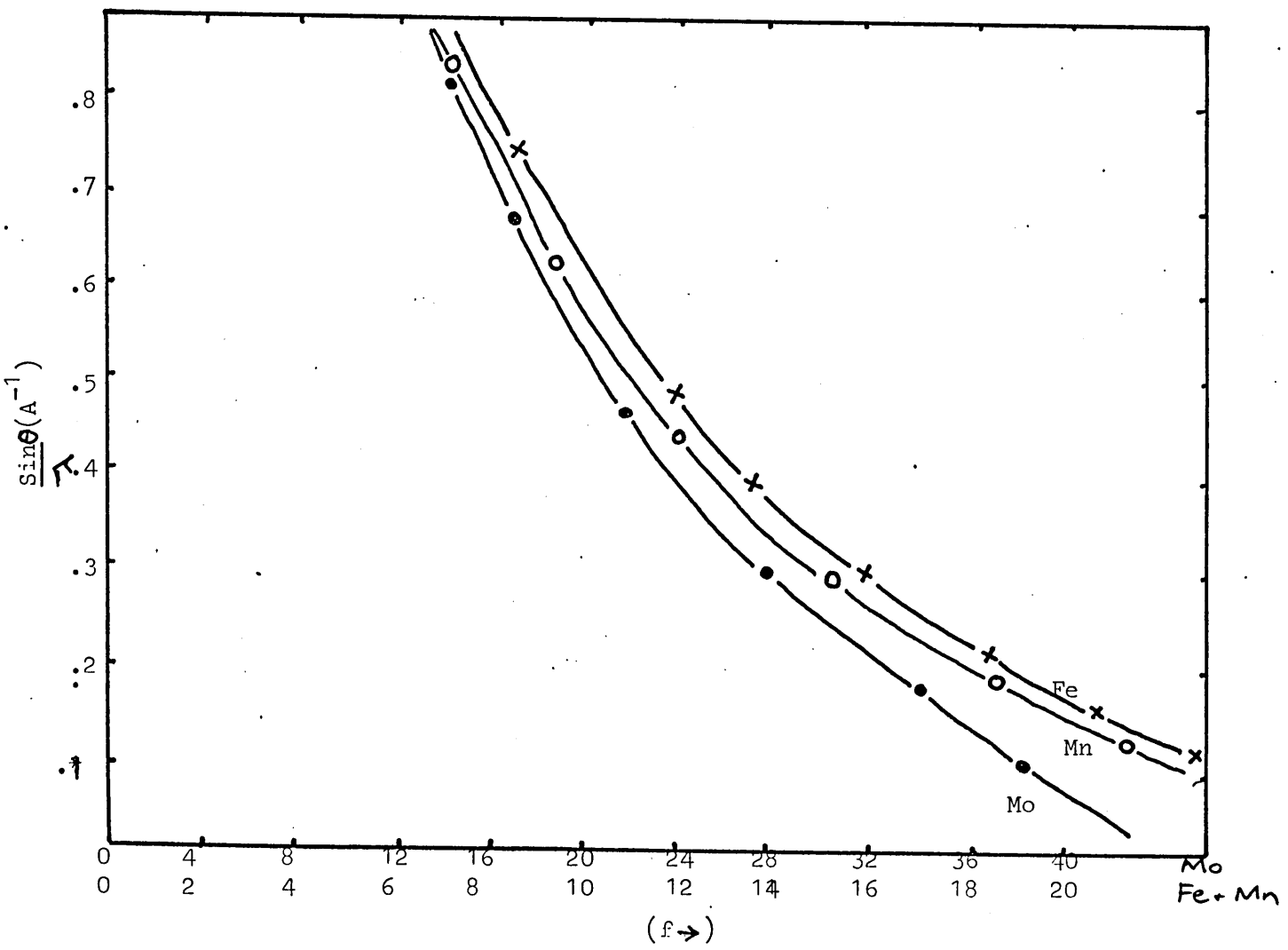
Sinθ/λ (A⁻¹)
.8
.7
.6
.5
.4
.3
.2
.1
Fe
Mn
Mo
0 4 8 12 16 20 24 28 32 36 40
0 2 4 6 8 10 12 14 16 18 20
Mo
Fe + Mn
(f →)

FIGURE 19

Temperature Factor e^{-2m} of Iron at 20°C as a Function of (Sin Θ/λ)

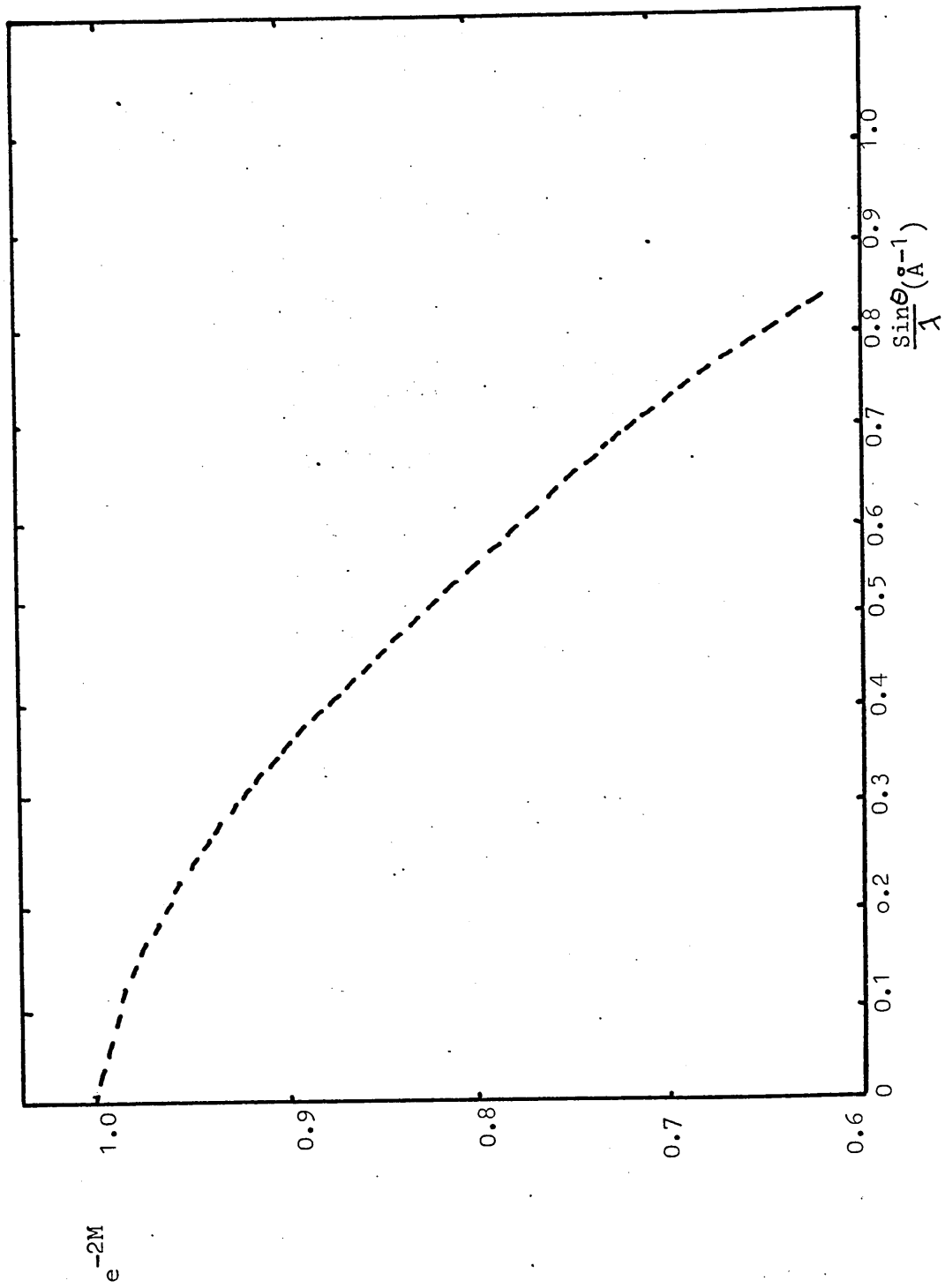
1.0
0.9
0.8
0.7
0.6
e^{-2M}
0
0.1
0.2
0.3
0.4
0.5
0.6
0.7
0.8
0.9
1.0
$\frac{\sin\theta}{\lambda}(\text{Å}^{-1})$

FIGURE 20

Diagram Showing the Effect of Embrittlement

on the Ductile to Brittle Transition Temperature

(after 12)

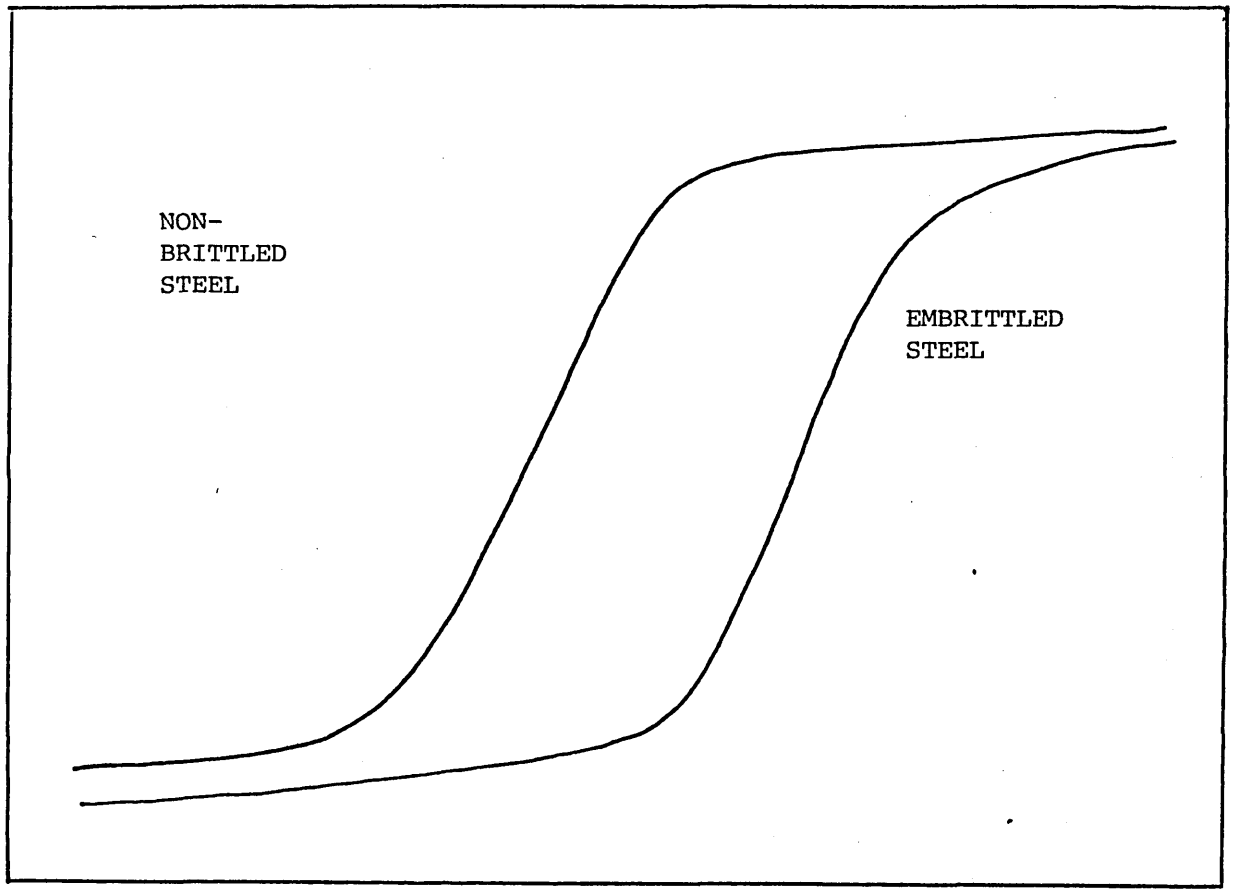
FRACTURE
ENERGY
NON-
BRITTLED
STEEL
EMBRITTLED
STEEL
TEST TEMPERATURE

FIGURE 21

The Effect of Embrittlement on the Brittle Fracture Mode of Ferrite Steel

As quenched (cleavage)

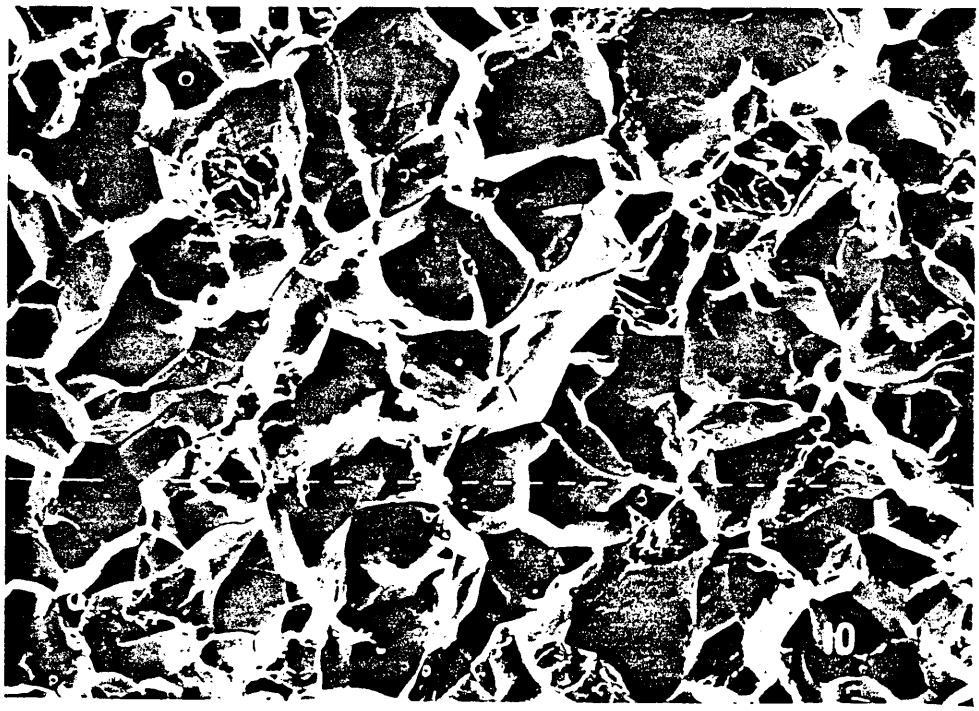

Embrittled (intergranular)

FIGURE 22

Differences in Chemical Composition of Embrittled and Unembrittled Steels. Note Build up of Embrittling Agent Sb. (After Palmberg & Marcus[13])

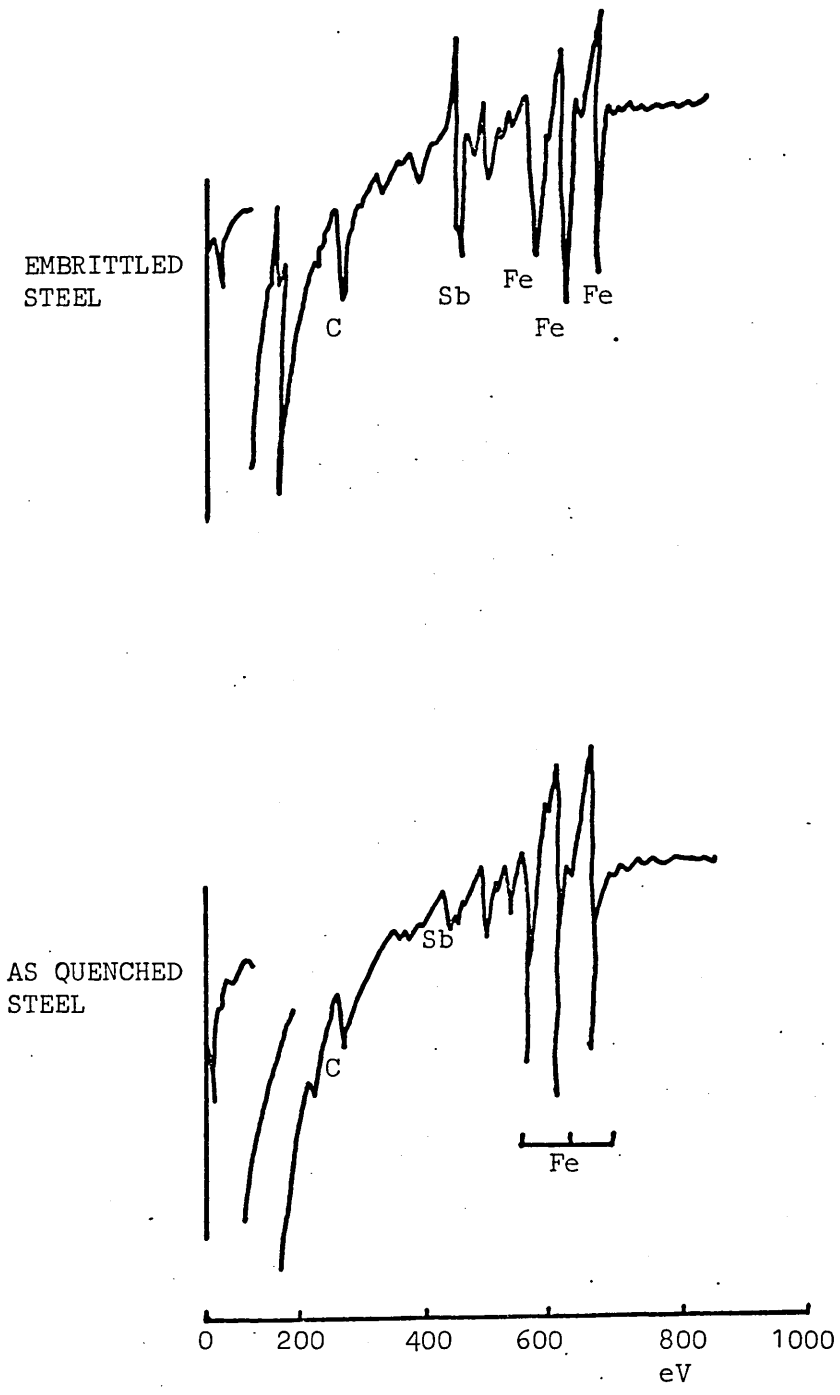
EMBRITTLED
STEEL
C
Sb
Fe
Fe
Fe
AS QUENCHED
STEEL
C
Sb
Fe
0
200
400
600
800
1000
eV

FIGURE 23

Influence of steel purity on embrittlement; effect of reheating on impact transition temperatures of commercial and high-purity Ni-Cr steels [18].

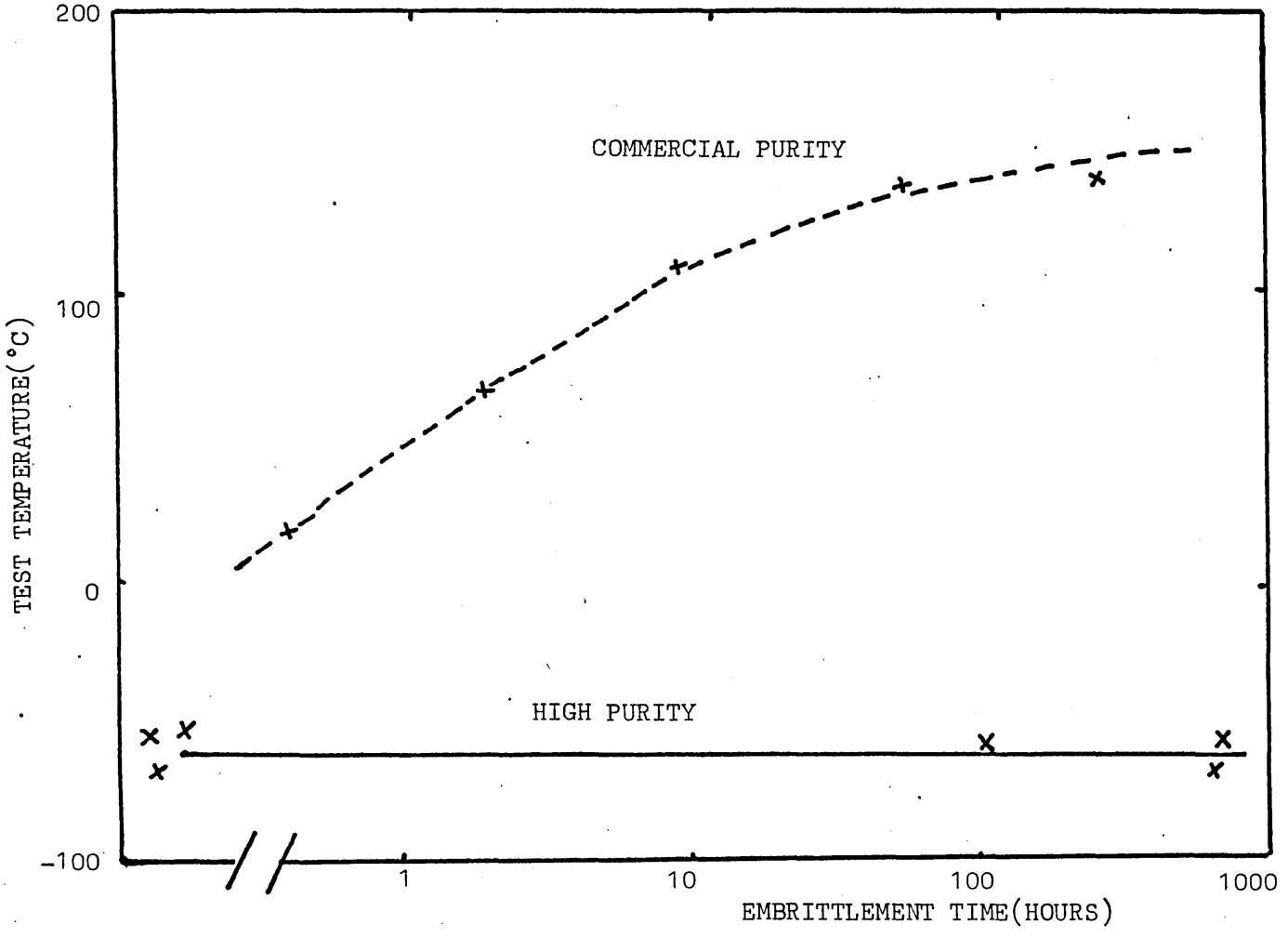
200
100
0
-100
TEST TEMPERATURE(°C)
COMMERCIAL PURITY
HIGH PURITY
1
10
100
1000
EMBRITTLEMENT TIME(HOURS)

FIGURE 24

Diffusivity of P as a function of Temperature in α-Fe.[24]

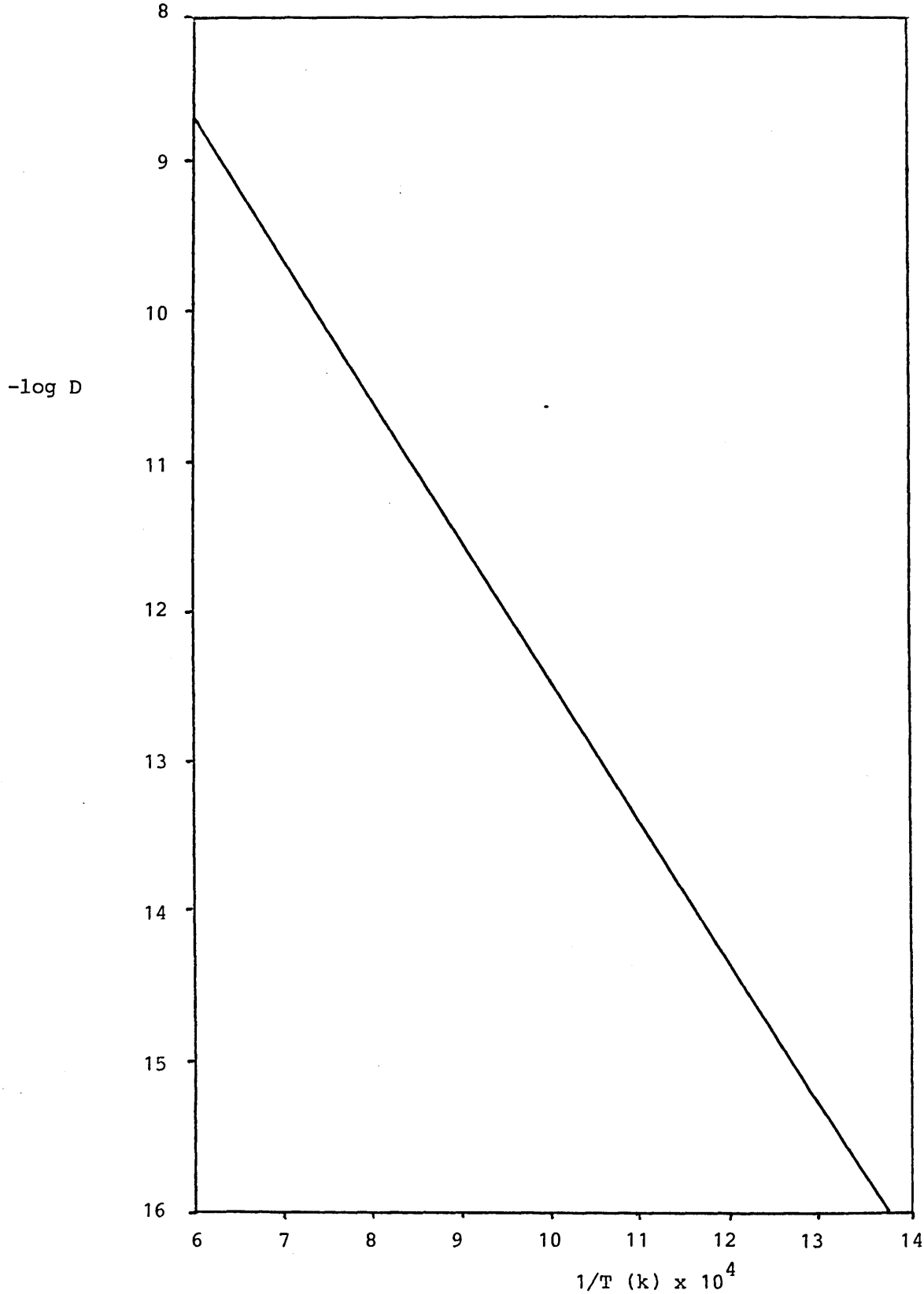
8
9
10
11
12
13
14
15
16
-log D
6
7
8
9
10
11
12
13
14
1/T (k) x 10^4

FIGURE 25

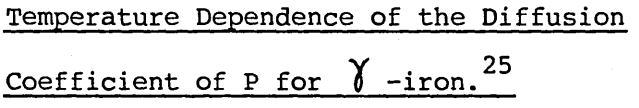

FIGURE 26

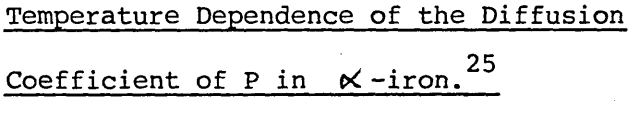

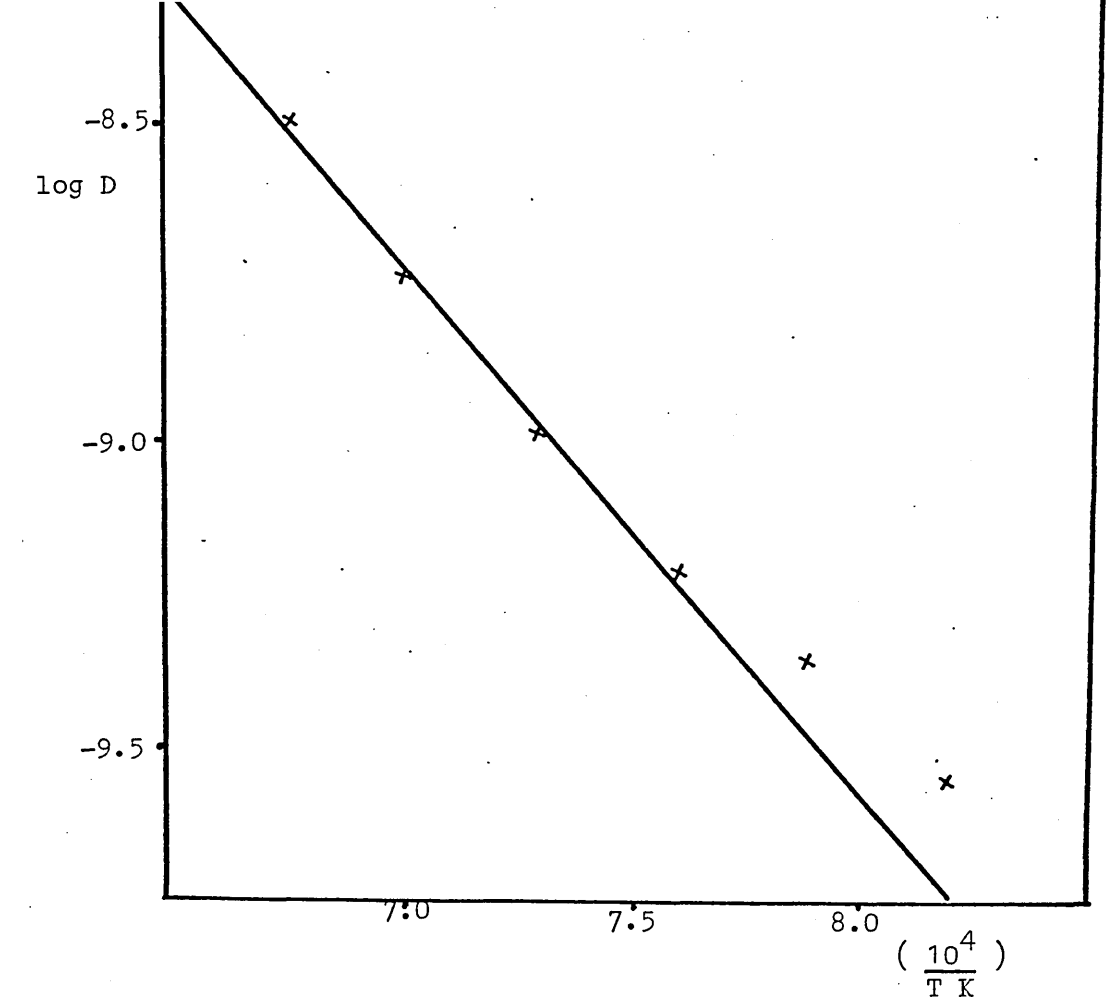
-8.5
log D
-9.0
-9.5
7.0
7.5
8.0
(10^4 / T K)

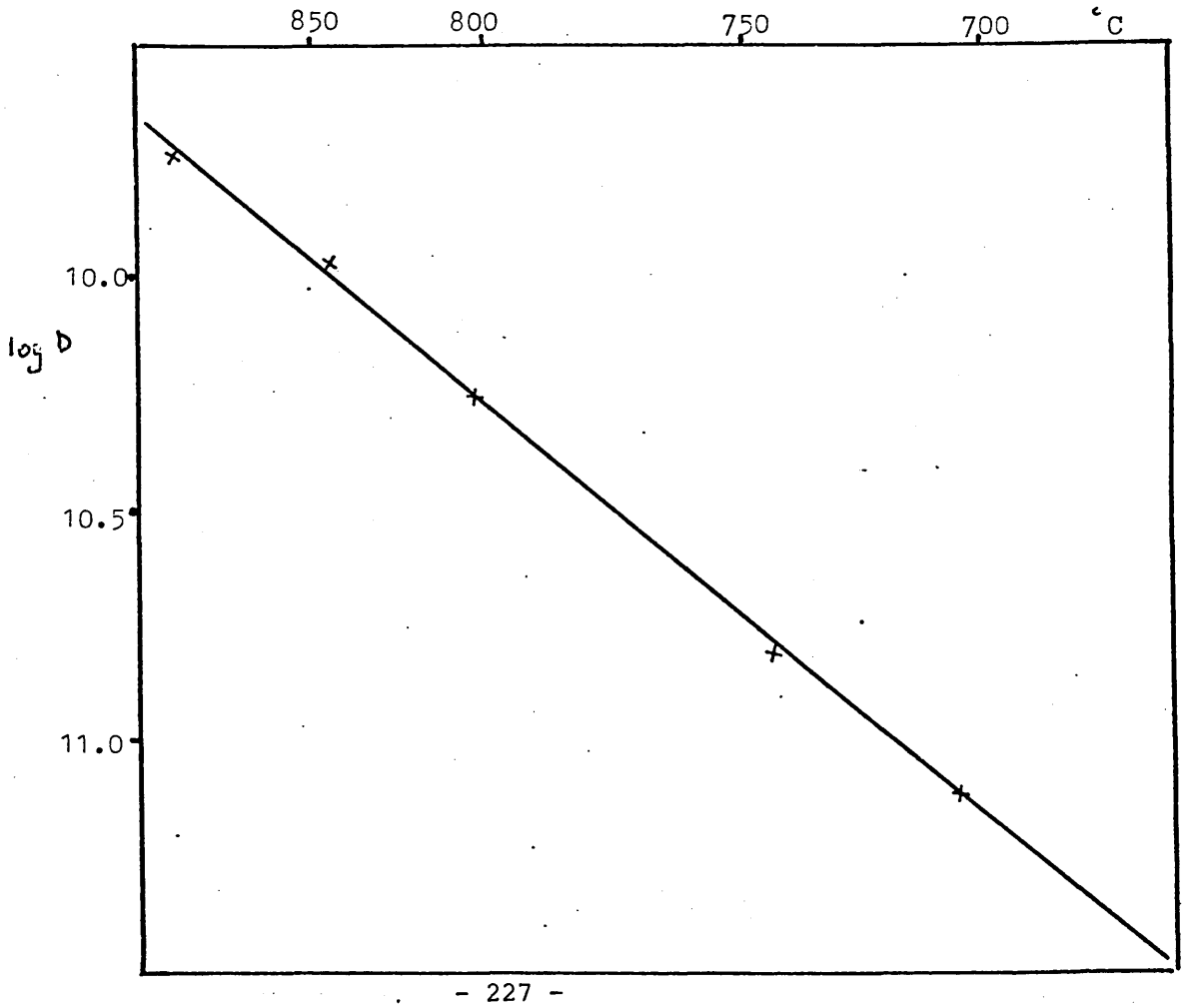
850
800
750
700
°C
10.0
log D
10.5
11.0

FIGURE 27

The Influence of Bulk P Content on the Surface Energy of Iron.[26]

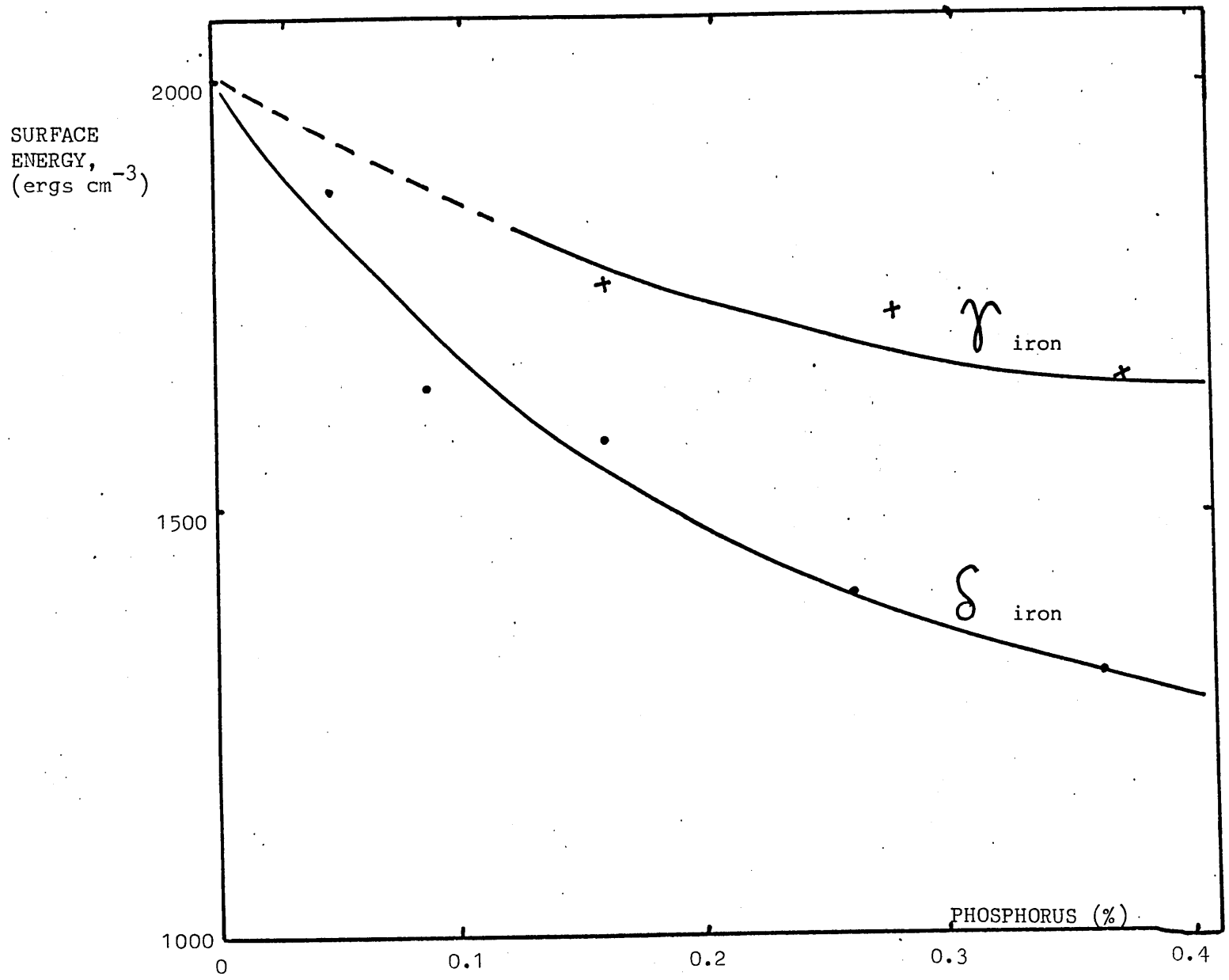
SURFACE
ENERGY,
(ergs cm^{-3})
2000
1500
1000
0
0.1
0.2
0.3
0.4
PHOSPHORUS (%)
γ iron
δ iron

FIGURE 28

Effect of Aging Temperature on Rate and Amount of P Segregation to Grain Boundaries in a Ni-Cr Steel.[31]

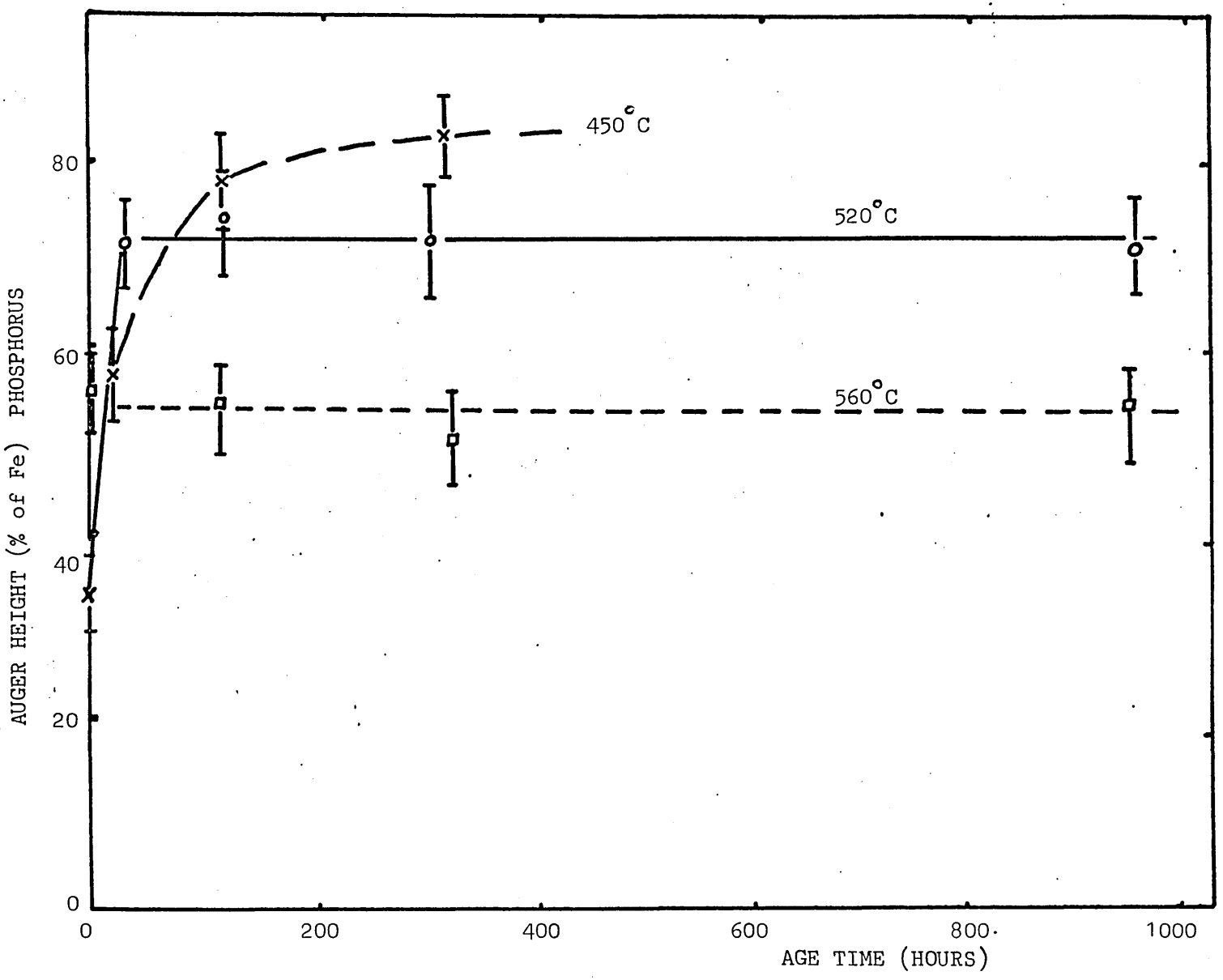
450°C
520°C
560°C
AUGER HEIGHT (% of Fe) PHOSPHORUS
AGE TIME (HOURS)
0
20
40
60
80
0
200
400
600
800
1000

FIGURE 29

Variation in the Grain Boundary Nickel Concentration as a Function of Aging Temperature and Time.[52]

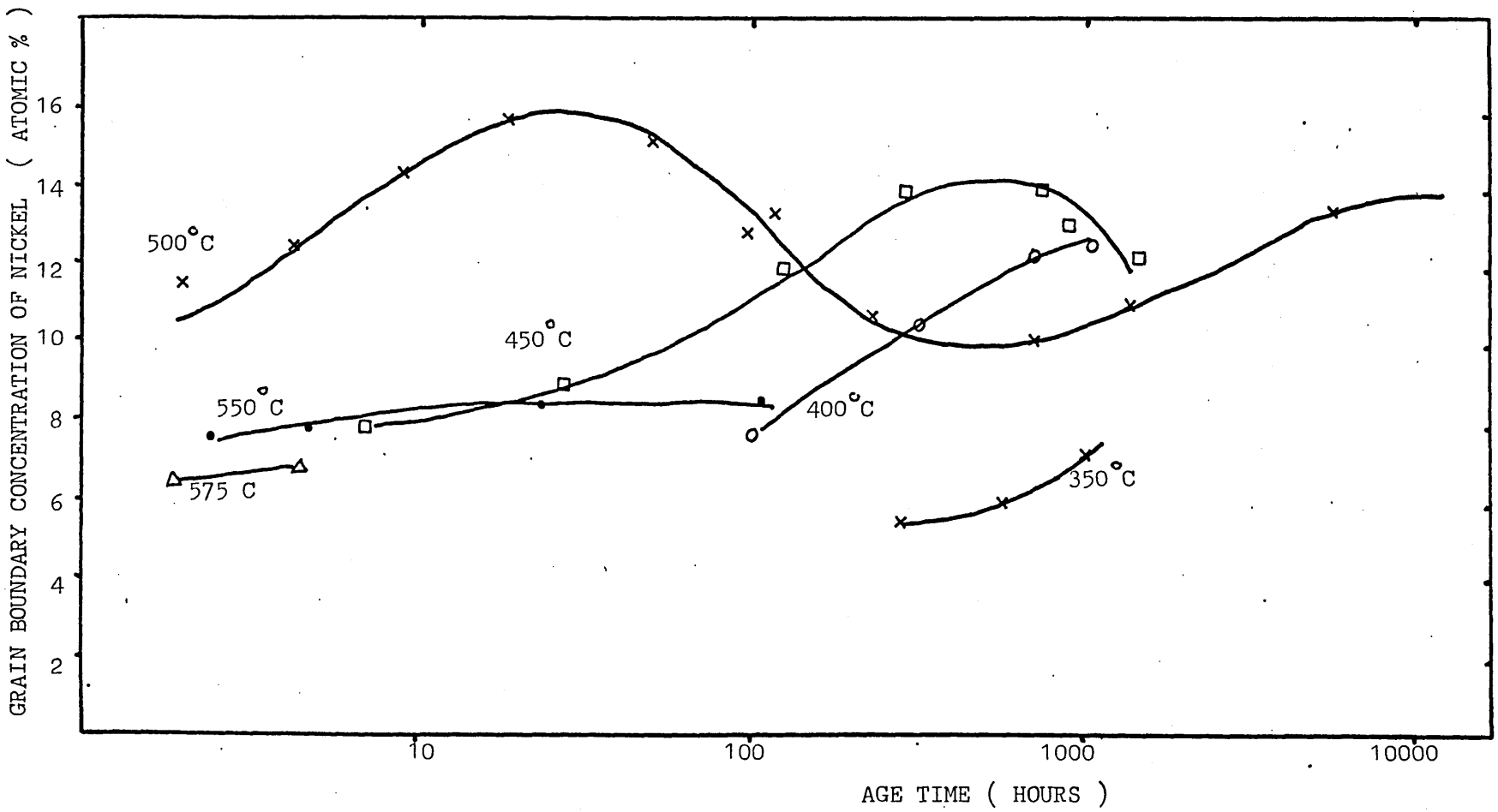
GRAIN BOUNDARY CONCENTRATION OF NICKEL (ATOMIC %)
16
14
12
10
8
6
4
2
500°C
450°C
550°C
400°C
575 C
350°C
10
100
1000
10000
AGE TIME (HOURS)

FIGURE 30

Ion Bombardment Concentration Profiles.[52]

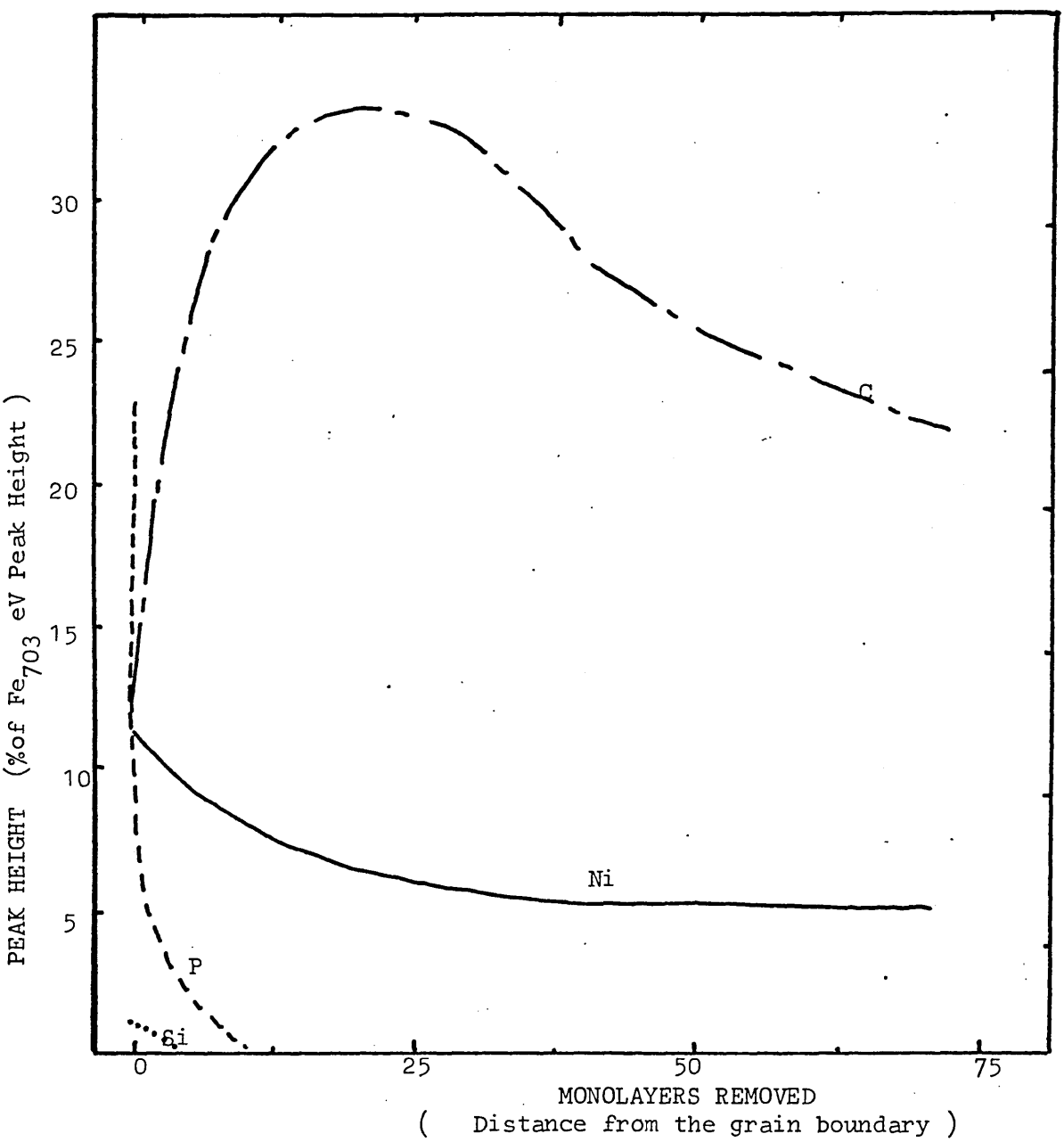
PEAK HEIGHT (%of Fe703 eV Peak Height)
30
25
20
15
10
5
C
Ni
P
Si
0
25
50
75
MONOLAYERS REMOVED
(Distance from the grain boundary)

FIGURE 31

Average Percentage Reduction of SF max for Various Increments of Molybdenum Content.[69]

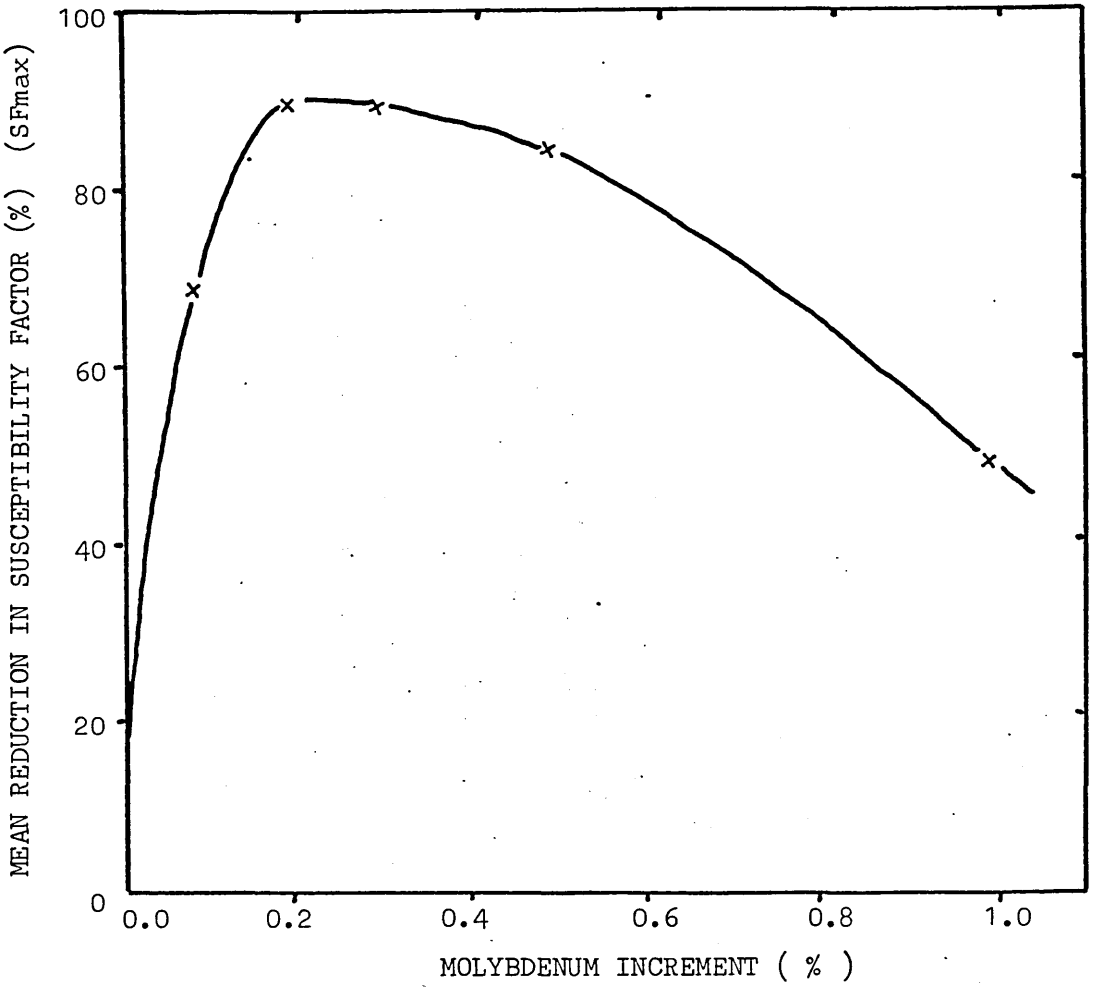
MEAN REDUCTION IN SUSCEPTIBILITY FACTOR (%) (SFmax)
100
80
60
40
20
0
0.0
0.2
0.4
0.6
0.8
1.0
MOLYBDENUM INCREMENT (%)

FIGURE 32

Effect of Mo Content on Improvement of the 35 ft. lb. Impact Transition Temperature[69]

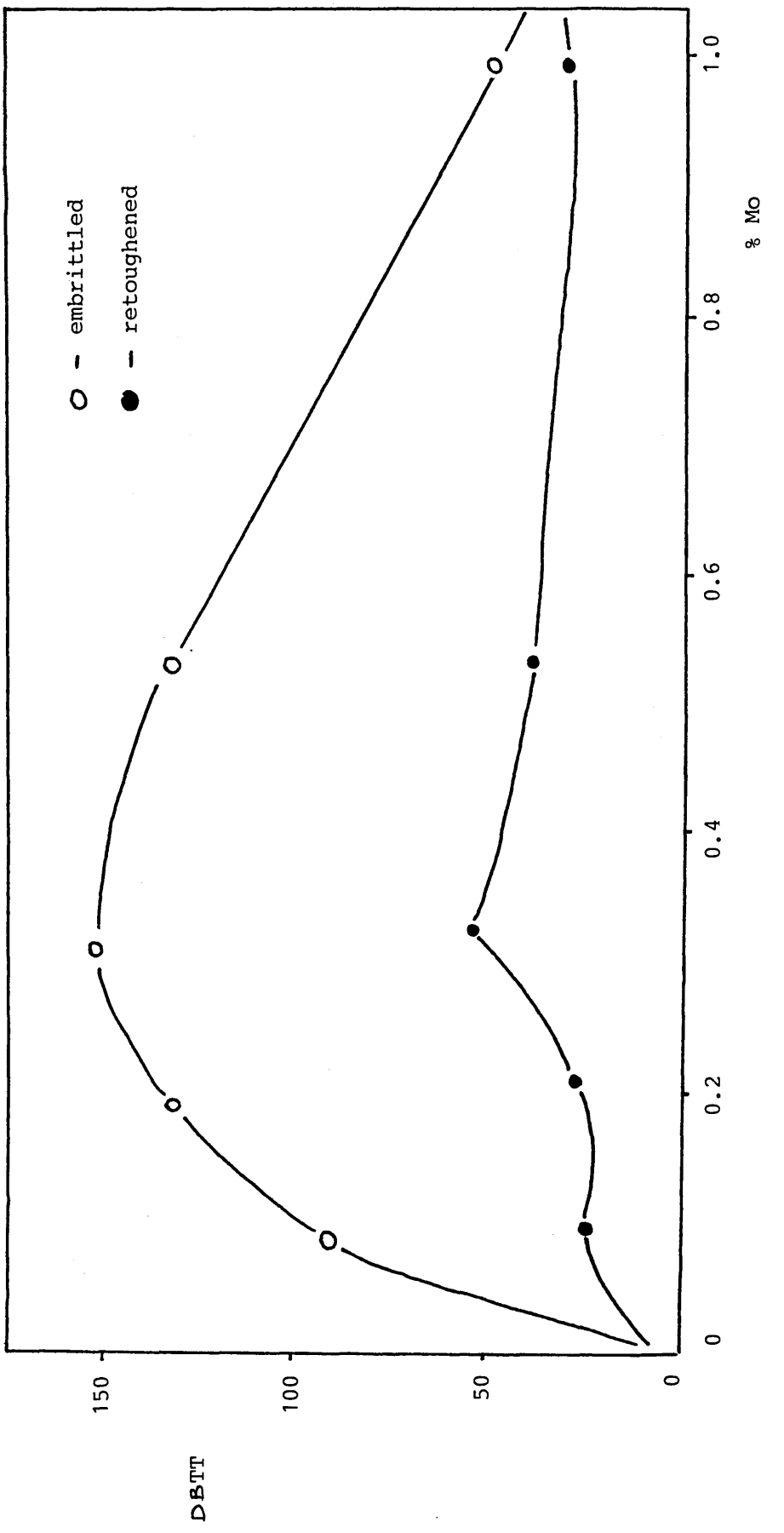
O - embrittled
● - retoughened
DBTT
150
100
50
0
0
0.2
0.4
0.6
0.8
1.0
% Mo

FIGURE 33

Effect of Mo Content on Various Strength Functions of Experimental Steels.[69]

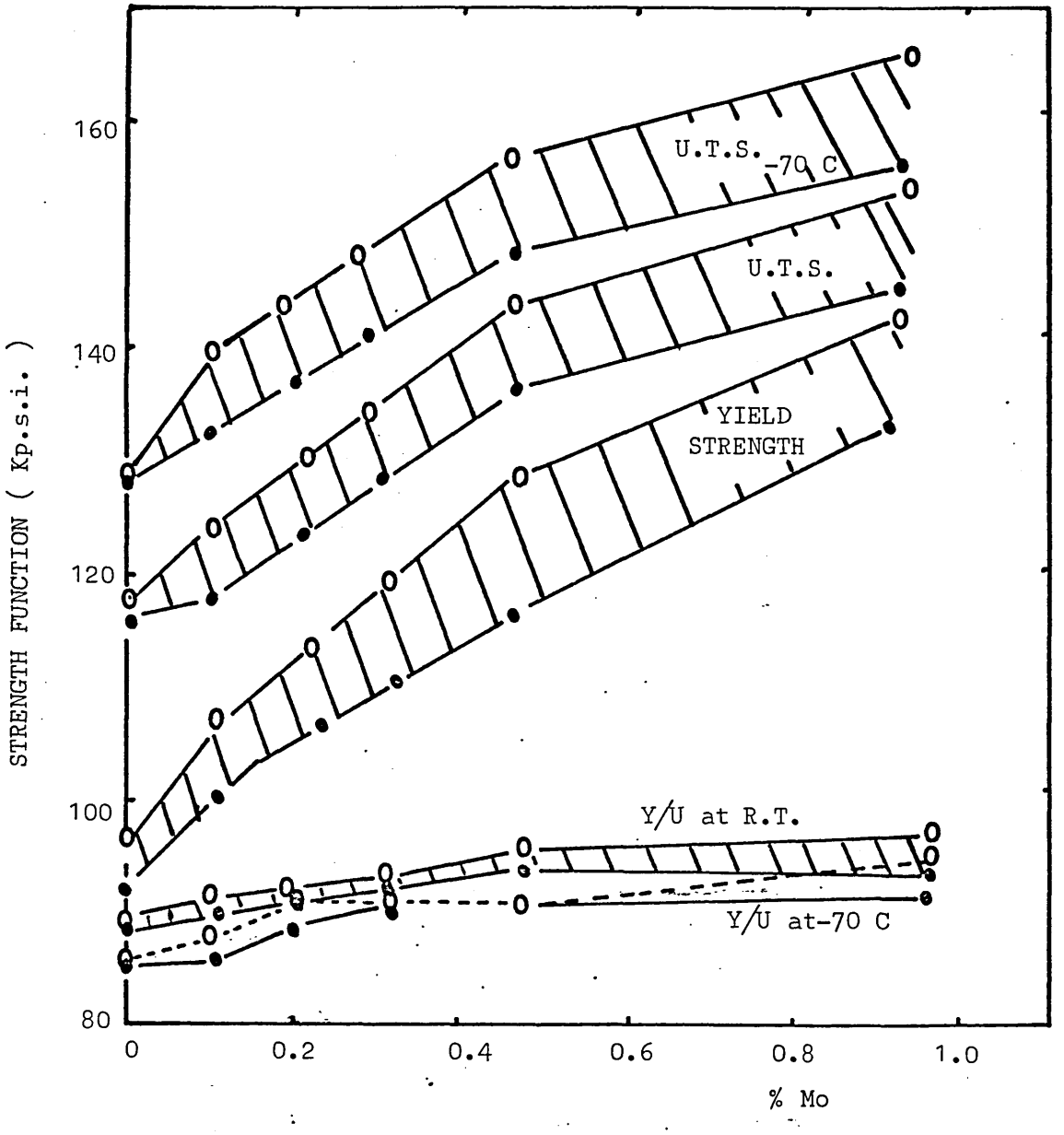
160
140
120
100
80
STRENGTH FUNCTION (Kp.s.i.)
U.T.S. -70 C
U.T.S.
YIELD STRENGTH
Y/U at R.T.
Y/U at-70 C
0
0.2
0.4
0.6
0.8
1.0
% Mo

FIGURE 34

Schematic Representation of Excess Grain Boundary Concentration as a Function of Temperature Showing Step Cooling Heat Treatment[67]

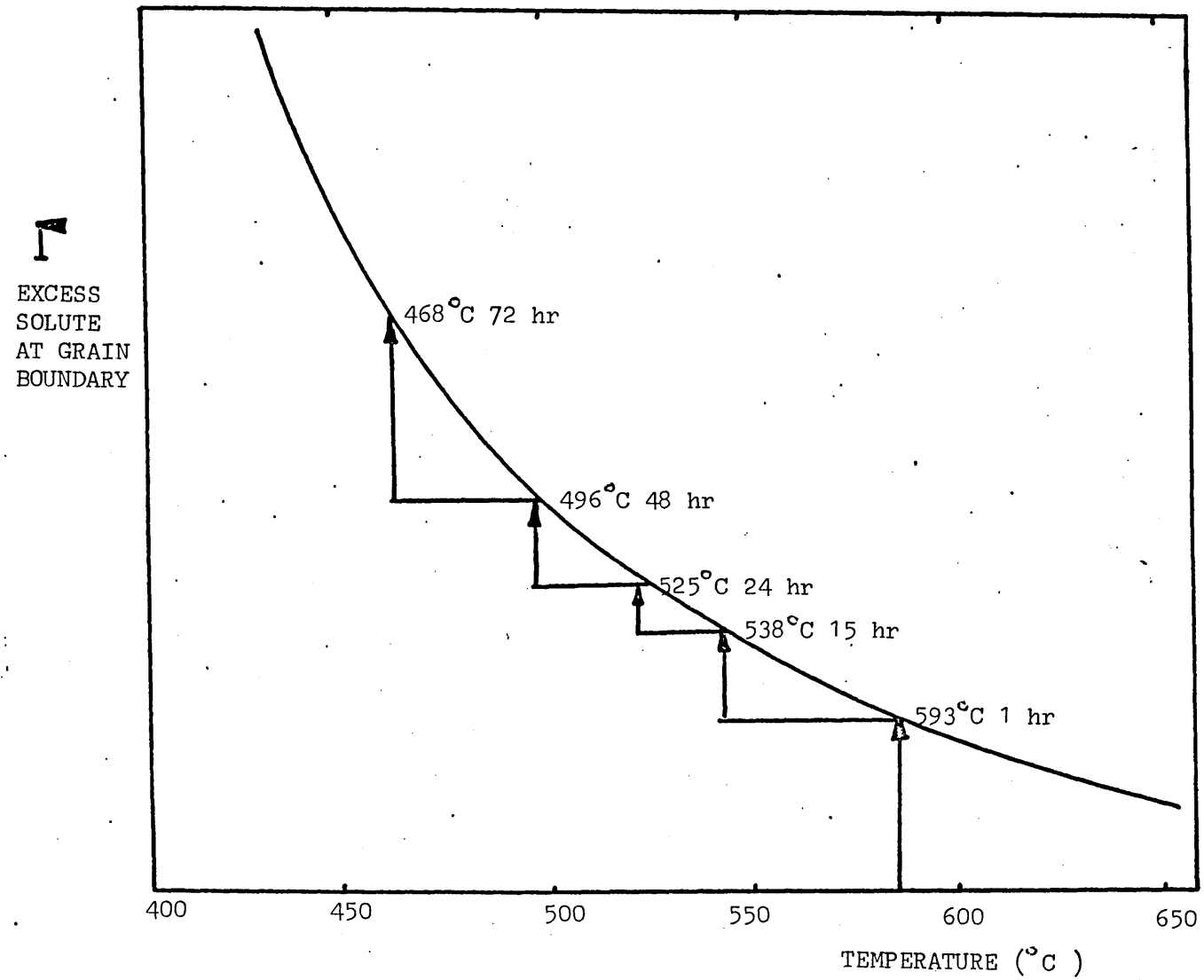
EXCESS
SOLUTE
AT GRAIN
BOUNDARY
468°C 72 hr
496°C 48 hr
525°C 24 hr
538°C 15 hr
593°C 1 hr
400
450
500
550
600
650
TEMPERATURE (°C)

FIGURE 35

Comparison of Stability of Various Compounds in Steel[133]

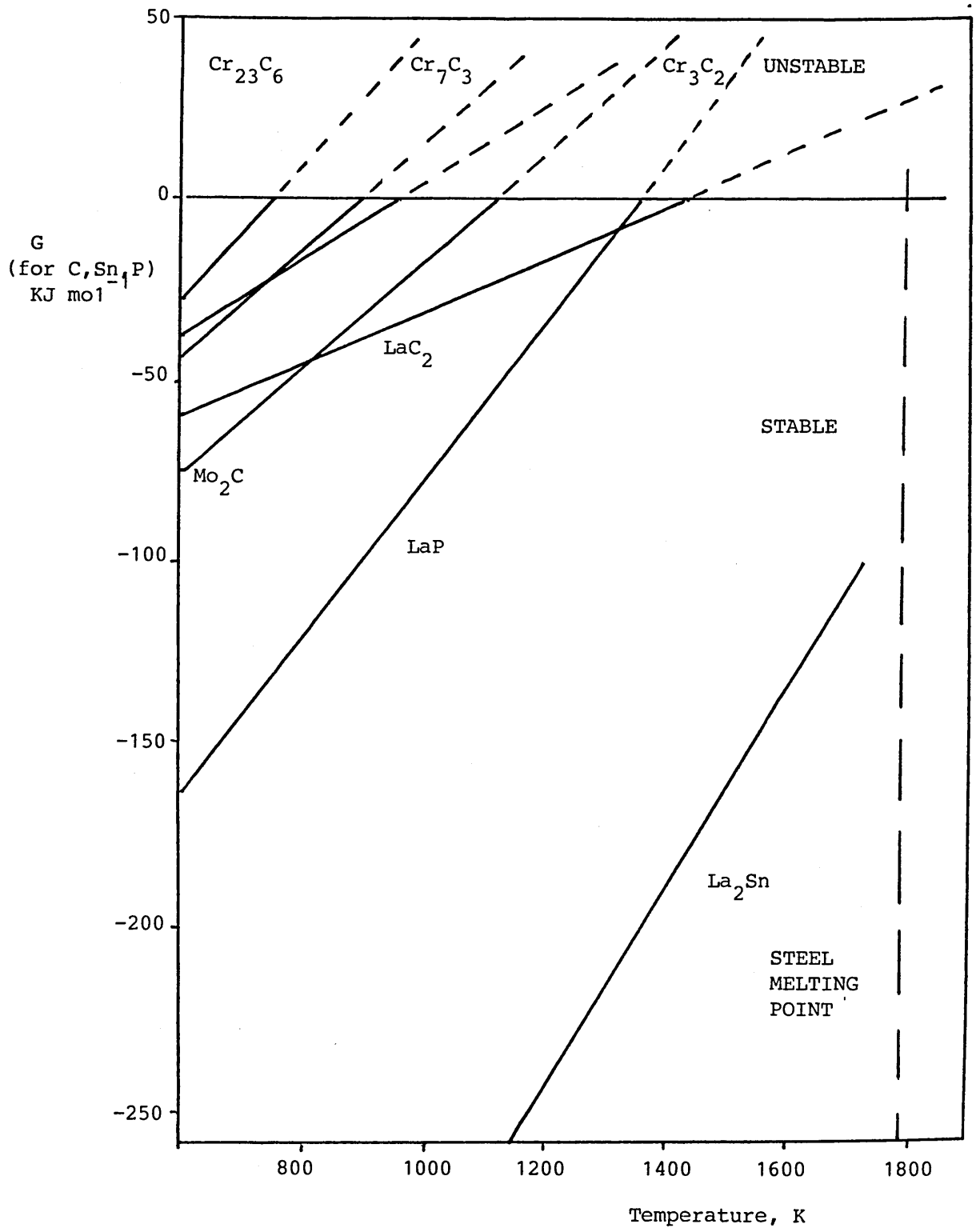
50
0
-50
-100
-150
-200
-250
G
(for C,Sn,P)
KJ mol^{-1}
$Cr_{23}C_6$
Cr_7C_3
Cr_3C_2
UNSTABLE
LaC_2
STABLE
Mo_2C
LaP
La_2Sn
STEEL
MELTING
POINT
800
1000
1200
1400
1600
1800
Temperature, K

FIGURE 36

Carbide-Ferrite Interface Cracks in Fe-Sb, Fe-Sn, and Fe-As. Tested at 77°K, 800x.[58]

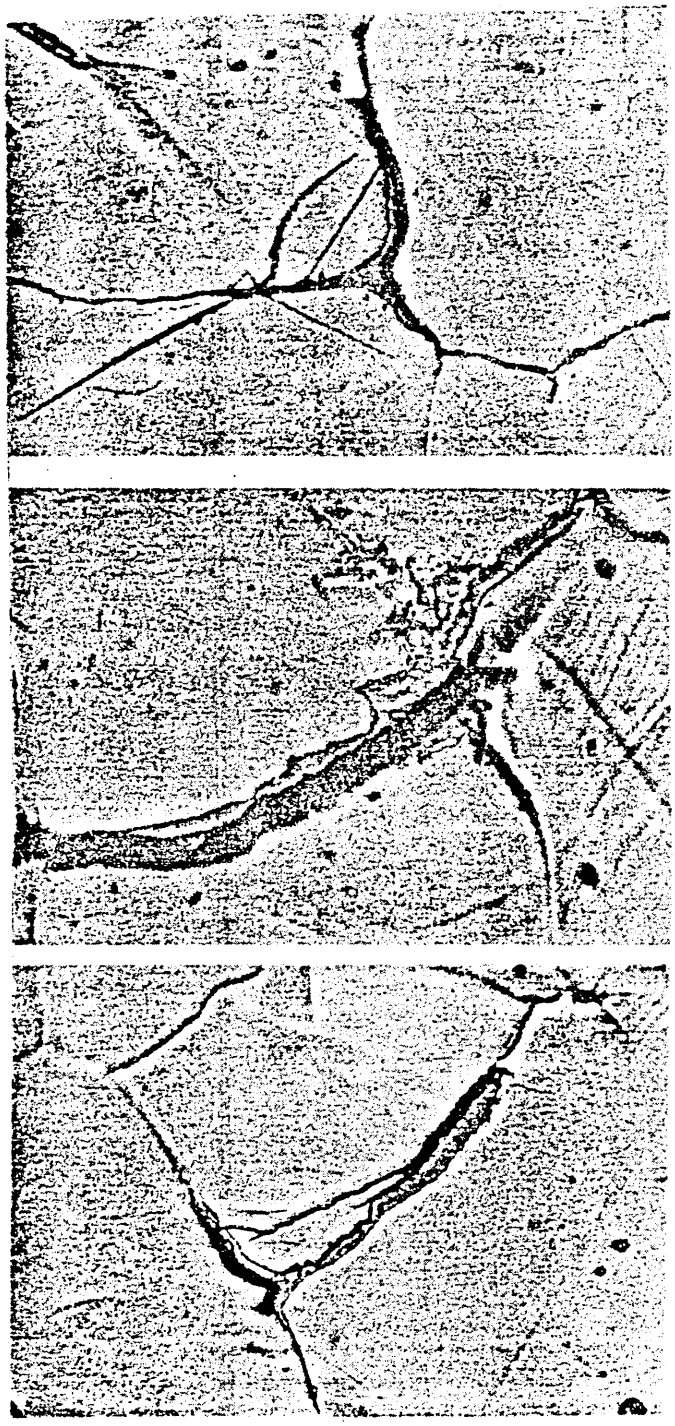

FIGURE 37

Variation of Ductility and Mode of Fracture with Quenching Temperature for Iron[74]

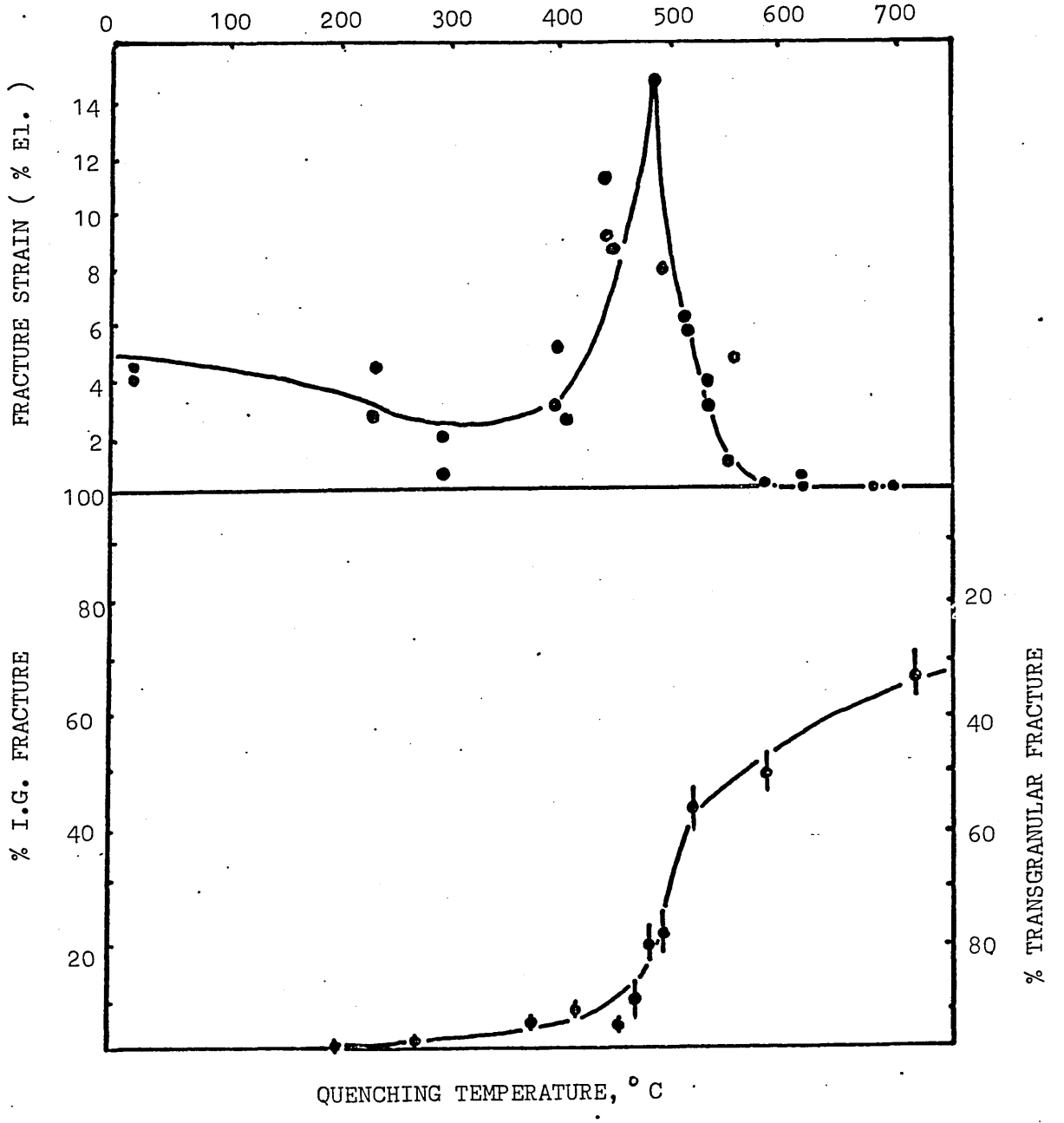
0
100
200
300
400
500
600
700
FRACTURE STRAIN (% El.)
14
12
10
8
6
4
2
100
80
60
40
20
% I.G. FRACTURE
20
40
60
80
% TRANSGRANULAR FRACTURE
QUENCHING TEMPERATURE, ° C

FIGURE 38

Typical Examples of Splitting Along the Carbide-Ferrite Interface in Embrittled Fe-0.04% C doped with Sb Tested in Tension at 110K.[77]


10 μ

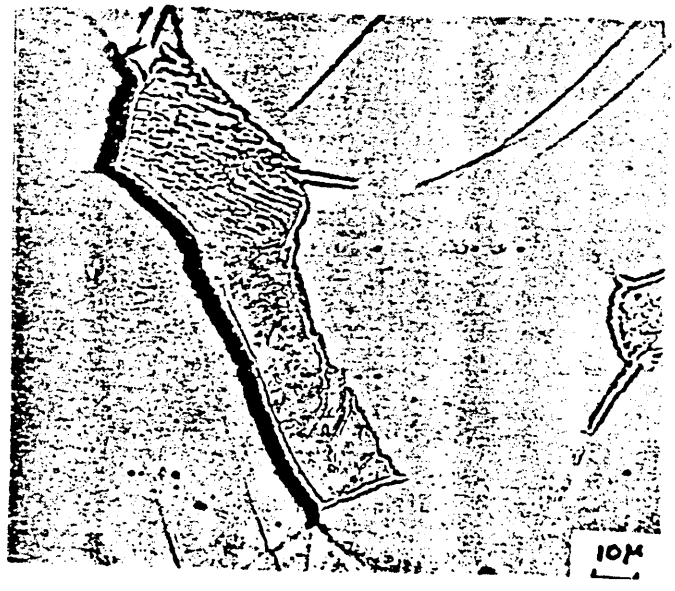
10μ

FIGURE 39

Schematic Representation of Embrittlement by Rejection of Embrittling Elements from Carbides.
(a) Initial Embrittlement by Slow Cooling from Austenite;
(b) Reversal by Heating to 650°C and Quenching;
(c) Re-Embrittlement by Reheating at 480°C.[77]

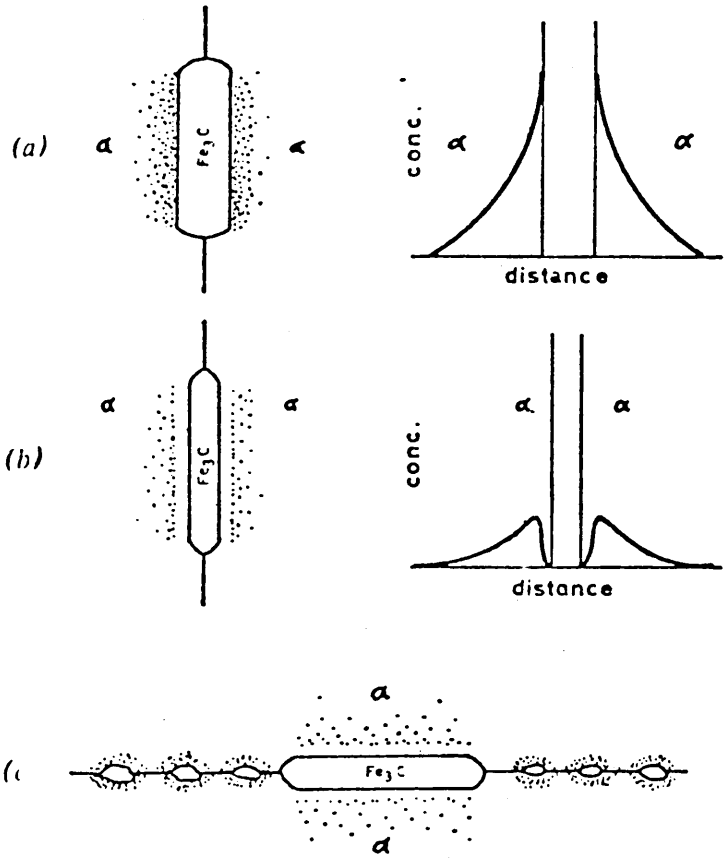
(a)
α
Fe3C
α
conc.
α
α
distance
(b)
α
Fe3C
α
conc.
α
α
distance
(c
α
Fe3C
α

FIGURE 40

Schematic Representation of Solute Distribution During the Growth of a β Plate into an α Matrix Under Isothermal Conditions where Partitioning is Complete and Growth Rate is Limited by Solute Diffusion in α.[77]

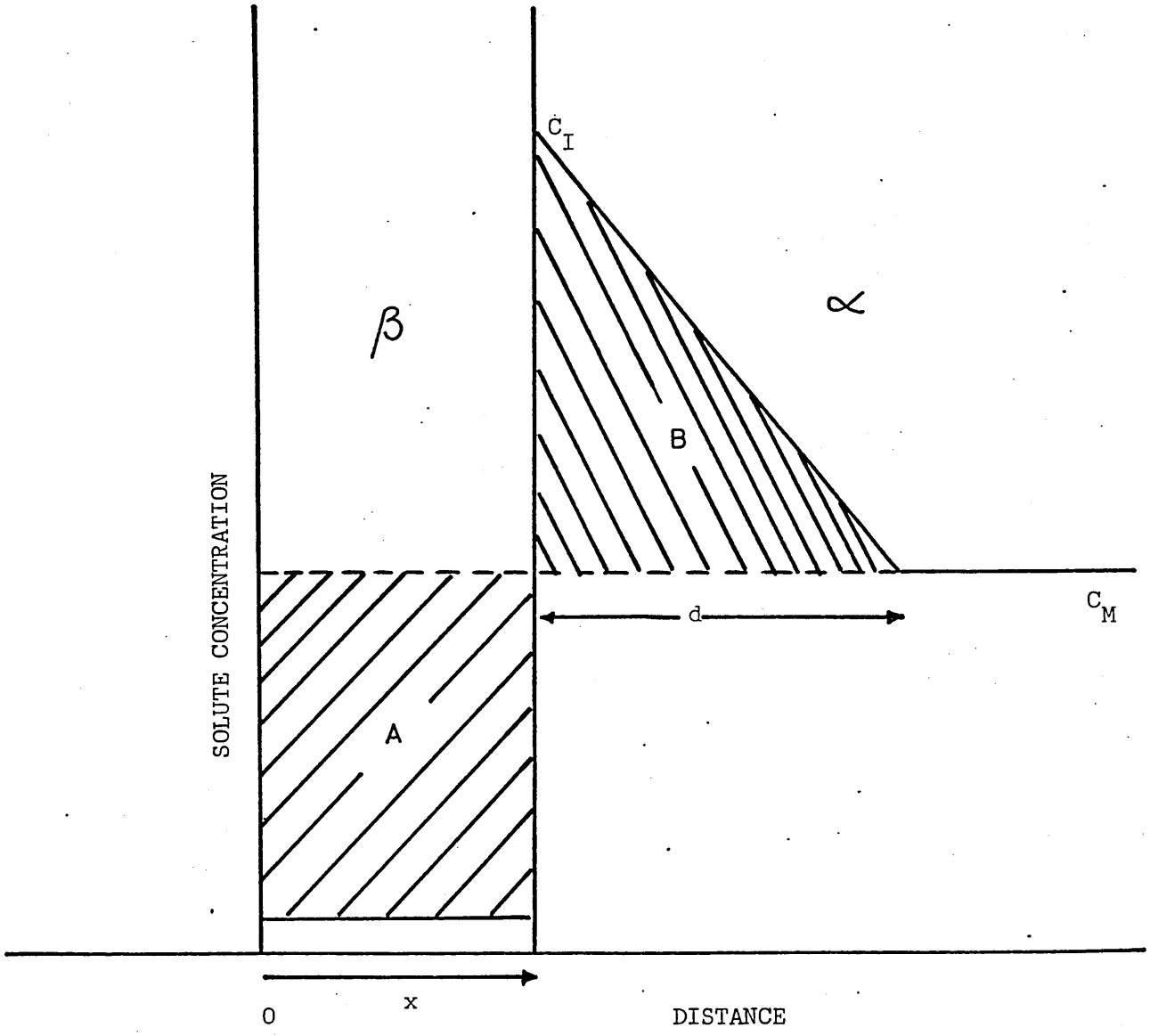
C_I
β
α
B
A
SOLUTE CONCENTRATION
d
C_M
0
x
DISTANCE

FIGURE 41

Solute Distribution Assumed for Carbide Precipitation during Continuous Cooling.[77]

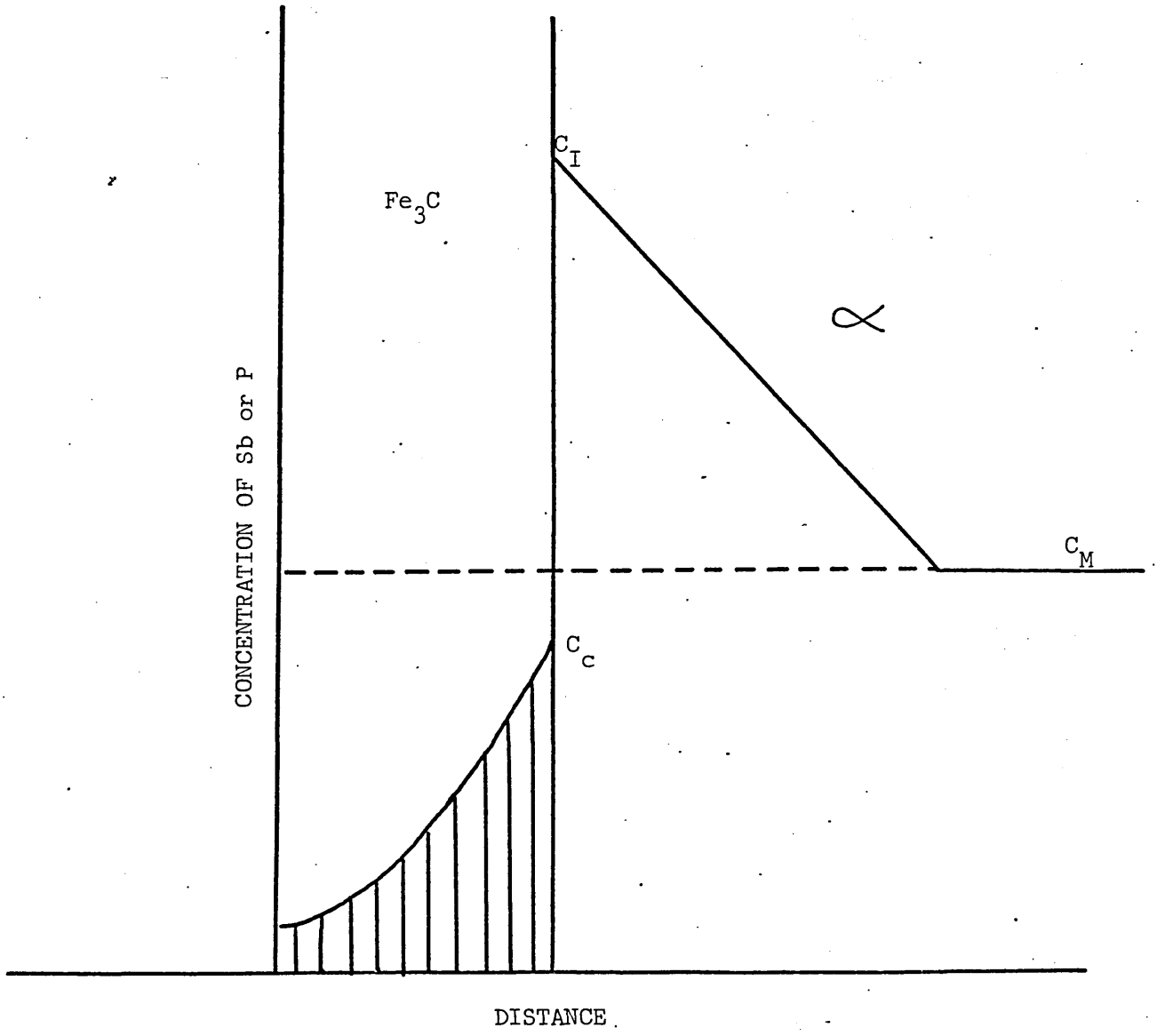
C_I
Fe_3C
α
C_M
C_C
CONCENTRATION OF Sb or P
DISTANCE

FIGURE 42

Effect of Austenite Grain Size on the Transition Temperature of Ni-Cr Steels Doped with P or Sn at a Fixed Hardness and Intergranular Dopant Concentration.[21, 31]

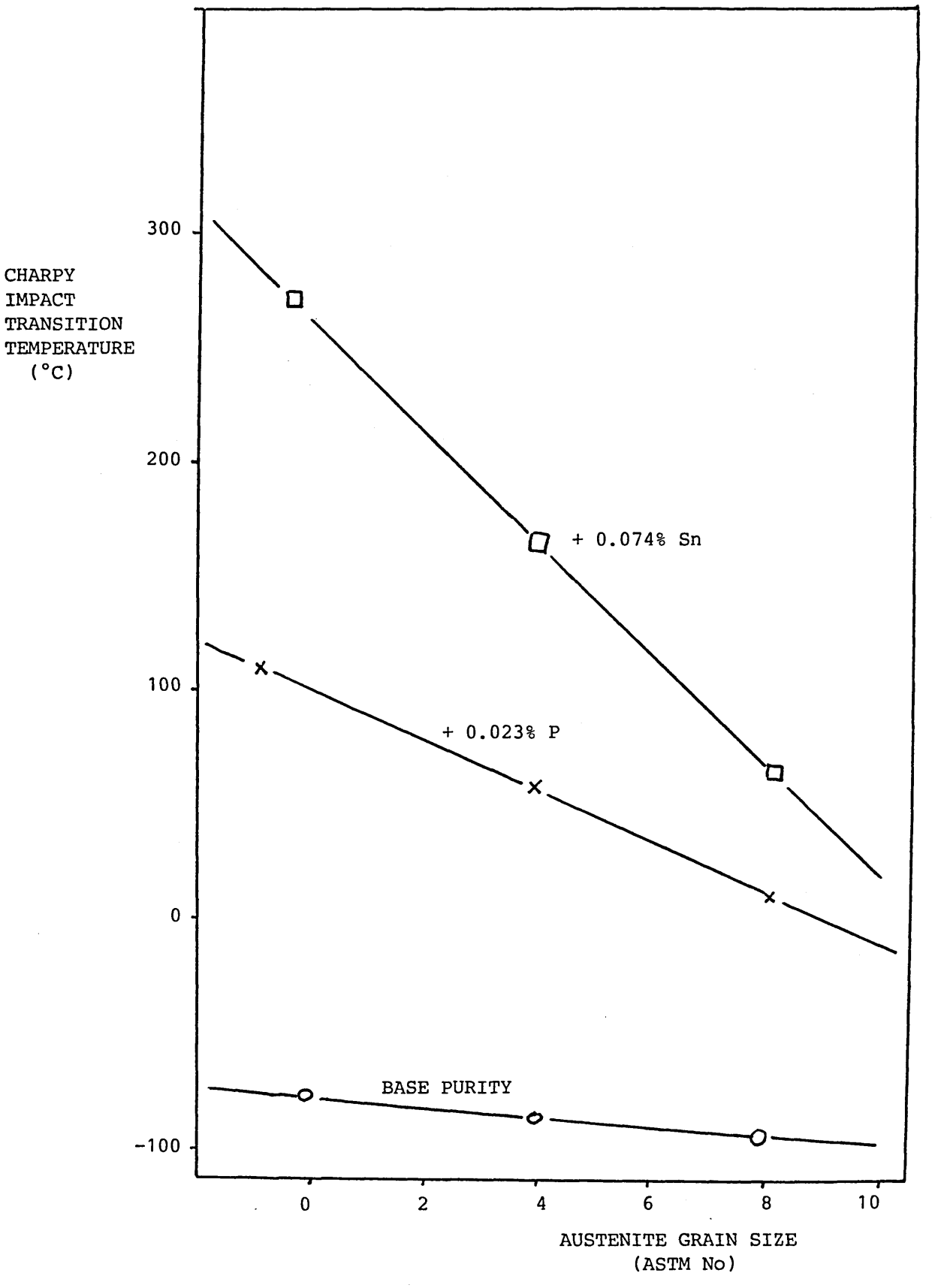
CHARPY
IMPACT
TRANSITION
TEMPERATURE
(°C)
300
200
100
0
-100
+ 0.074% Sn
+ 0.023% P
BASE PURITY
0
2
4
6
8
10
AUSTENITE GRAIN SIZE
(ASTM No)

FIGURE 43

The Time-Temperature Diagram for Embrittlements of SAE 3140 Corrected to Constant Hardness.[89]

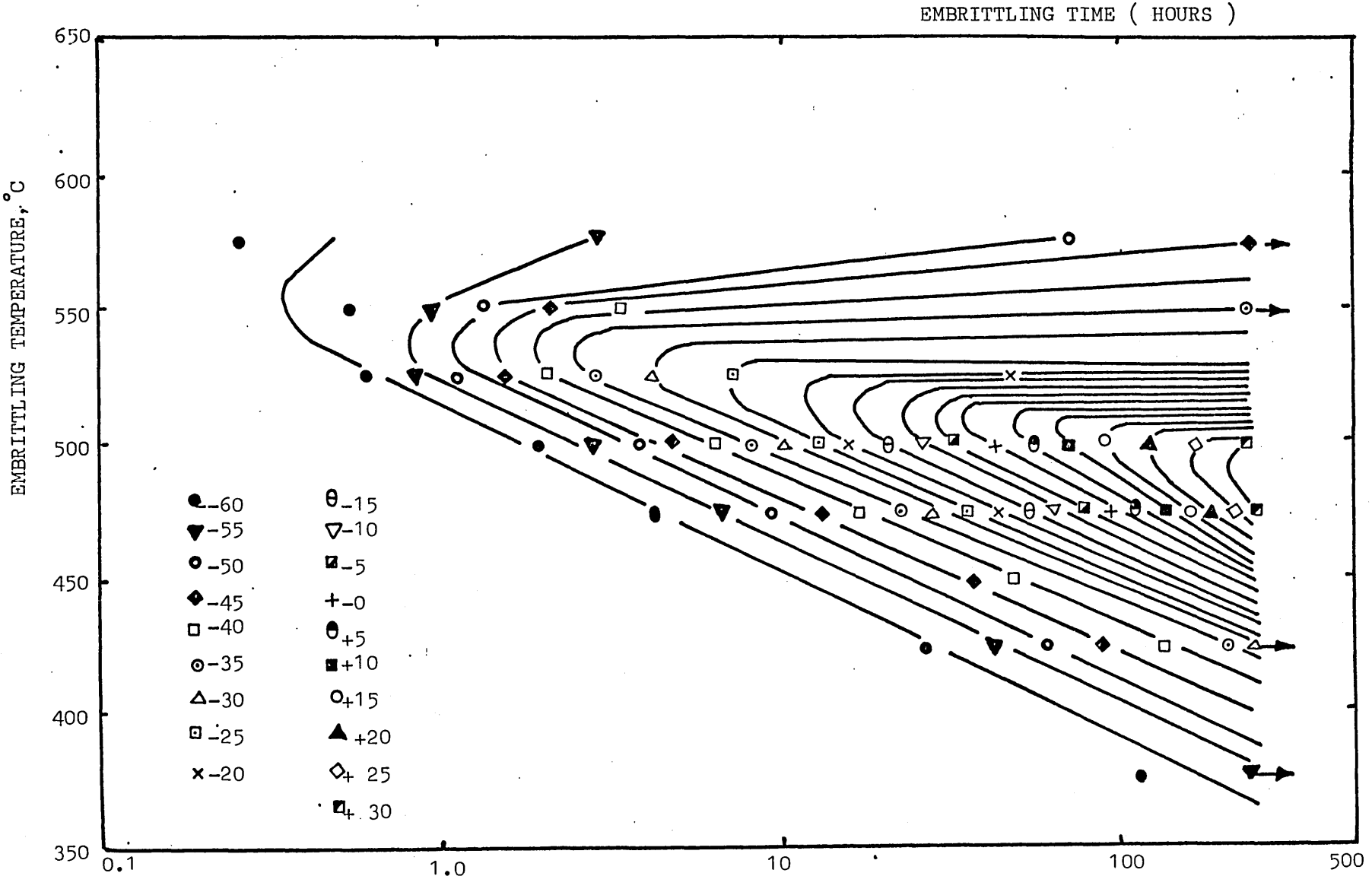
EMBRITTLING TIME (HOURS)
EMBRITTLING TEMPERATURE, °C
650
600
550
500
450
400
350
0.1
1.0
10
100
500
-60
-55
-50
-45
-40
-35
-30
-25
-20
-15
-10
-5
-0
+5
+10
+15
+20
+ 25
+ 30

FIGURE 44

Schematic Representation of a Model for Temper Embrittlement[87] Showing Effect of Tempering Temperature on Toughness

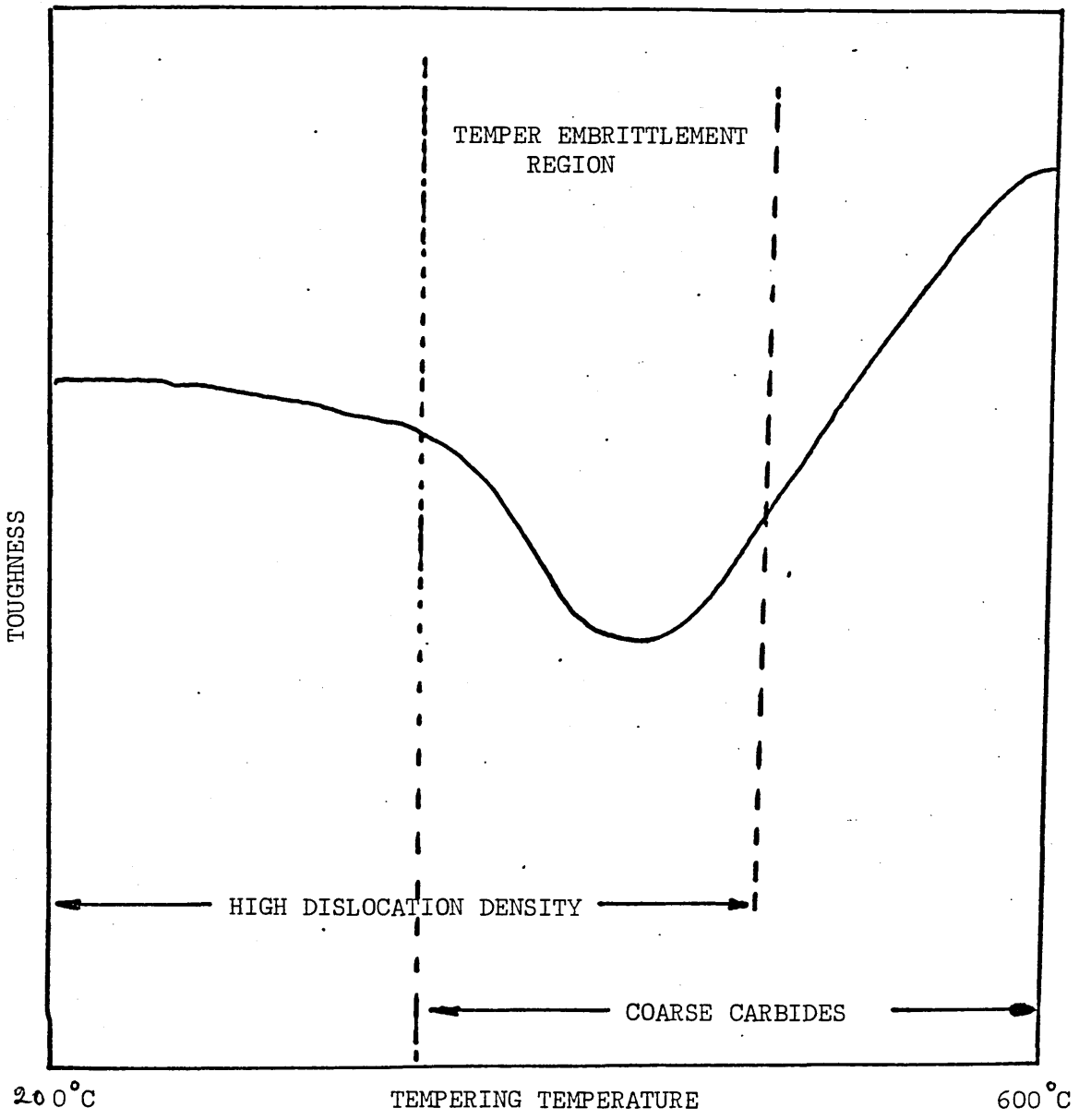
TEMPER EMBRITTLEMENT
REGION
TOUGHNESS
HIGH DISLOCATION DENSITY
COARSE CARBIDES
200°C
TEMPERING TEMPERATURE
600°C

FIGURE 45

The Predicted Extra Segregation of Phosphorus[88] as a Result of a 200h Embrittlement as a Function of Isothermal Holding Temperature with Experimental Data of Carr et al.[89]

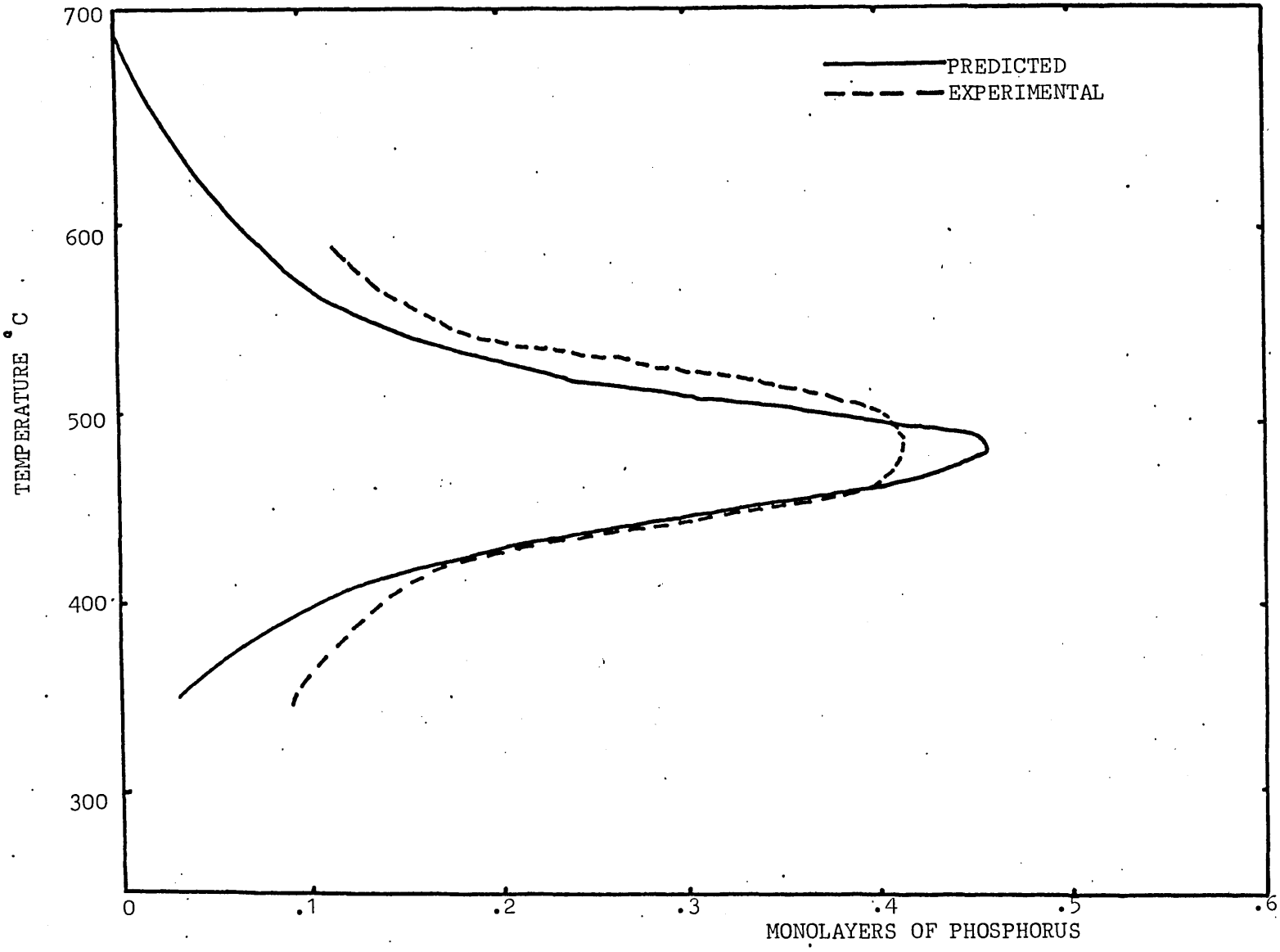
700
600
500
400
300
TEMPERATURE °C
PREDICTED
EXPERIMENTAL
0
.1
.2
.3
.4
.5
.6
MONOLAYERS OF PHOSPHORUS

FIGURE 46

Heat Treatment Involved in One Step

Temper Embrittlement

Two Step Temper Embrittlement.

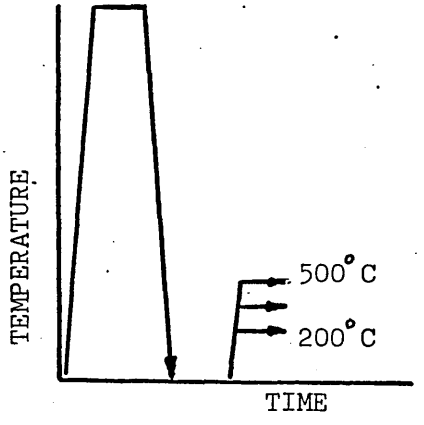
TEMPERATURE
500°C
200°C
TIME

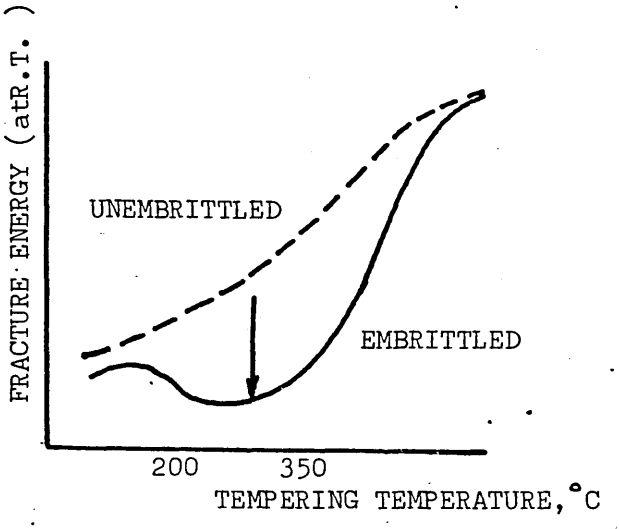
FRACTURE ENERGY (at R.T.)
UNEMBRITTLED
EMBRITTLED
200
350
TEMPERING TEMPERATURE, °C

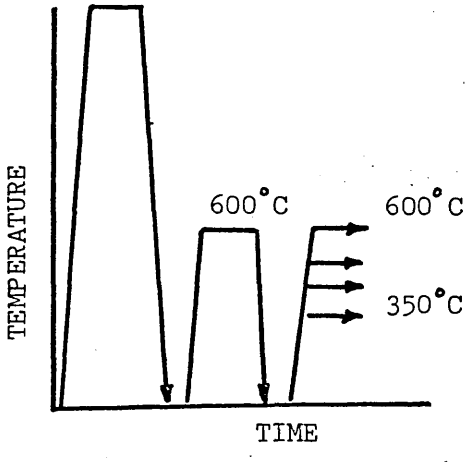
TEMPERATURE
600°C
600°C
350°C
TIME

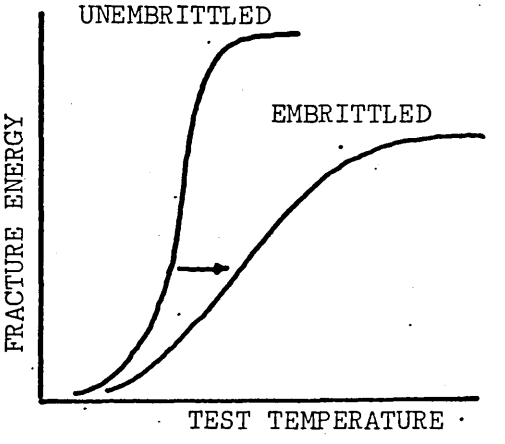
UNEMBRITTLED
EMBRITTLED
FRACTURE ENERGY
TEST TEMPERATURE

FIGURE 47

Correlation of Grain Boundary Enrichment Factors with Atomic Solid Solubility. Open Circles are Obtained by the Interface Energy Approach; Filled Circles by Auger Electron Spectroscopy; Open Triangles by Self Diffusion in the Lattice and Grain Boundaries; Open Diamond by Sulphur Diffusion.[98,99]

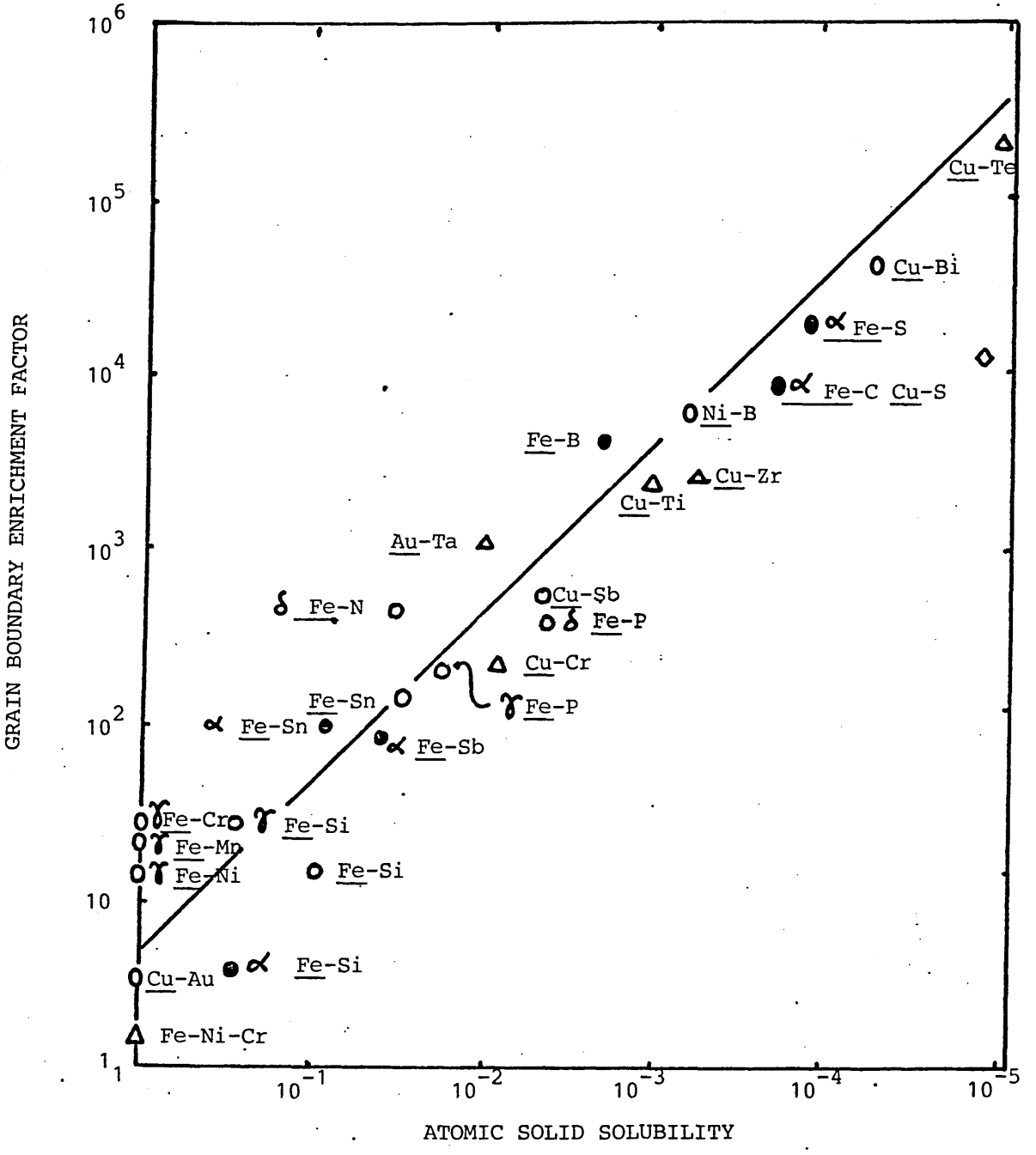
GRAIN BOUNDARY ENRICHMENT FACTOR
10^6
10^5
10^4
10^3
10^2
10
1
10^{-1}
10^{-2}
10^{-3}
10^{-4}
10^{-5}
ATOMIC SOLID SOLUBILITY
Cu-Te
Cu-Bi
Fe-S
Fe-C Cu-S
Ni-B
Fe-B
Cu-Zr
Cu-Ti
Au-Ta
Fe-N
Cu-Sb
Fe-P
Cu-Cr
Fe-Sn
Fe-P
Fe-Sn
Fe-Sb
Fe-Cr
Fe-Si
Fe-Mn
Fe-Ni
Fe-Si
Cu-Au
Fe-Si
Fe-Ni-Cr

FIGURE 48

Hardness Profiles (1g. load) Near a Grain Boundary in Zinc with 100 ppm Al, and in Zinc with 100 ppm Au.[101]

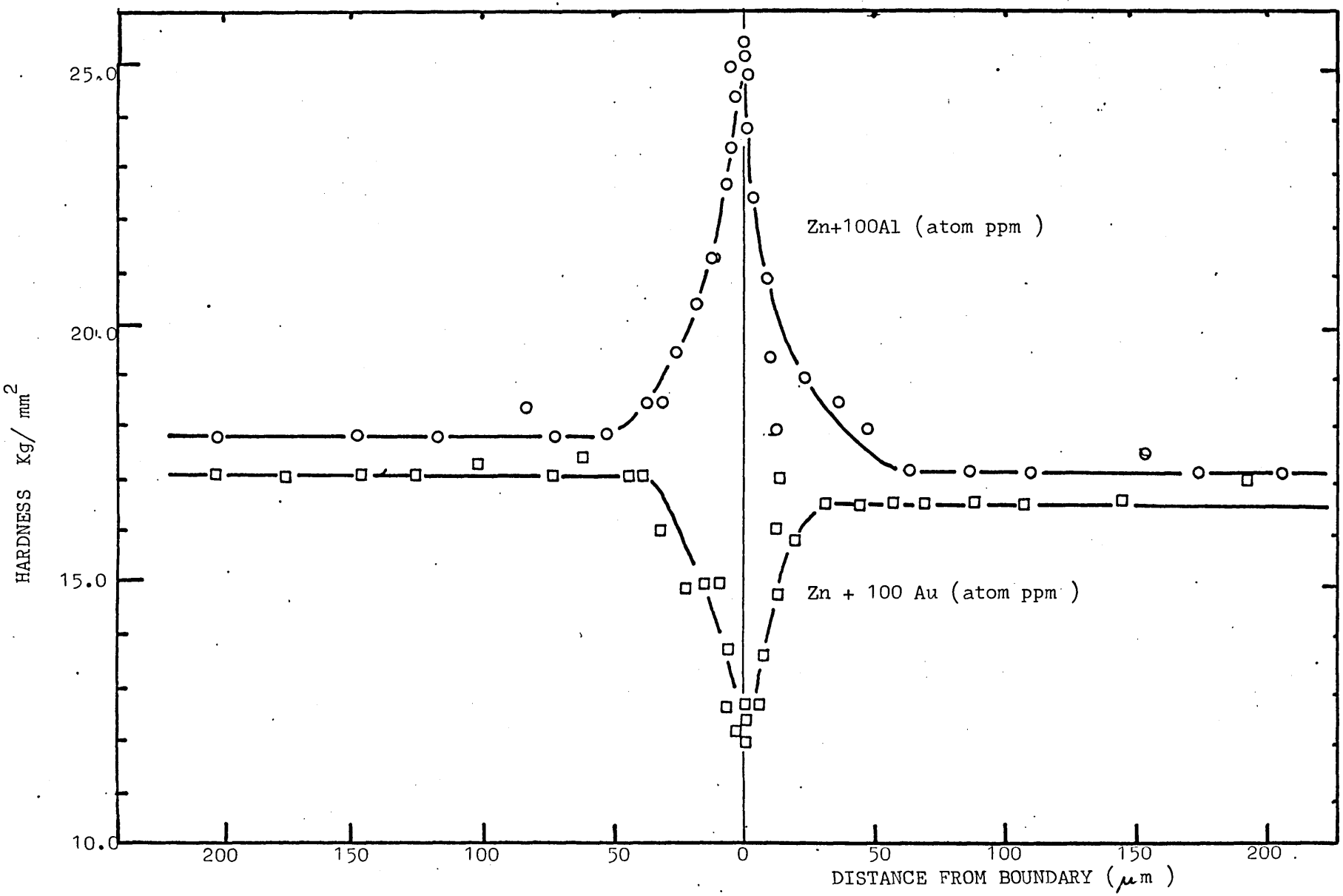
25.0
20.0
15.0
10.0
HARDNESS Kg/ mm^2
Zn+100Al (atom ppm)
Zn + 100 Au (atom ppm)
200
150
100
50
0
50
100
150
200
DISTANCE FROM BOUNDARY (μm)

FIGURE 49

Energy Level Diagram in an Atom Depicting a Single Event in Electron-Atom Interactions. Example Shows a Core Level, K, Hole Created by an Incident Electron. The Hole is Rapidly Filled by the Drop of an Electron from an Outer Level Resulting in an X-ray Emission with Energy ($E_k - E_L$) or Alternatively an Auger Electron with Approximate Energy ($E_K - E_{L1} - E_{L2}$)

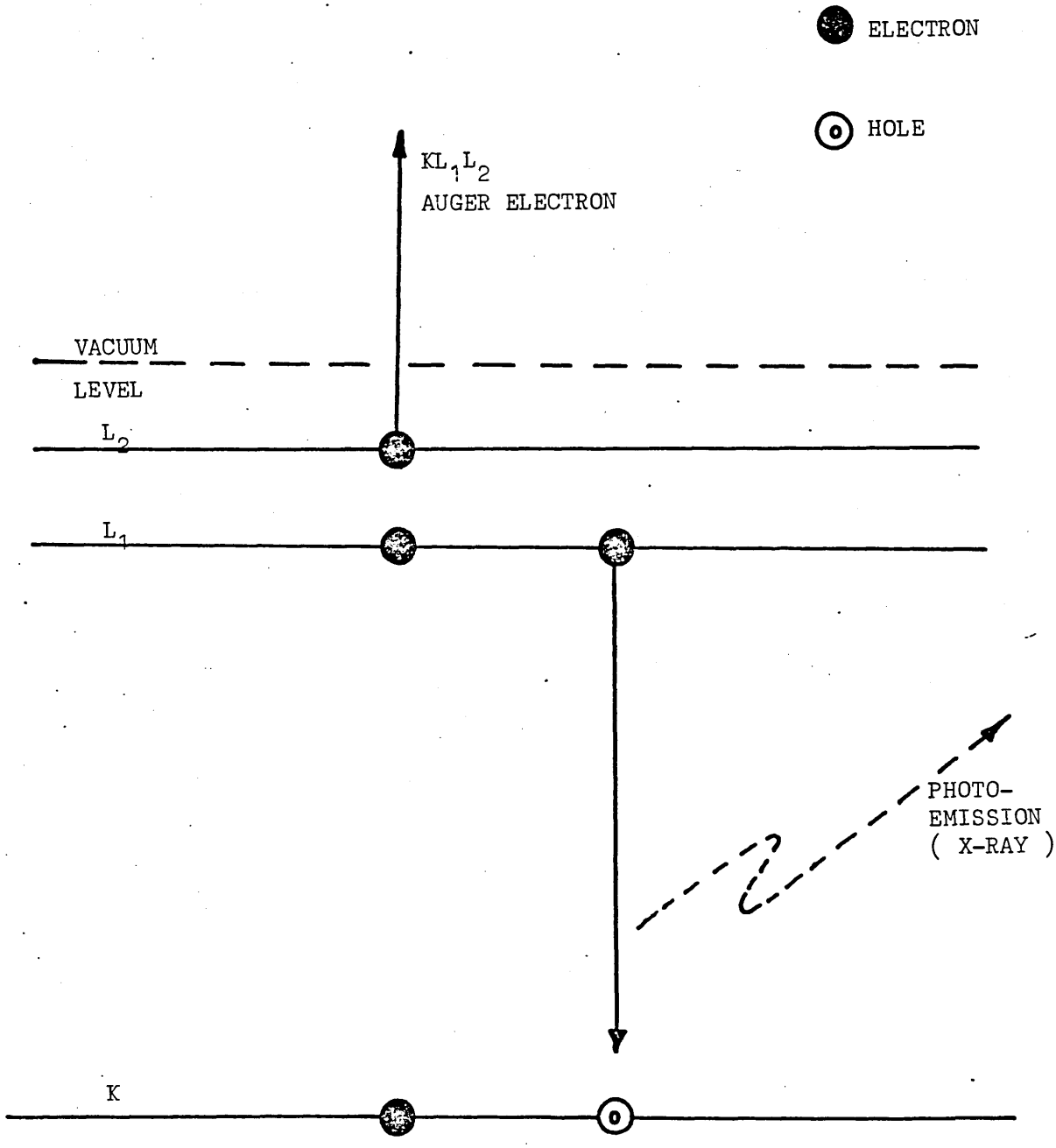
ELECTRON
HOLE
KL_1L_2
AUGER ELECTRON
VACUUM
LEVEL
L_2
L_1
PHOTO-
EMISSION
(X-RAY)
K

FIGURE 50

X-ray Excitation Volume in a Solid Specimen.[102]

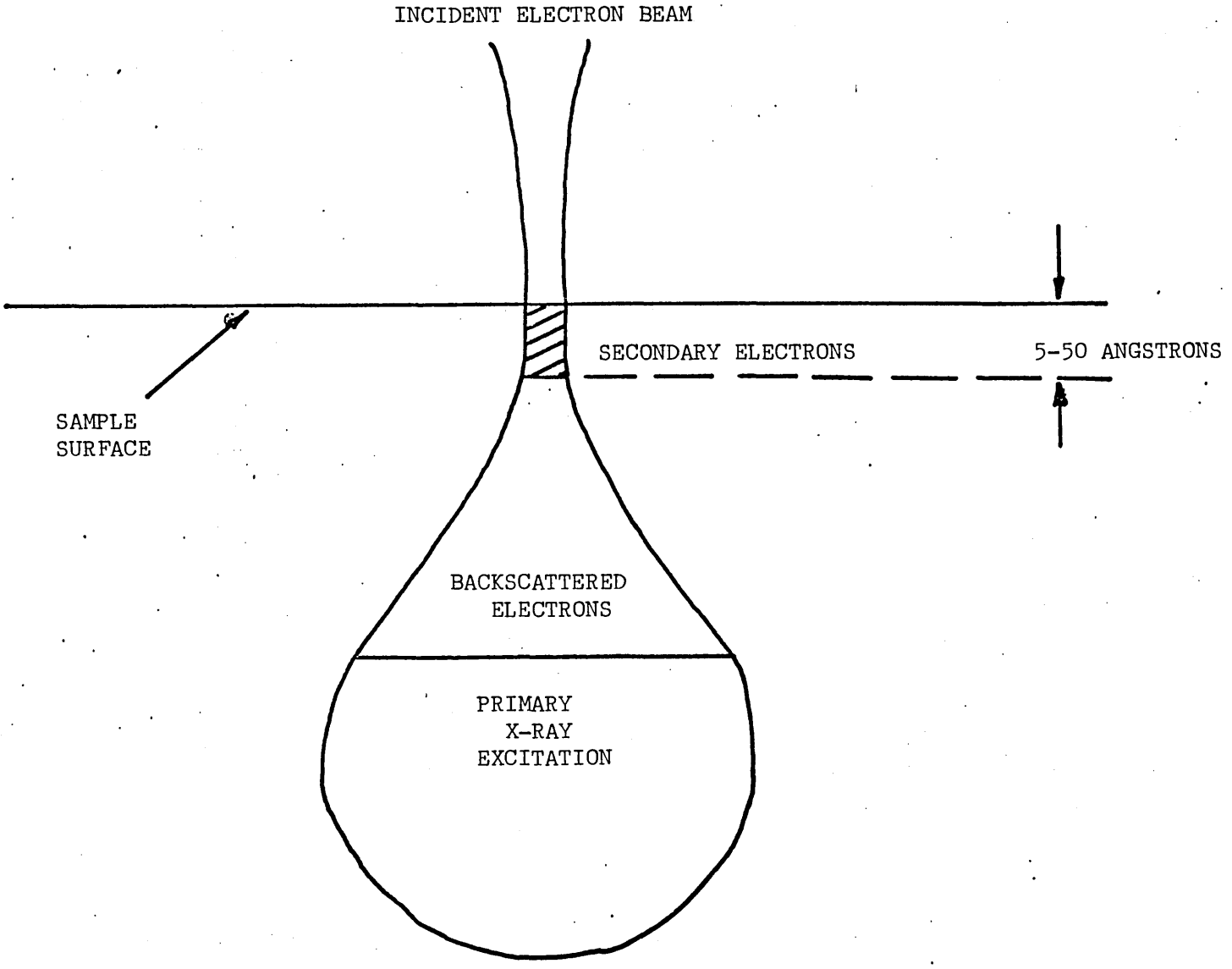
INCIDENT ELECTRON BEAM
SECONDARY ELECTRONS
5-50 ANGSTRONS
SAMPLE
SURFACE
BACKSCATTERED
ELECTRONS
PRIMARY
X-RAY
EXCITATION

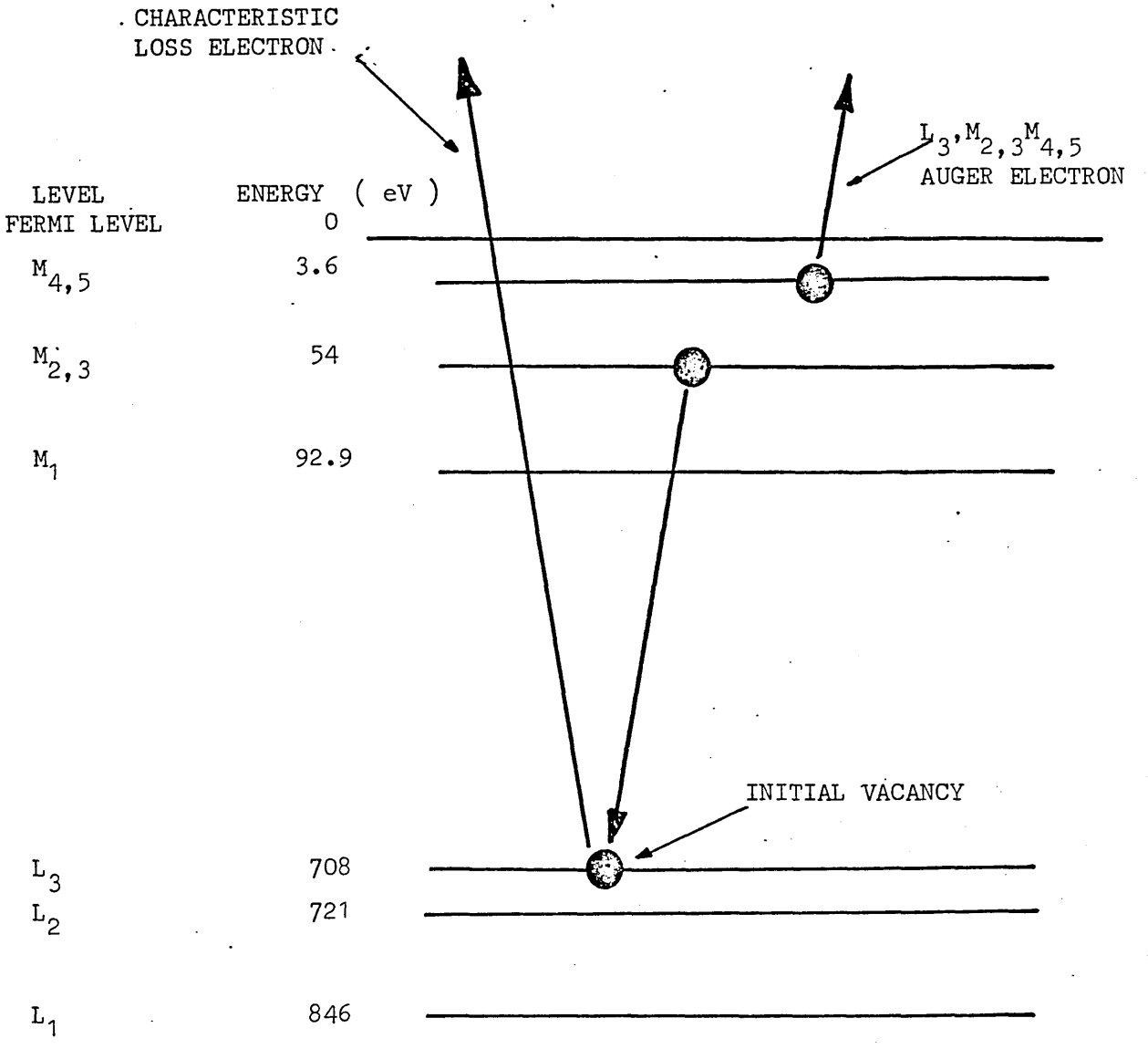
CHARACTERISTIC LOSS ELECTRON
$L_3, M_{2,3} M_{4,5}$ AUGER ELECTRON
LEVEL
ENERGY (eV)
FERMI LEVEL
0
$M_{4,5}$
3.6
$M_{2,3}$
54
M_1
92.9
INITIAL VACANCY
L_3
708
L_2
721
L_1
846
K
7112

FIGURE 52

General Form of a Secondary Emission Curve, Showing Auger Peaks and Plasmon Loss Features Near the Elastic Peak. The Auger Peak is Usually Displayed in the Differentiated Form (inset).

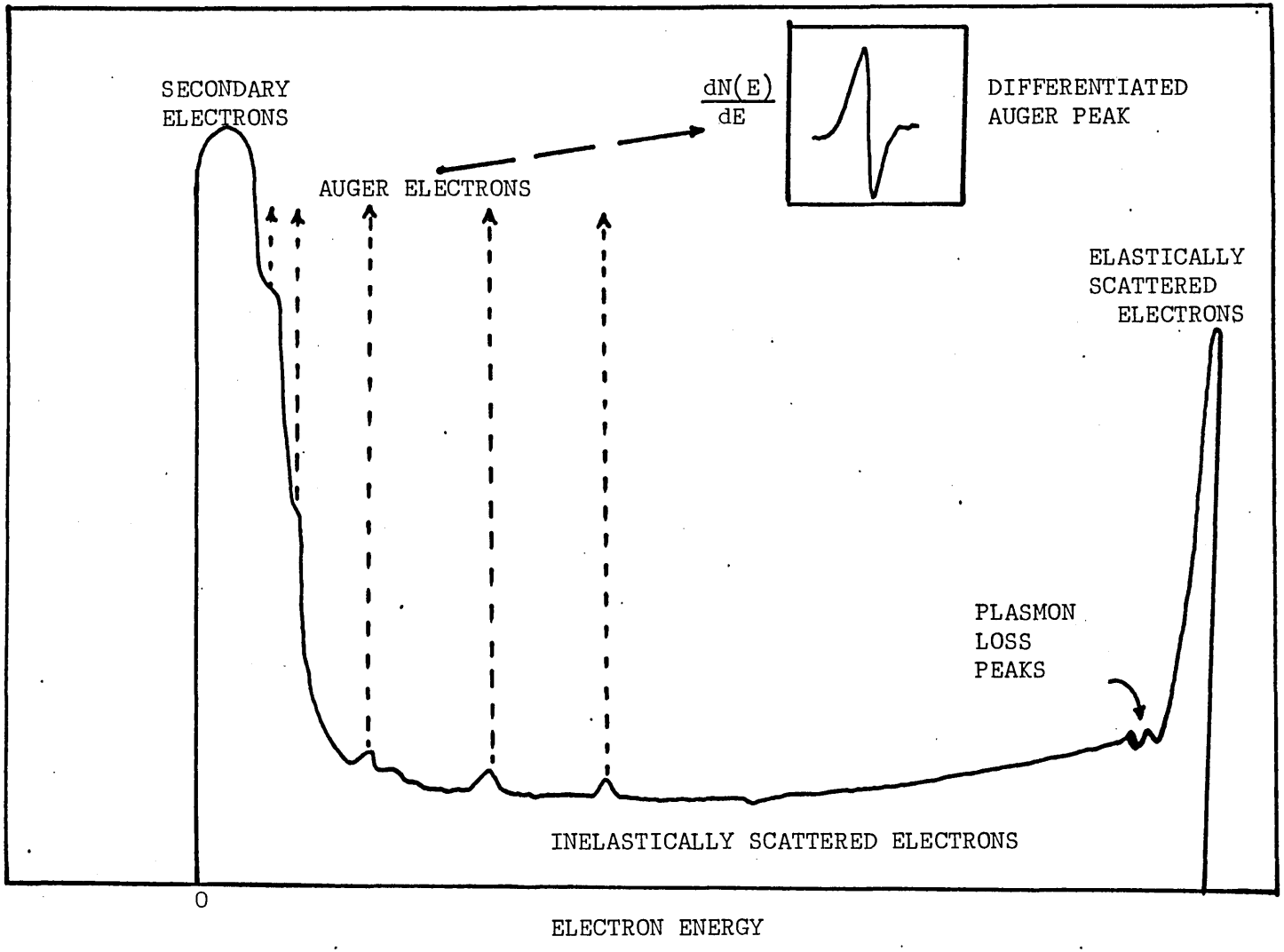
SECONDARY ELECTRONS
dN(E)/dE
DIFFERENTIATED AUGER PEAK
AUGER ELECTRONS
ELASTICALLY SCATTERED ELECTRONS
PLASMON LOSS PEAKS
INELASTICALLY SCATTERED ELECTRONS
N(E)
0
ELECTRON ENERGY

FIGURE 53

Variation of Escape Depth with Kinetic Energy. The Data is From Many Sources and Assembled by Riviére.[108]

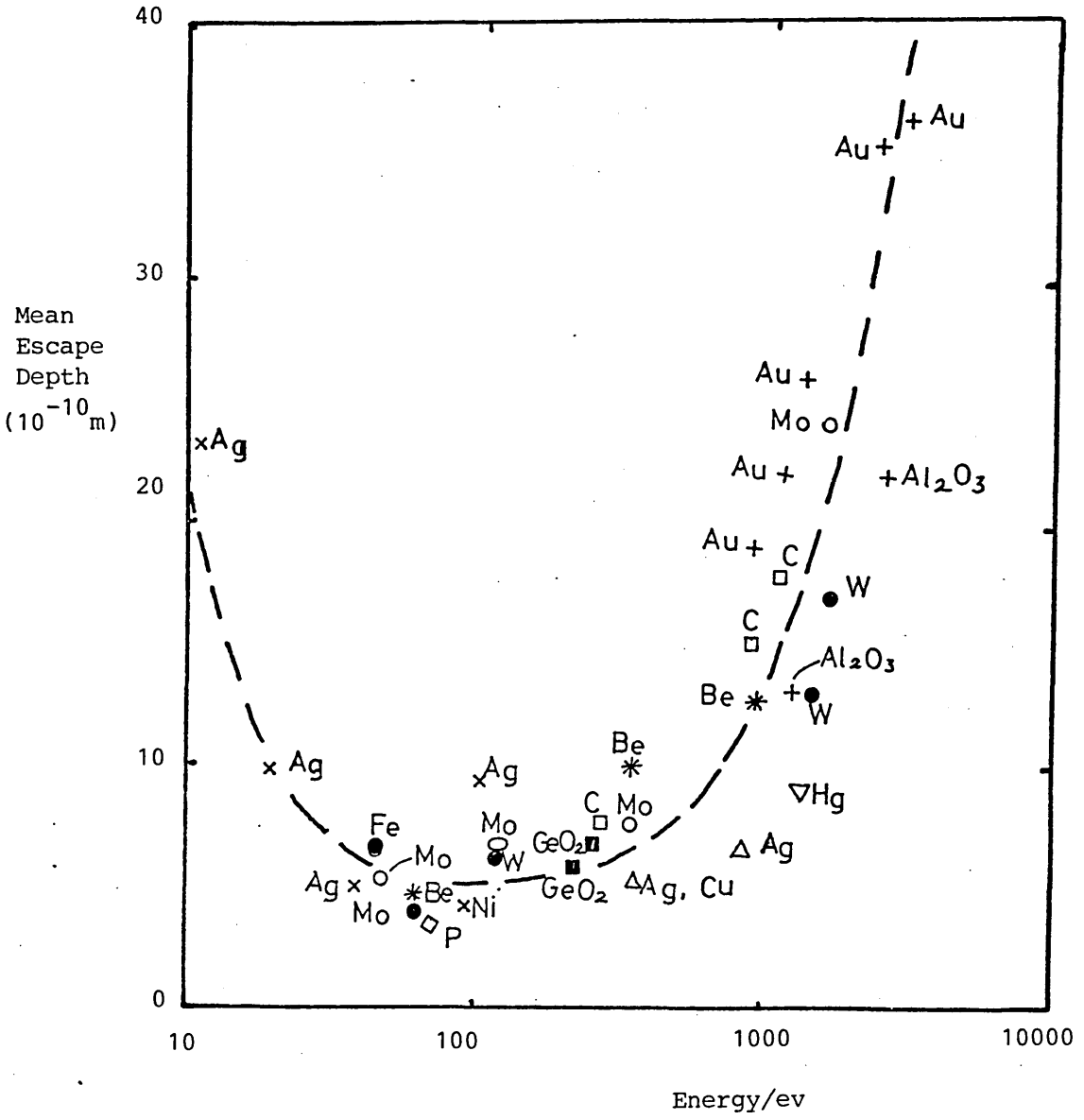
40
30
20
10
0
Mean
Escape
Depth
(10^{-10}m)
10
100
1000
10000
Energy/ev
Au
Au
Au
Mo
Au
Al_2O_3
Au
C
W
C
Al_2O_3
Be
W
Ag
Ag
Be
C
Mo
Hg
Fe
Mo
GeO_2
Ag
Ag
Mo
Be
Ni
GeO_2
Ag, Cu
Mo
P

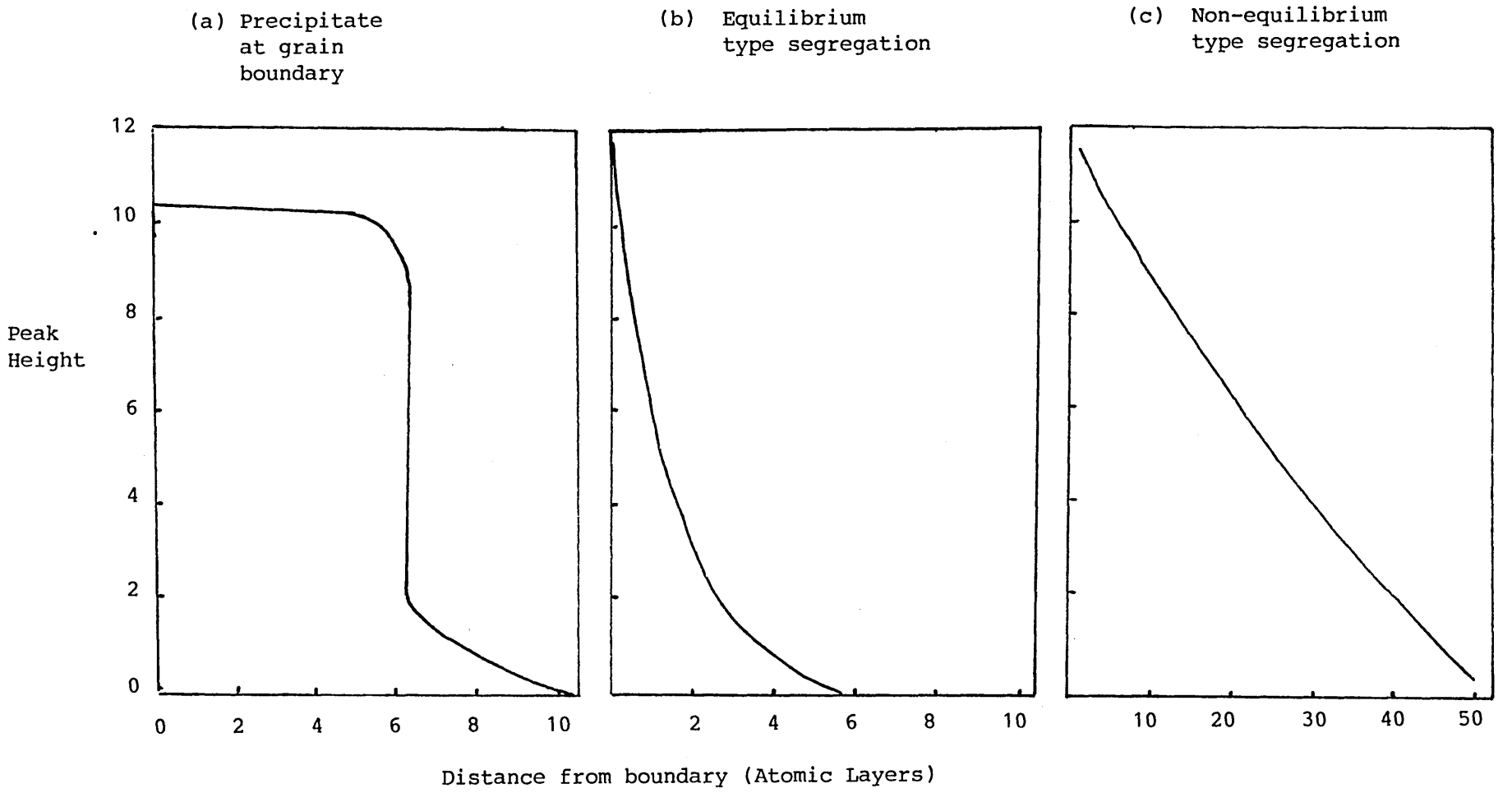
(a) Precipitate at grain boundary
(b) Equilibrium type segregation
(c) Non-equilibrium type segregation
Peak Height
12
10
8
6
4
2
0
0
2
4
6
8
10
2
4
6
8
10
10
20
30
40
50
Distance from boundary (Atomic Layers)

FIGURE 55

Effect of Temperature on the Tensile Properties of 0.2% C Steel.

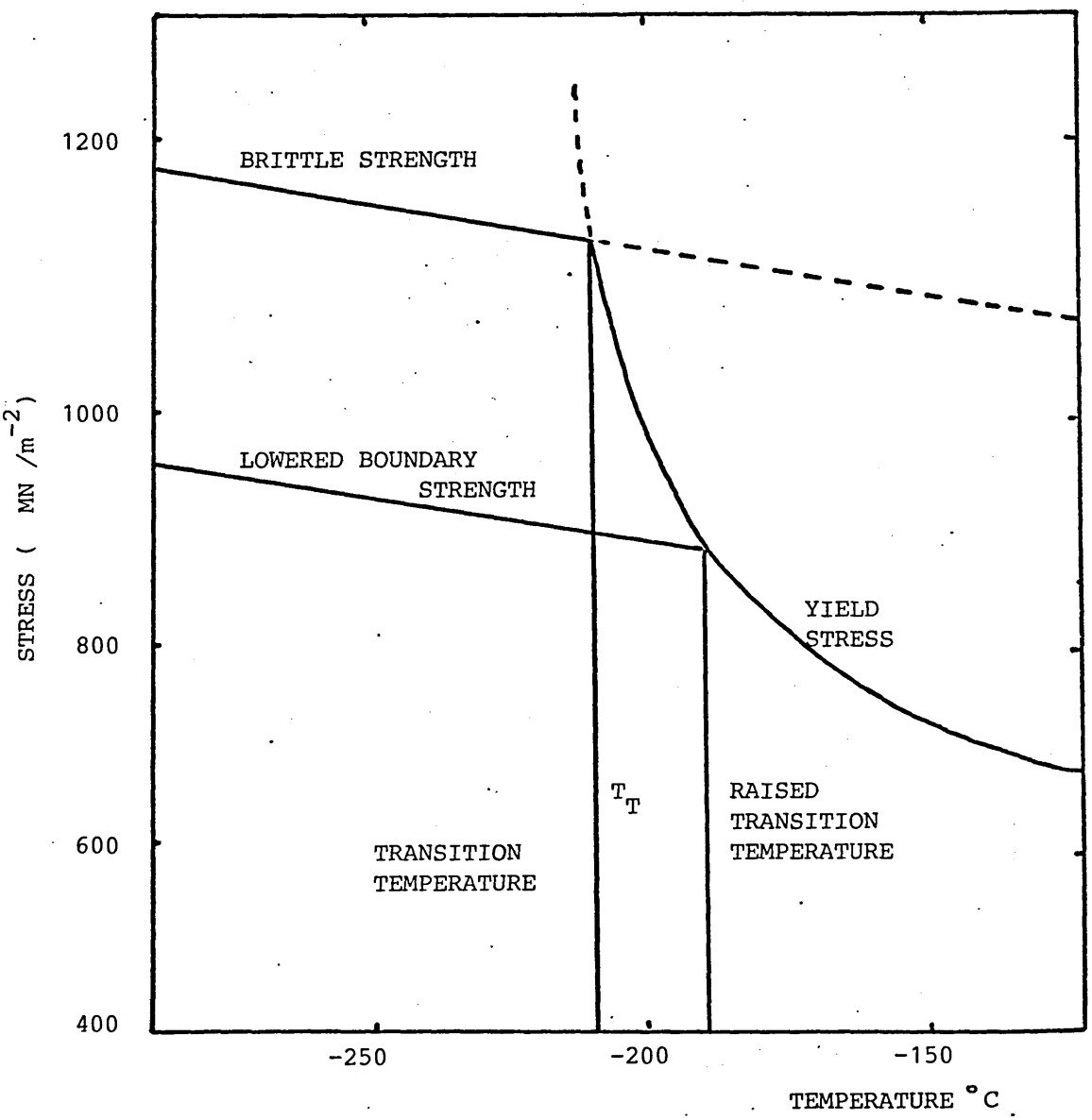
1200
1000
800
600
400
STRESS (MN /m^{-2})
BRITTLE STRENGTH
LOWERED BOUNDARY
STRENGTH
YIELD
STRESS
T_T
TRANSITION
TEMPERATURE
RAISED
TRANSITION
TEMPERATURE
-250
-200
-150
TEMPERATURE °C

FIGURE 56

Schematic Curves for the Cohesion Between the Atom Planes Across a Grain Boundary as a Function of their Separation.[110]

a_o = Equilibrium Separation for a Clean Boundary.

a_e = Equilibrium Separation of a Boundary + Impurities.

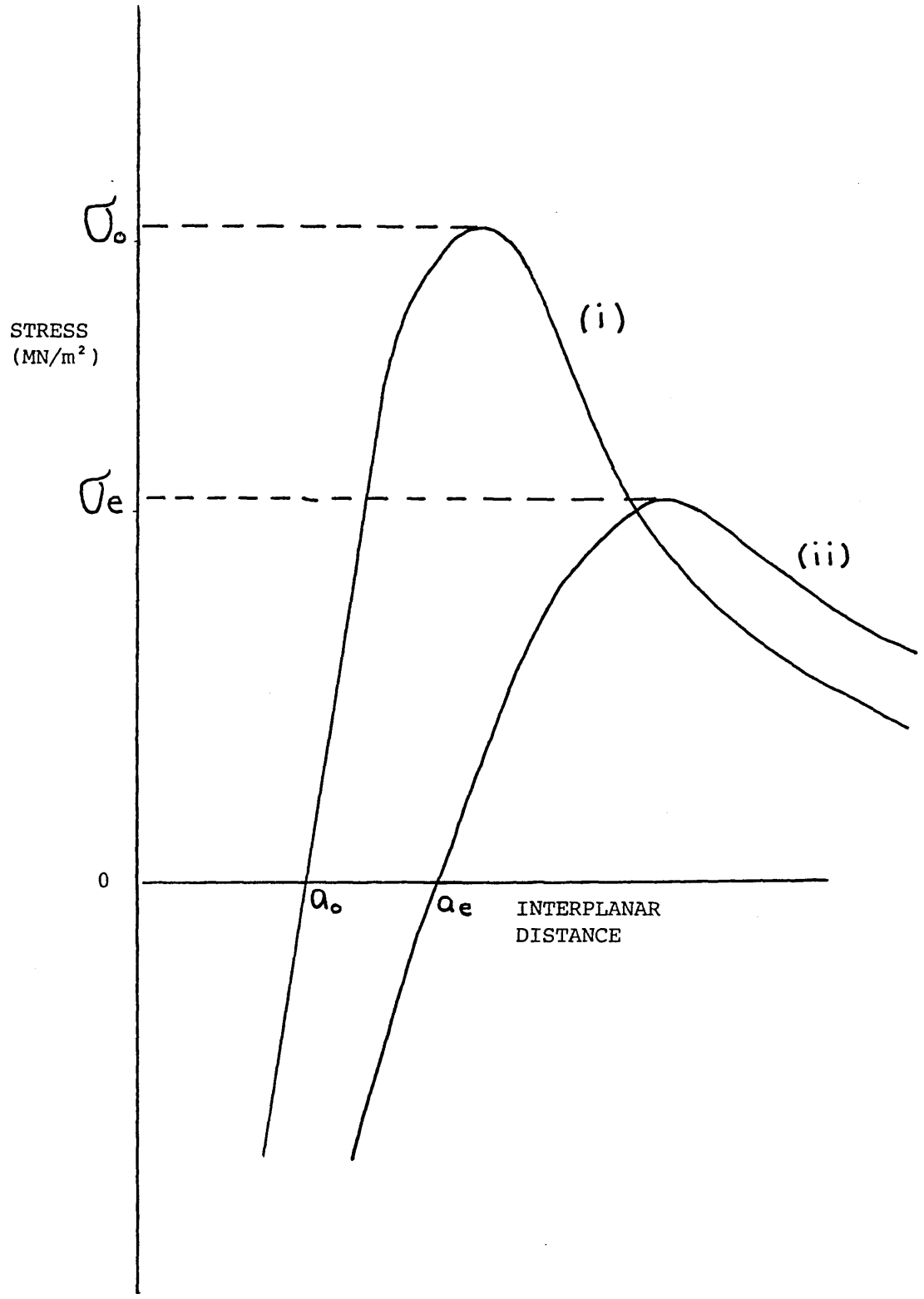
σ_o
σ_e
STRESS
(MN/m²)
(i)
(ii)
0
a_o
a_e
INTERPLANAR
DISTANCE

FIGURE 57

Fractographs of Alloy K1525 (Fe-8Mn) After an Austenitizing Treatment of 1000°C for 1 Hour Followed by Water Quenching.

BRITTLE (INTERGRANULAR) x1180

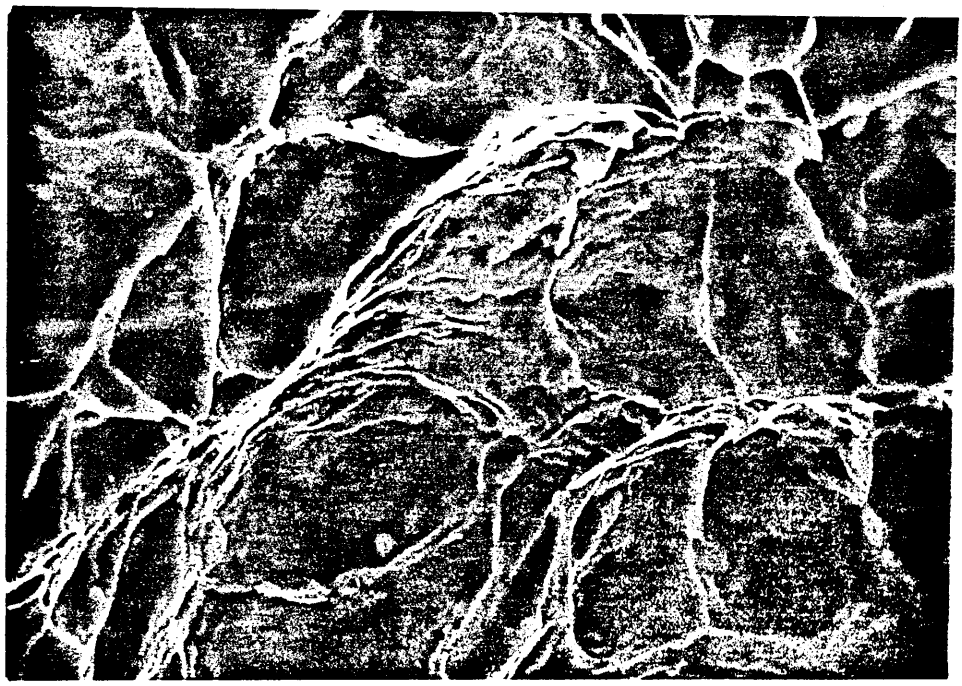

DUCTILE x1220

FIGURE 58

Effect of Holding at 450°C on Ductile-Brittle Transition Temperature in Alloy 181 (Fe-8Mn)[134] After Being Ice-Brine Quenched.

FIGURE 59

Effect of Holding at 450°C on Ductile-Brittle Transition Temperature in Alloy 193 (Fe-8.5Mn 0.17 Ti - 0.18 Al) After Being Ice-Brine Quenched.[134]

Key :- (a) Ice-Brine Quenched

(b) 6 mins at 450°C

(c) 1 hour at 450°C

(d) 10 hours at 450°C

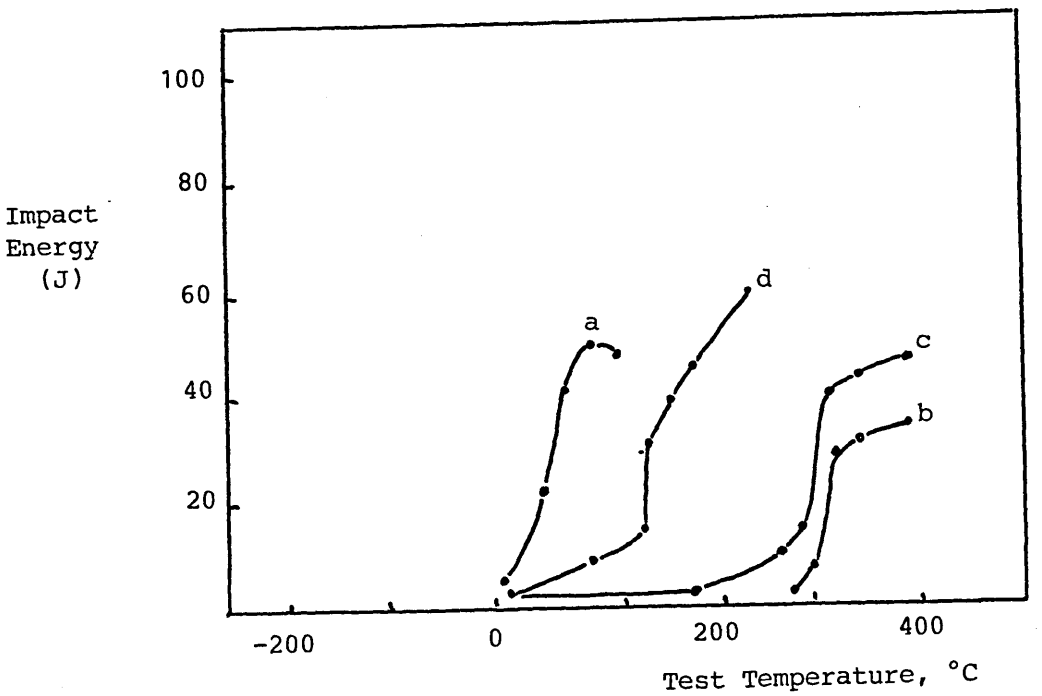
Impact
Energy
(J)
100
80
60
40
20
a
d
c
b
-200
0
200
400
Test Temperature, °C

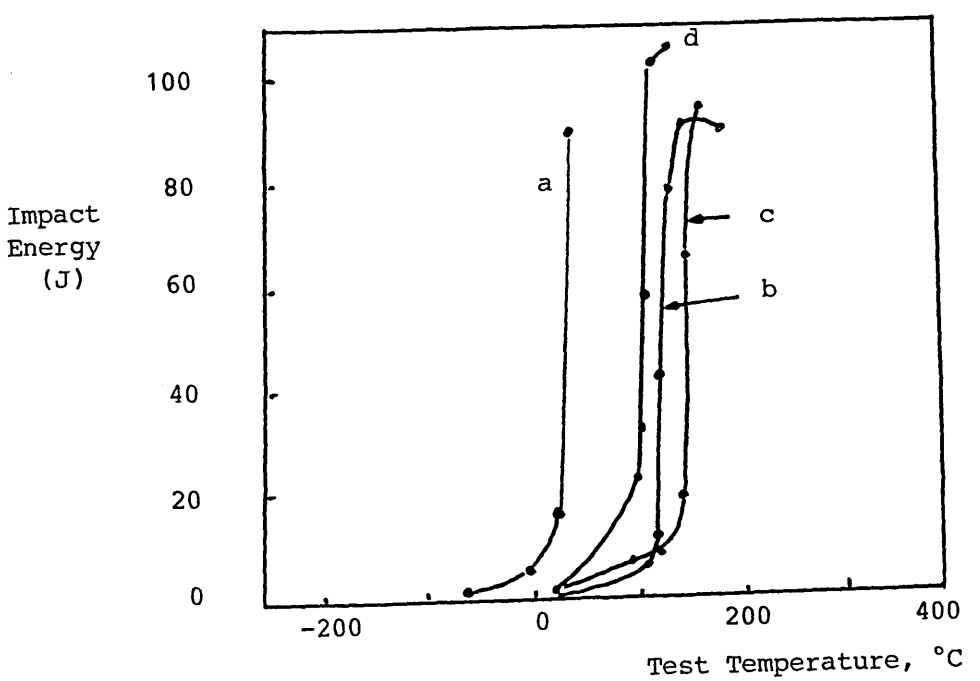
Impact
Energy
(J)
100
80
60
40
20
0
a
d
c
b
-200
0
200
400
Test Temperature, °C

FIGURE 60

Effect of Prior Heat Treatment at 1300°C on the Ductile to Brittle Transition Temperature of Alloy K1526 (Fe-8Mn-2.5Mo).

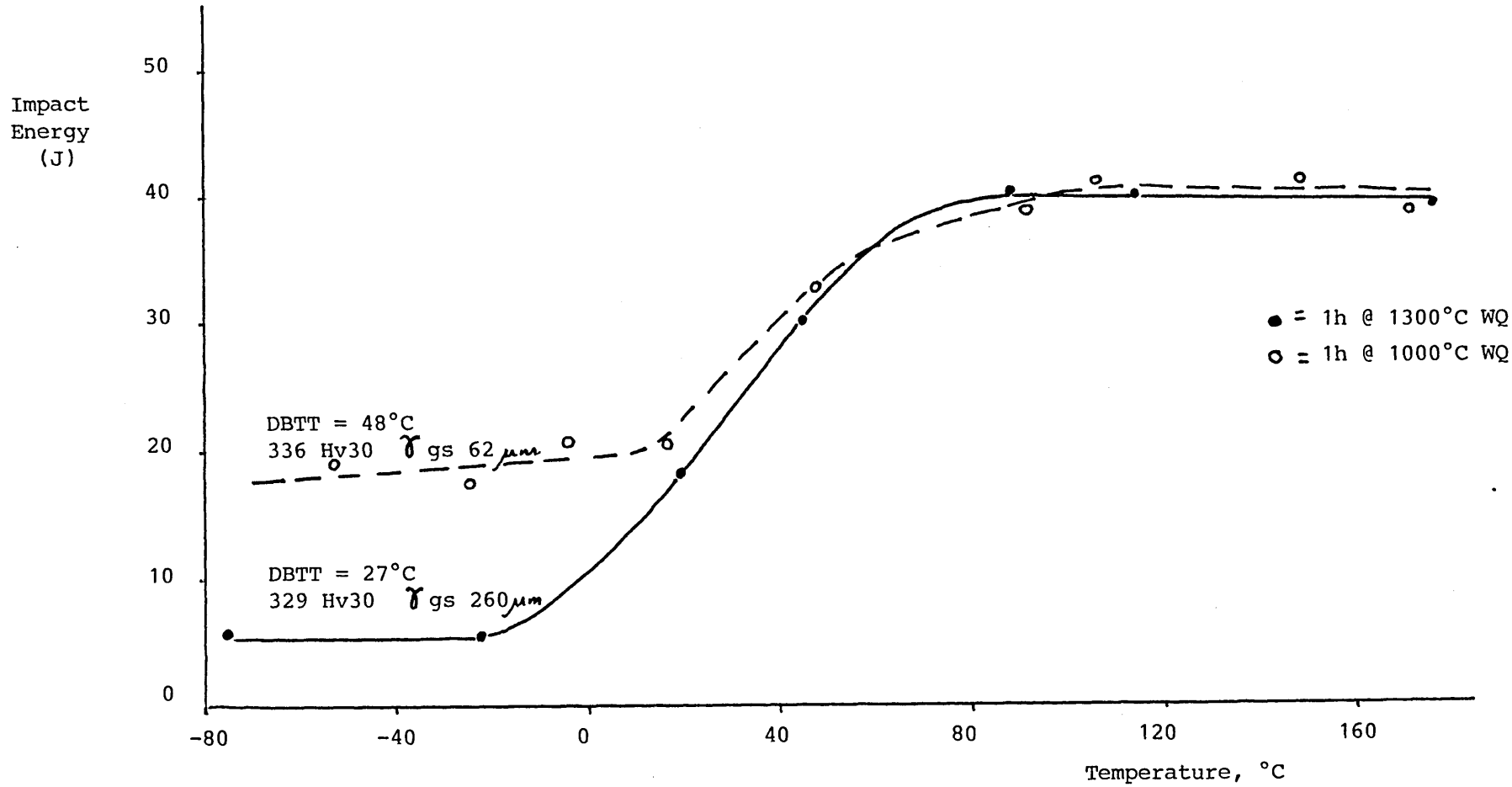
Impact
Energy
(J)
50
40
30
20
10
0
-80
-40
0
40
80
120
160
Temperature, °C
● = 1h @ 1300°C WQ
o = 1h @ 1000°C WQ
DBTT = 48°C
336 Hv30 γ gs 62 μm
DBTT = 27°C
329 Hv30 γ gs 260μm

FIGURE 61

Effect of Prior Heat Treatment at 1300°C Followed by 1000°C on the Ductile to Brittle Transition Temperature of Alloy K1526 (Fe-8Mn-2.5Mo).

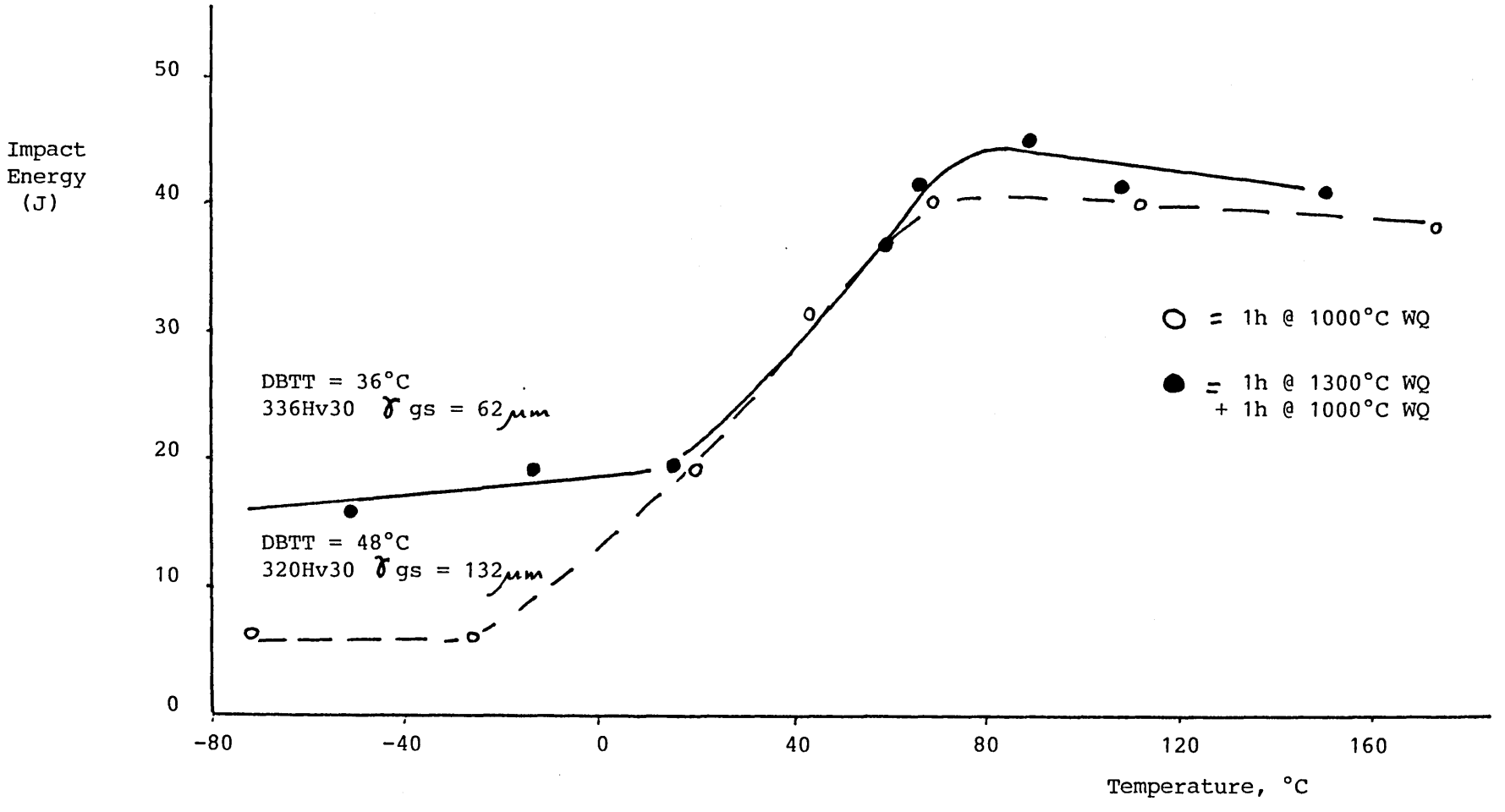
Impact
Energy
(J)
50
40
30
20
10
0
-80
-40
0
40
80
120
160
Temperature, °C
DBTT = 36°C
336Hv30 γ gs = 62 μm
DBTT = 48°C
320Hv30 γ gs = 132 μm
= 1h @ 1000°C WQ
= 1h @ 1300°C WQ
+ 1h @ 1000°C WQ

FIGURE 62

Impact Transition Curves for Alloy K1526

After Different Heat Treatment Temperatures.

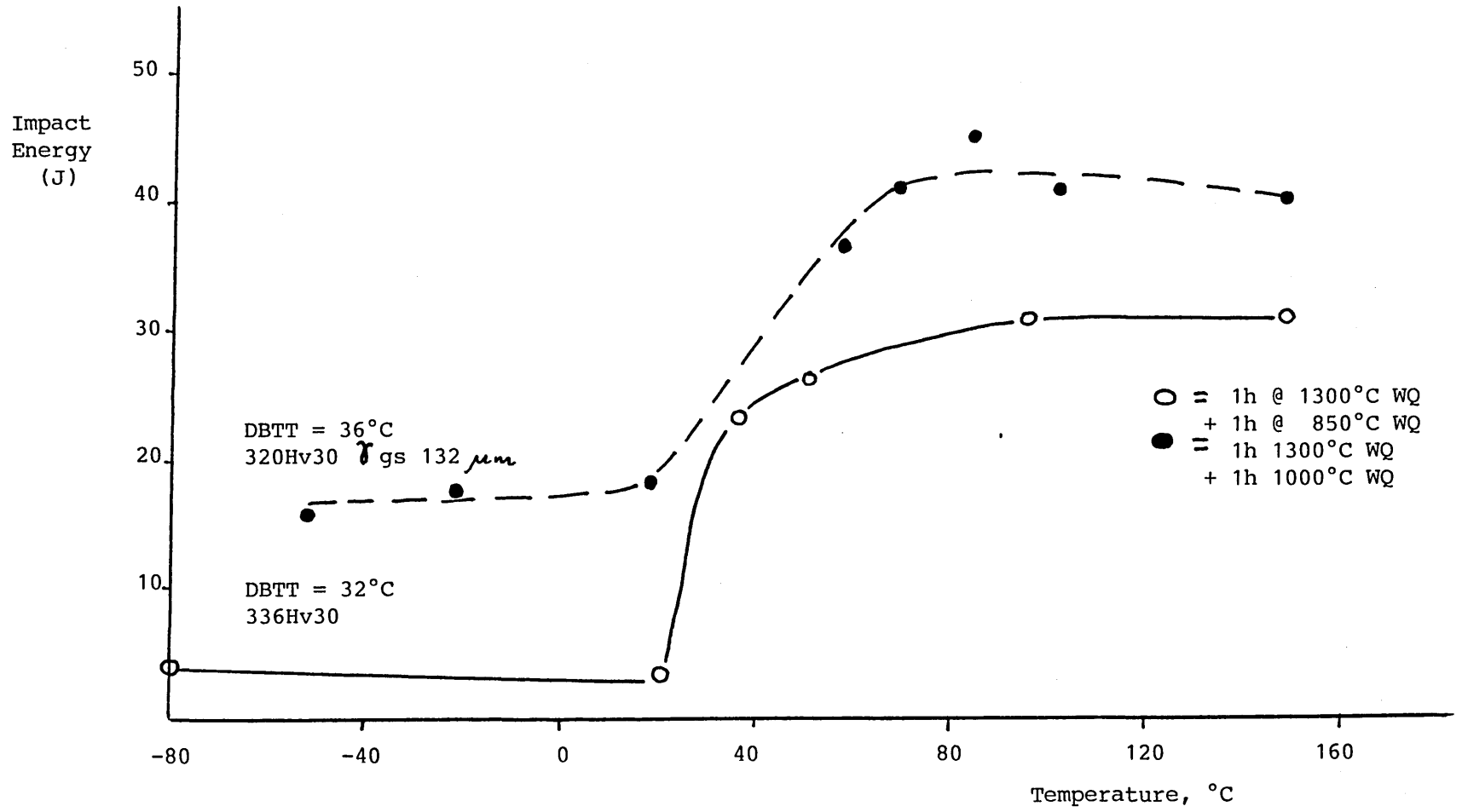
Impact
Energy
(J)
50
40
30
20
10
DBTT = 36°C
320Hv30 γgs 132 μm
DBTT = 32°C
336Hv30
O = 1h @ 1300°C WQ
+ 1h @ 850°C WQ
● = 1h 1300°C WQ
+ 1h 1000°C WQ
-80
-40
0
40
80
120
160
Temperature, °C

FIGURE 63

Impact Transition Curves for Alloy K1525 (Fe-8Mn), K1526 (Fe-8Mn) and K1527 After Solution Treating at 1000°C for 1 Hour Followed by Water Quenching.

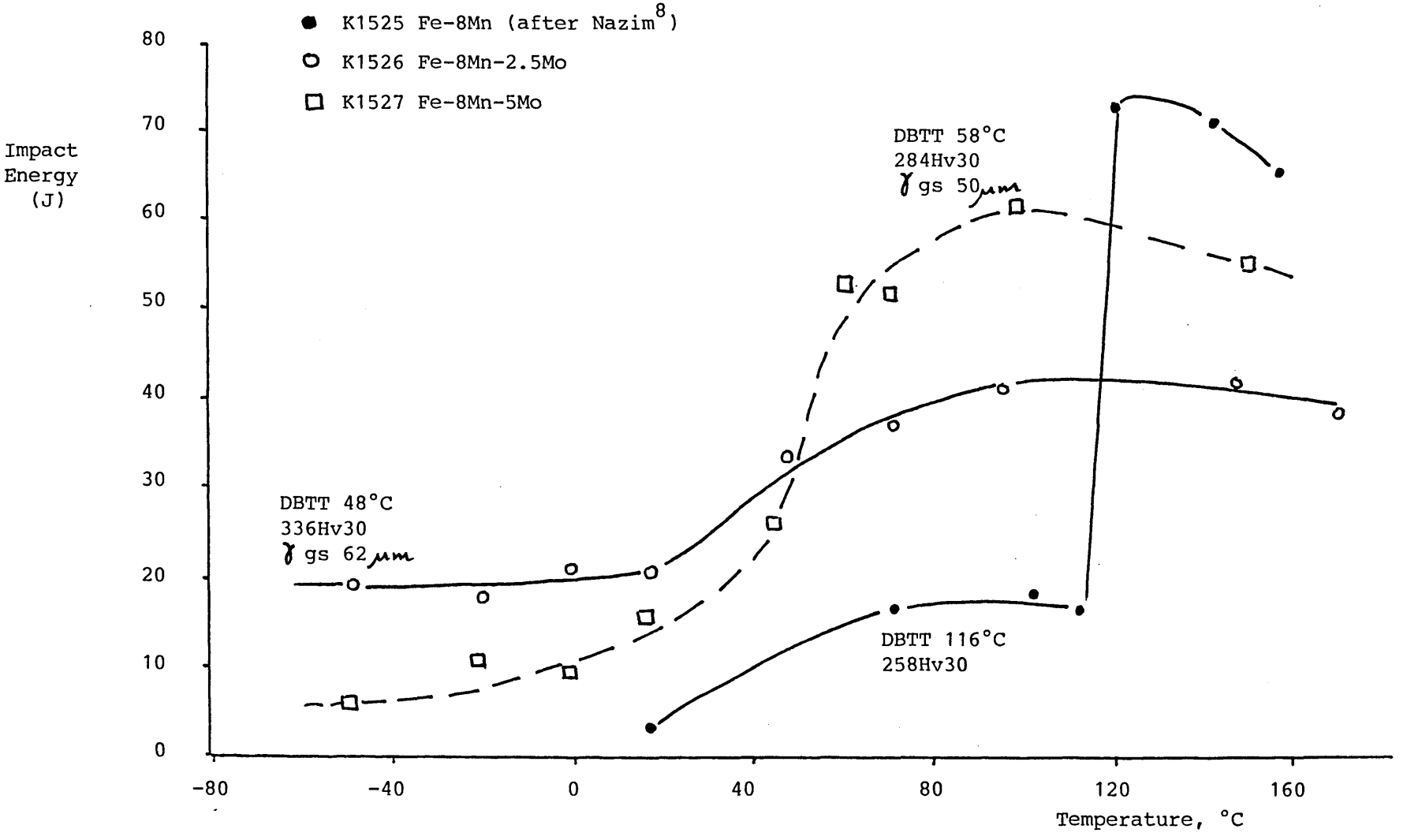
K1525 Fe-8Mn (after Nazim[8])
K1526 Fe-8Mn-2.5Mo
K1527 Fe-8Mn-5Mo
Impact Energy (J)
80
70
60
50
40
30
20
10
0
-80
-40
0
40
80
120
160
Temperature, °C
DBTT 58°C
284Hv30
γ gs 50μm
DBTT 48°C
336Hv30
γ gs 62μm
DBTT 116°C
258Hv30

FIGURE 64

Effect of Prior Heat Treatment at 1300°C on the Ductile to Brittle Transition Curve for Alloy K1527 (Fe-8Mn-5Mo).

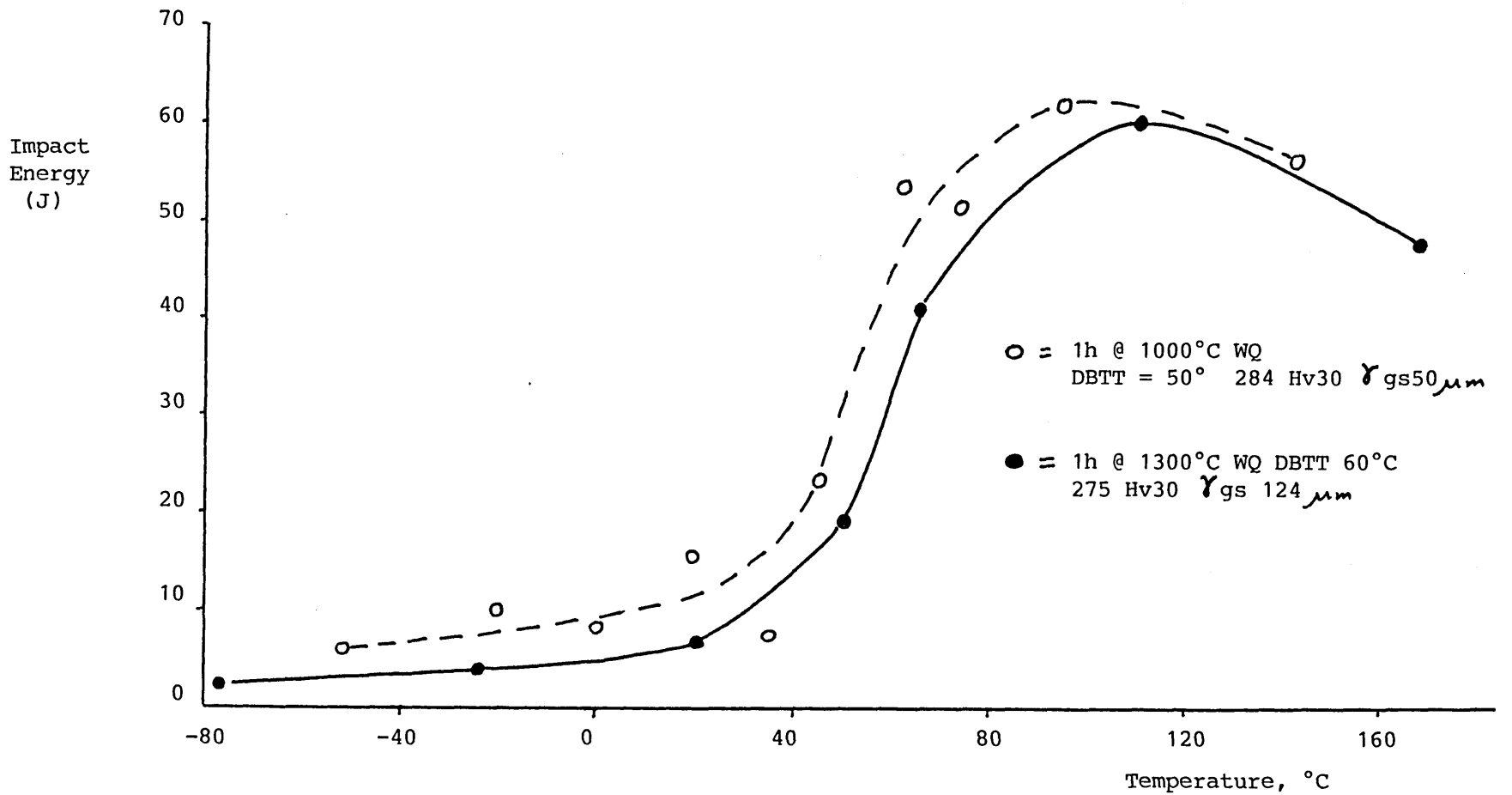
Impact
Energy
(J)
70
60
50
40
30
20
10
0
-80
-40
0
40
80
120
160
Temperature, °C
o = 1h @ 1000°C WQ
DBTT = 50° 284 Hv30 γgs50μm
● = 1h @ 1300°C WQ DBTT 60°C
275 Hv30 γgs 124μm

FIGURE 65

The Effect of a Double Austenitising Treatment of 1300°C and the 1000°C on the Impact Transition Curve for Alloy K1527 (Fe-8Mn-5Mo).

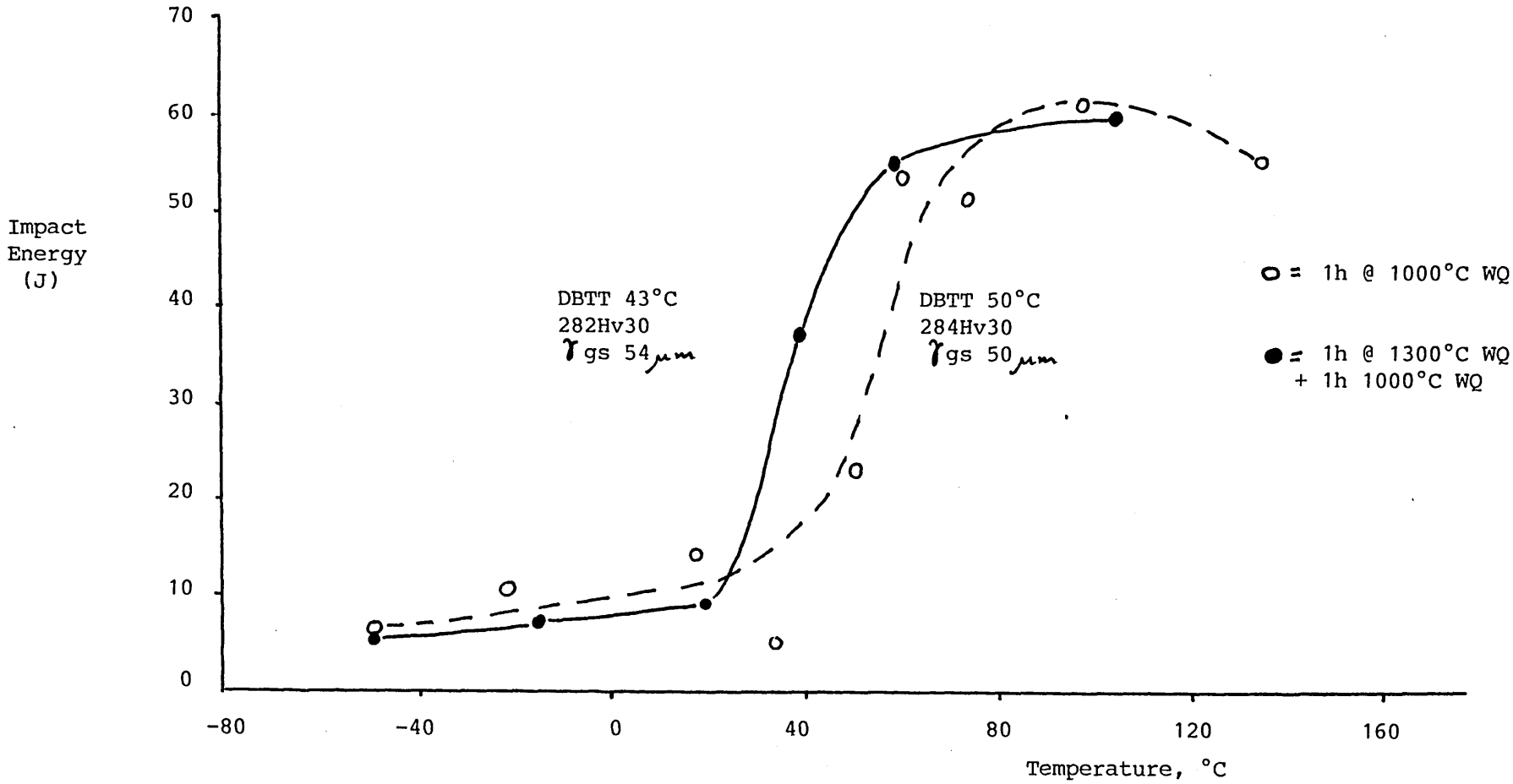
Impact
Energy
(J)
70
60
50
40
30
20
10
0
-80
-40
0
40
80
120
160
Temperature, °C
DBTT 43°C
282Hv30
γgs 54μm
DBTT 50°C
284Hv30
γgs 50μm
o = 1h @ 1000°C WQ
● = 1h @ 1300°C WQ
+ 1h 1000°C WQ

FIGURE 66

Impact Transition Curves for Alloy K1527 after Different Heat Treatments.

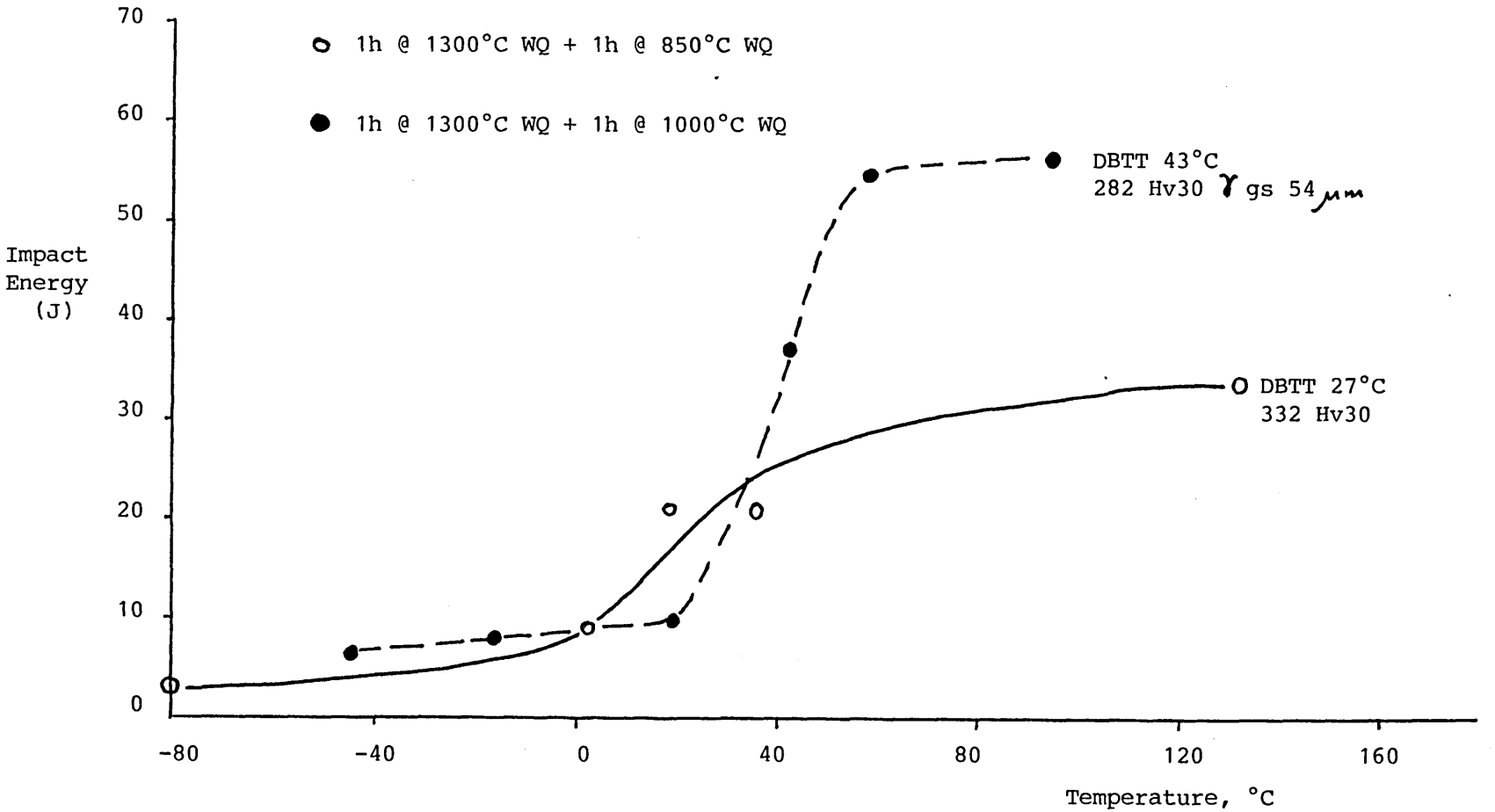
o 1h @ 1300°C WQ + 1h @ 850°C WQ
● 1h @ 1300°C WQ + 1h @ 1000°C WQ
DBTT 43°C
282 Hv30 γ gs 54 μm
O DBTT 27°C
332 Hv30
Impact Energy (J)
70
60
50
40
30
20
10
0
-80
-40
0
40
80
120
160
Temperature, °C

FIGURE 67

Effect of Addition of 2.5Mo to an Fe-8Mn Alloy and the Effect of Austenitising Treatment on the Alloy.

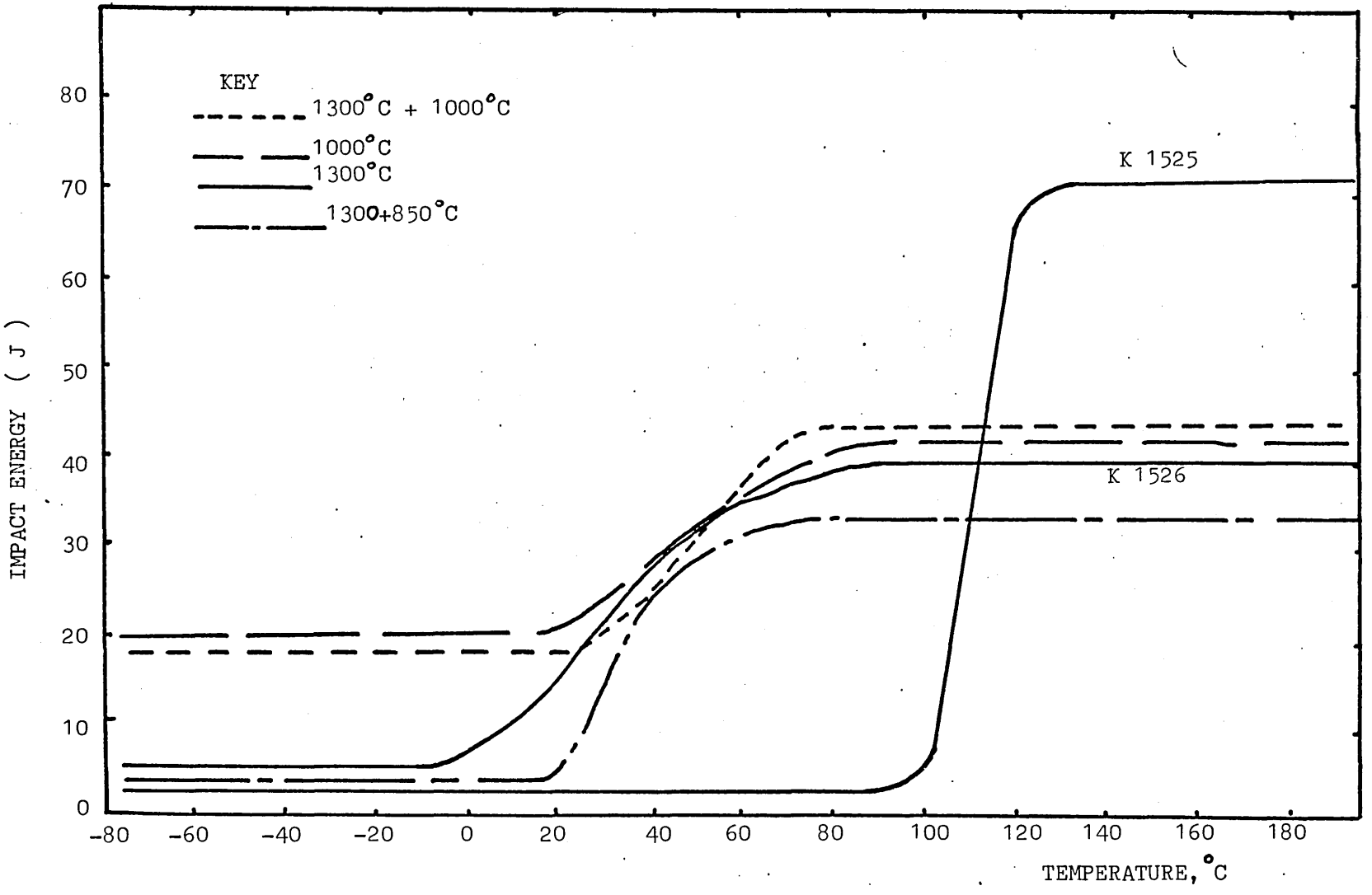
KEY
1300°C + 1000°C
1000°C
1300°C
1300+850°C
K 1525
K 1526
IMPACT ENERGY (J)
TEMPERATURE, °C
0
10
20
30
40
50
60
70
80
-80
-60
-40
-20
0
20
40
60
80
100
120
140
160
180

FIGURE 68

Fractography of Alloy K1526 (Fe-8Mn-2.5Mo) after a Solution Treatment of 1000^{o}C for 1 Hour Followed by Water Quenching.

BRITTLE x400

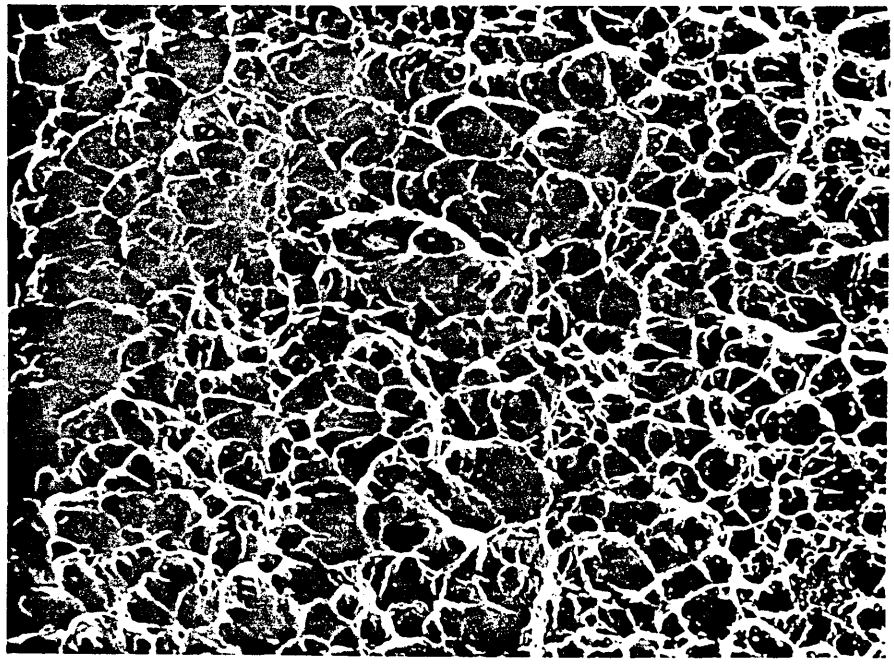

DUCTILE x400

FIGURE 69

Fractographs of Alloy K1526 (Fe-8Mn-2.5Mo) After a Solution Treatment of 1300°C for 1 Hour Followed by Water Quenching.

BRITTLE x400

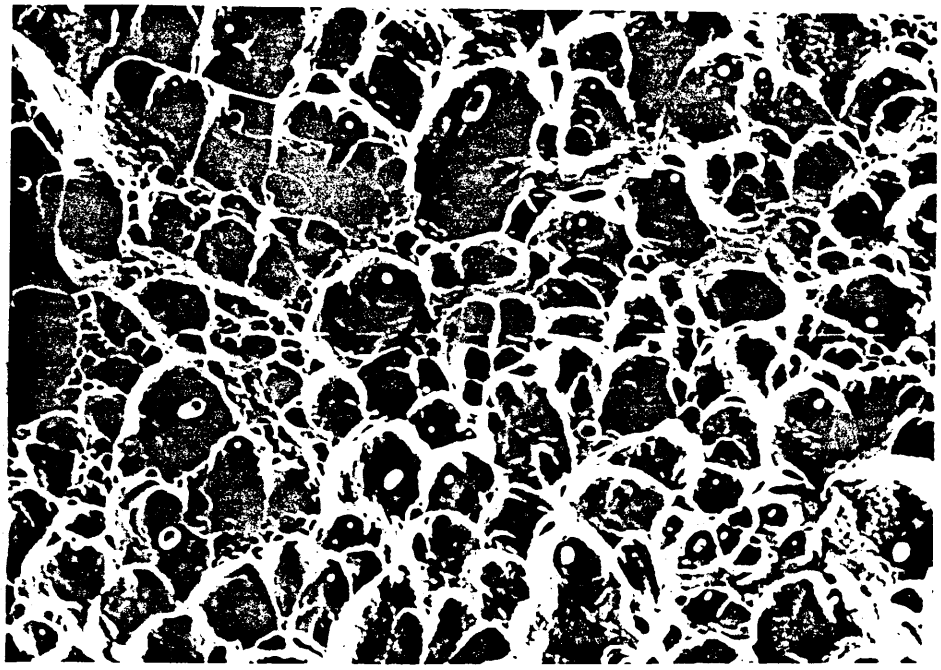

DUCTILE x400

FIGURE 70

Fractographs of Alloy K1526 after a Solution Treatment of 1300°C for 1 Hour Followed by Water Quenching and then a Further 1000°C for 1 Hour Followed by Water Quenching.

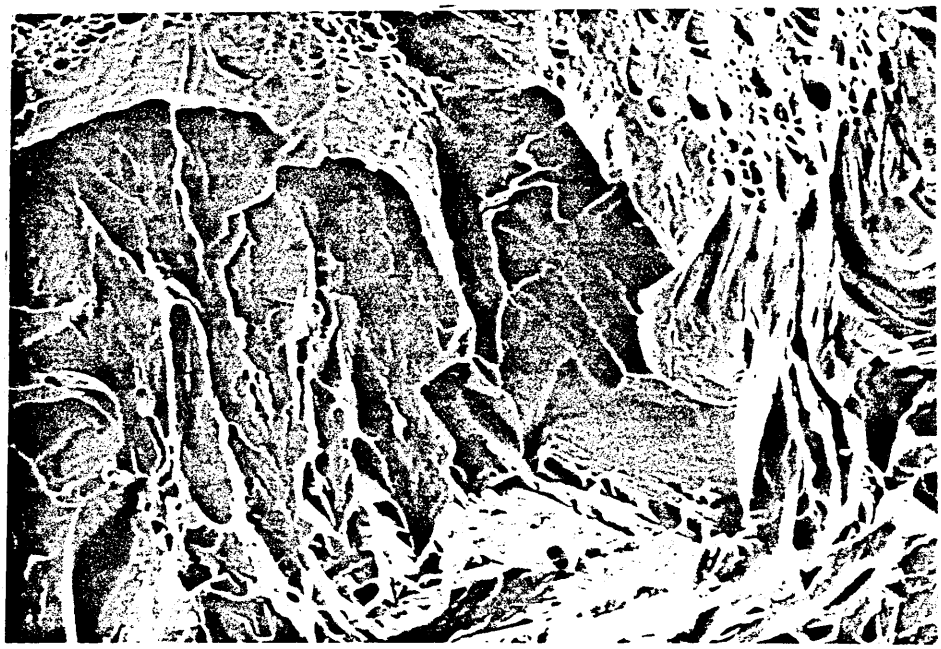

BRITTLE x960

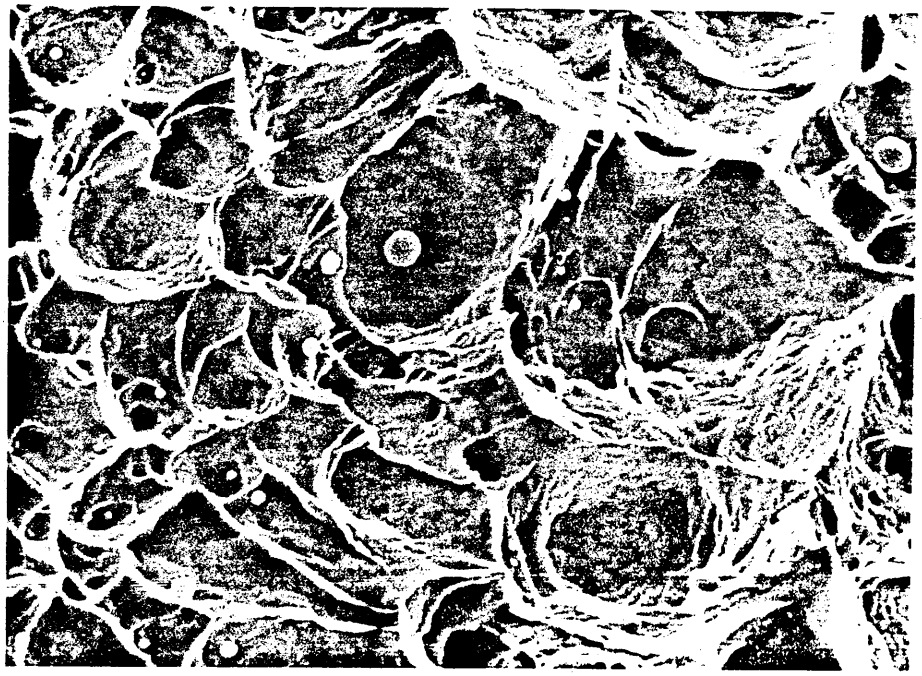

DUCTILE x960

FIGURE 71

Fractographs of K1526 after a Solution Treatment of 1300°C for 1 Hour Followed by a Water Quench and then 850°C for 1 Hour Followed by a Water Quench.

BRITTLE x400

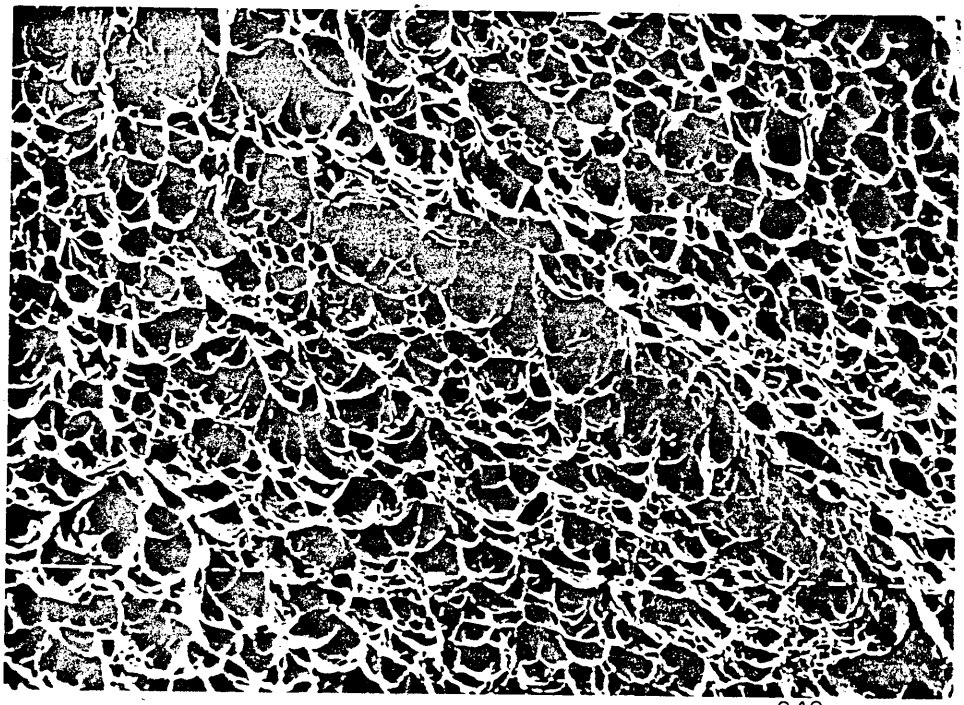

DUCTILE x240

FIGURE 72

Effect of the Addition of 5%Mo to an Fe-8Mn Alloy on the Impact Transition Curve. Also Showing the Effect of Prior Austenitising Temperature of the Impact Transition of the Alloy.

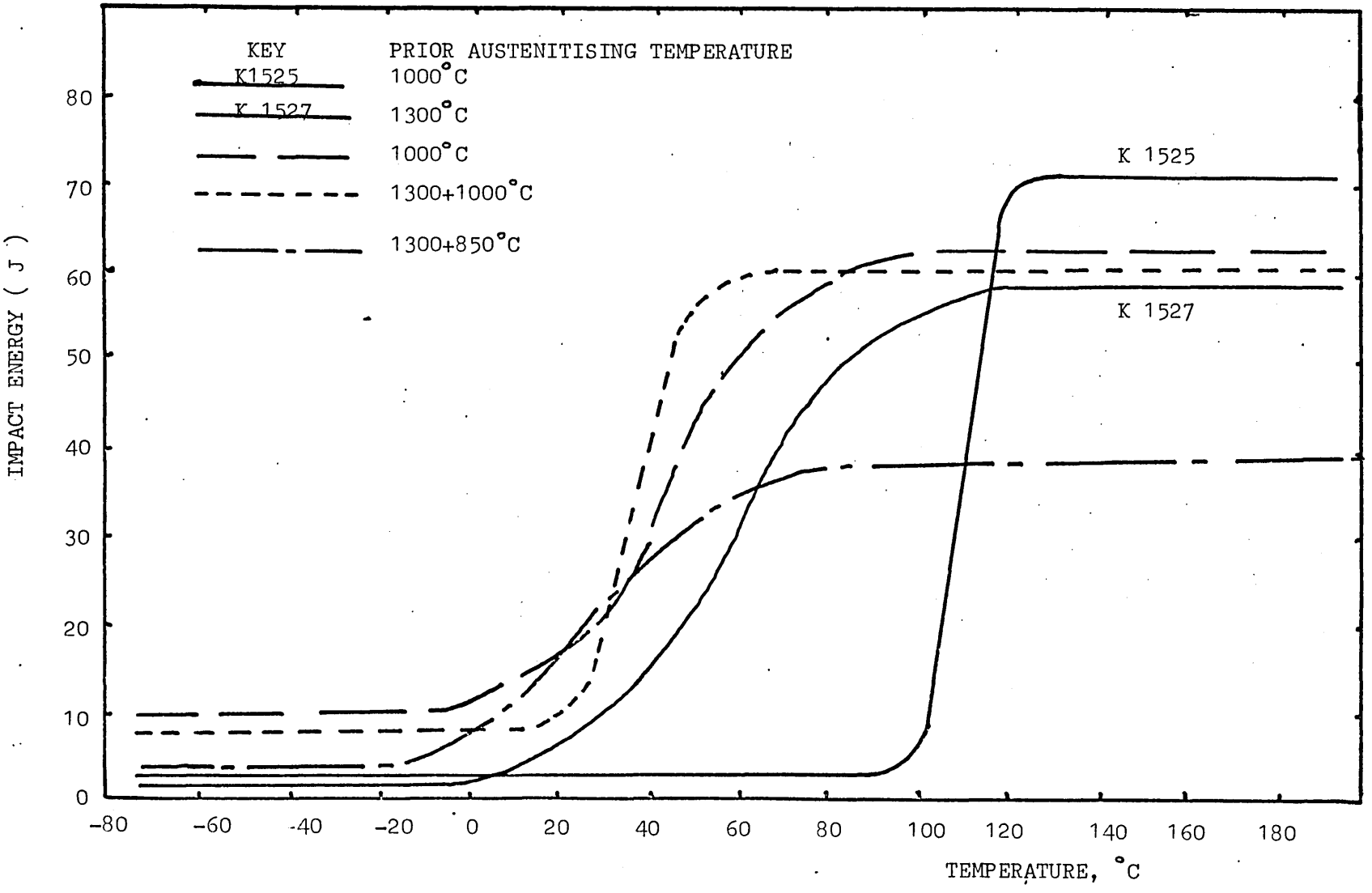
KEY
K1525
K 1527
PRIOR AUSTENITISING TEMPERATURE
1000°C
1300°C
1000°C
1300+1000°C
1300+850°C
K 1525
K 1527
IMPACT ENERGY (J)
0
10
20
30
40
50
60
70
80
-80
-60
-40
-20
0
20
40
60
80
100
120
140
160
180
TEMPERATURE, °C

FIGURE 73

Fractographs of Alloy K1527 (Fe-8Mn-5Mo) After an Austenitising Treatment of 1000^{o}C for 1 Hour Followed by Water Quenching.

BRITTLE x400

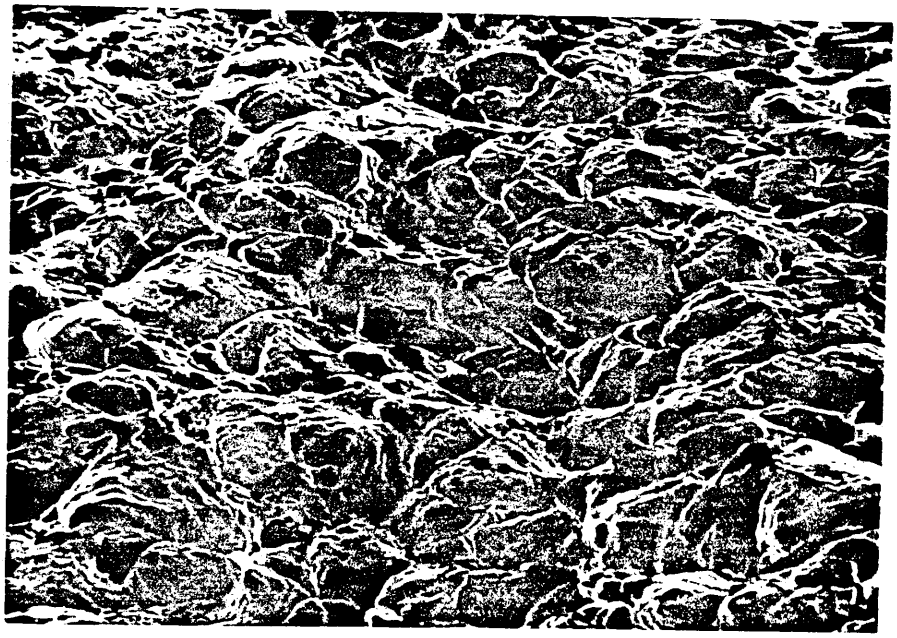

DUCTILE x400

FIGURE 74

Fractographs of K1527 after a Solution Treatment of 1300°C for 1 Hour Followed by a Water Quench.

BRITTLE x400

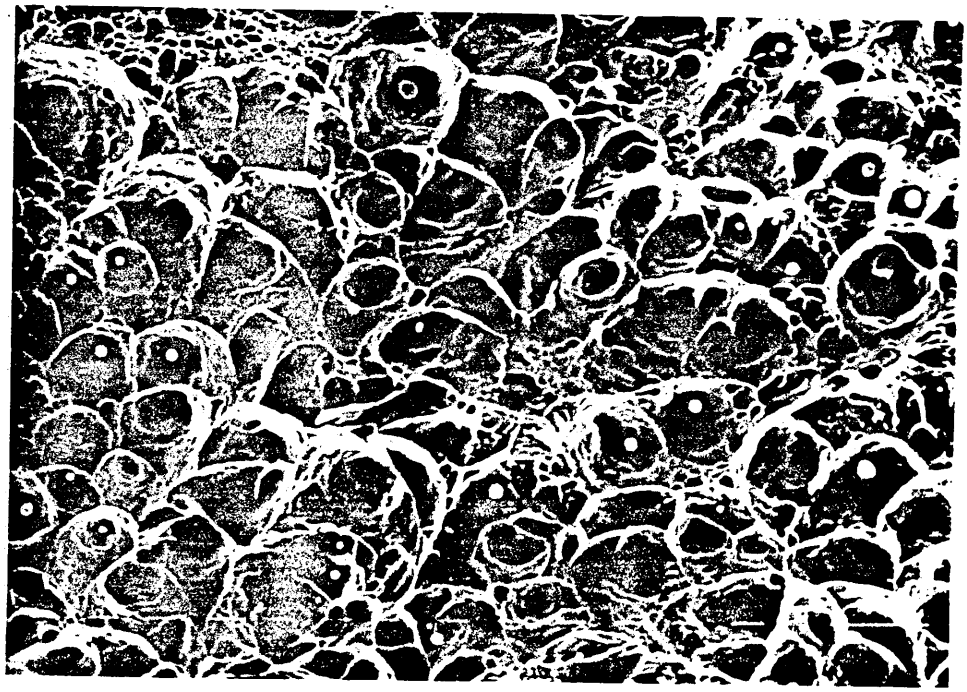

DUCTILE x400

FIGURE 75

Fractographs of Alloy K1527 after a Solution Treatment of 1300°C for 1 Hour Followed by Water Quenching and then 1 Hour at 1000°C Followed by Water Quenching.

BRITTLE x960

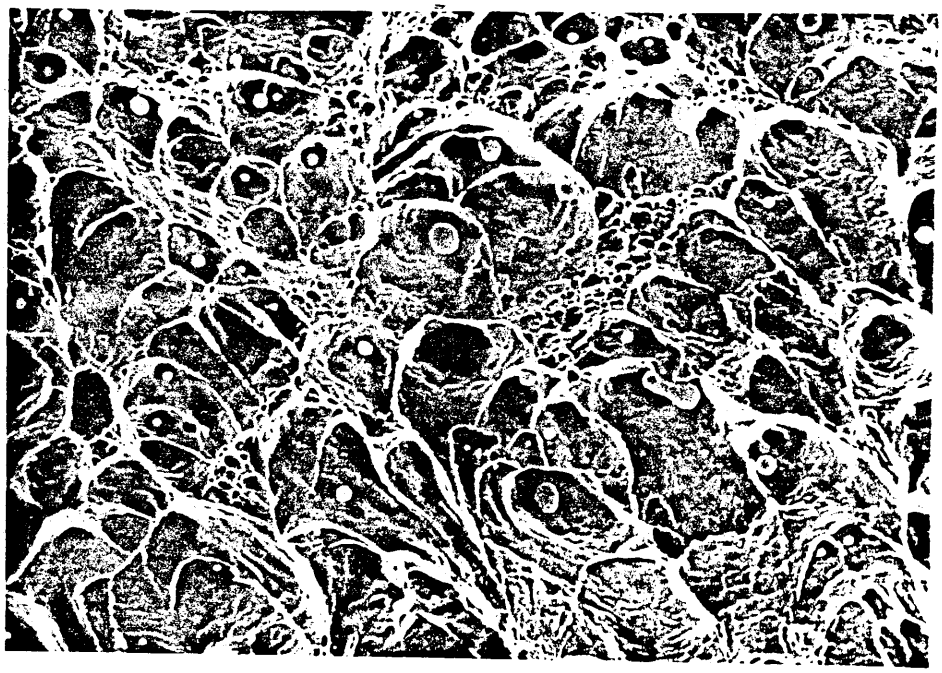

DUCTILE x480

FIGURE 76

Fractographs of Alloy K1527 after Solution Treatment at 1300°C for 1 Hour Followed by Water Quenching and then 1 Hour at 850°C Followed by Water Quenching.

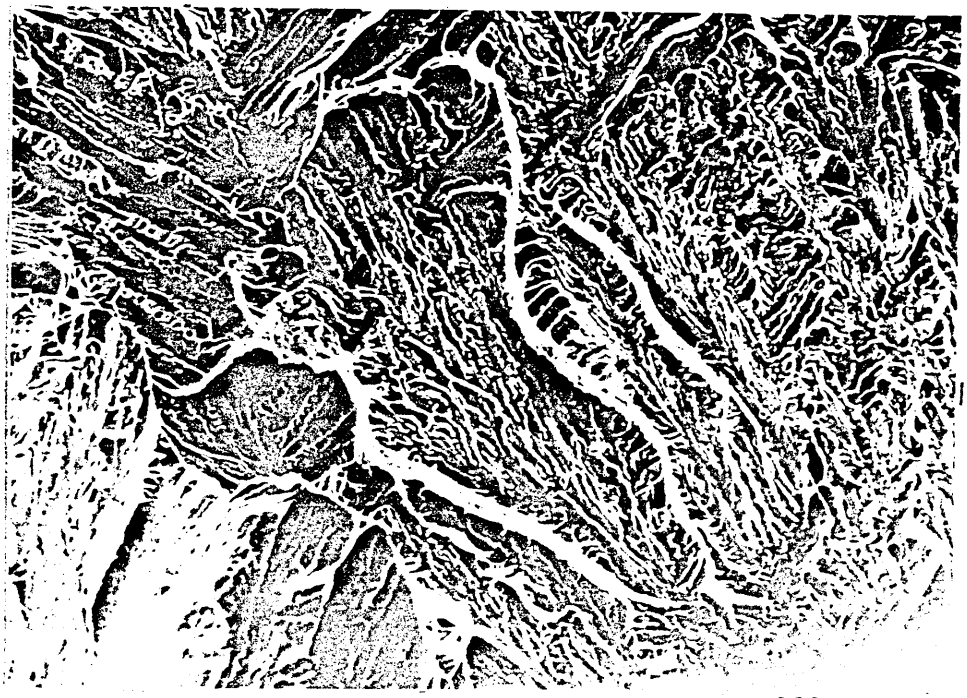

BRITTLE x200

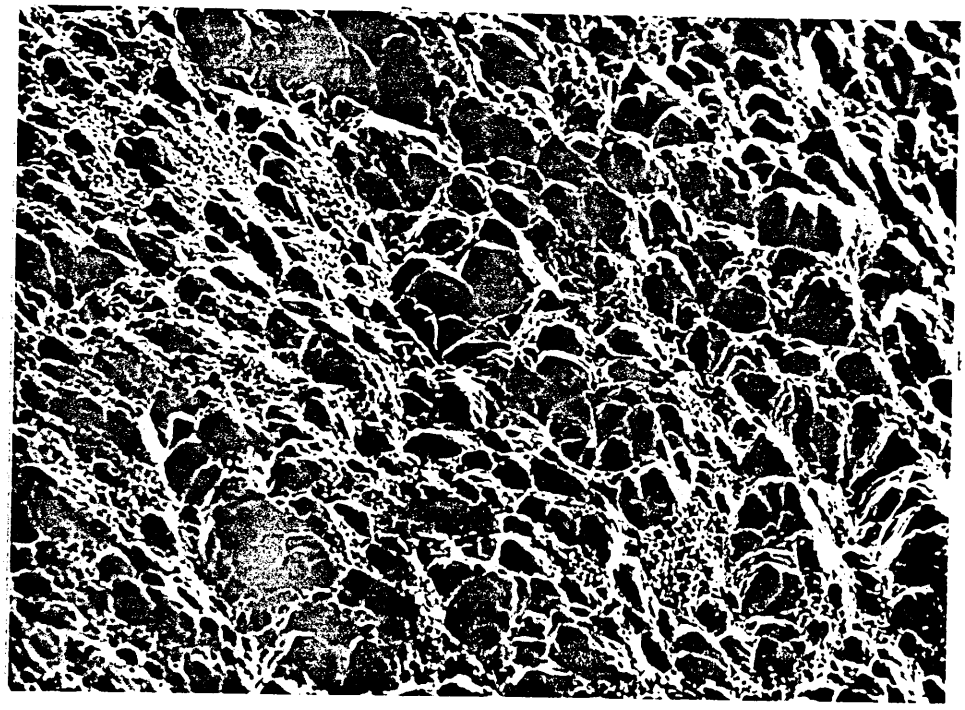

DUCTILE x200

FIGURE 77

Comparison of the Effect of Austenitising Treatment on the Impact Transition Curves for Alloys K1525 (Fe-8Mn), K1526 (Fe-8Mn-2.5Mo) and K1527 (Fe-8Mn-5Mo).

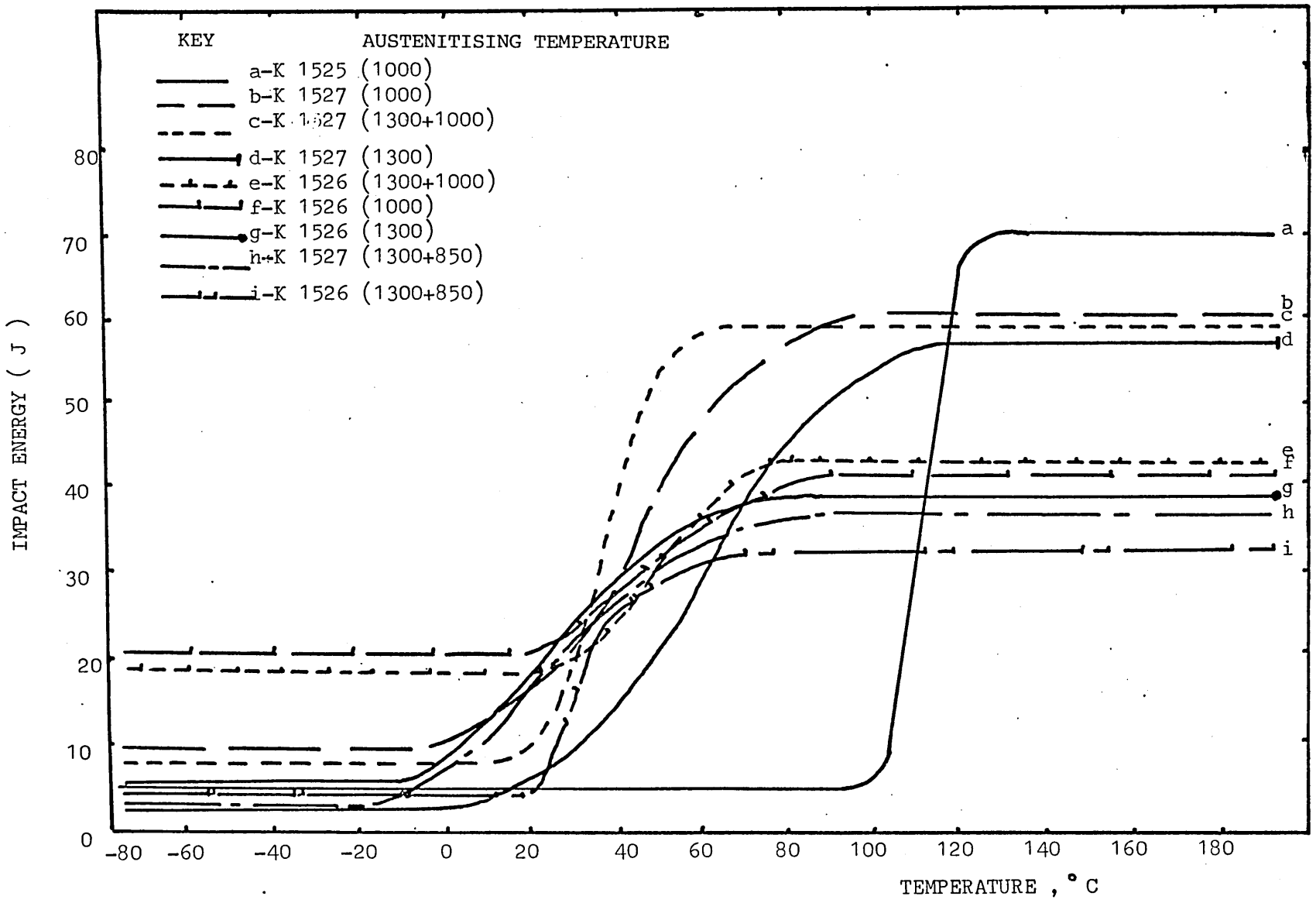
KEY
AUSTENITISING TEMPERATURE
a-K 1525 (1000)
b-K 1527 (1000)
c-K 1527 (1300+1000)
d-K 1527 (1300)
e-K 1526 (1300+1000)
f-K 1526 (1000)
g-K 1526 (1300)
h-K 1527 (1300+850)
i-K 1526 (1300+850)
IMPACT ENERGY (J)
0
10
20
30
40
50
60
70
80
-80
-60
-40
-20
0
20
40
60
80
100
120
140
160
180
TEMPERATURE , ° C
a
b
c
d
e
f
g
h
i

FIGURE 78

Effect of Molybdenum Content on the Impact Transition Curves After Single Austenitising Treatments.

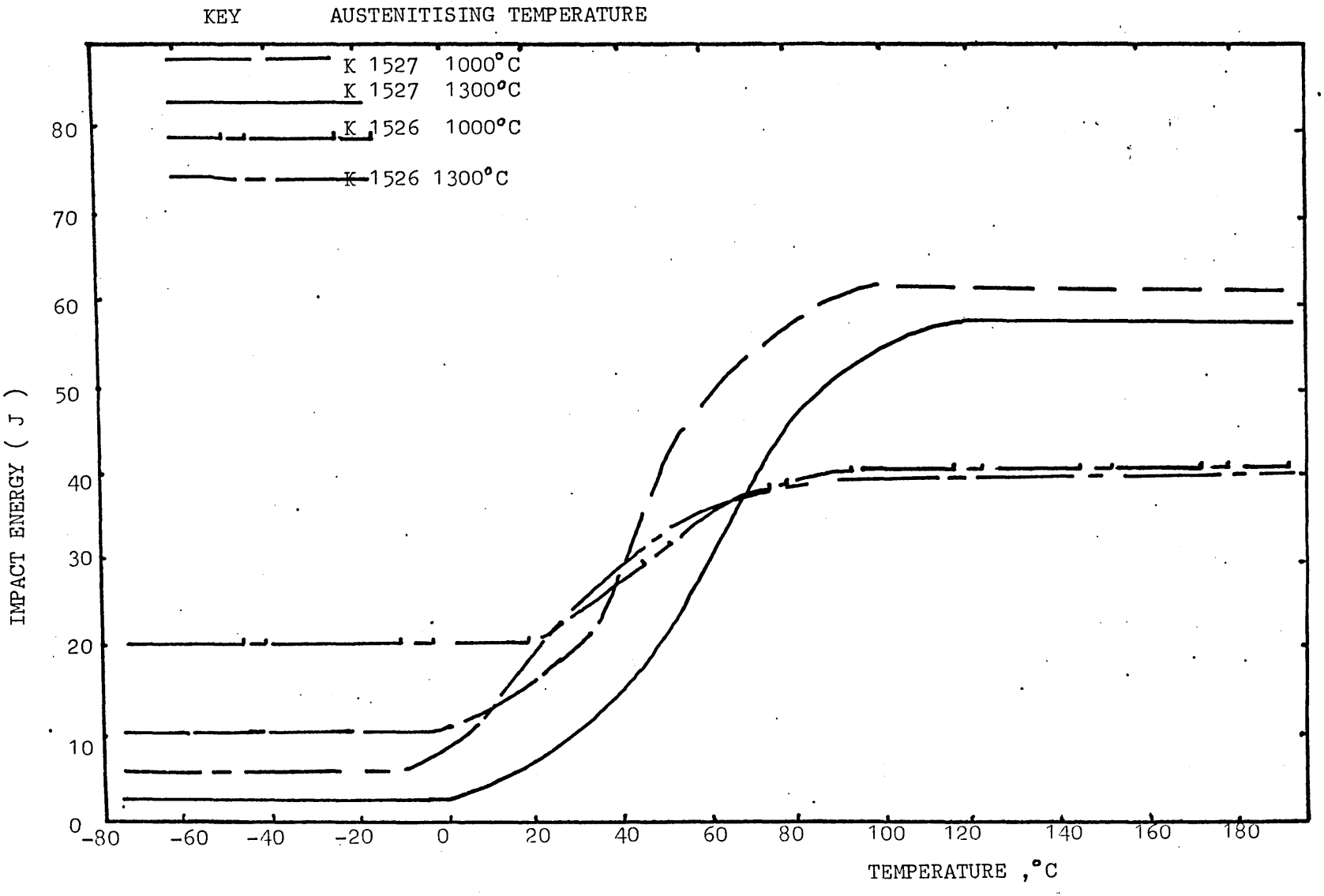
KEY
AUSTENITISING TEMPERATURE
K 1527 1000°C
K 1527 1300°C
K 1526 1000°C
K 1526 1300°C
IMPACT ENERGY (J)
0
10
20
30
40
50
60
70
80
-80
-60
-40
-20
0
20
40
60
80
100
120
140
160
180
TEMPERATURE ,°C

FIGURE 79

Comparison of the Impact Transition Curves for Alloys K1526 and K1527 in the As Quenched Condition, Austenitised at 1300°C and then 850°C.

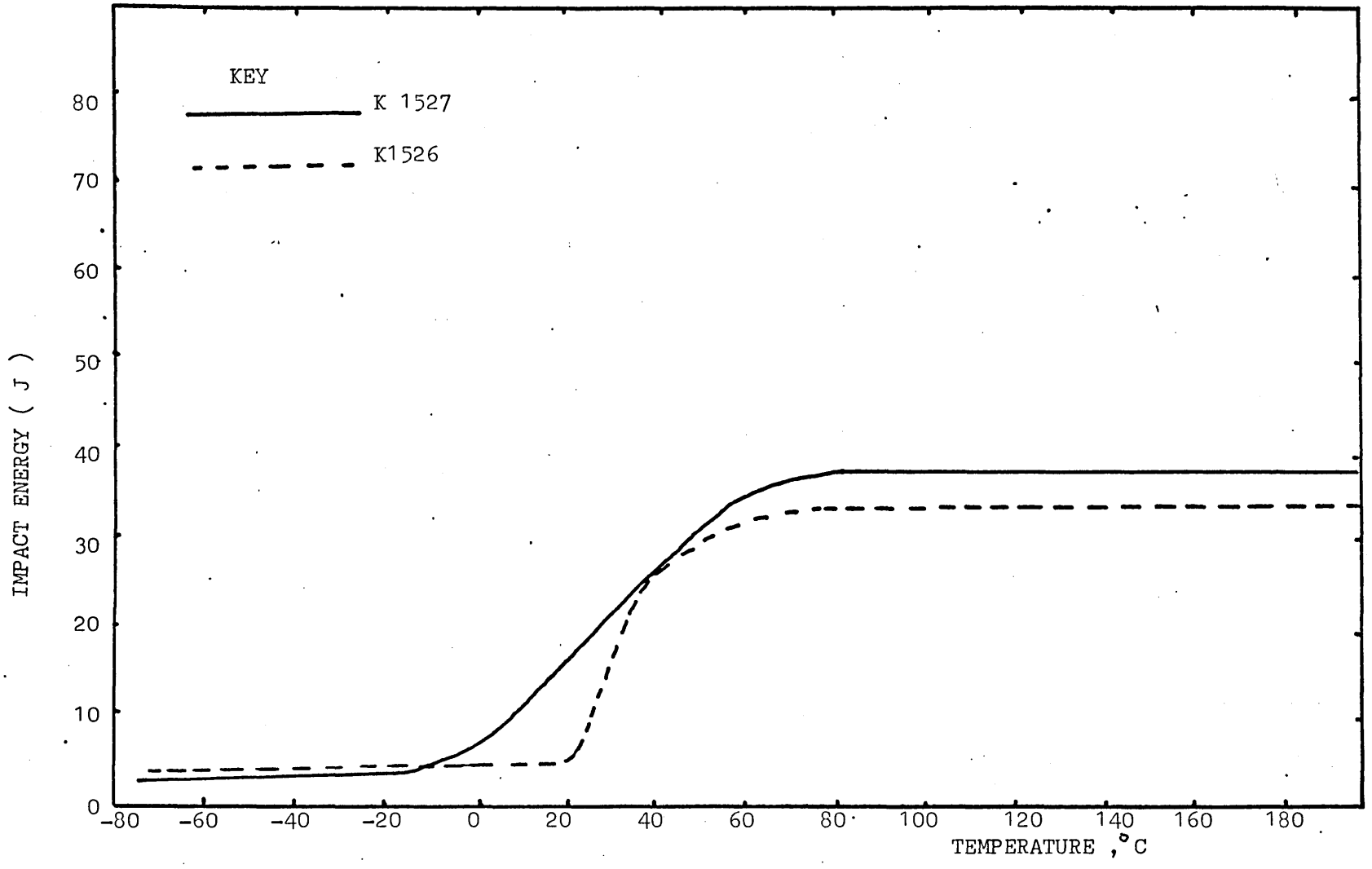
KEY
K 1527
K1526
IMPACT ENERGY (J)
0
10
20
30
40
50
60
70
80
-80
-60
-40
-20
0
20
40
60
80
100
120
140
160
180
TEMPERATURE , °C

FIGURE 80

Comparison of the Impact Transition Curves for Alloys K1526 and K1527 in the As Quenched Condition After Double Austenitising at 1300°C and then 1000°C.

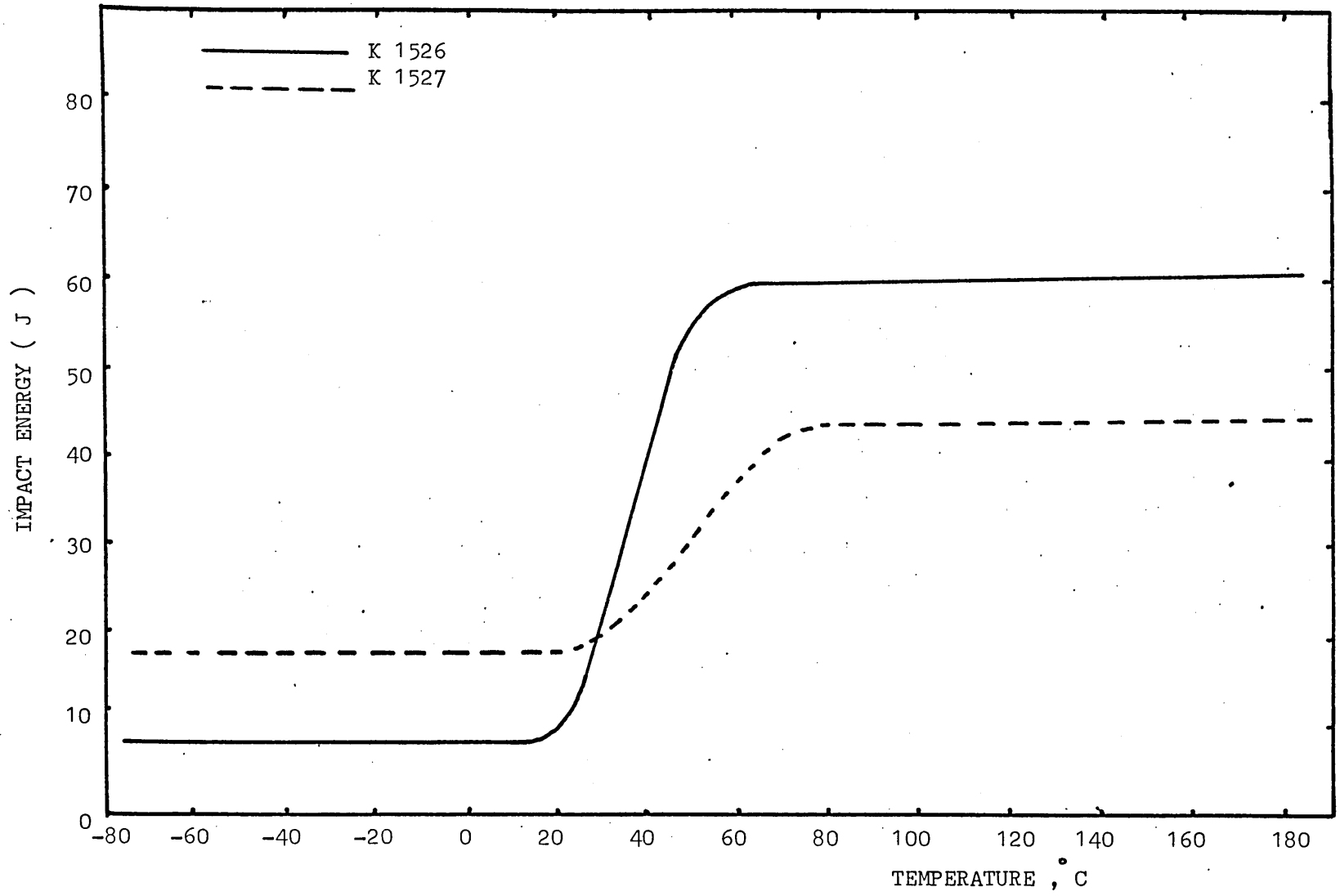
K 1526
K 1527
IMPACT ENERGY (J)
0
10
20
30
40
50
60
70
80
-80
-60
-40
-20
0
20
40
60
80
100
120
140
160
180
TEMPERATURE , °C

FIGURE 81

Comparison of the Impact Transition Curves for Alloys K1525 (Fe-8Mn), K1526 (Fe-8Mn-2.5Mo) and K1527 (Fe-Mn-5Mo) in the As Quenched Condition After Austenitising at 1000°C.

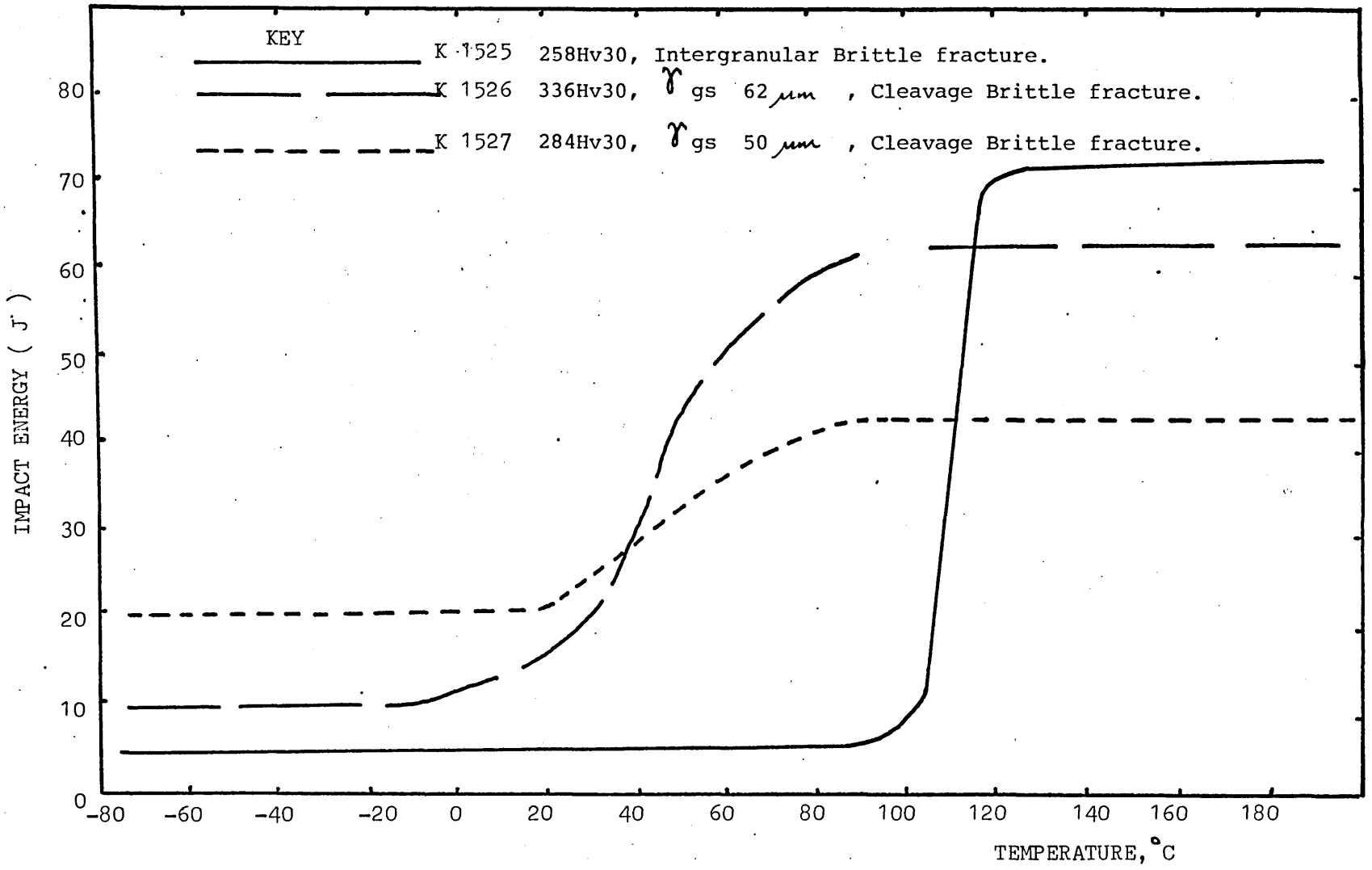
KEY
K 1525 258Hv30, Intergranular Brittle fracture.
K 1526 336Hv30, γgs 62 μm , Cleavage Brittle fracture.
K 1527 284Hv30, γgs 50 μm , Cleavage Brittle fracture.
IMPACT ENERGY (J)
0
10
20
30
40
50
60
70
80
-80
-60
-40
-20
0
20
40
60
80
100
120
140
160
180
TEMPERATURE, °C

FIGURE 82

Comparison of the Impact Transition Curves for Alloys K1526 (Fe-8Mn-2.5Mo) and K1527 (Fe-8Mn-5Mo) As Quenched from 1300°C.

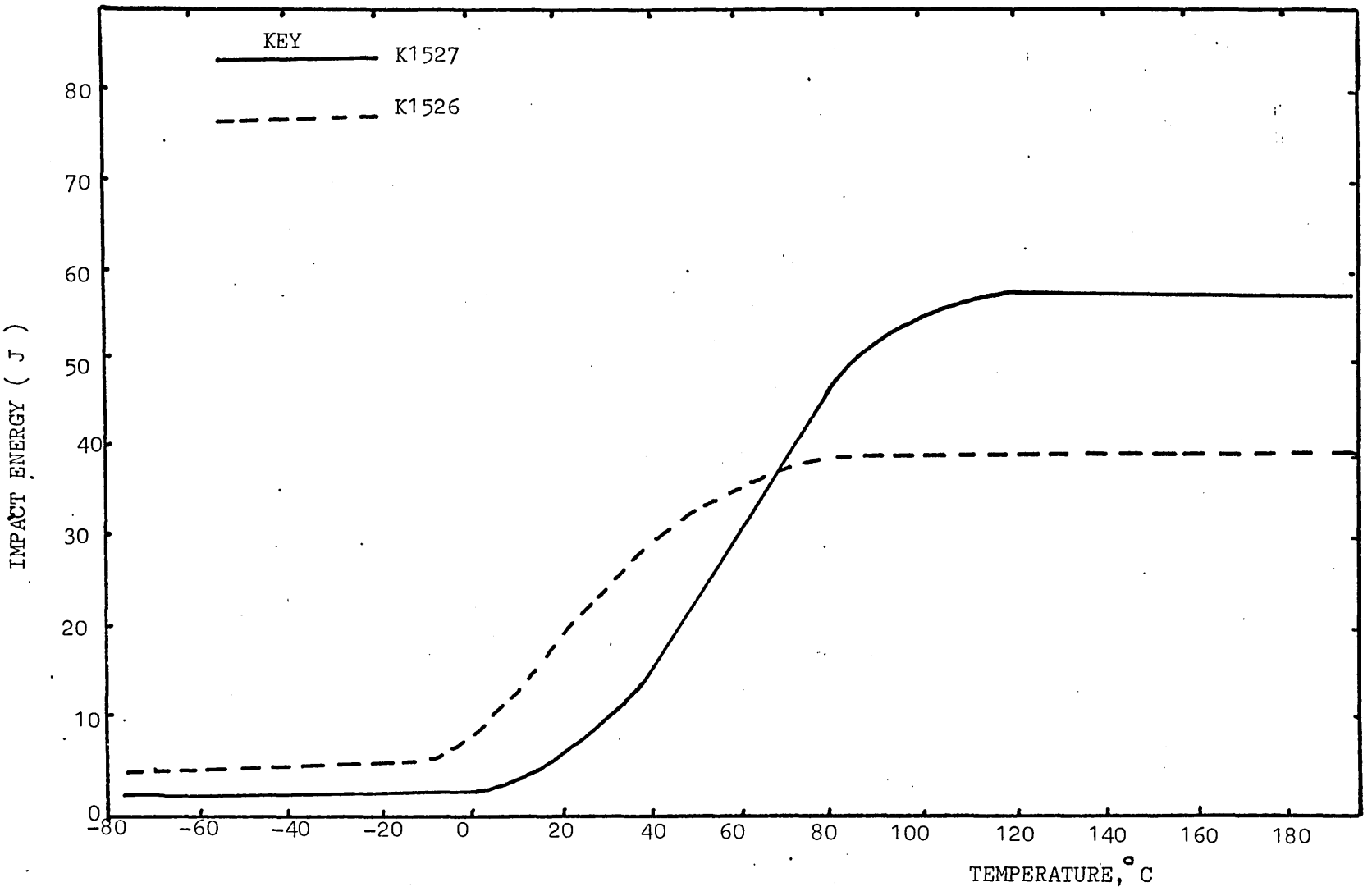
KEY
K1527
K1526
IMPACT ENERGY (J)
0
10
20
30
40
50
60
70
80
-80
-60
-40
-20
0
20
40
60
80
100
120
140
160
180
TEMPERATURE, °C

FIGURE 83

The Age Hardening Characteristics of Alloy K1526 (Fe-8Mn-2.5Mo) and K1527 (Fe-8Mn-5Mo) Aged at 450°C. Prior Austenitising Taken Place at 1000°C and 1300°C.

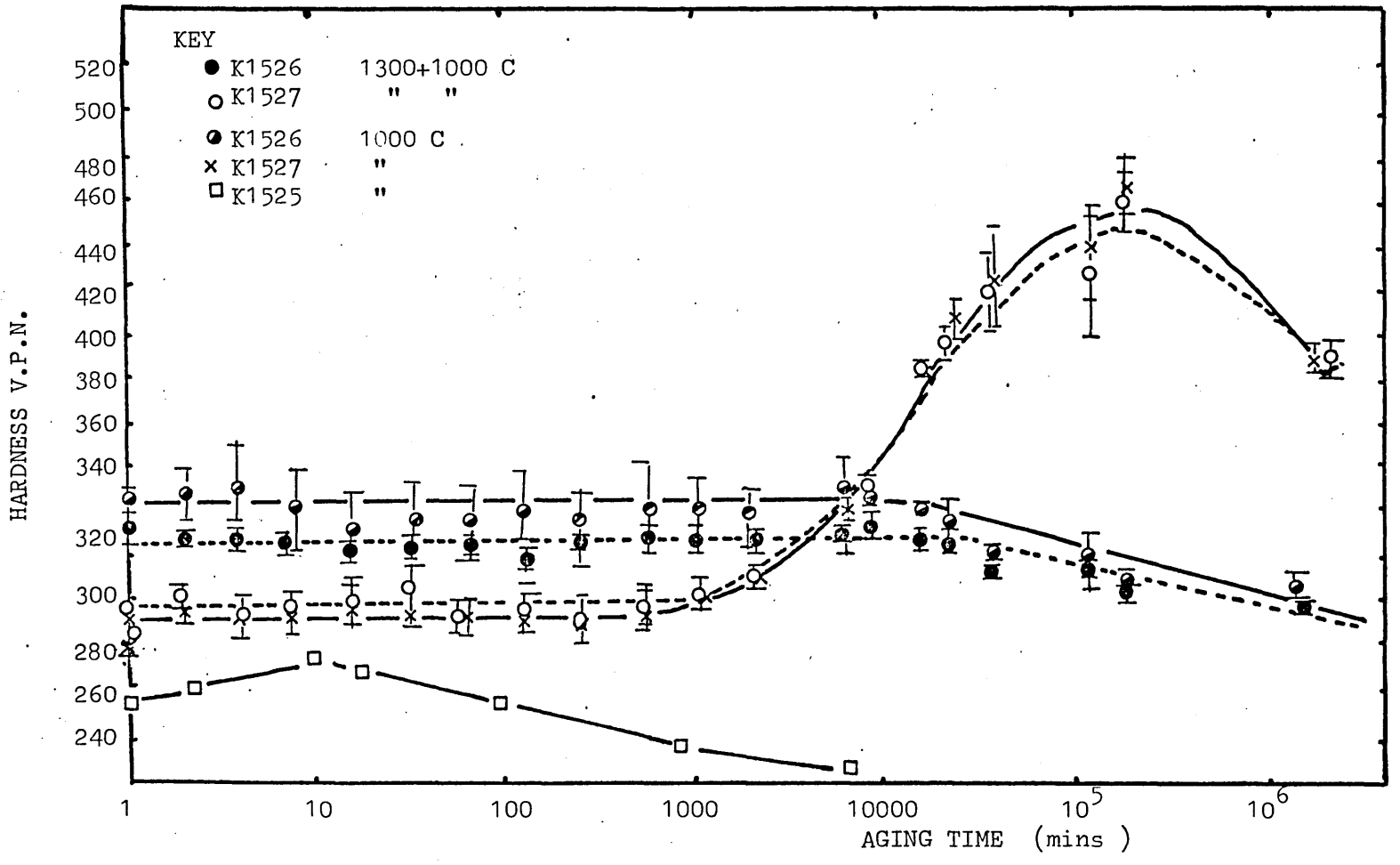
KEY
K1526 1300+1000 C
K1527 " "
K1526 1000 C
K1527 "
K1525 "
HARDNESS V.P.N.
520
500
480
460
440
420
400
380
360
340
320
300
280
260
240
1
10
100
1000
10000
10^5
10^6
AGING TIME (mins)

FIGURE 84

Electron Micrographs of Alloy K1527 (Fe-8Mn-5Mo) in the As-Quenched and in the Aged Condition.

AS QUENCHED x4500

AGED FOR 368 HOURS x15000

AT 450°C.

FIGURE 85

Electron Micrograph of K1527 in the As Quenched Condition.

Diffraction Pattern From the Iron Matrix in K1527.

Solution of the Diffraction Pattern gives a Zone Axis (011).

x3000

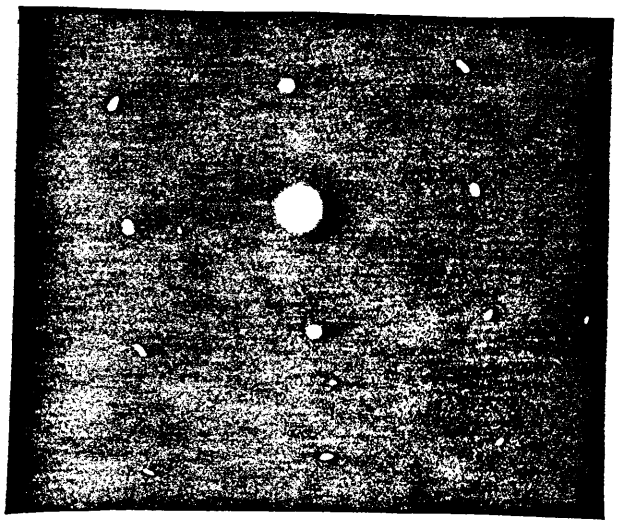

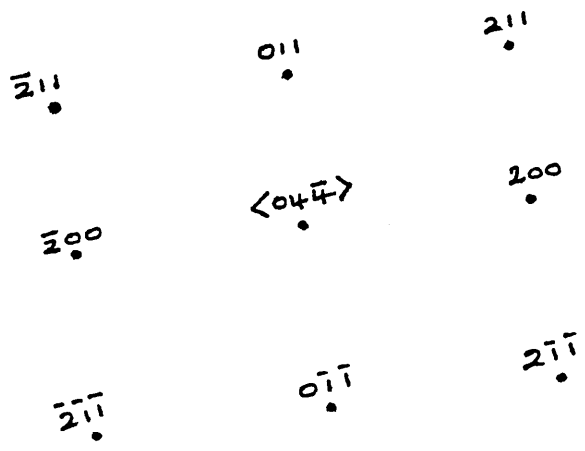
$\bar{2}11$
011
211
$\bar{2}00$
$\langle 04\bar{4} \rangle$
200
$\bar{2}1\bar{1}$
$01\bar{1}$
$21\bar{1}$

FIGURE 86

Diffraction Pattern Taken from the Matrix Shown in Figure 87.

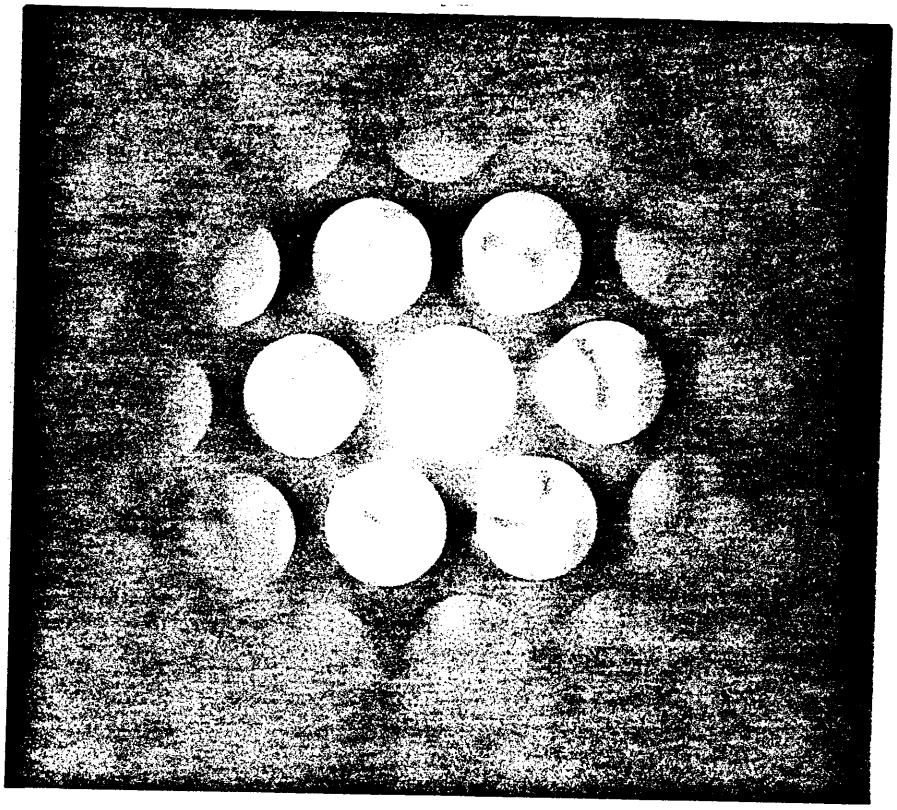


202
101
110
112
011
111
022
220
110
101
112
202

FIGURE 87

Precipitation in Alloy K1527 (Fe-8Mn-5Mo) after Aging for 480 Hours at 450°C.

x184000

FIGURE 88

Dark Field of Precipitates in Alloy K1527 (Fe-8Mn-5Mo) Aged for 480 Hours at 450°C Using the Diffraction Pattern from Figure 89.

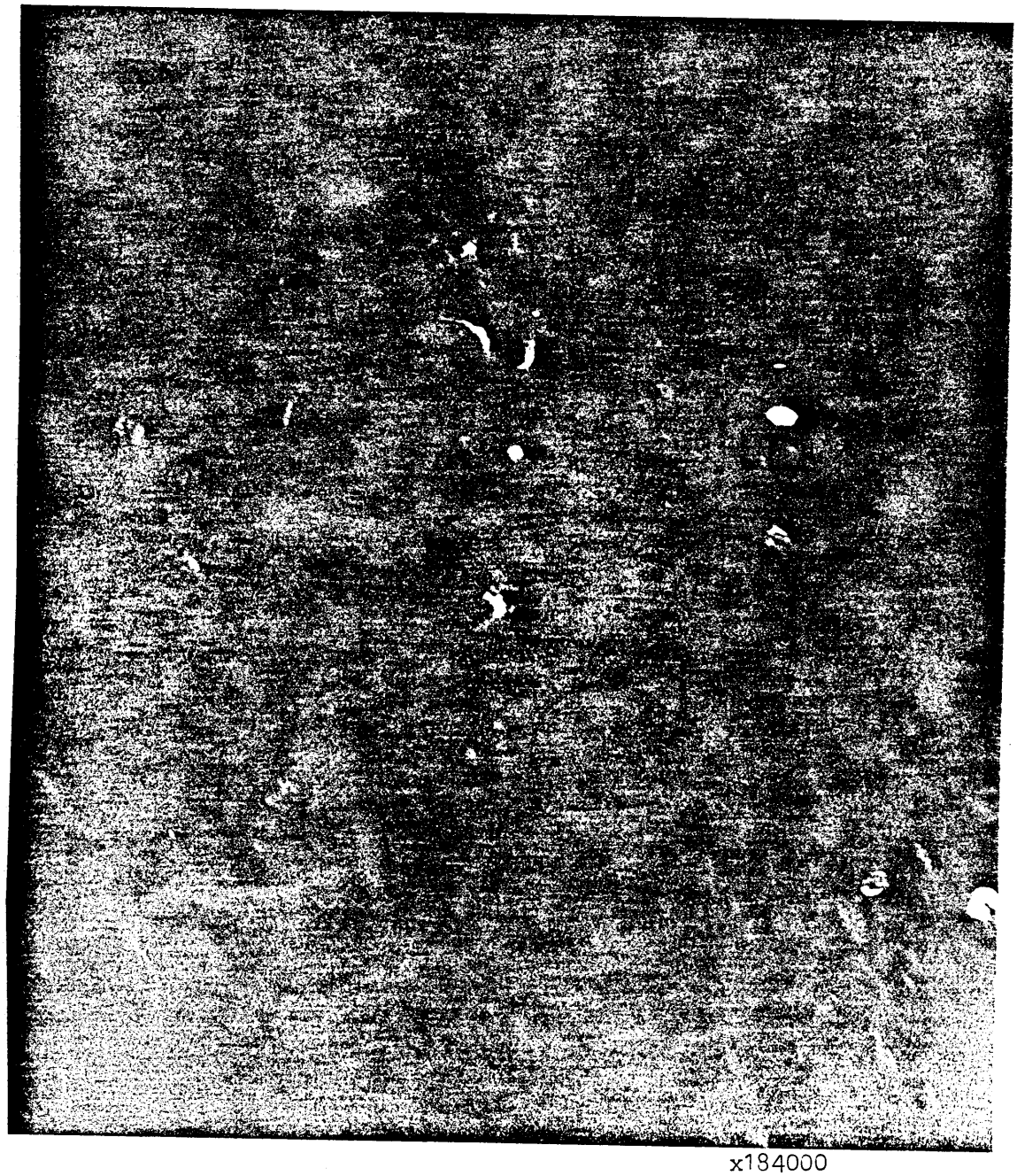

x184000

FIGURE 89

Diffraction Pattern for Precipitates Shown in Figure 87.

Solution for Laves Fe_2Mo Phase

Zone Axis = $\langle \bar{1}\bar{1}2 \rangle$ = $[112]$ type.

Solution for Fe-Mo σ Phase

Zone Axis $\langle 0\bar{5}0 \rangle$ = $[010]$ type.

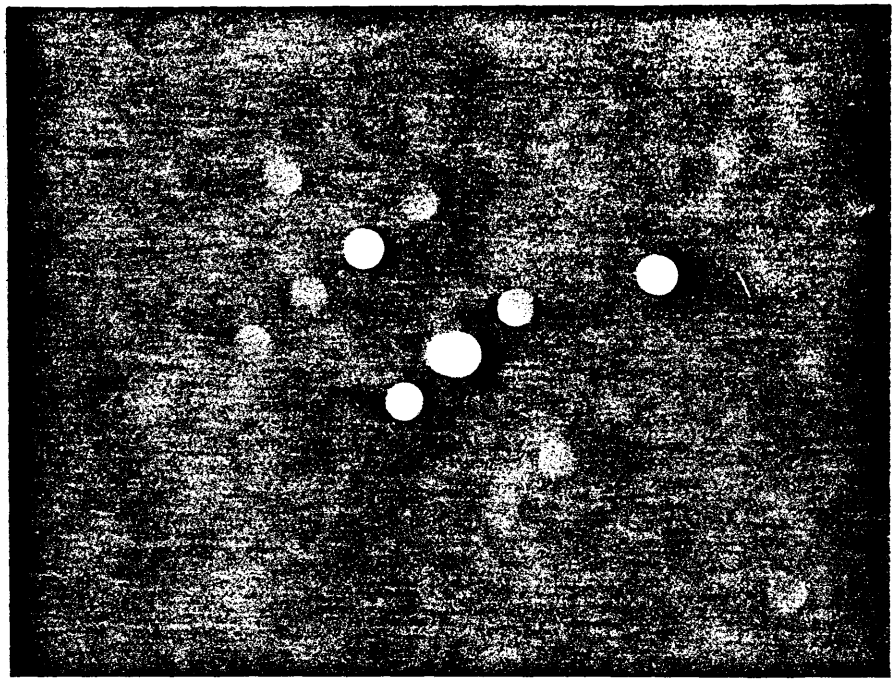

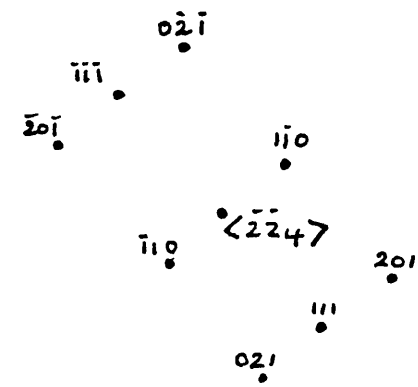
02$\bar{1}$
$\bar{1}$11
$\bar{2}$0$\bar{1}$
1$\bar{1}$0
<$\bar{2}\bar{2}$4>
$\bar{1}$10
201
111
021

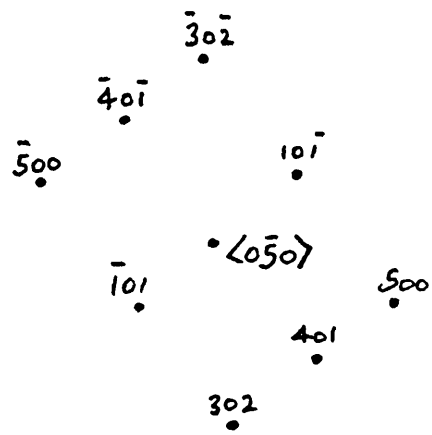
$\bar{3}$0$\bar{2}$
$\bar{4}$0$\bar{1}$
$\bar{5}$00
10$\bar{1}$
<0$\bar{5}$0>
$\bar{1}$01
500
401
302

FIGURE 90

Effect of Aging at 450°C and 525°C on the Impact Transition Curve of Alloy K1527 (Fe-8Mn-5Mo) After Austenitising at 1000°C.

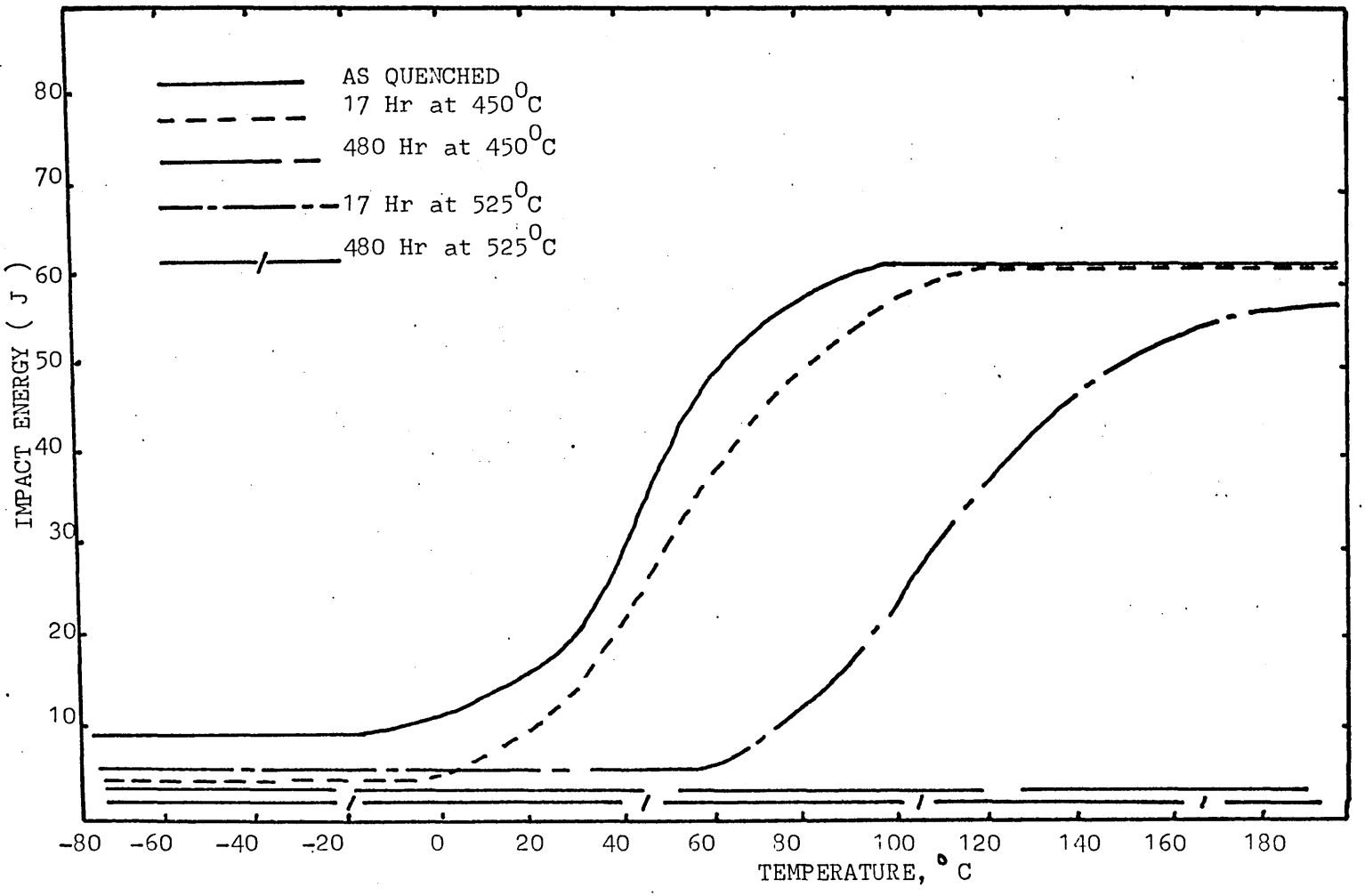
AS QUENCHED
17 Hr at 450°C
480 Hr at 450°C
17 Hr at 525°C
480 Hr at 525°C
IMPACT ENERGY (J)
80
70
60
50
40
30
20
10
-80
-60
-40
-20
0
20
40
60
80
100
120
140
160
180
TEMPERATURE, °C

FIGURE 91

The Effect of Aging at 450°C and 525°C on the Impact Transition Curves for Alloy K1526 (Fe-8Mn-2.5Mo) After Austenitising at 1000°C.

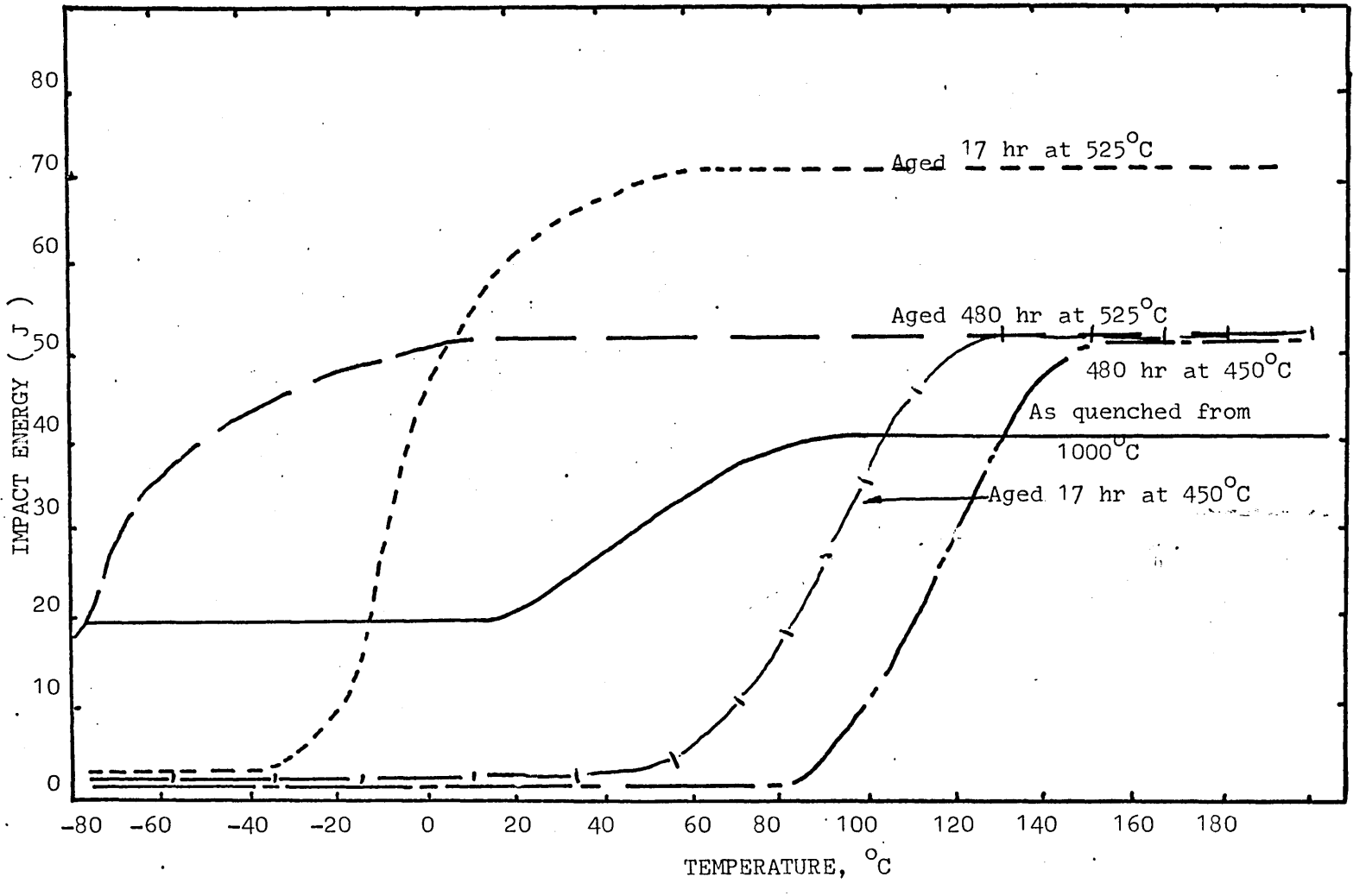
80
70
60
50
40
30
20
10
0
IMPACT ENERGY (J)
Aged 17 hr at 525°C
Aged 480 hr at 525°C
480 hr at 450°C
As quenched from 1000°C
Aged 17 hr at 450°C
-80 -60 -40 -20 0 20 40 60 80 100 120 140 160 180
TEMPERATURE, °C

FIGURE 92

SEM Fractographs of Alloy K1526 (Fe-8Mn-2.5Mo)

After 17 Hours at 450°C.

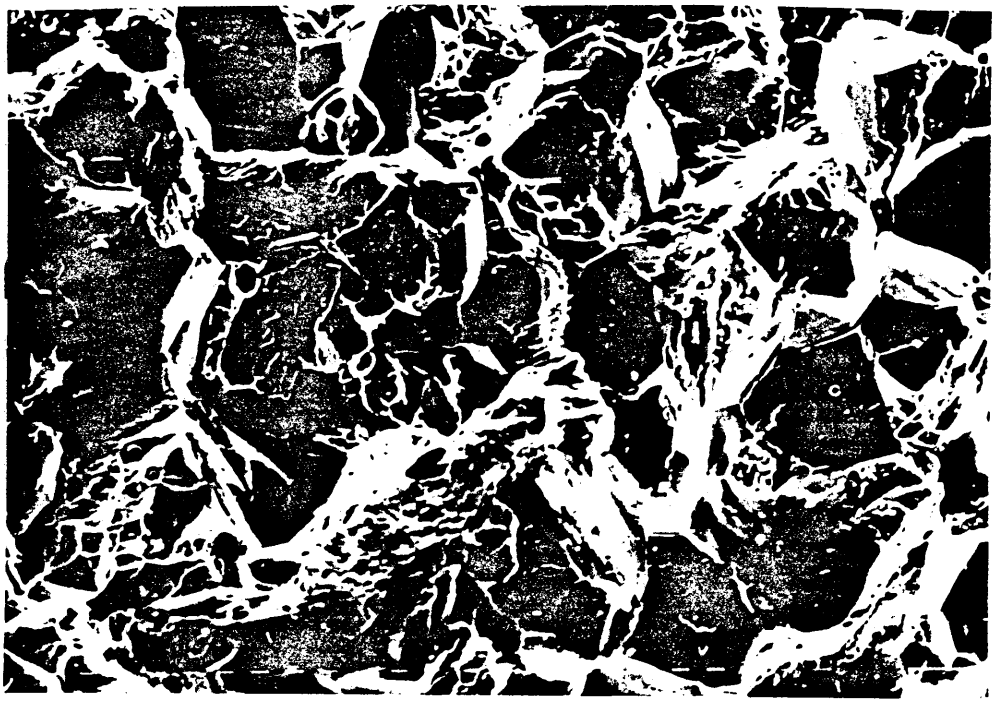

BRITTLE x280

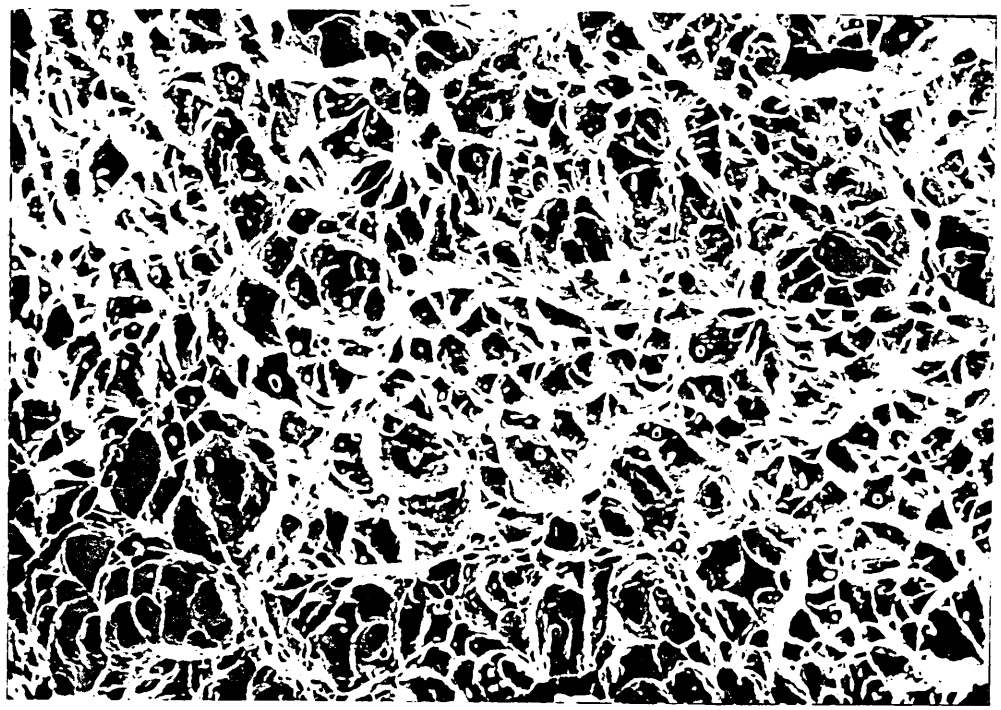

DUCTILE x257

FIGURE 93

SEM Fractographs of Alloy K1526 (Fe-8Mn-2.5Mo)

After 480 Hours at 450°C.

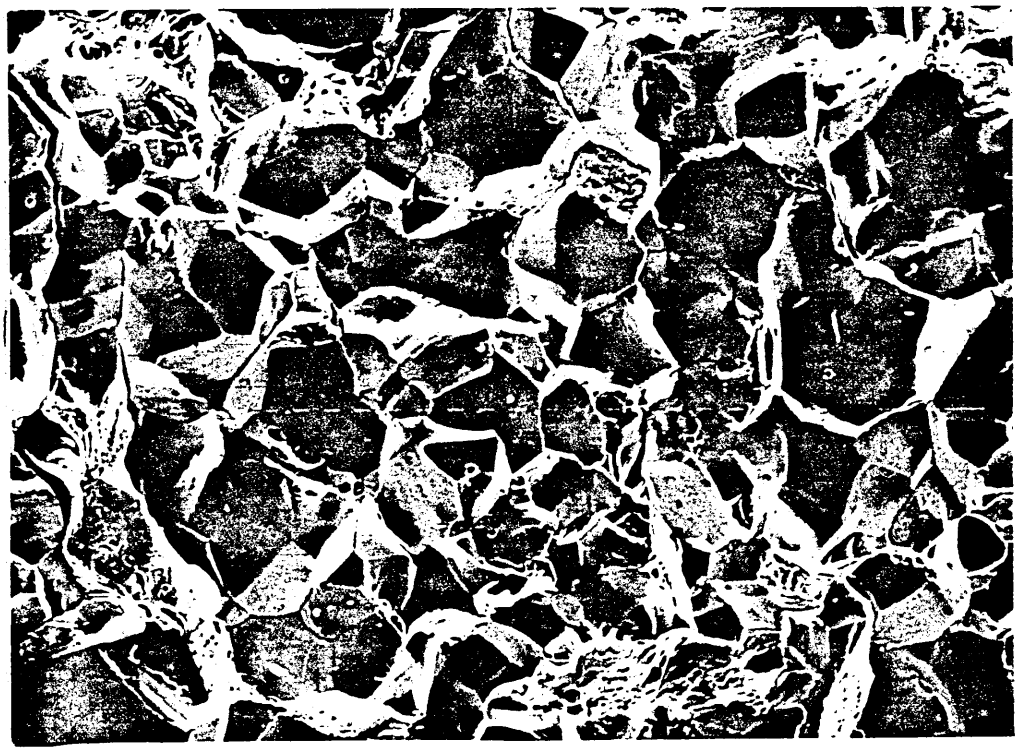

BRITTLE x257

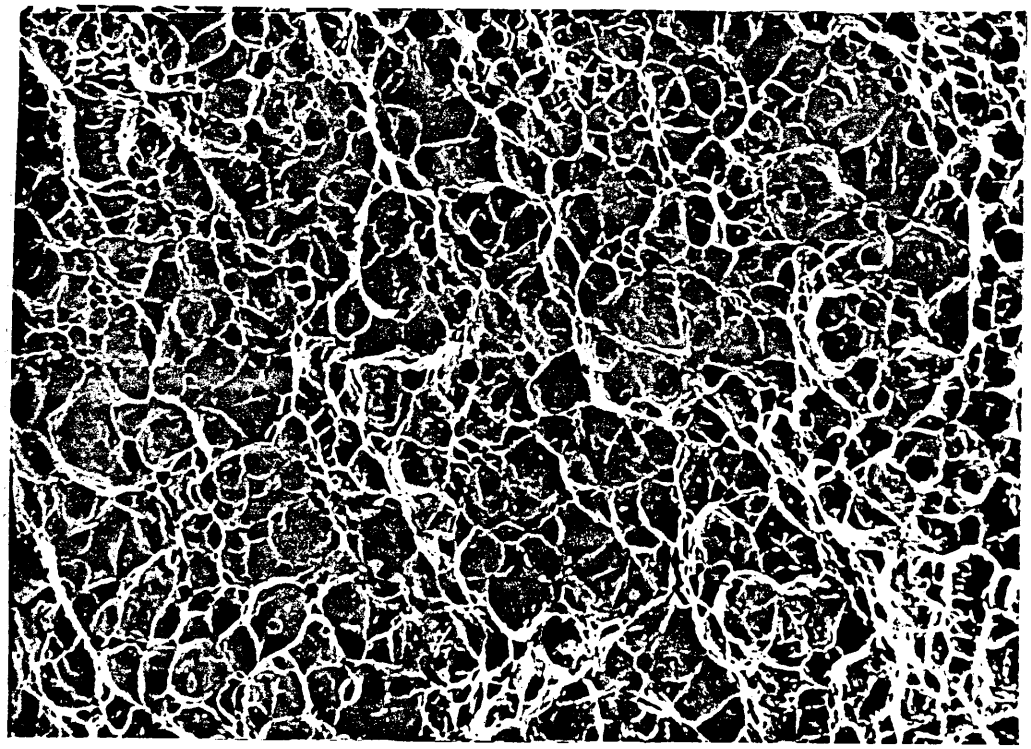

DUCTILE x234

FIGURE 94

SEM Fractographs of Alloy K1526 (Fe-8Mn-2.5Mo)

After Aging for 17 Hours at 525°C.

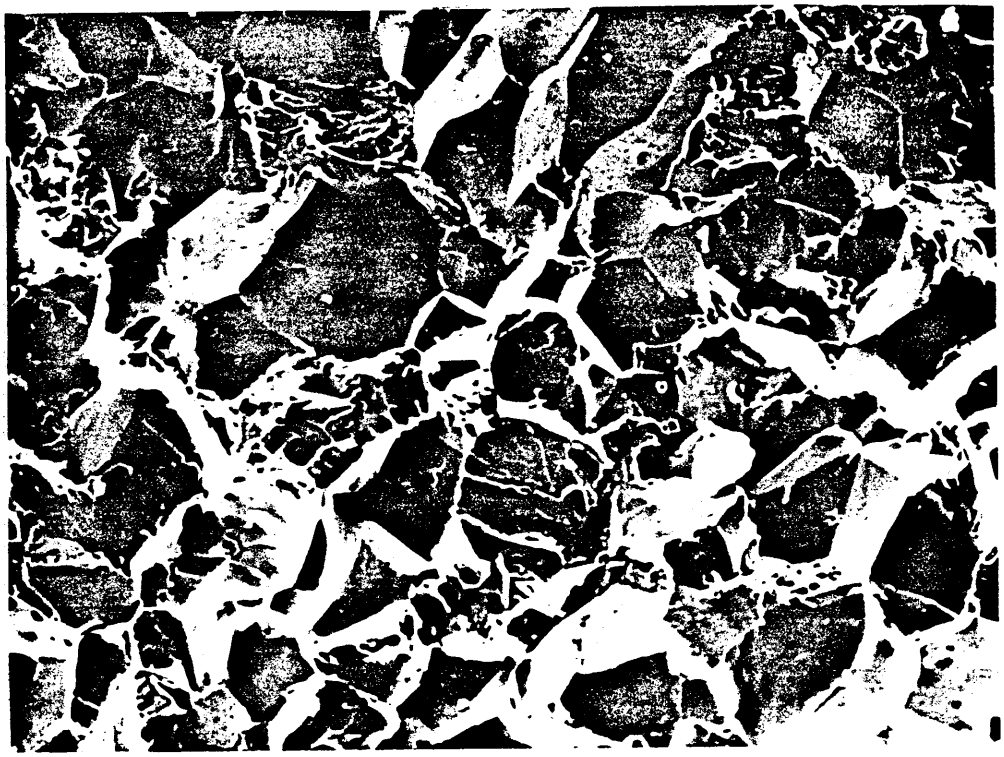

BRITTLE x234

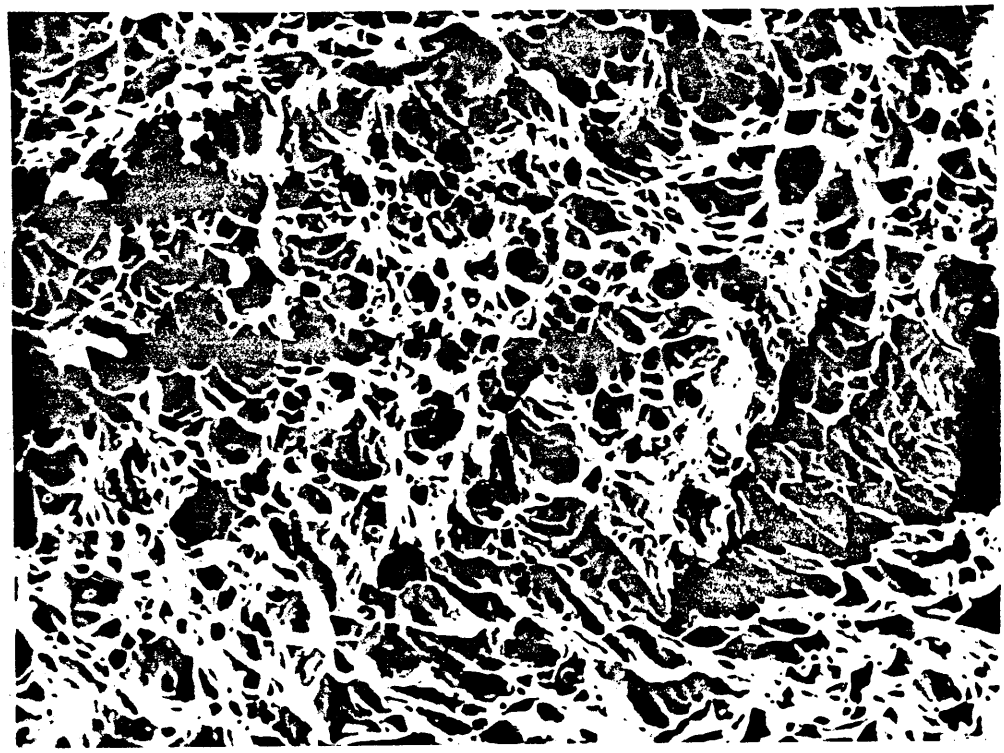

DUCTILE x257

FIGURE 95

SEM Fractographs of Alloy K1526 (Fe-8Mn-2.5Mo)

After Aging for 480 Hours at 525°C.

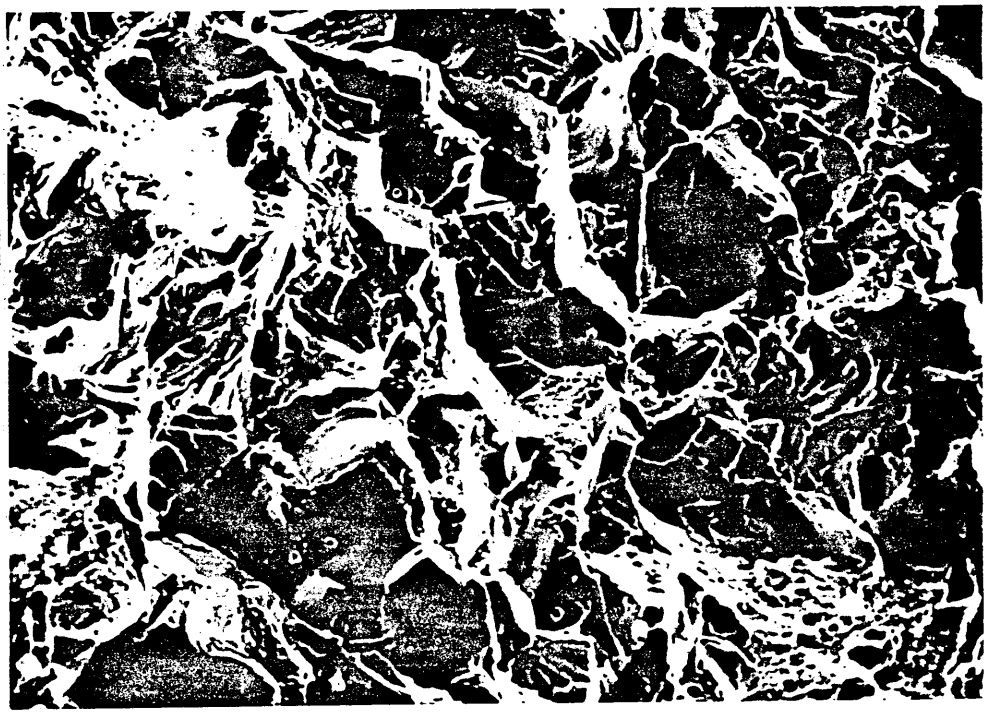

BRITTLE x257

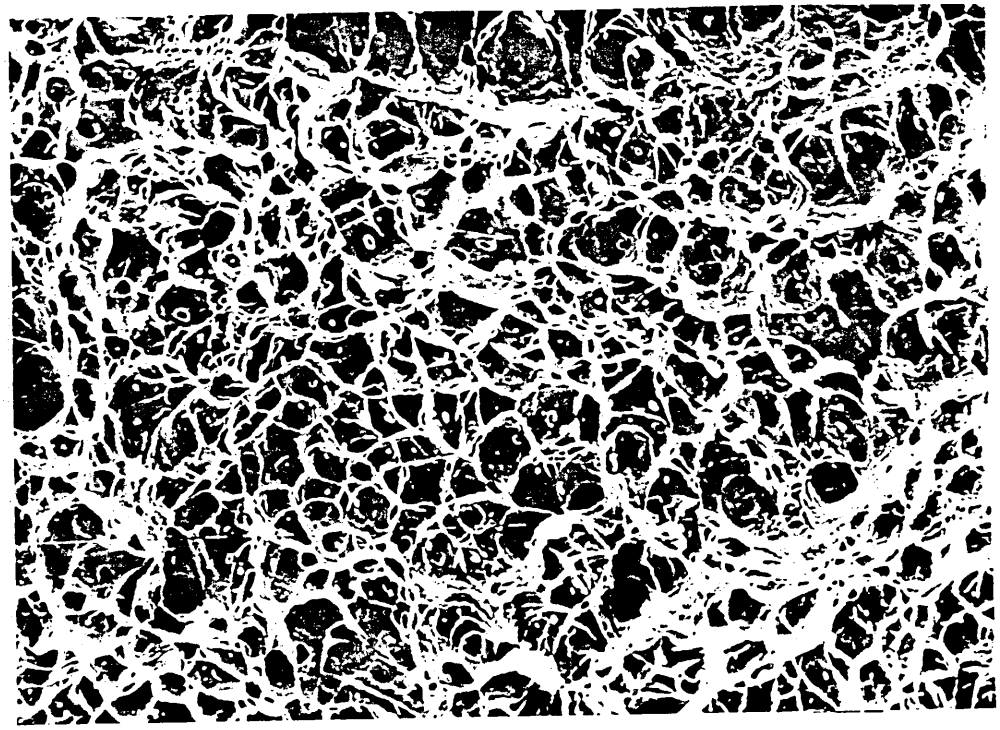

DUCTILE x222

FIGURE 96

SEM Fractographs of Alloy K1527 (Fe-8Mn-5Mo)

After Aging for 17 Hours at 450°C.

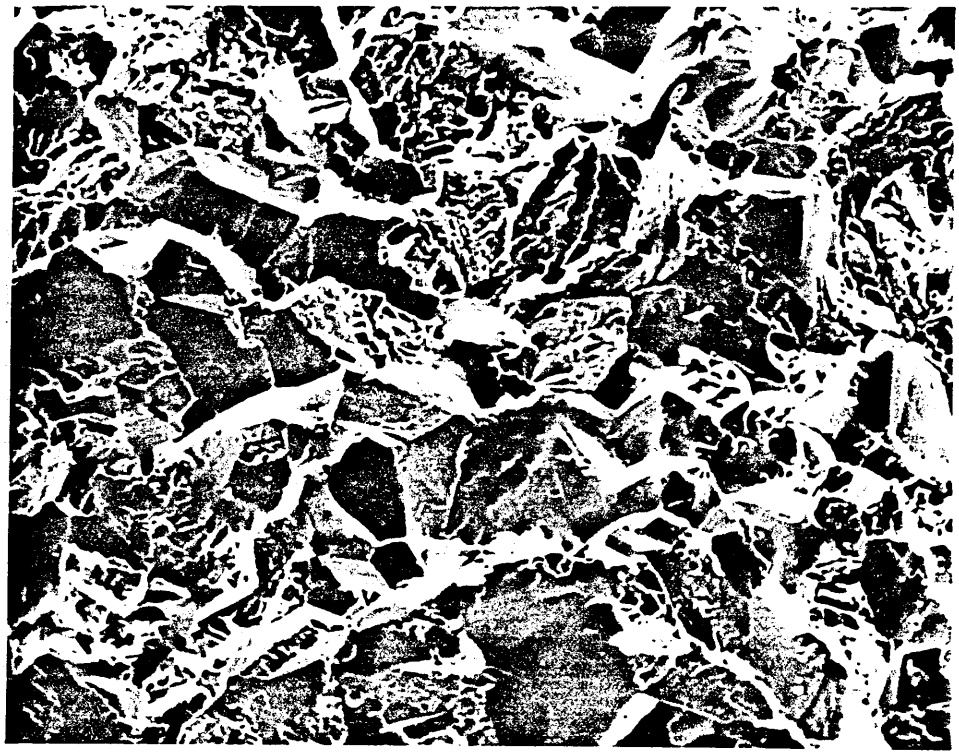

BRITTLE x562

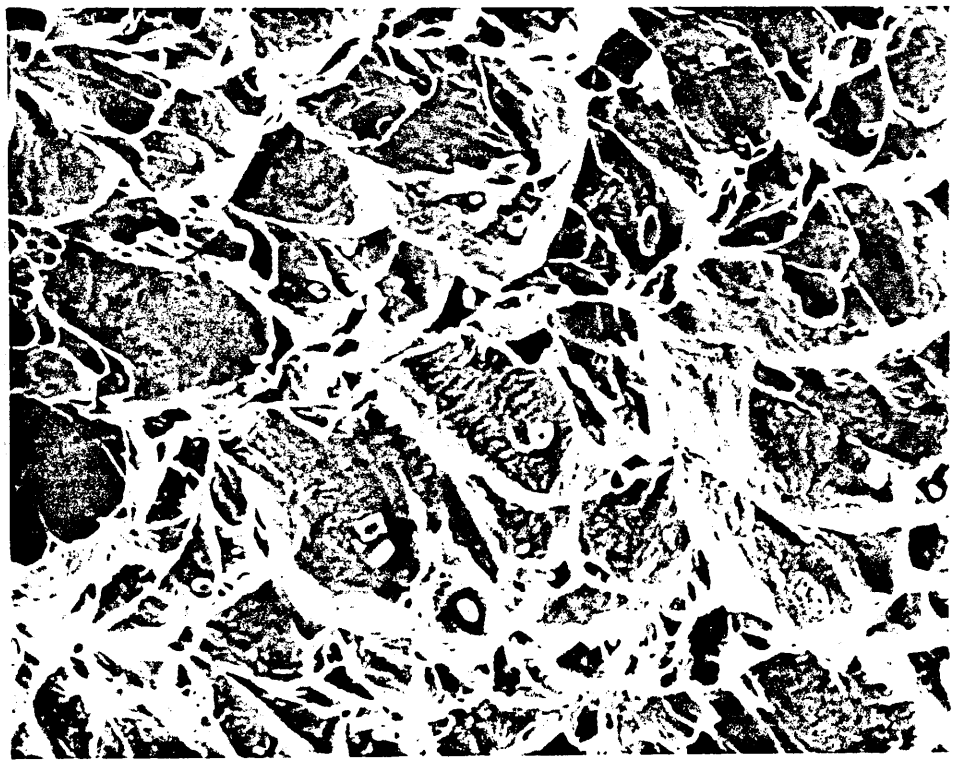

DUCTILE x562

FIGURE 97

SEM Fractographs of Alloy K1527 (Fe-8Mn-5Mo)

After Aging for 480 Hours at 450°C.

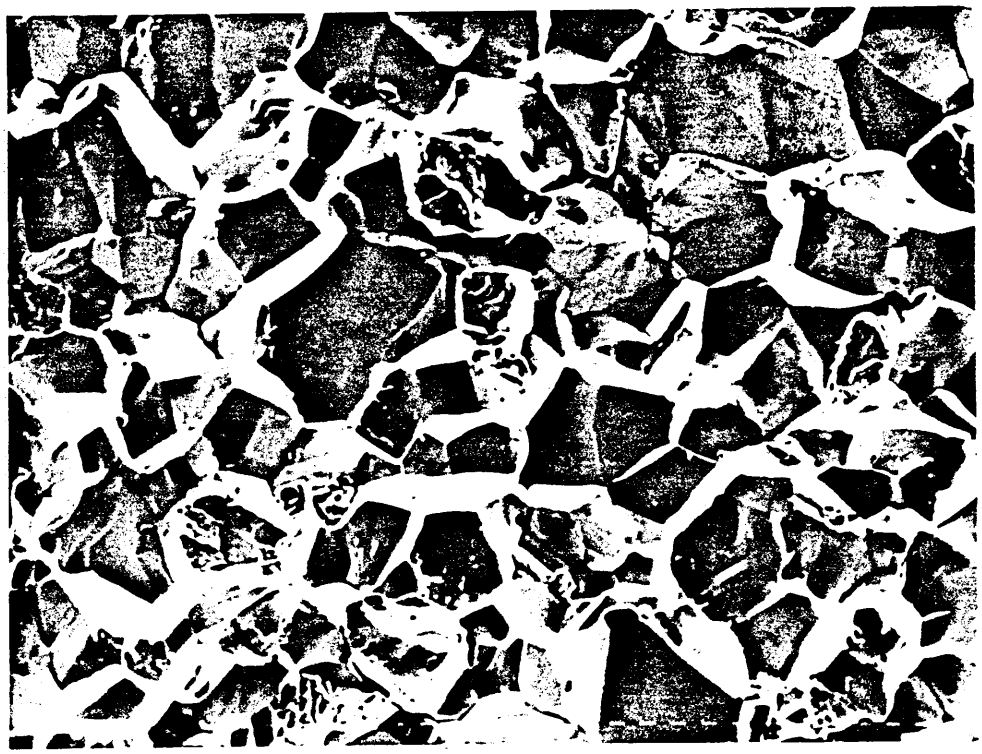

BRITTLE (fracture at 23°C) x280

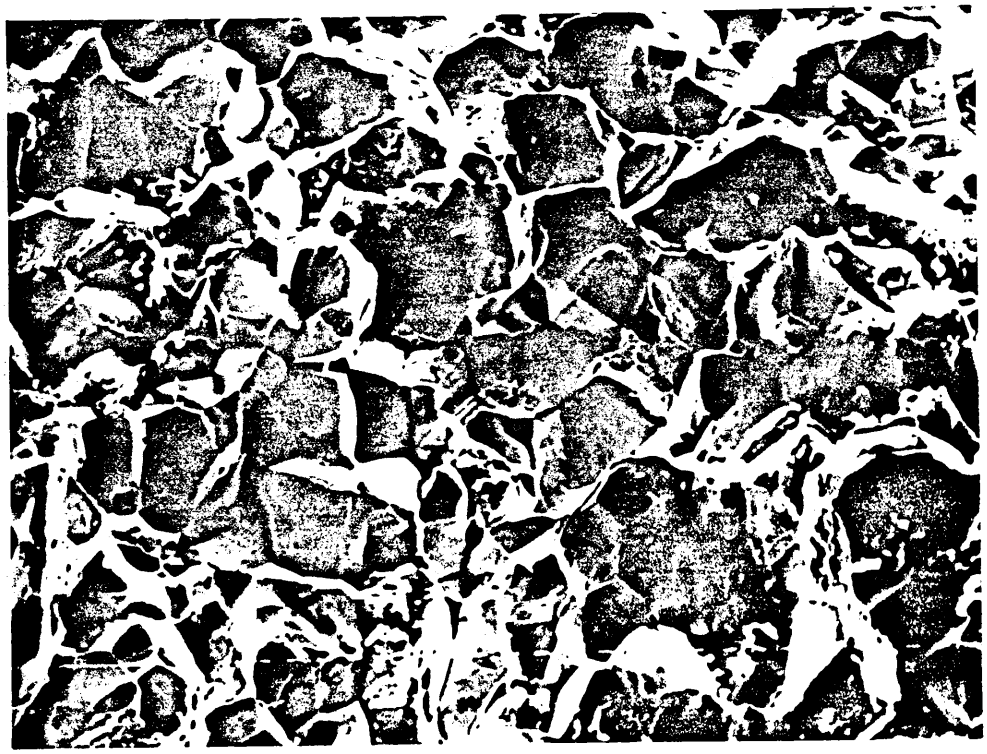

BRITTLE (fracture at 256°C) x257

FIGURE 98

SEM Fractographs of Alloy K1527 (Fe-8Mn-5Mo)

After Aging for 17 Hours at 525°C.

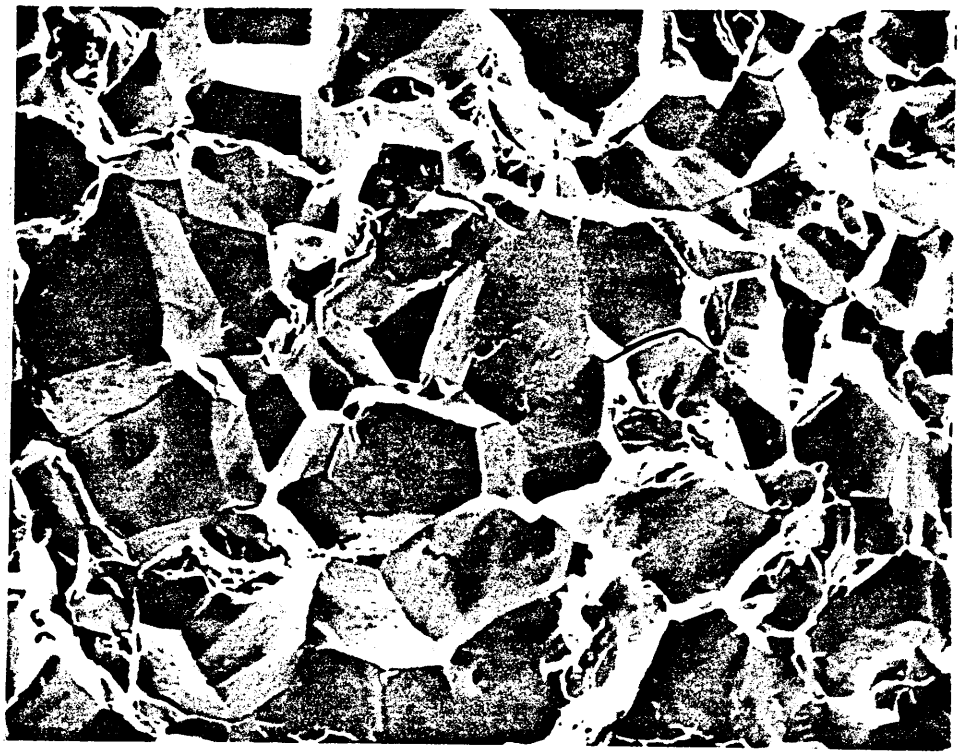

BRITTLE x304

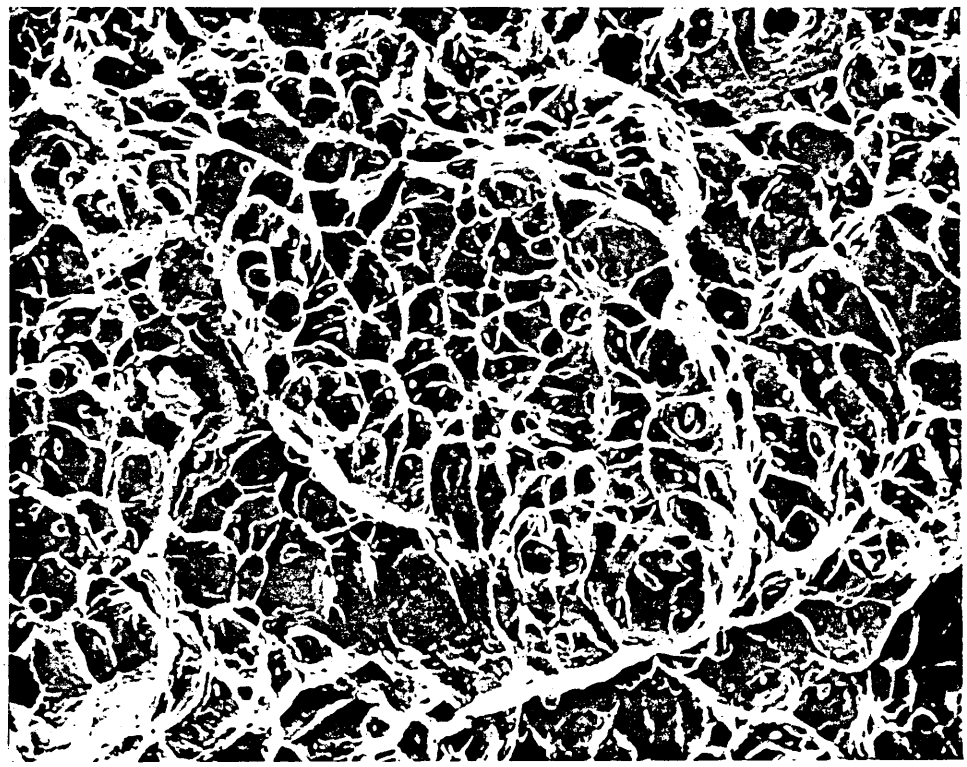

DUCTILE x280

FIGURE 99

SEM Fractographs of Alloy K1527 after Aging for 480 Hours at 525°C.

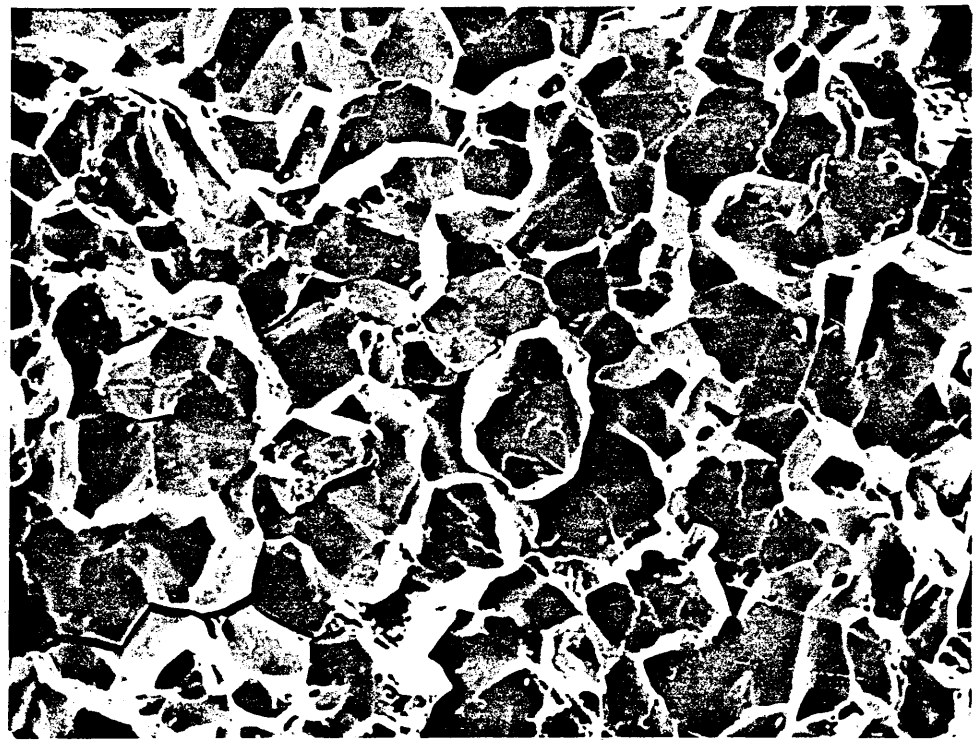

BRITTLE (fracture at 23°C) x257

BRITTLE (fracture at 256°C) x514

FIGURE 100

The Variation with Charpy Impact Transition Temperature with the Aging Time at Two Different Aging Temperatures Showing the Effect of Varying the Molybdenum Content of a Fe-8Mn Alloy.

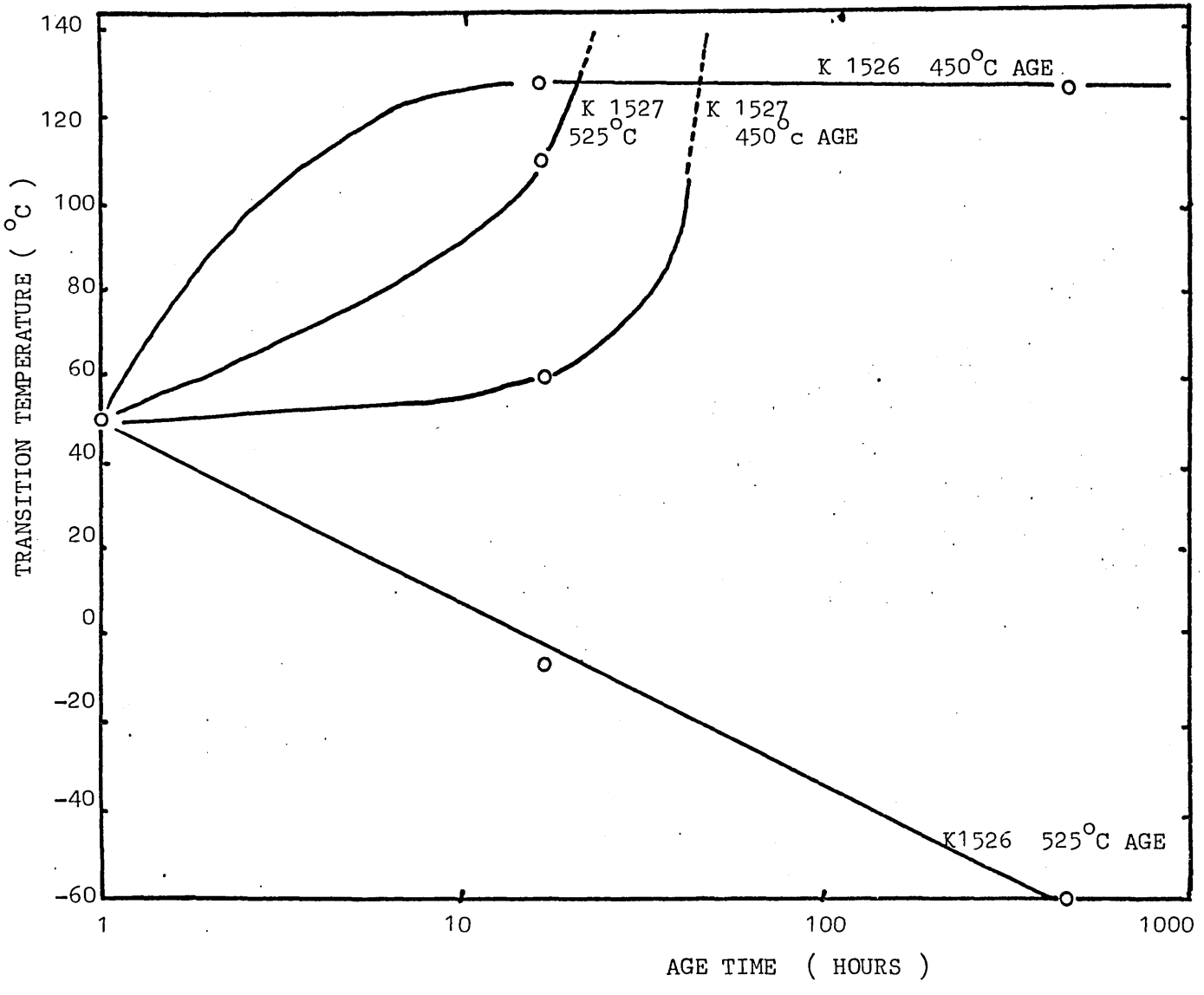
140
120
100
80
60
40
20
0
-20
-40
-60
TRANSITION TEMPERATURE (°C)
1
10
100
1000
AGE TIME (HOURS)
K 1526 450°C AGE
K 1527
525°C
K 1527
450°C AGE
K1526 525°C AGE

FIGURE 101

Changes in Hardness, Ductile-Brittle Transition Temperature, Segregation of Manganese and Nitrogen in Alloy K1525 and 181 (Fe-8Mn) on Aging at 450°C.[134]

(a) Hardness, H_v30 (K1525)

(b) Ductile-Brittle Transition Temperature (181)

(c) Atomic Percent Manganese (K1525) at Grain Boundaries (AES)

(d) Atomic Percent Nitrogen (K1525) at Grain Boundaries (AES)

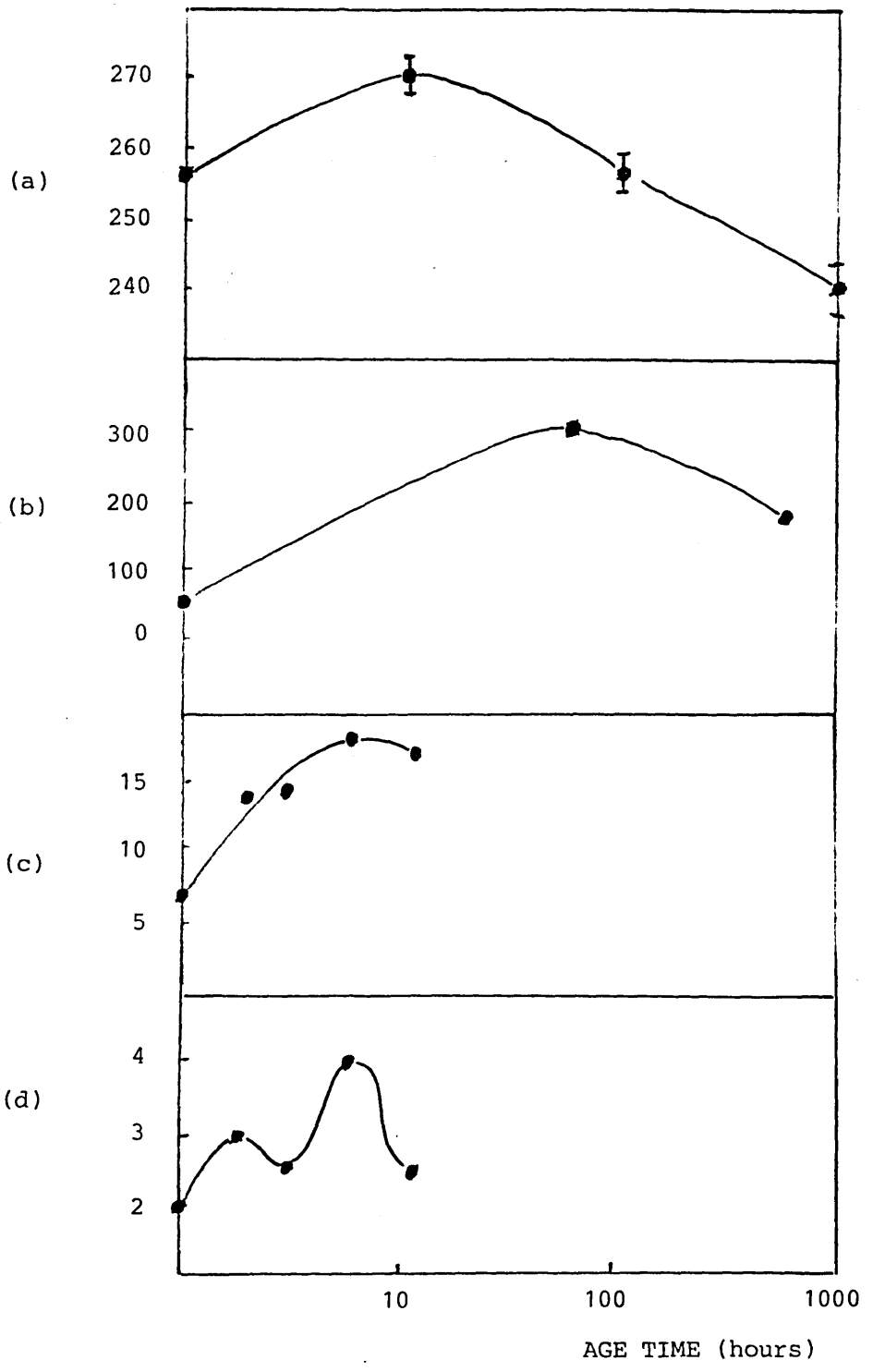
(a)
270
260
250
240
(b)
300
200
100
0
(c)
15
10
5
(d)
4
3
2
10
100
1000
AGE TIME (hours)

FIGURE 102

Changes in Hardness, Ductile-Brittle Transition Temperature, Segregation of Manganese and Nitrogen in Alloy K1526 (Fe-8Mn-2.5Mo) on Aging at 450°C.

(a) Hardness, H_v30

(b) Ductile-Brittle Transition Temperature

(c) Atomic Percent Manganese at Grain Boundaries (AES)

(d) Atomic Percent Nitrogen at Grain Boundaries (AES)

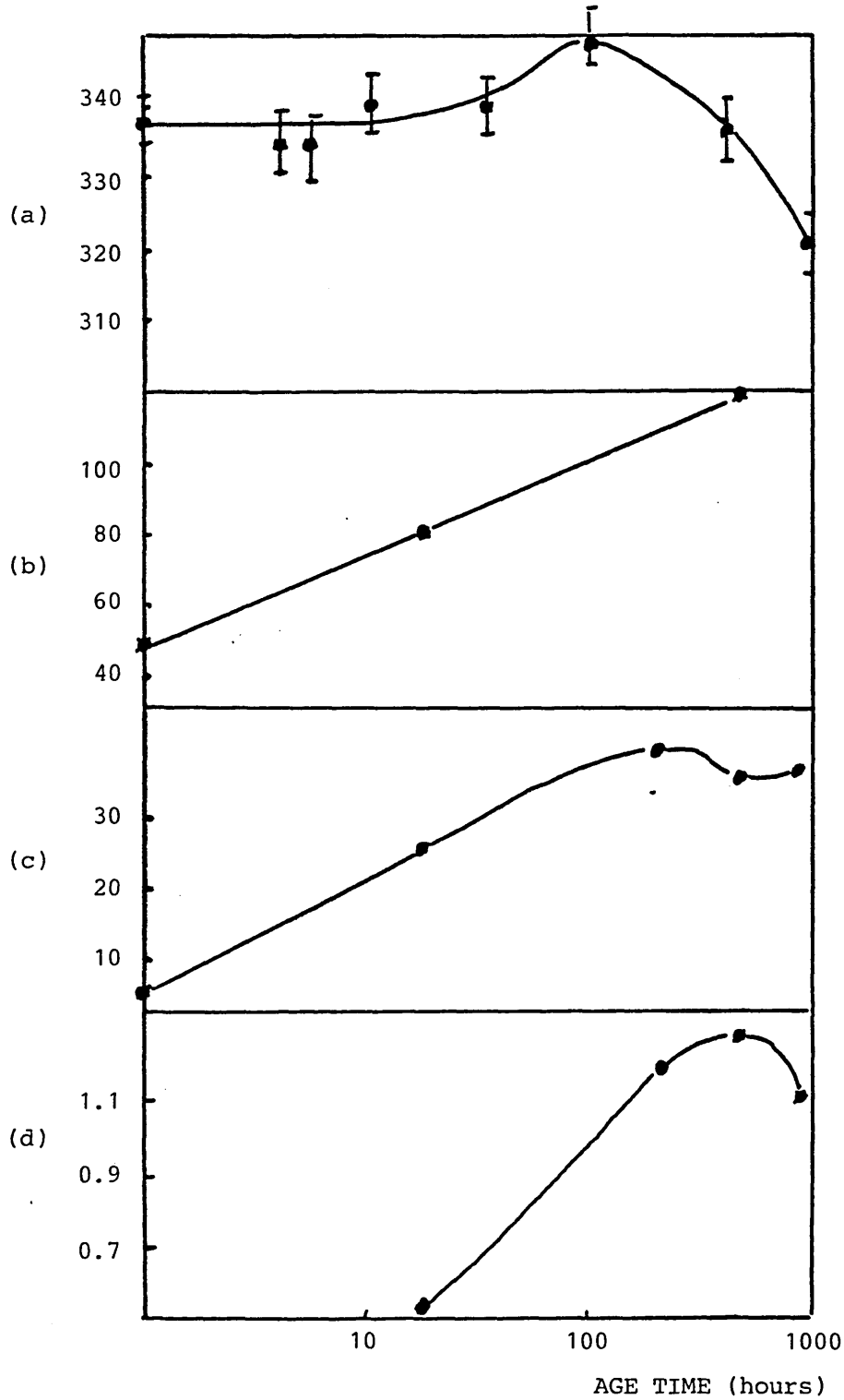
(a)
340
330
320
310
(b)
100
80
60
40
(c)
30
20
10
(d)
1.1
0.9
0.7
10
100
1000
AGE TIME (hours)

FIGURE 103

Changes in Hardness, Ductile-Brittle Transition Temperature, Segregation of Manganese and Nitrogen in Alloy K1527 (Fe-8Mn-5Mo) on Aging at 450°C.

(a) Hardness, H_v30

(b) Ductile-Brittle Transition Temperature

(c) Atomic Percentage Manganese at Grain Boundaries (AES)

(d) Atomic Percentage Nitrogen at Grain Boundaries (AES)

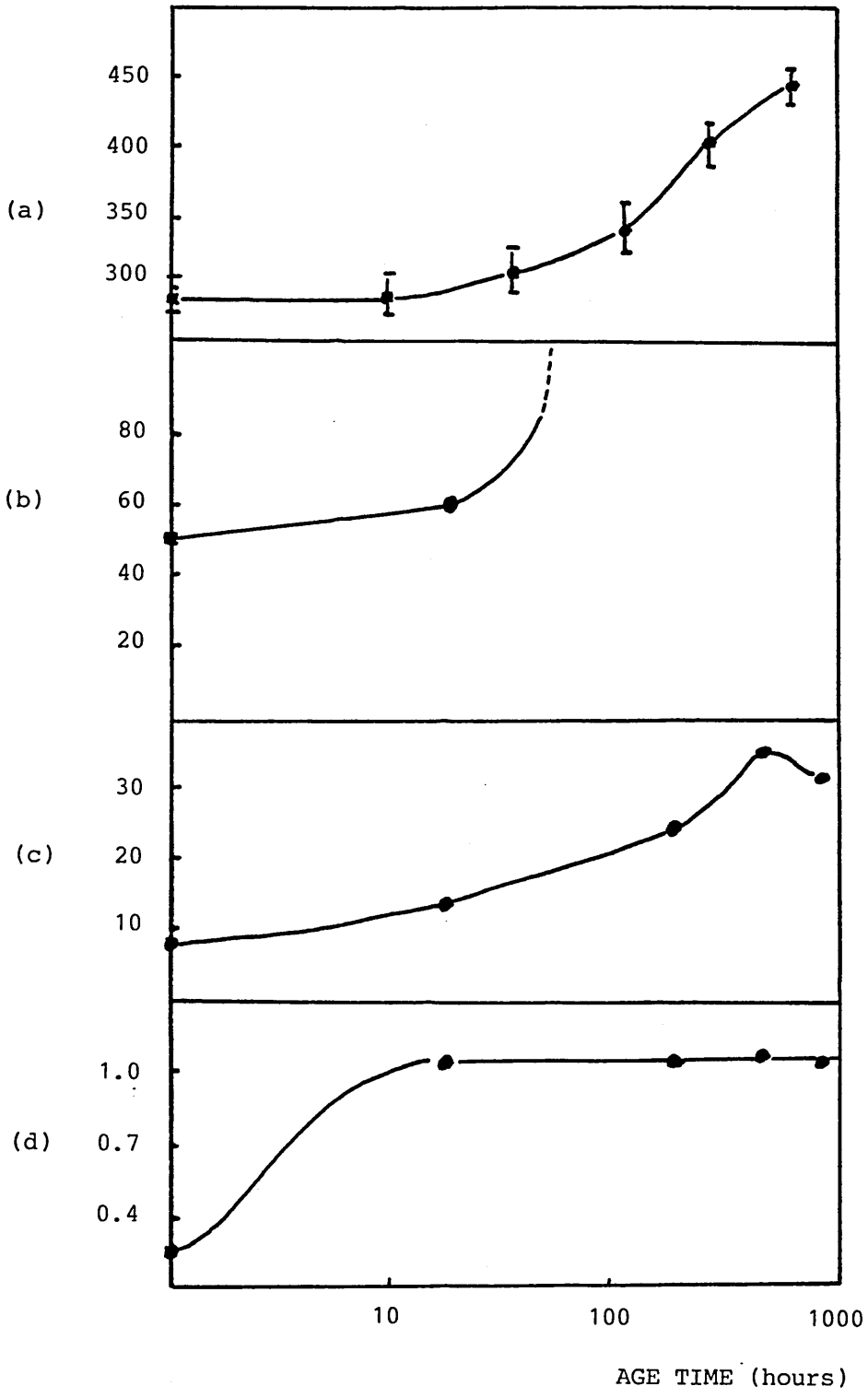
(a)
450
400
350
300
(b)
80
60
40
20
(c)
30
20
10
(d)
1.0
0.7
0.4
10
100
1000
AGE TIME (hours)

FIGURE 104

Changes in Hardness and Ductile-Brittle Transition Temperature of Alloy K1526 on Aging at 525°C.

FIGURE 105

Changes in Hardness and Ductile-Brittle Transition Temperature of Alloy K1527 on Aging at 525°C.

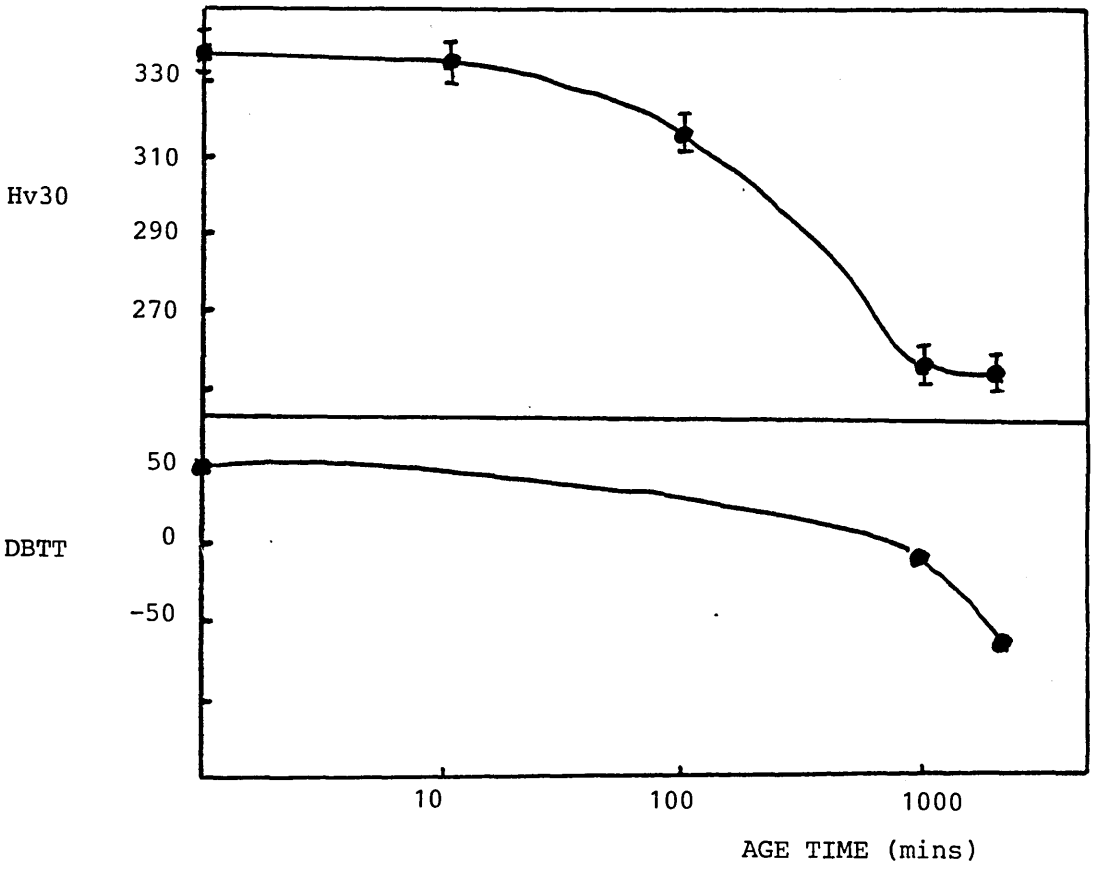
330
310
290
270
Hv30
50
0
-50
DBTT
10
100
1000
AGE TIME (mins)

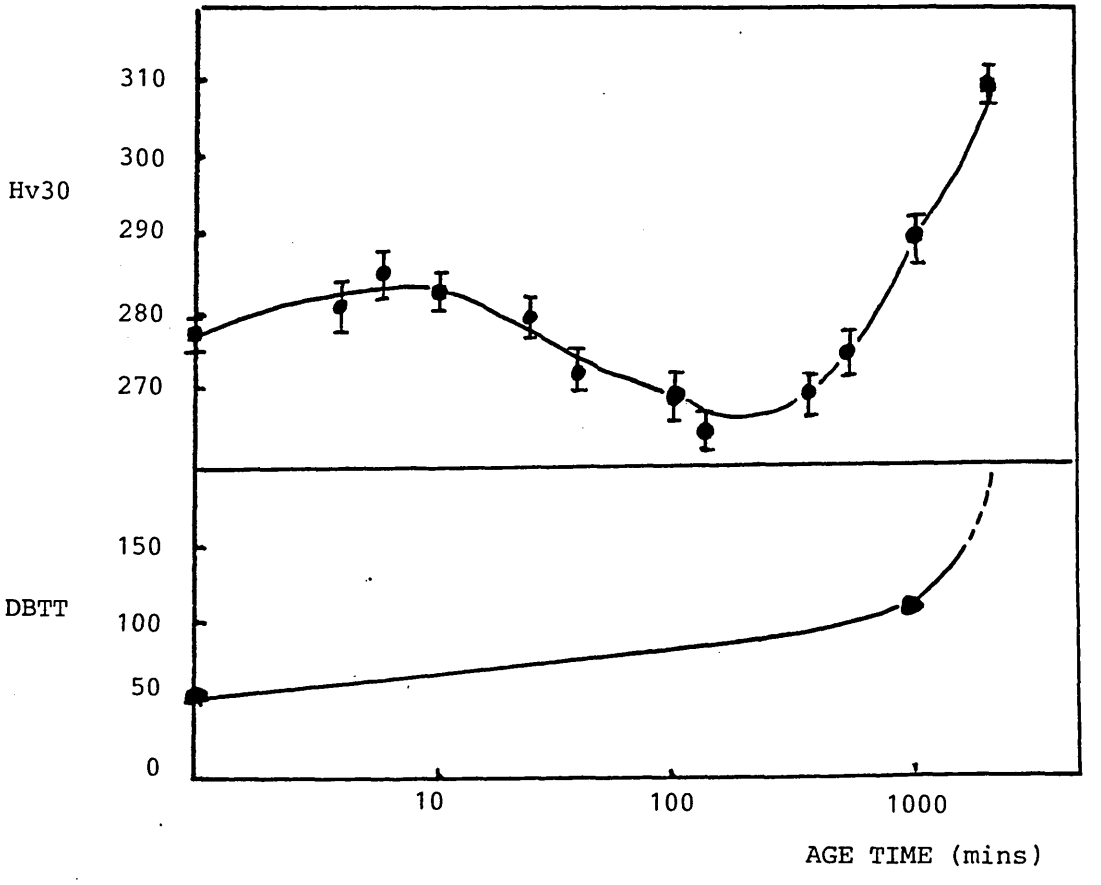
310
300
290
280
270
Hv30
150
100
50
0
DBTT
10
100
1000
AGE TIME (mins)

FIGURE 106

Comparison of Impact Transition Curves

for Alloy K1526 after Aging at 450°C and 525°C

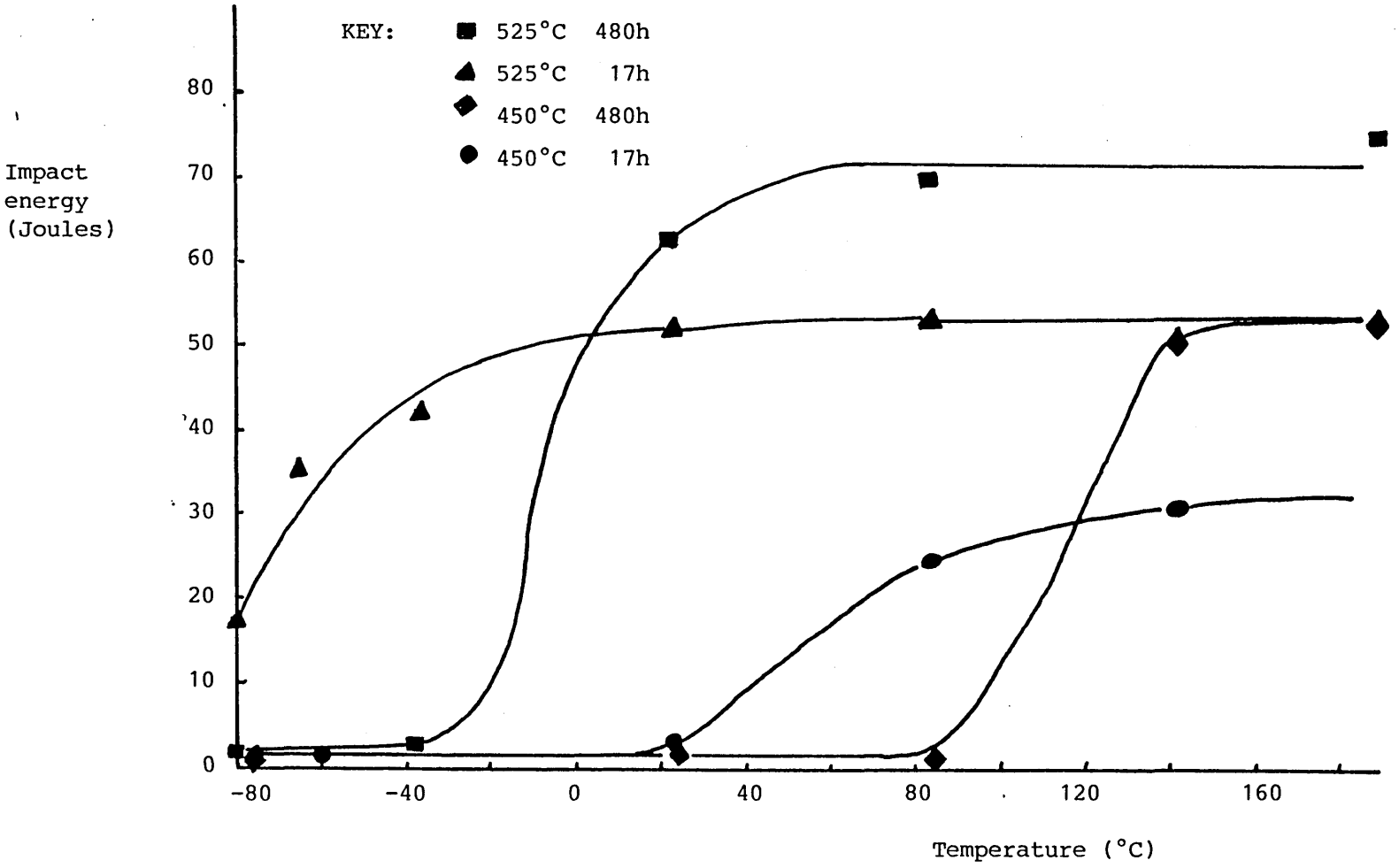
KEY:
525°C 480h
525°C 17h
450°C 480h
450°C 17h
Impact energy (Joules)
80
70
60
50
40
30
20
10
0
-80
-40
0
40
80
120
160
Temperature (°C)

FIGURE 107

Comparison of Impact Transition Curves for Alloy K1527 after Aging at 450°C and 525°C

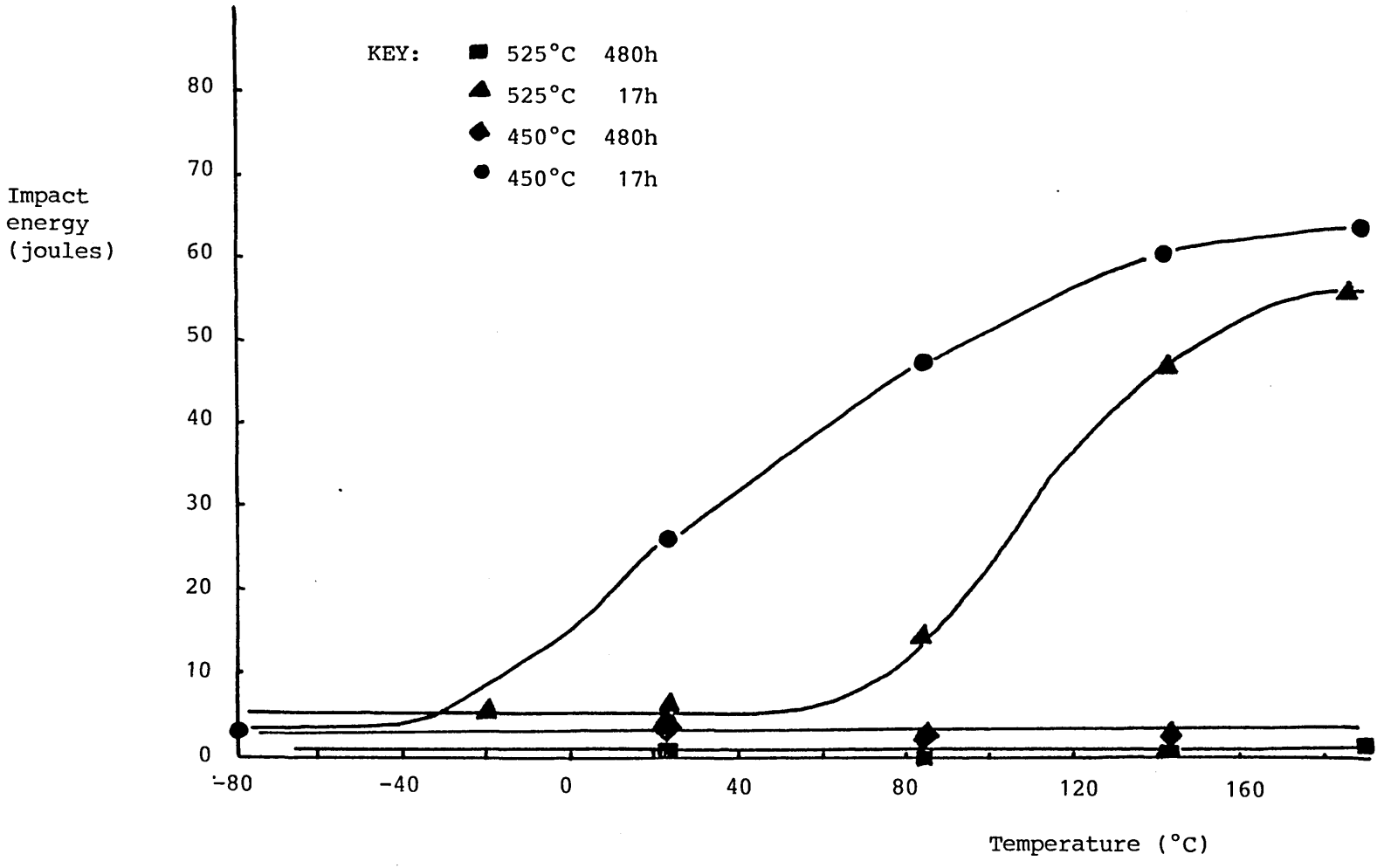
KEY:
525°C 480h
525°C 17h
450°C 480h
450°C 17h
Impact energy (joules)
80
70
60
50
40
30
20
10
0
-80
-40
0
40
80
120
160
Temperature (°C)

FIGURE 108

The Variation in the hardness of alloys A217, A317 and A417 (compositions table II) on aging at 525°C

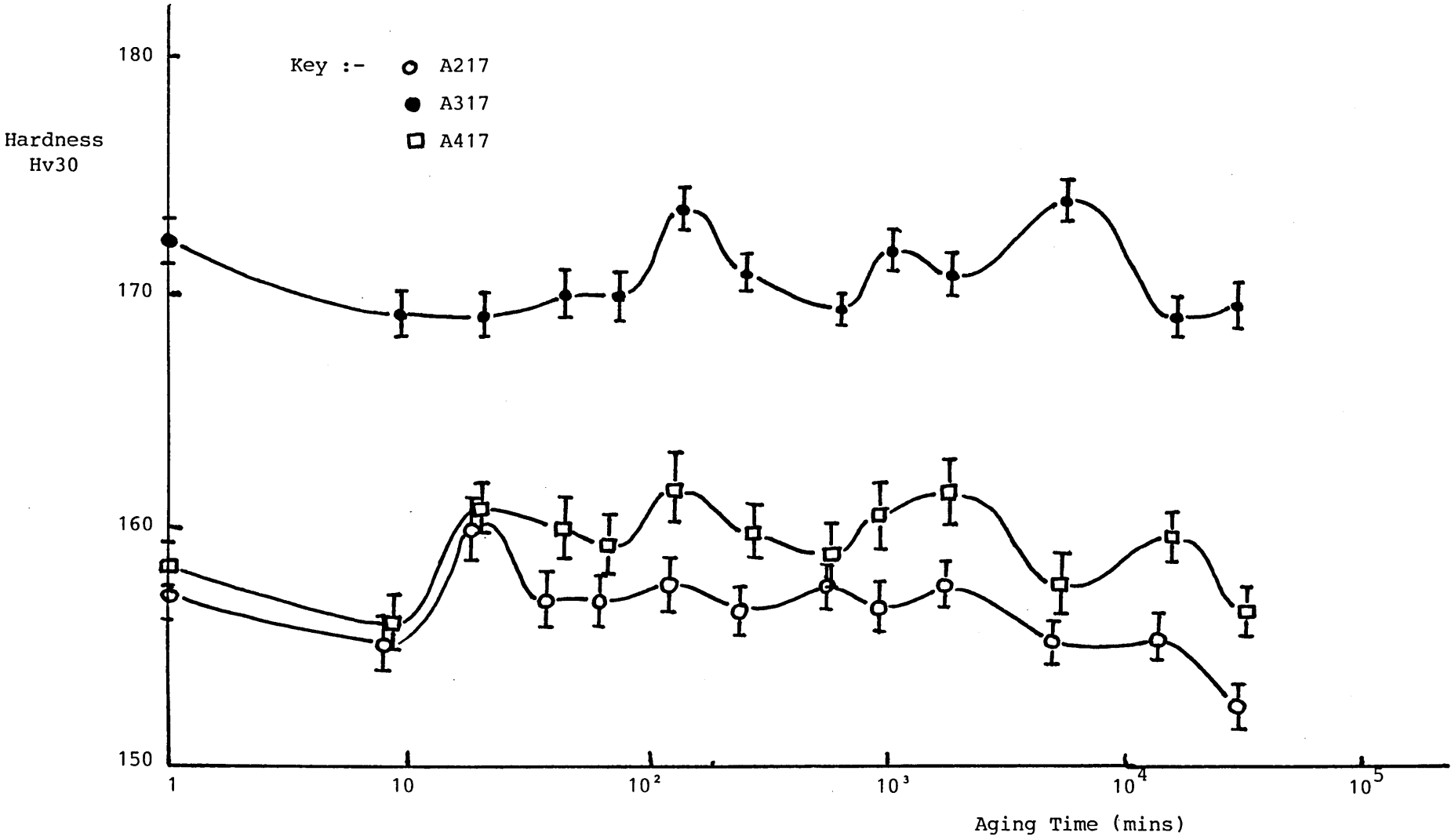
Key :- A217
A317
A417
Hardness
Hv30
180
170
160
150
1
10
10²
10³
10⁴
10⁵
Aging Time (mins)

FIGURE 109

Optical Micrographs of K1526 Etched in 4% Nital for 15 Secs After a Solution Treatment of 1000°C for 1 Hour Followed by Water Quenching.

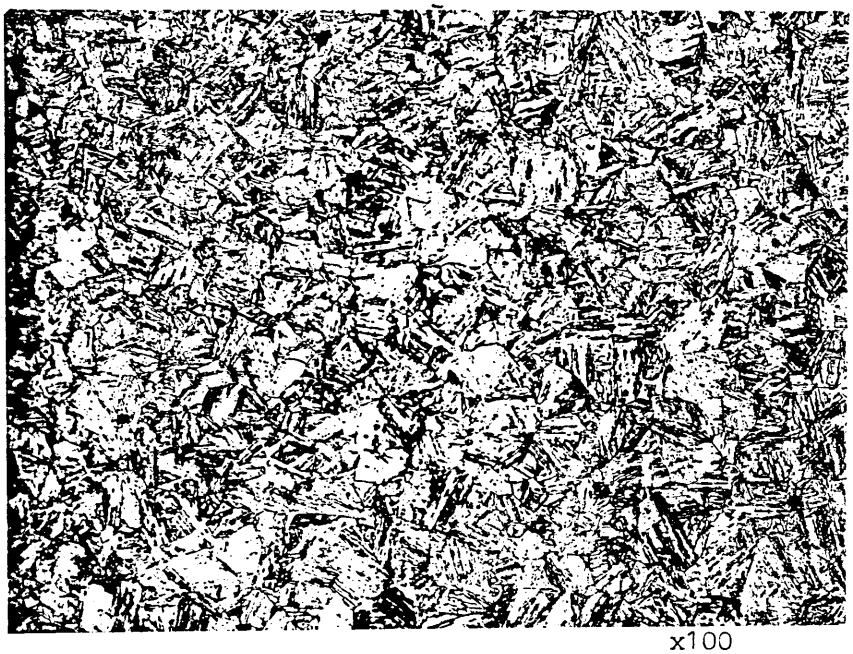

x100

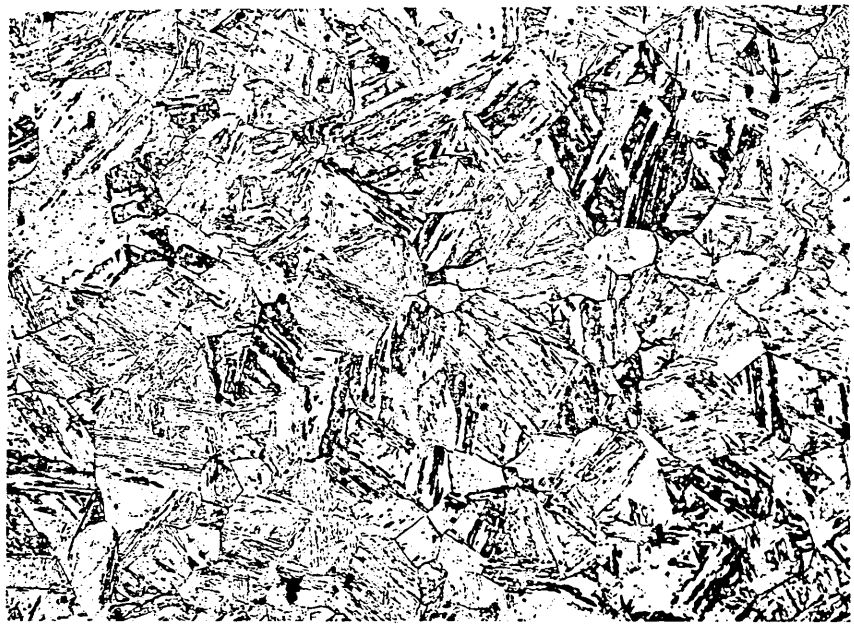

x200

Prior austenite

grain size = 62μm

FIGURE 110

Optical Micrographs of K1526 Etched in 4% Nital for 15 Seconds after a Solution Treatment of 1300°C for 1 Hour Followed by Water Quenching.

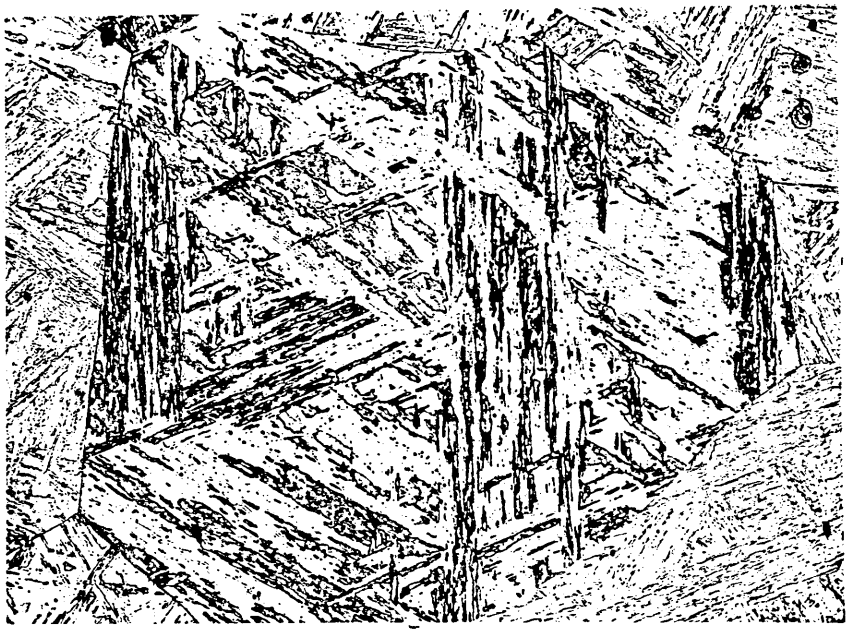

x200

x200

Prior austenite

grain size = 260μm

FIGURE 111

Optical Micrographs of K1526 Etched in 2% Nital for 15 Seconds after a Solution Treatment at 1300°C for 1 Hour Followed by Water Quenching, and then 1 Hour at 1000°C followed by Water Quenching.

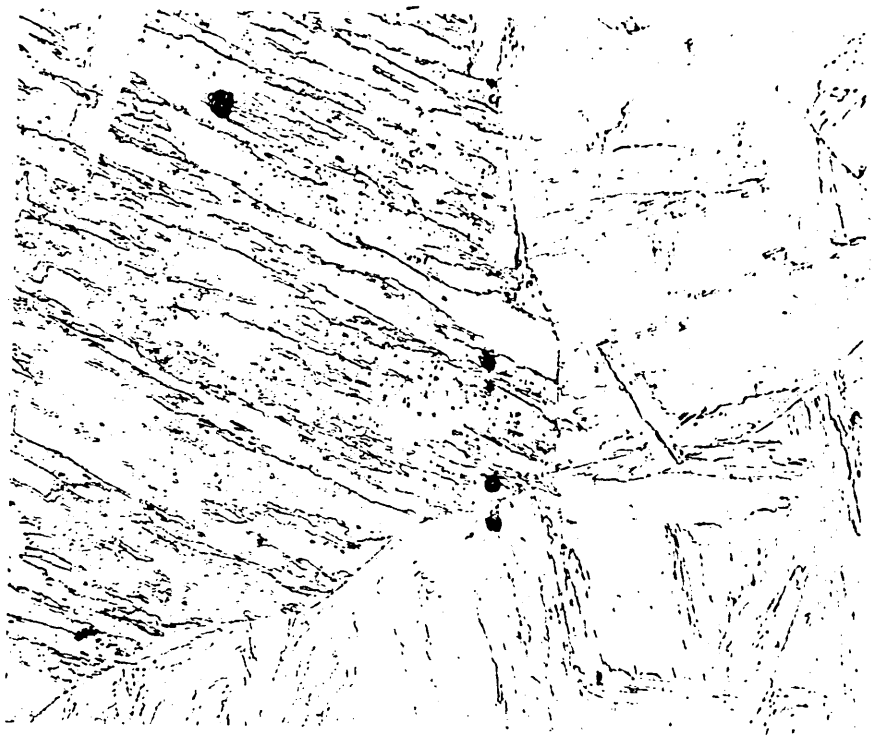

x400

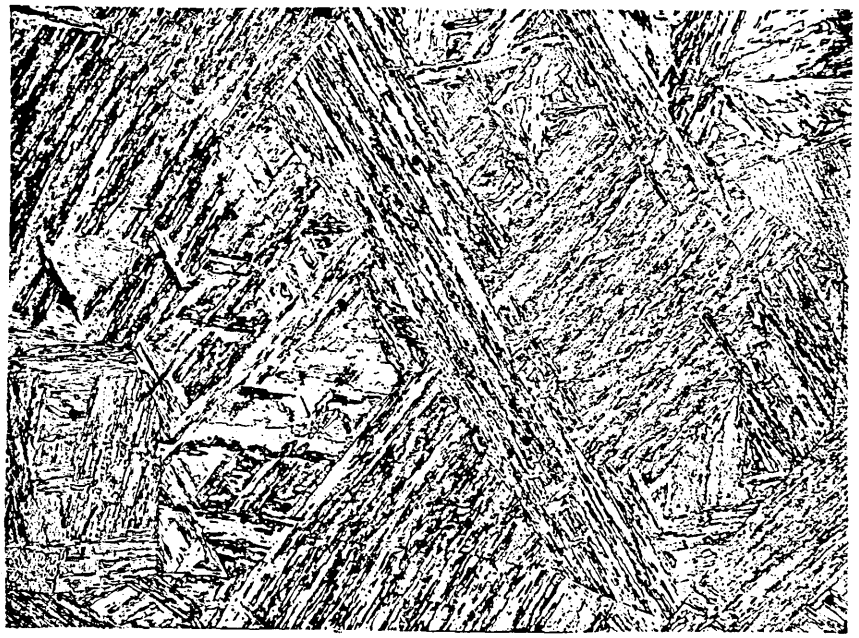

x200

Prior austenite

grain size = 132 μm

FIGURE 112

Optical Micrographs of K1527 Etched in 4% Nital for 15 Seconds After a Solution Treatment of 1000°C for 1 Hour Followed by Water Quenching.

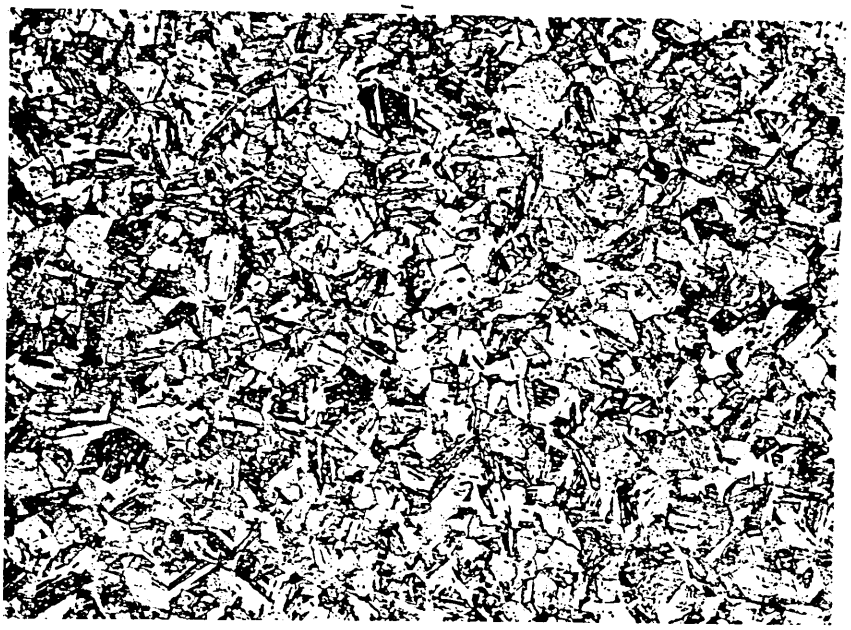

x100

x200

Prior austenite

grain size = 50μm

FIGURE 113

Optical Micrographs of K1527 Etched in 4% Nital for 15 Seconds After a Solution Treatment of 1300°C for 1 Hour Followed by Water Quenching.

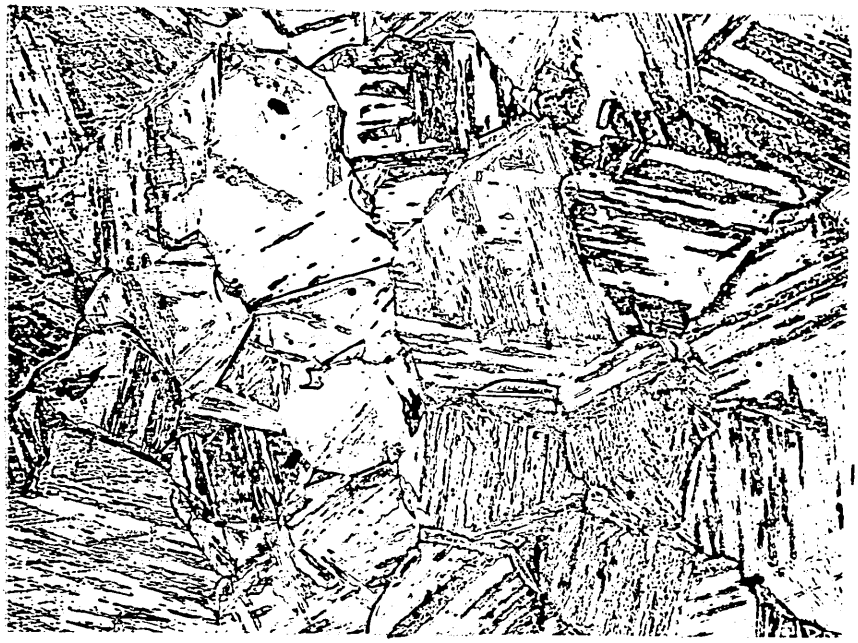

x200

Prior austenite grain size = 124 m

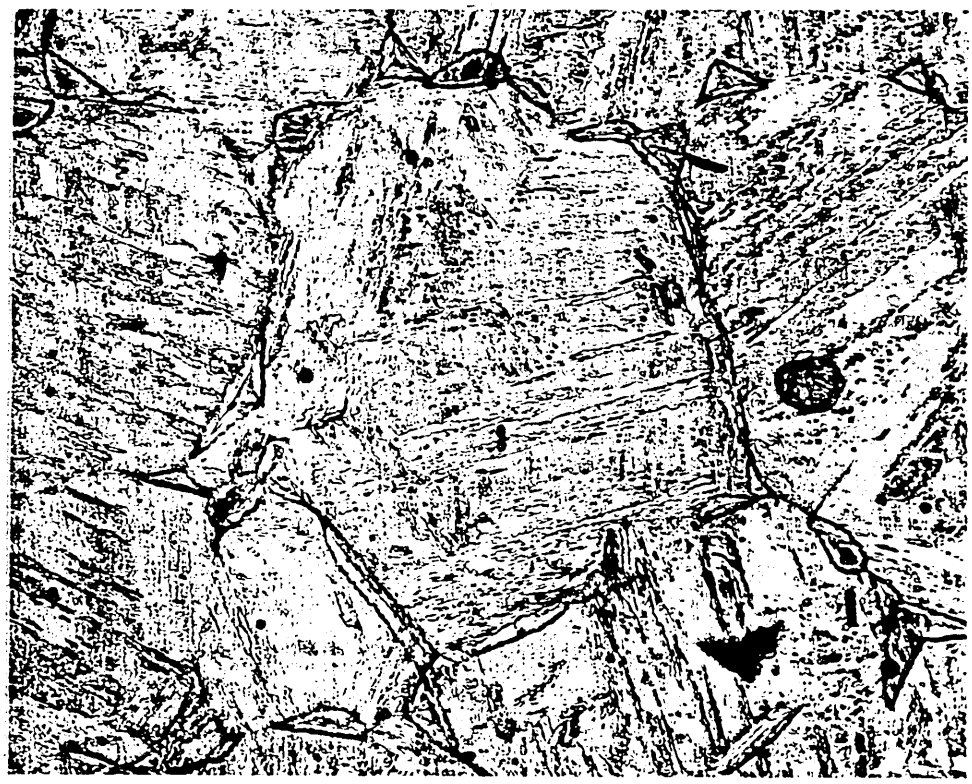

x500

NOTE- δ - ferrite at prior austenite grain boundaries.

FIGURE 114

Optical Micrographs of K1527 Etched in 2% Nital for 15 Seconds after Solution Treatment at 1300°C for 1 Hour Followed by Water Quenching and then 1000°C for 1 Hour Followed by Water Quenching.

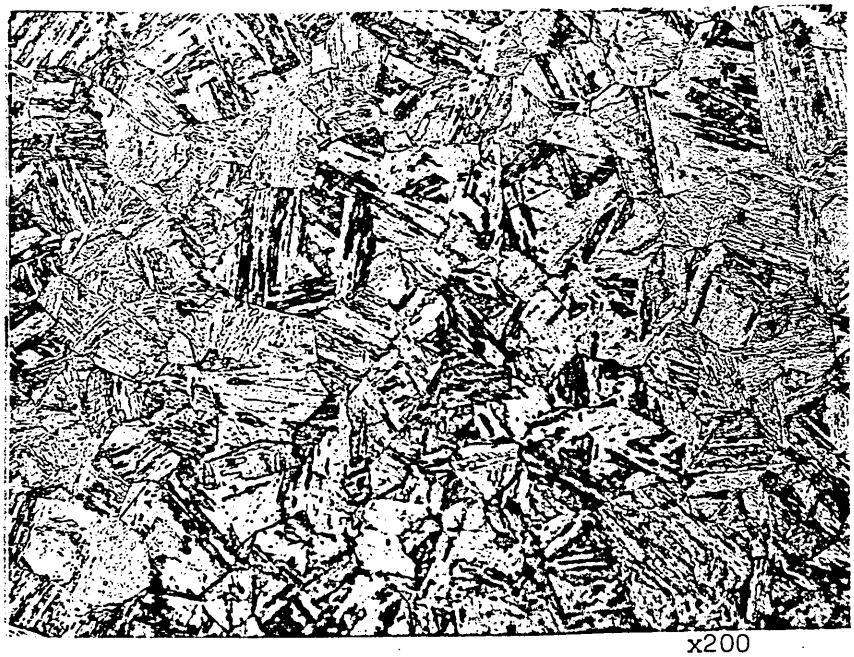

Prior austenite

grain size = 54 μm

FIGURE 115

An Inclusion Typical of the Ones Found in the As Quenched K1526 and K1527 Alloys Showing their Dual Phase Structure.

X-Ray Map Showing Distribution of Oxygen.

X-Ray Map Showing Distribution of Sulphur.

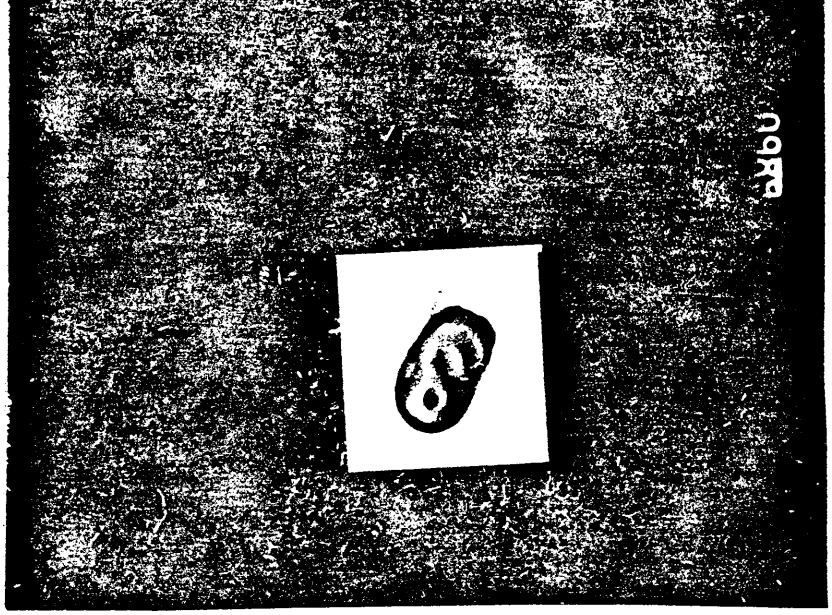

x2000

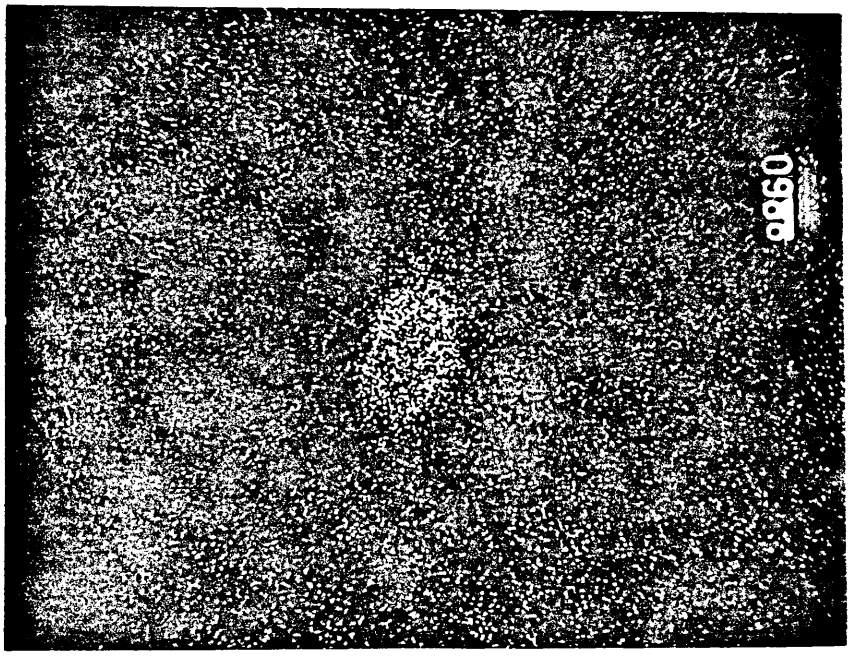

x2000

x2000

FIGURE 116

Optical Micrograph of Alloy K1526 in the Unetched Condition After Austenitizing at 1000°C for 1 Hour Followed by Water Quenching.

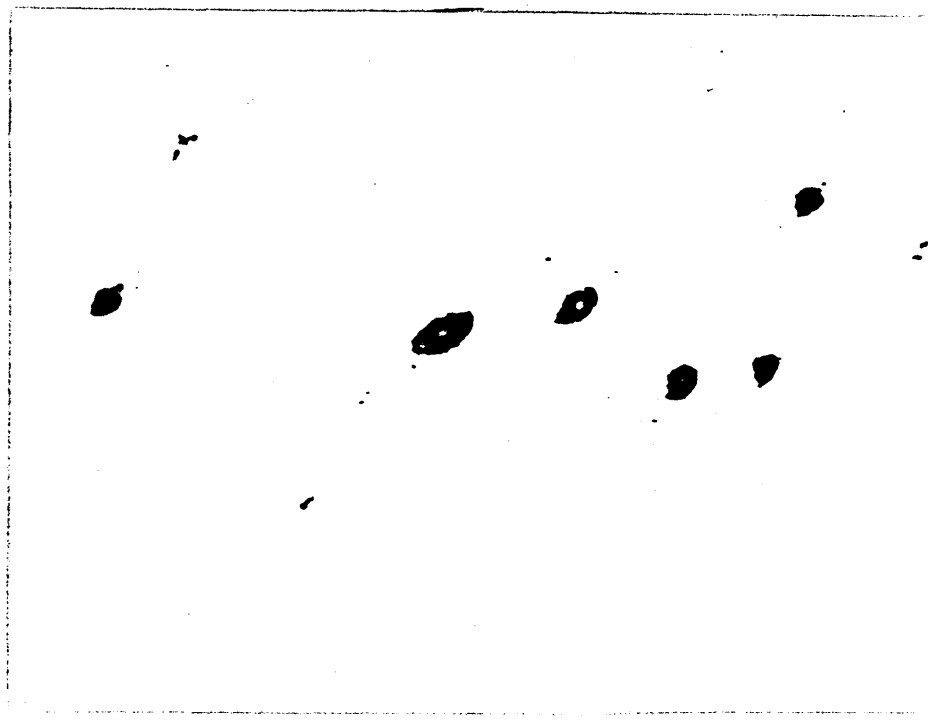

x400

VOLUME FRACTION OF INCLUSIONS ANALYSED = 0.004 %

(Number of points analysed = 13200)

FIGURE 117

Optical Micrograph of Alloy K1526 in the Unetched Condition after Austenitising at 1300°C for 1 Hour Followed by Water Quenching and then 1000°C for 1 Hour Followed by Water Quenching.

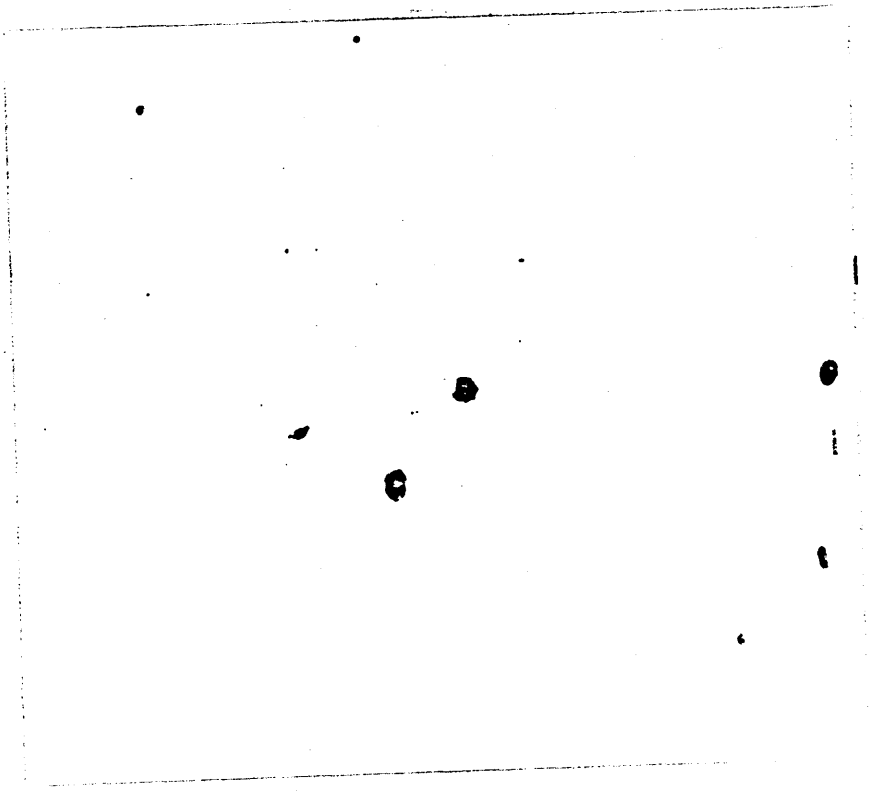

x400

VOLUME FRACTION OF INCLUSIONS = 0.004 %

(Number of points analysed = 13200)

FIGURE 118

Optical Micrograph of Alloy K1527 in the Unetched Condition After Austenitising at 1000°C for 1 Hour Followed by Water Quenching.

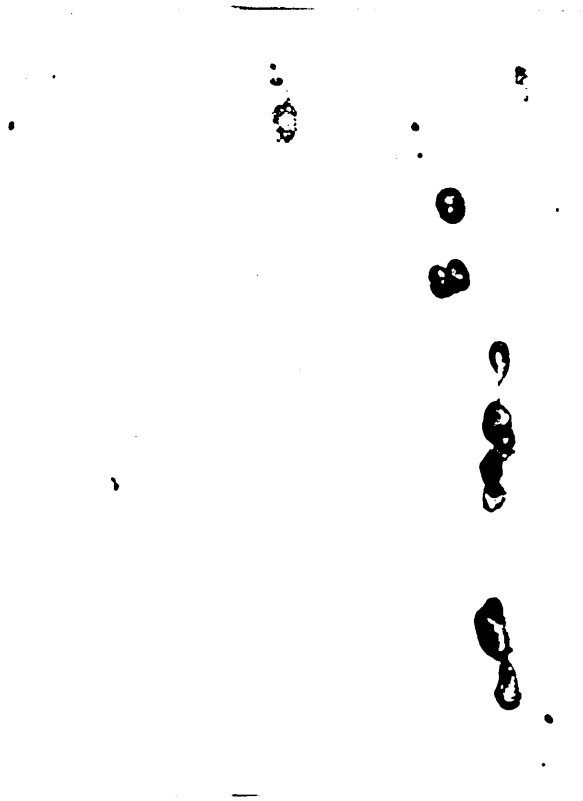

x400

GLASSY, MULTI-PHASE INCLUSIONS

VOLUME FRACTION = 0.002 %

(Number of points analysed = 13200)

FIGURE 119

Optical Micrographs of K1527 in the Unetched Condition after Austenitising at 1300°C for 1 Hour Followed by Water Quenching and then at 1000°C for 1 Hour Followed by Water Quenching.

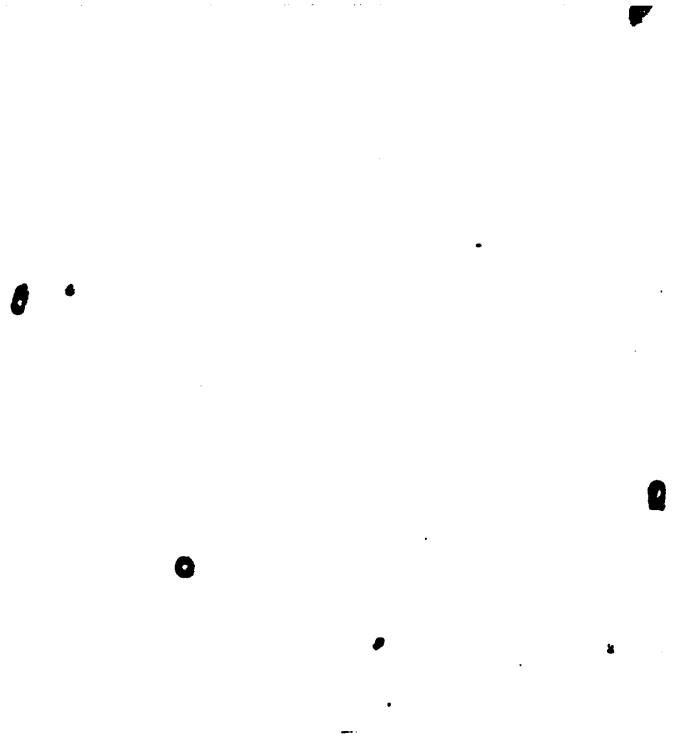

x400

VOLUME FRACTION = 0.002 %

(Number of points analysed = 13200)

FIGURE 120

Graph Showing the Build-Up of Manganese and Molybdenum at Prior Austenite Grain Boundaries in Alloys K1526 and K1527 During Aging at 450°C.

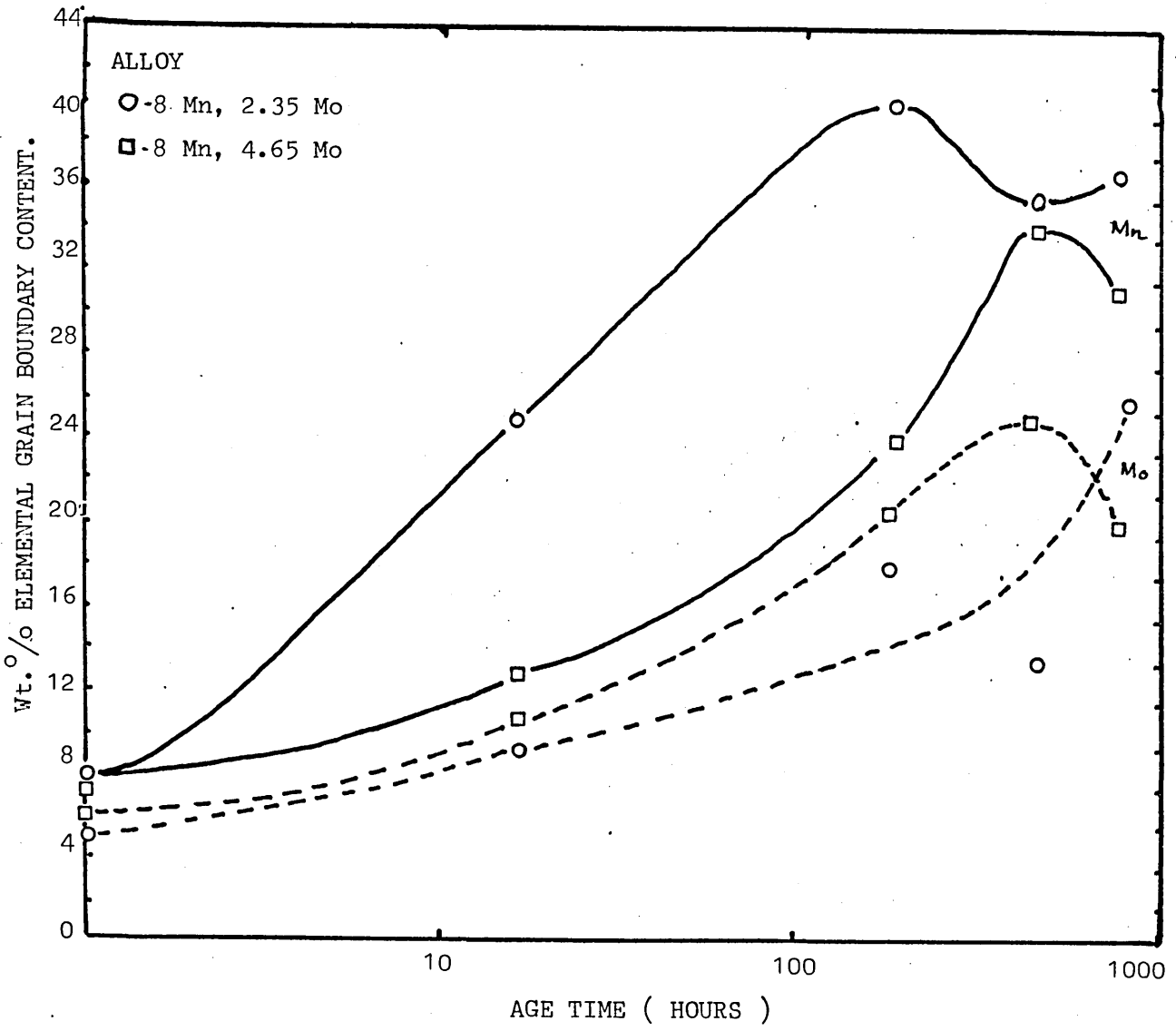
ALLOY
O-8 Mn, 2.35 Mo
□-8 Mn, 4.65 Mo
Mn
Mo
Wt.°/o ELEMENTAL GRAIN BOUNDARY CONTENT.
AGE TIME (HOURS)
0
4
8
12
16
20
24
28
32
36
40
44
10
100
1000

FIGURE 121

AES Spectrum of the As Quenched K1526 Alloy.

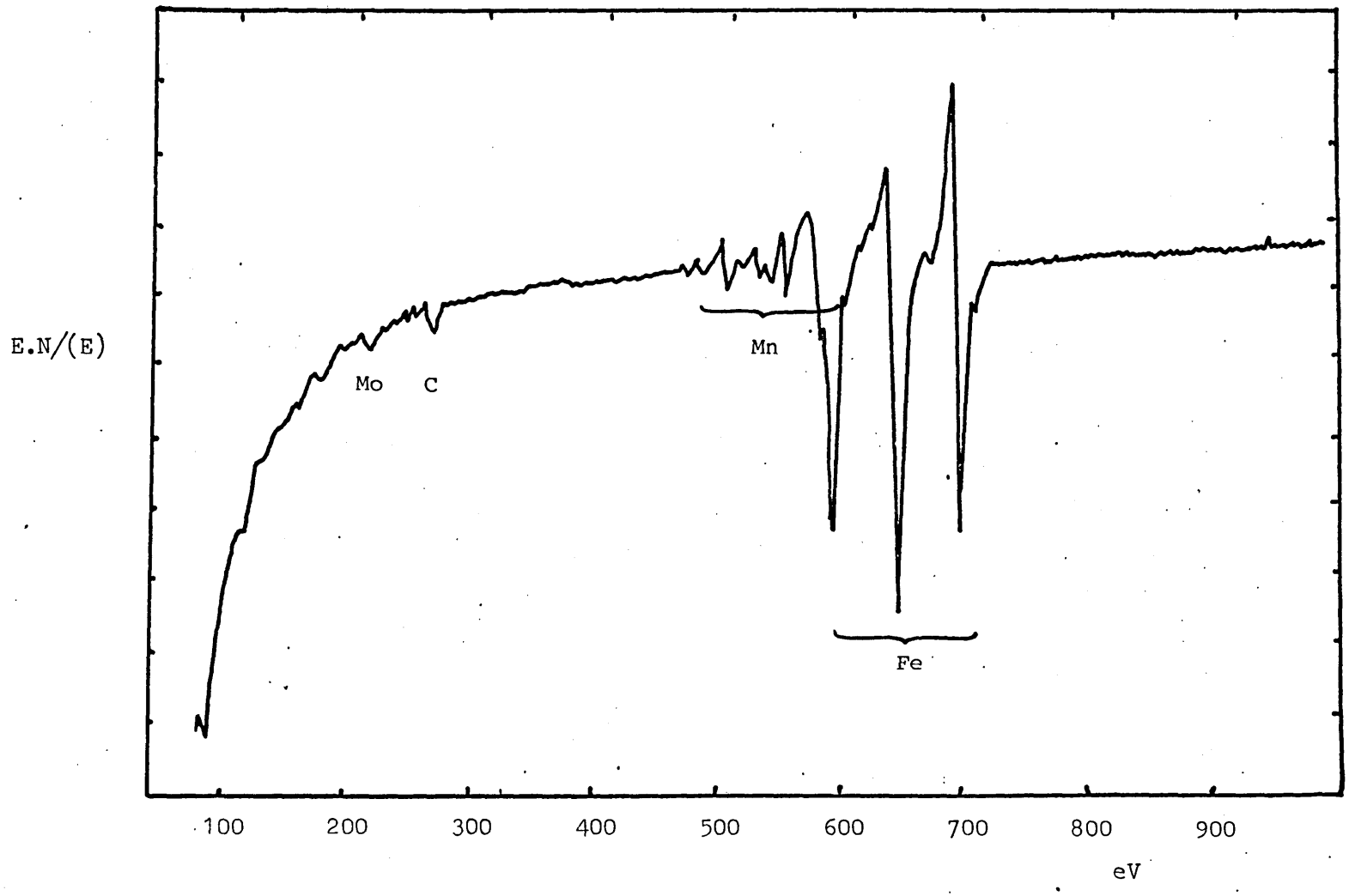
E.N/(E)
Mo
C
Mn
Fe
100
200
300
400
500
600
700
800
900
eV

FIGURE 122

AES Spectrum of Alloy K1526 in the Embrittled State After 858 Hours at 450°C.

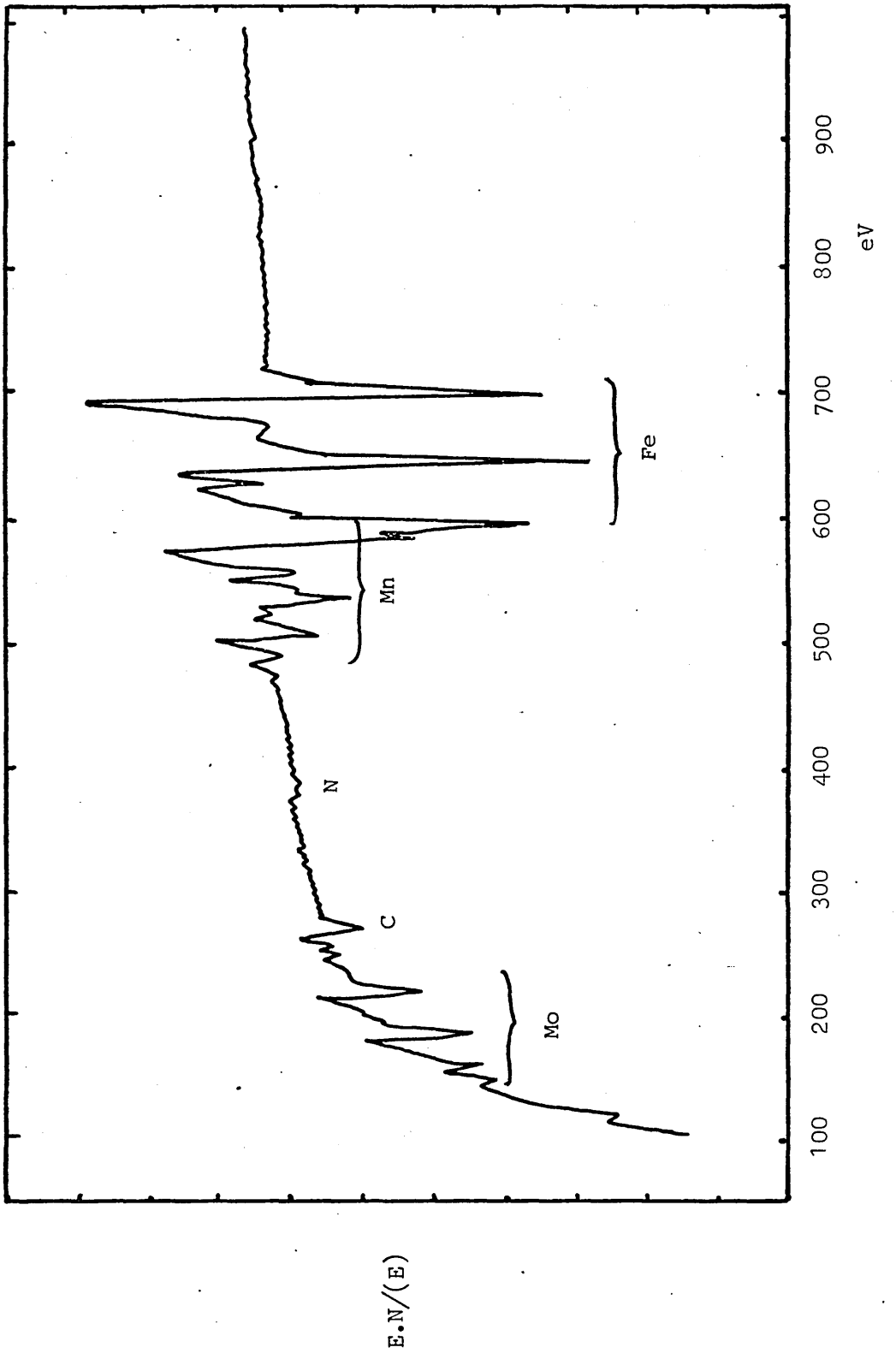
E.N/(E)
100
200
300
400
500
600
700
800
900
eV
Mo
C
N
Mn
Fe

FIGURE 123

AES Spectrum of the As Quenched K1527 Alloy.

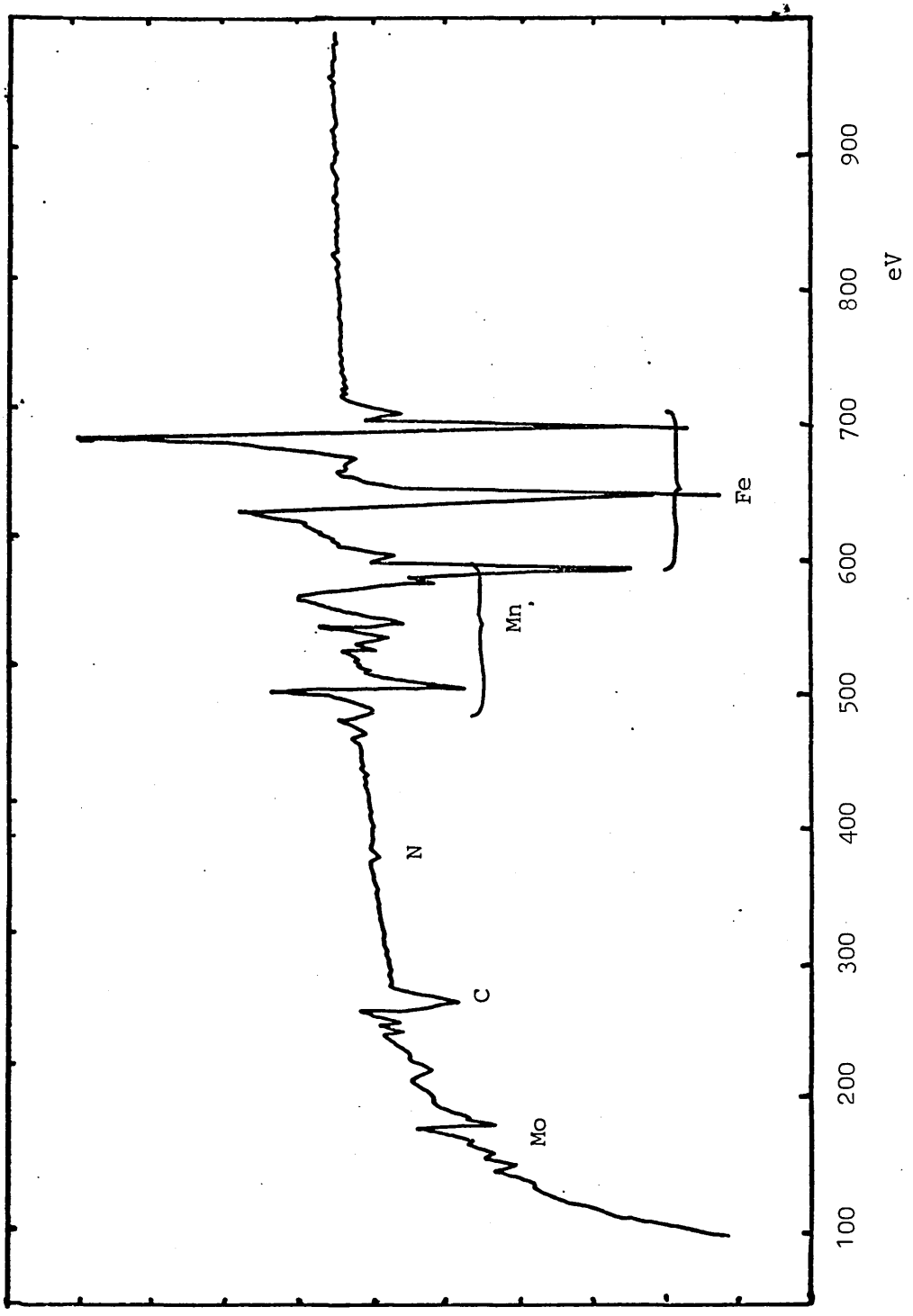
E.N/(E)
100
200
300
400
500
600
700
800
900
eV
Mo
C
N
Mn
Fe

FIGURE 124

AES Spectrum of Alloy K1527 in the Embrittled Condition After 858 Hours at 450°C.

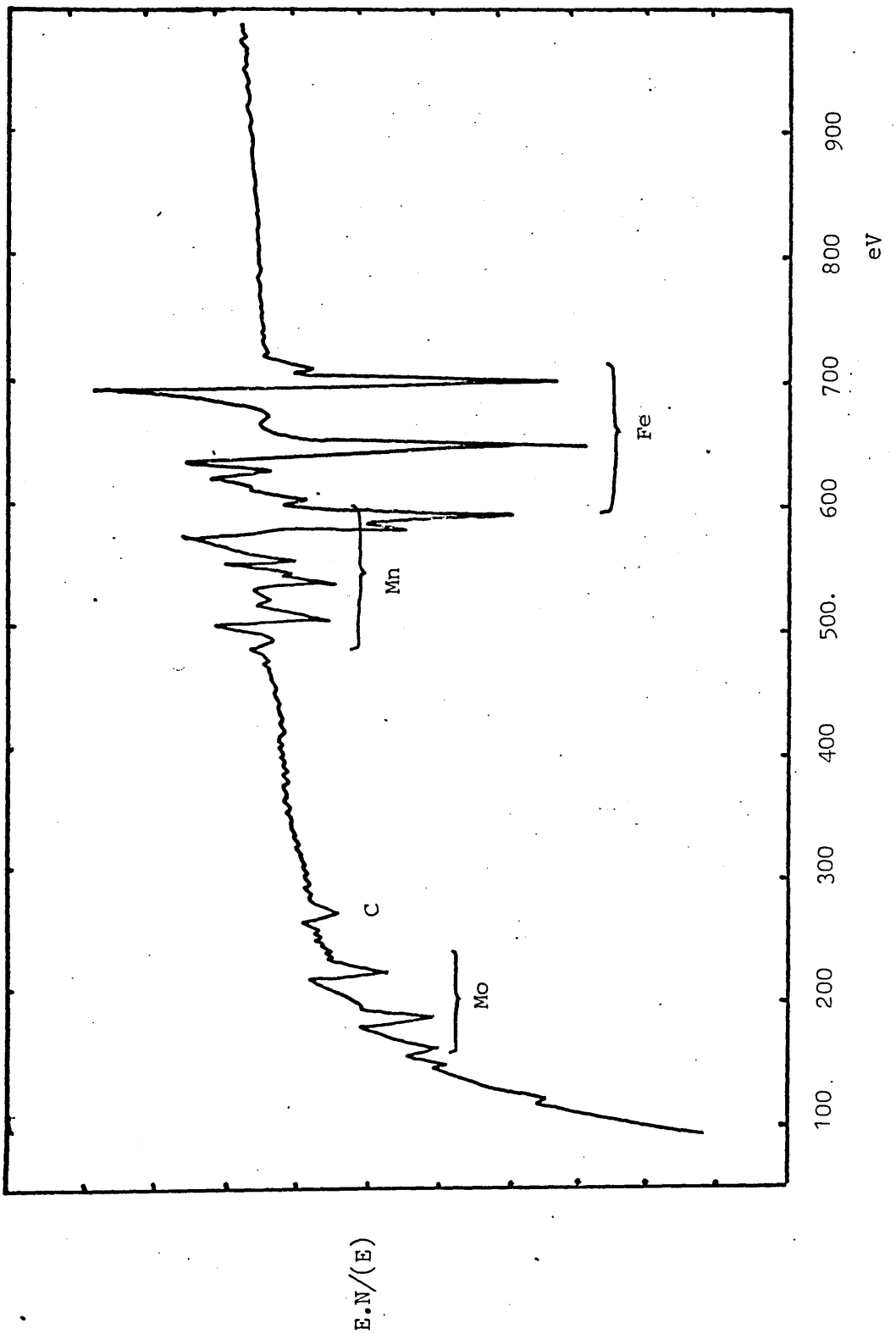
E.N/(E)
100
200
300
400
500.
600
700
800
900
eV
Mo
C
Mn
Fe

FIGURE 125

Variation of Hardness on Aging Alloy K1525 at 350°C, 400°C, and 450°C after being Solution Treated at 1000°C for 1 Hour and then Water Quenched.

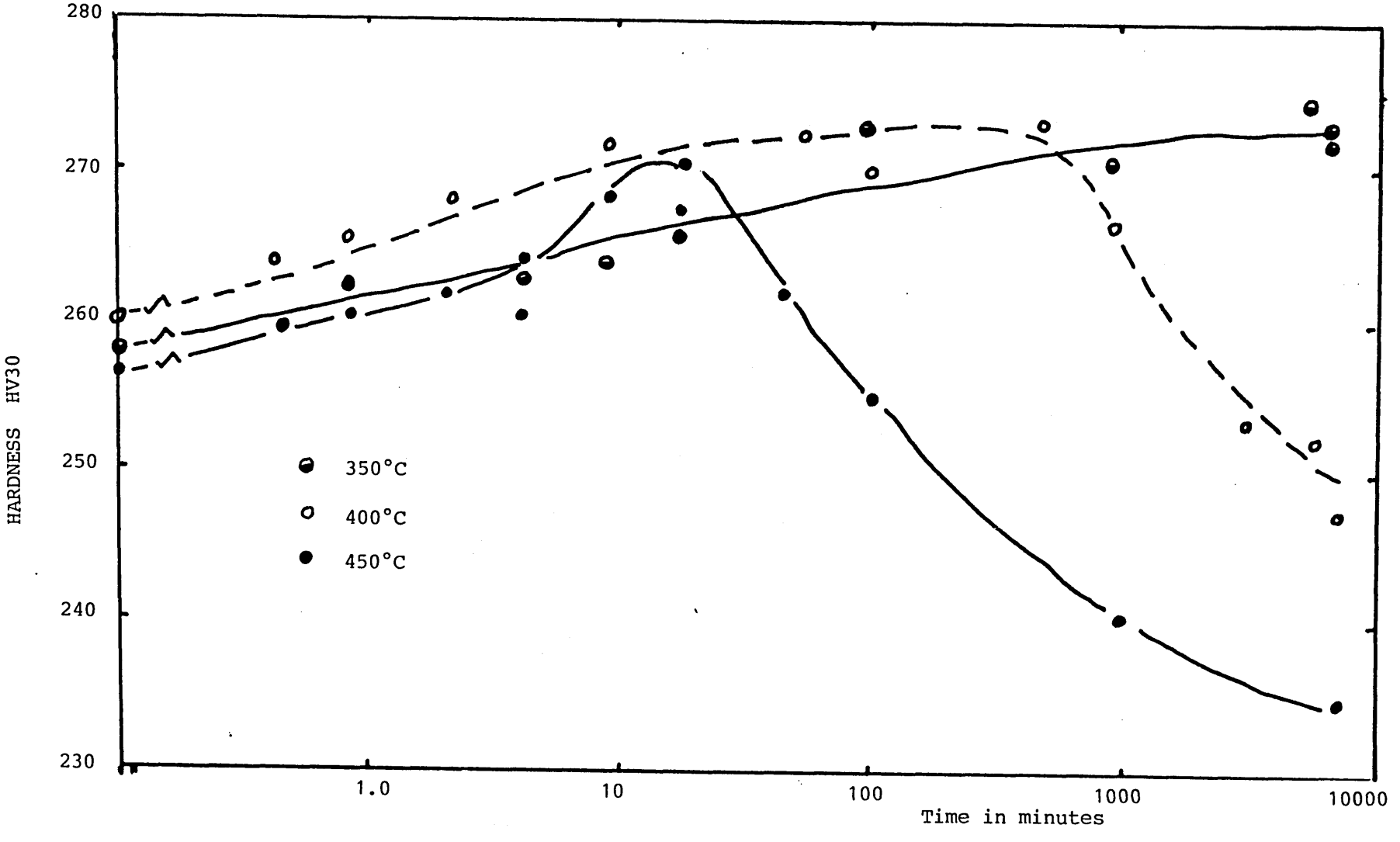
280
270
260
250
240
230
HARDNESS HV30
350°C
400°C
450°C
1.0
10
100
1000
10000
Time in minutes

FIGURE 126

Electron Micrographs of Alloys K1526 and K1527 in the As Quenched Condition after Solution Treatment at 1000°C for 1 Hour Followed by Water Quenching.

K 1526 x60 k

K 1527 x20 k

FIGURE 127

Electron Micrographs of Alloy K1526 Solution Treated at 1000°C for 1 Hour Followed by Water Quenching and then Aged for 193½ Hours at 450°C Followed by Water Quenching.

x160 k

FIGURE 128

The Variation of Hardness with Aging Time at 525°C for Alloys K1526 and K1527.

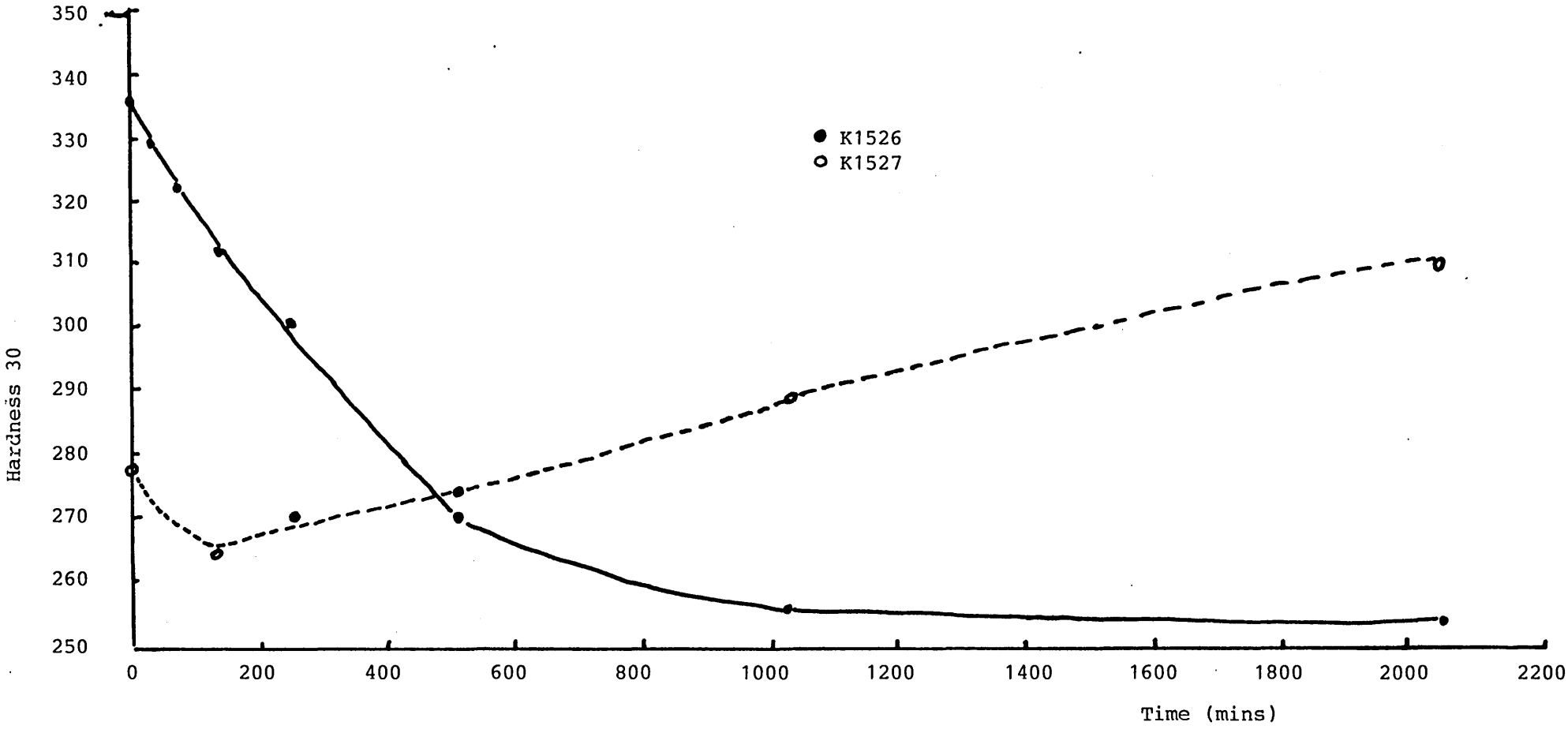
Hardness 30
350
340
330
320
310
300
290
280
270
260
250
0
200
400
600
800
1000
1200
1400
1600
1800
2000
2200
Time (mins)
K1526
K1527

FIGURE 129

The Variation of Nitrogen Content at the Fracture Surface of Alloys K1526 and K1527 with Age Time at 450°C.

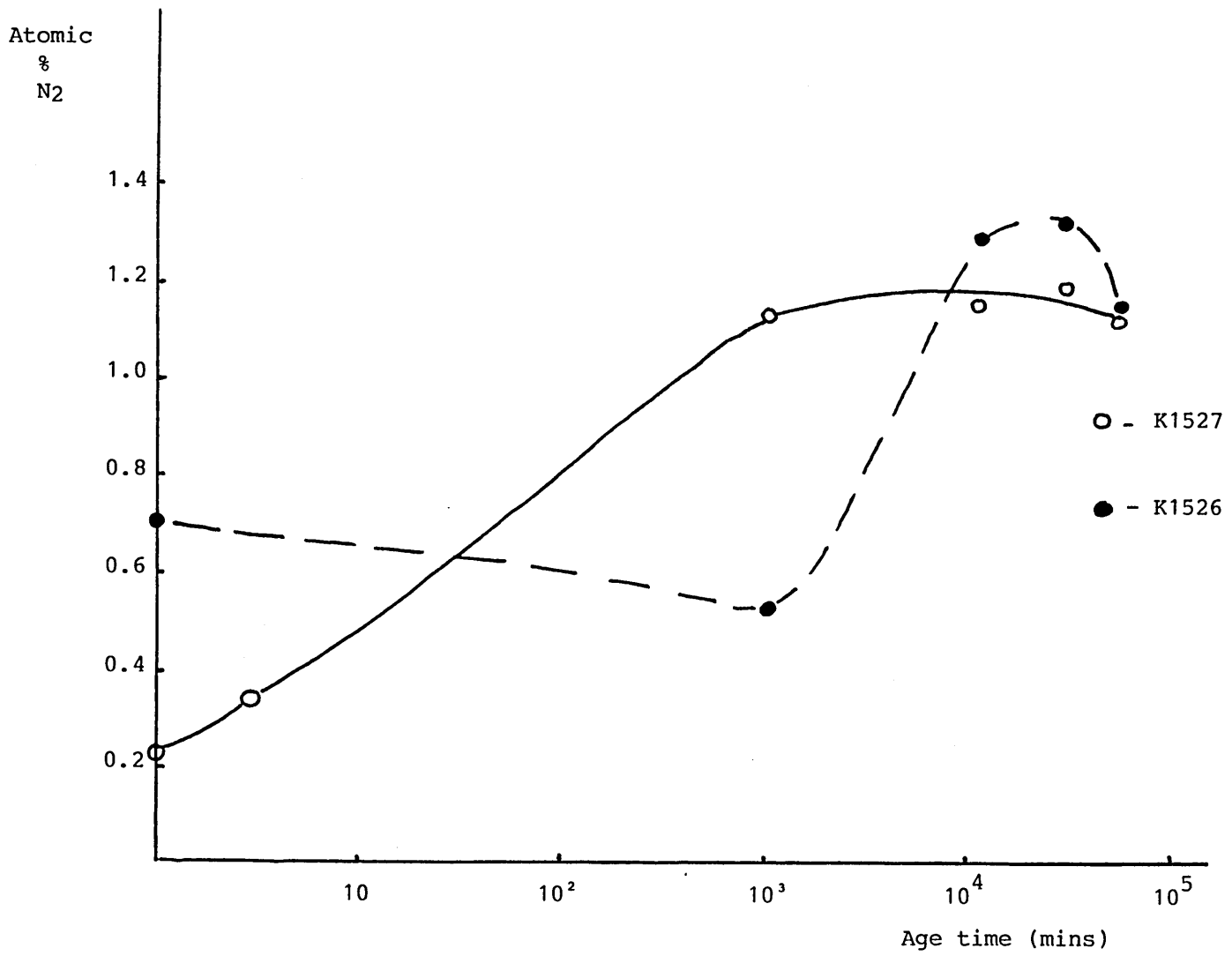
Atomic
%
N_2
1.4
1.2
1.0
0.8
0.6
0.4
0.2
10
10^2
10^3
10^4
10^5
Age time (mins)
O - K1527
● - K1526

FIGURE 130

Ion Bombardment Profiles Showing the Distribution of Manganese and Molybdenum about the Grain Boundaries of Alloy K1526 after Aging for 480 Hours at 450°C.

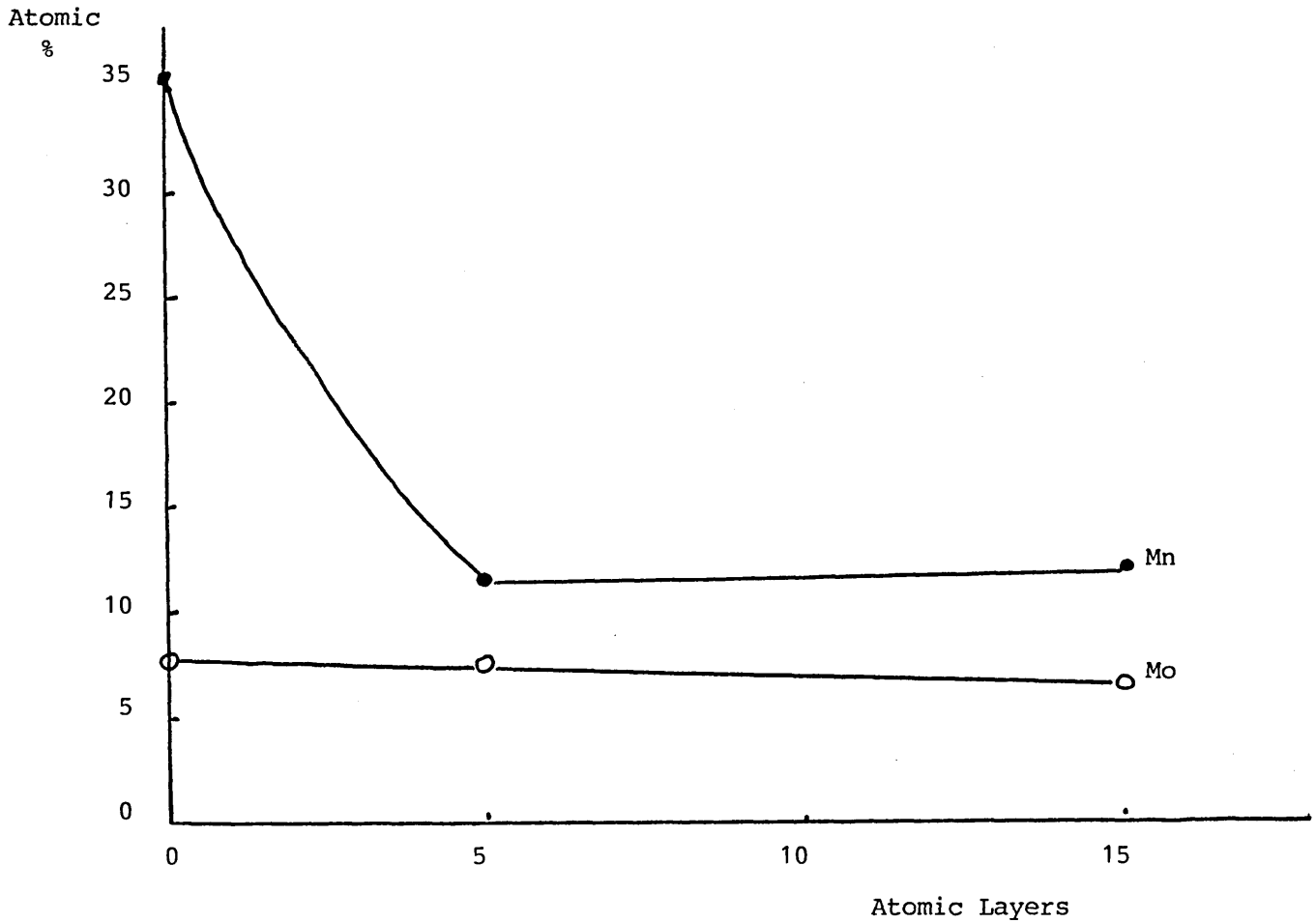
Atomic
%
35
30
25
20
15
10
5
0
0
5
10
15
Atomic Layers
Mn
Mo

FIGURE 131

Optical Micrographs of Alloy A217 Etched in 6% Nital for 12 Seconds.

(a) After a Solution Treatment of 1000°C for One Hour Followed by Water Quenching.

(b) Solution Treatment as above Followed by a Tempering Treatment of One Hour at 650°C Followed by a Water Quench.

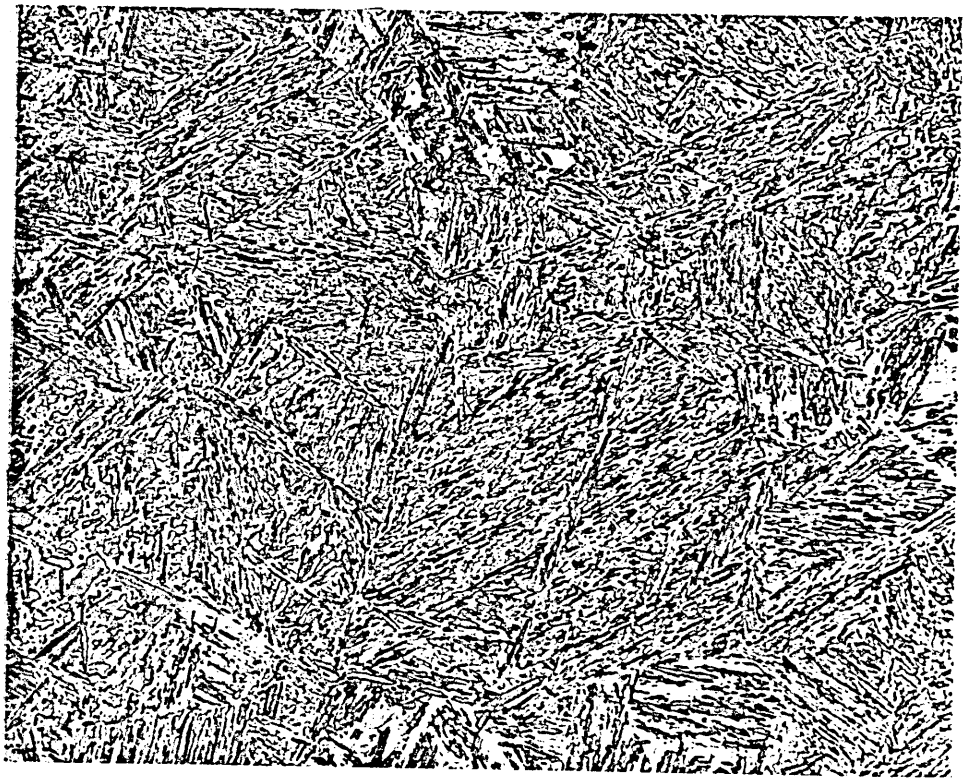

x208

x208

FIGURE 132

Optical Micrographs of Alloy A317 Etched in 6% Nital for 12 Seconds.

(a) After a Solution Treatment of 1000°C for One Hour Followed by Water Quenching.

(b) Solution Treatment as above Followed by a Tempering Treatment of One Hour at 650°C Followed by a Water Quench.

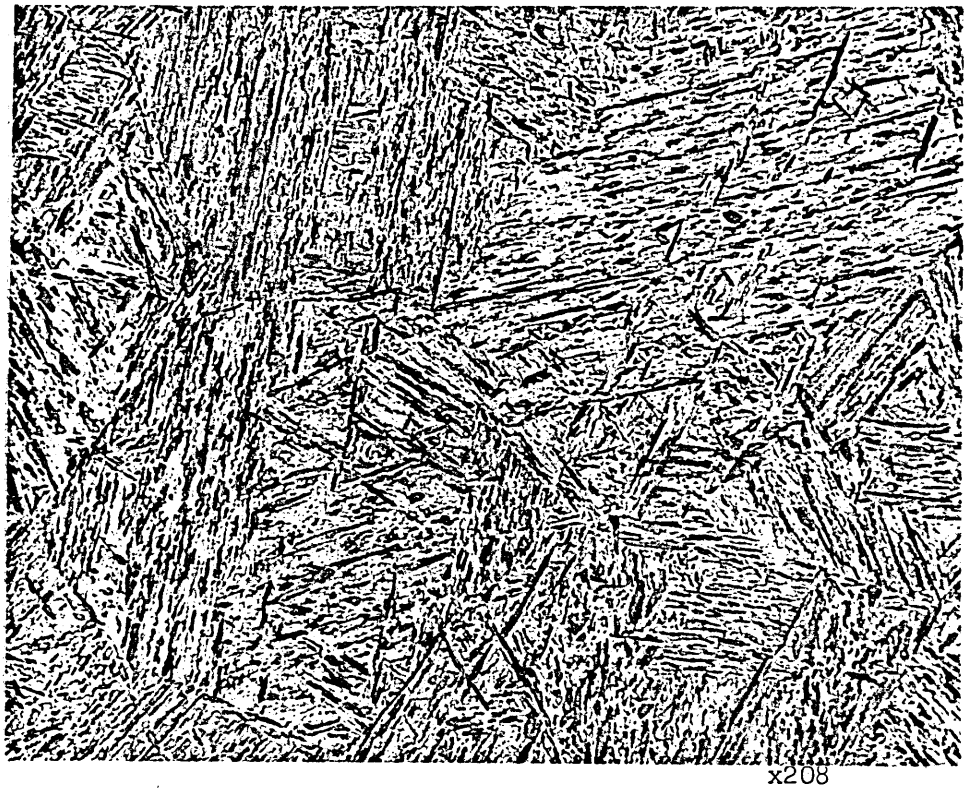

x208

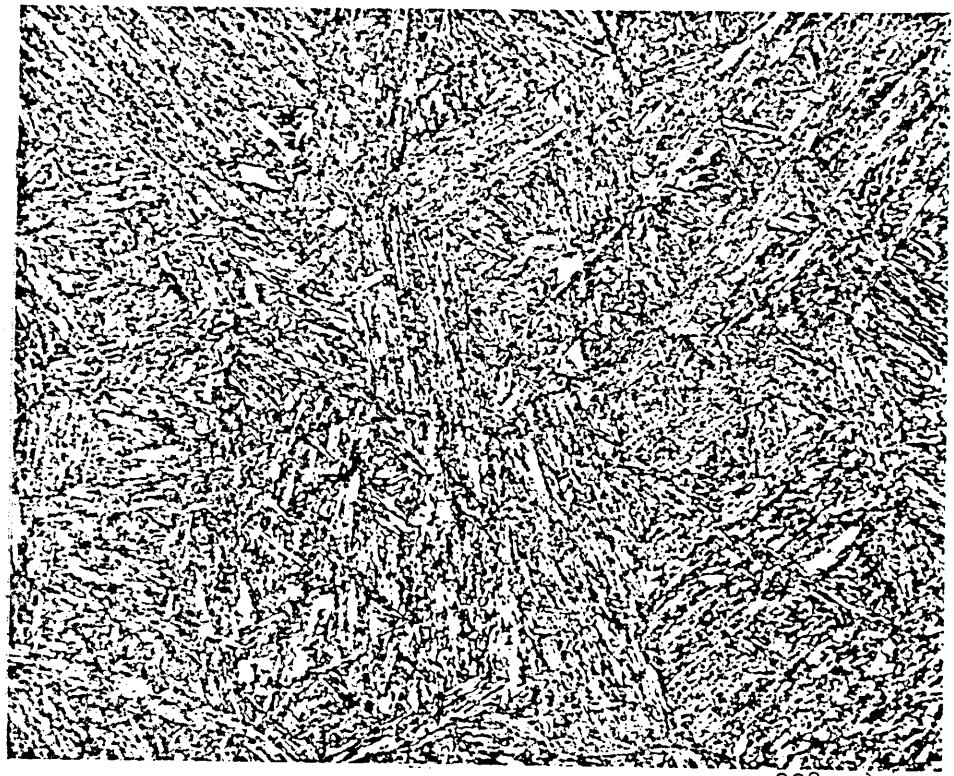

x208

FIGURE 133

Optical Micrographs of Alloy A417 Etched in 6% Nital for 12 Seconds.

(a) After a Solution Treatment of 1000°C for One Hour Followed by Water Quenching.

(b) Solution Treatment as Above Followed by a Tempering Treatment of One Hour at 650°C Followed by a Water Quench.

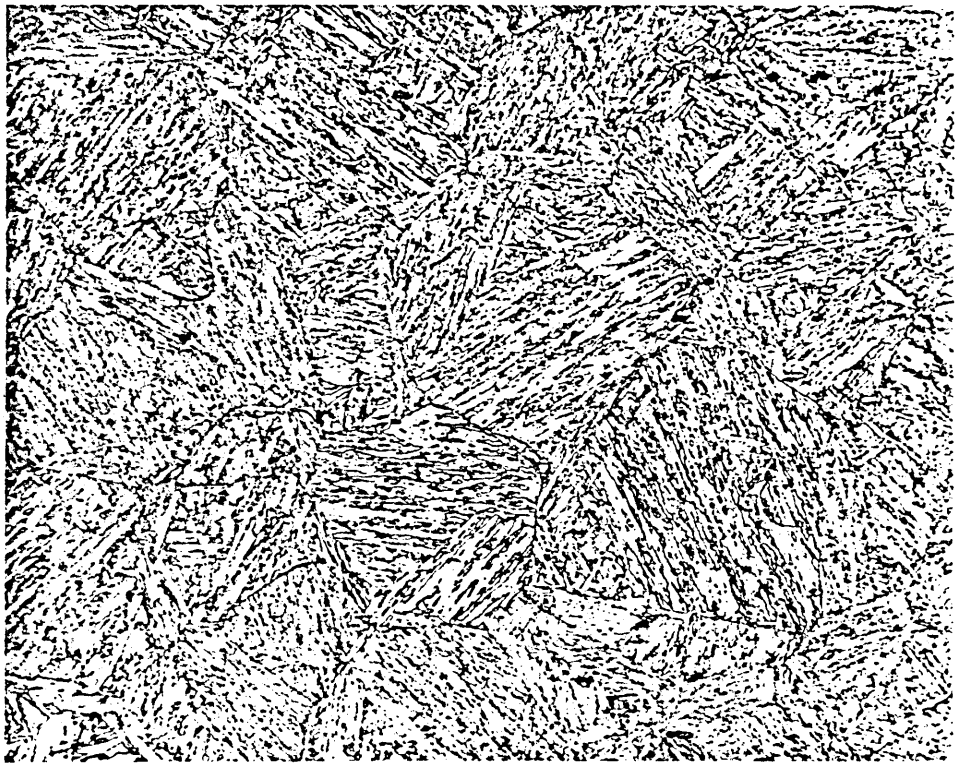

x208

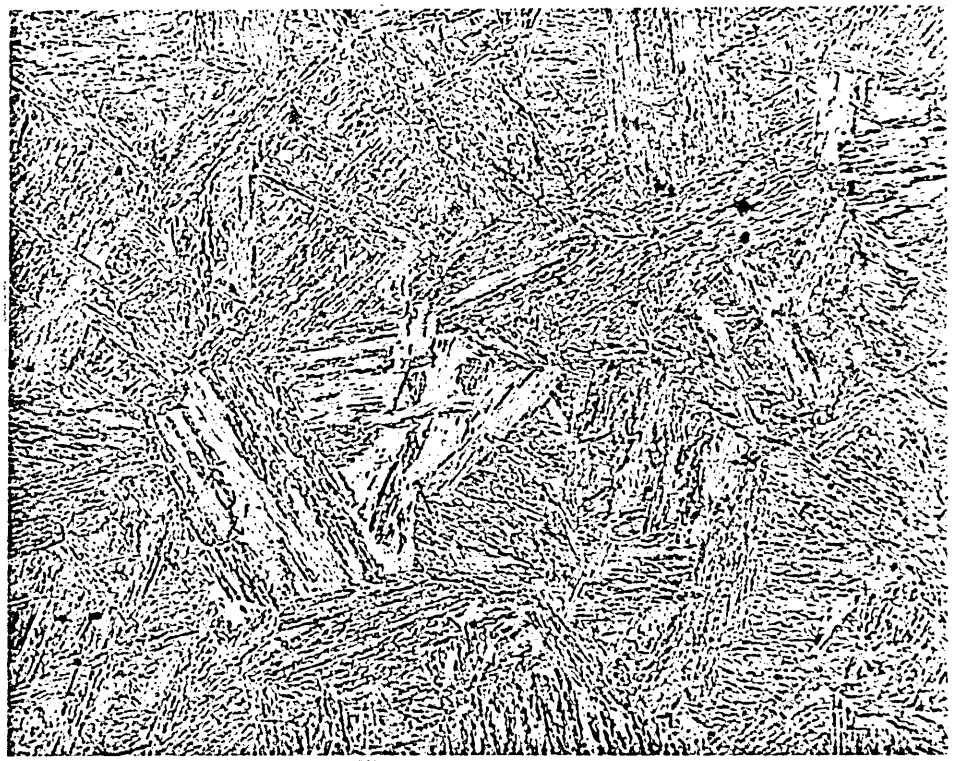

x208

FIGURE 134

The Charpy Impact Transition Diagrams for A217 Fe - 0.25C, 1.4Mn, 0.5Mo, 0.6Ni, 0.3Si A317 Fe - 0.25C, 1.4Mn, 0.5Mo, 0.6Ni, 0.3Si, 0.4Cu A417 Fe - 0.25C, 1.4Mn, 0.5Mo, 0.6Ni, 0.3Si, 0.04P in the Solution Treated Condition after 1 Hour at 1000°C Followed by Water Quenching and the Quenched Tempered Condition (Tempering at 650°C for 1 Hour Followed by Water Quenching).

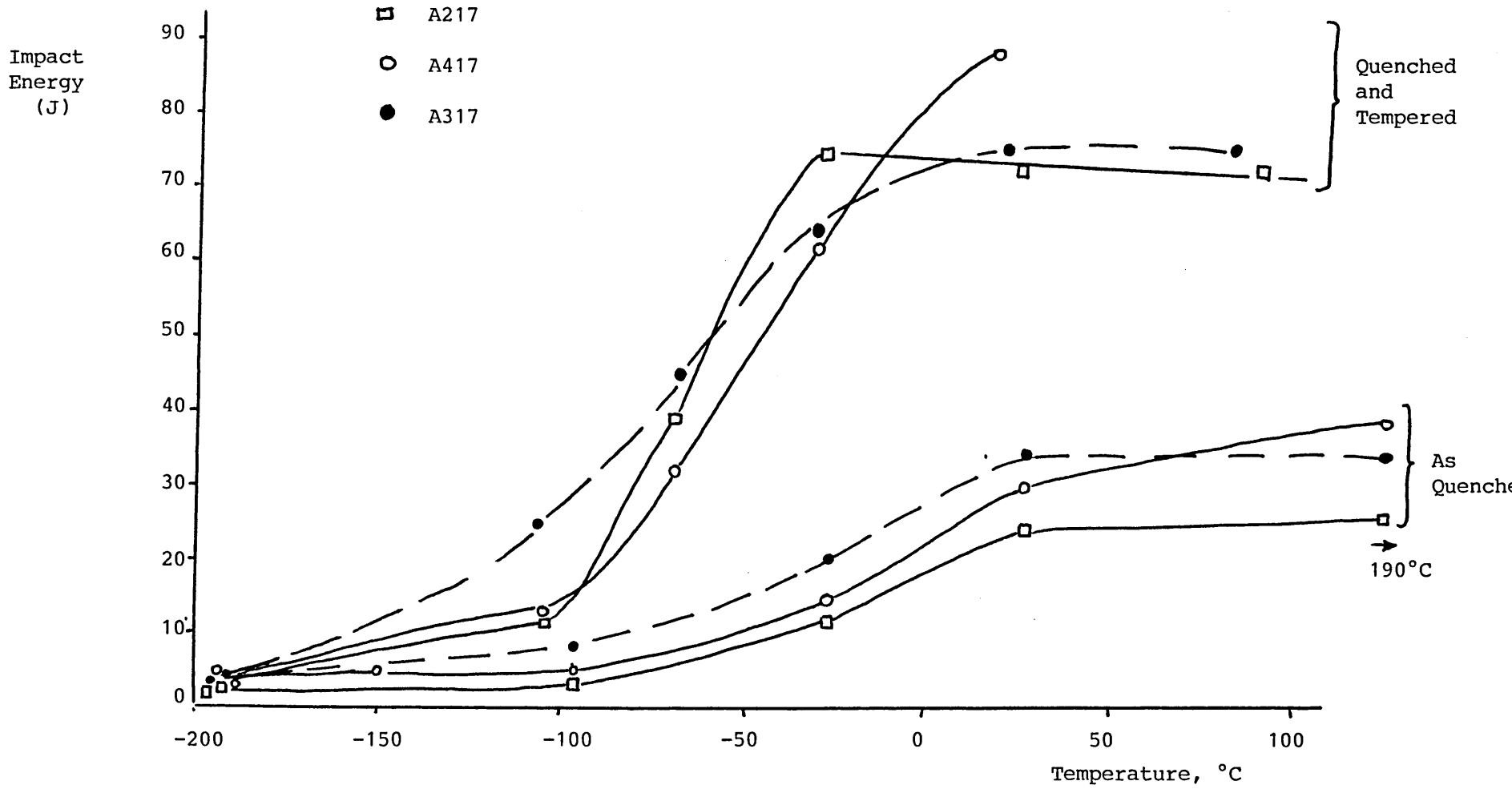
A217
A417
A317
Impact Energy (J)
90
80
70
60
50
40
30
20
10
0
-200
-150
-100
-50
0
50
100
Temperature, °C
Quenched and Tempered
As Quenche
190°C

FIGURE 135

Fractographs Showing Brittle and Ductile Fracture of Impact Specimens from Alloy A217 in the Quenched and Tempered Condition.

X 1204

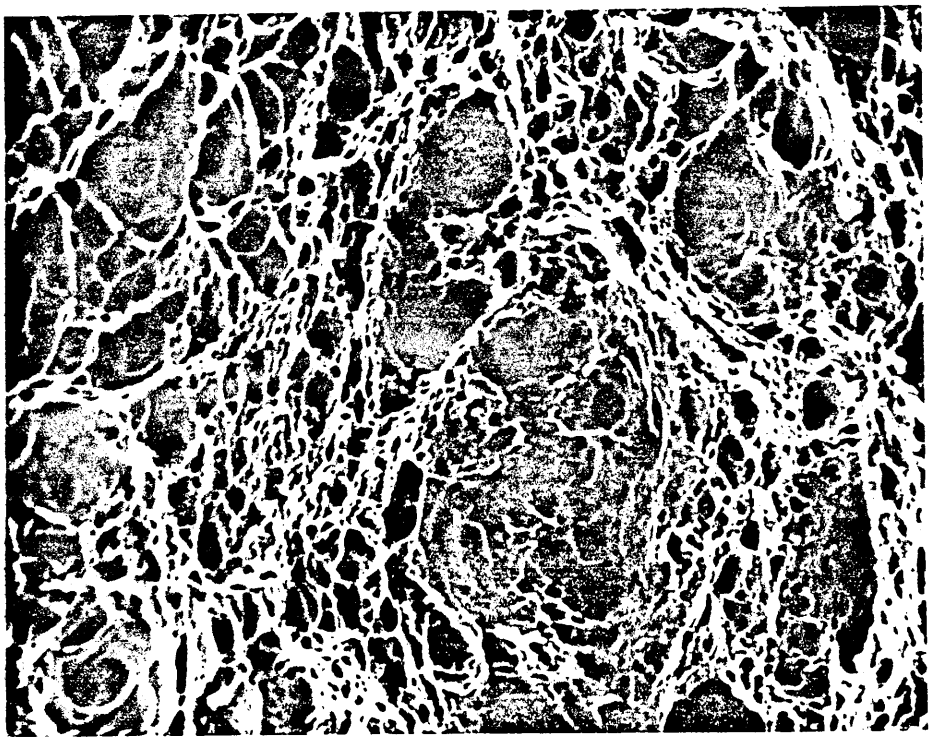

X 301

FIGURE 136

Charpy Fractograph Showing Fracture Below the Ductile to Brittle Transition Temperature for Alloy A317 in the Quenched and Tempered Condition

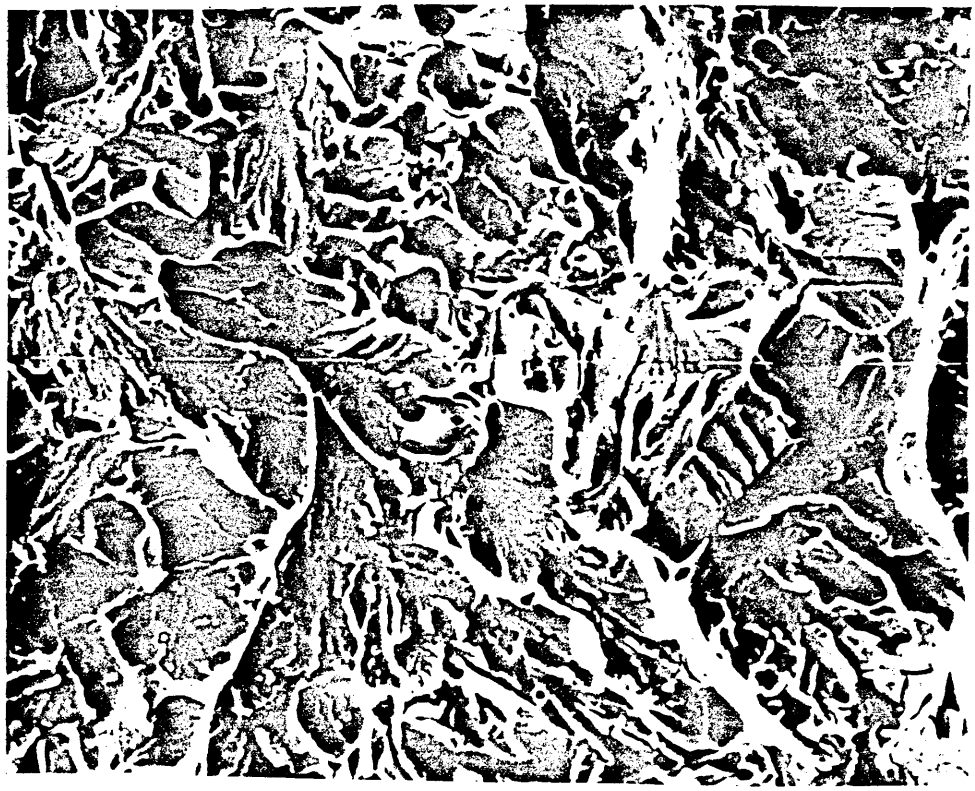

X 800

FIGURE 137

Charpy Fractographs from Above and Below the Ductile to Brittle Transition Temperature for Alloy A417 in the Quenched and Tempered Condition.

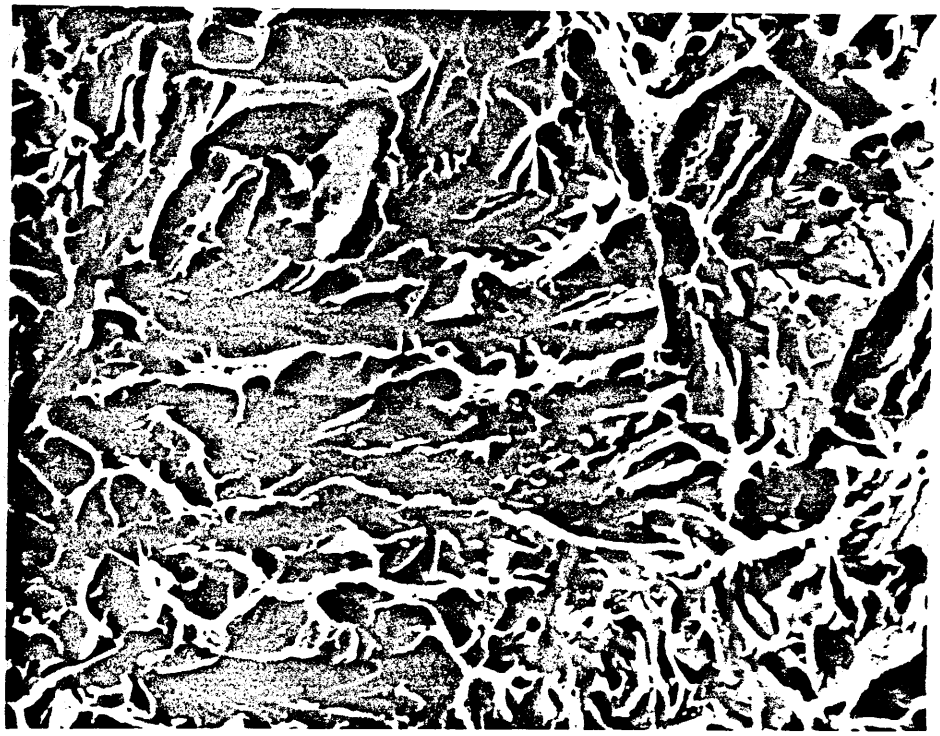

BRITTLE x 1111

DUCTILE x 1111

FIGURE 138

Variation in Hardness with Age Time at 450°C for Alloys A217, A317 and A417.

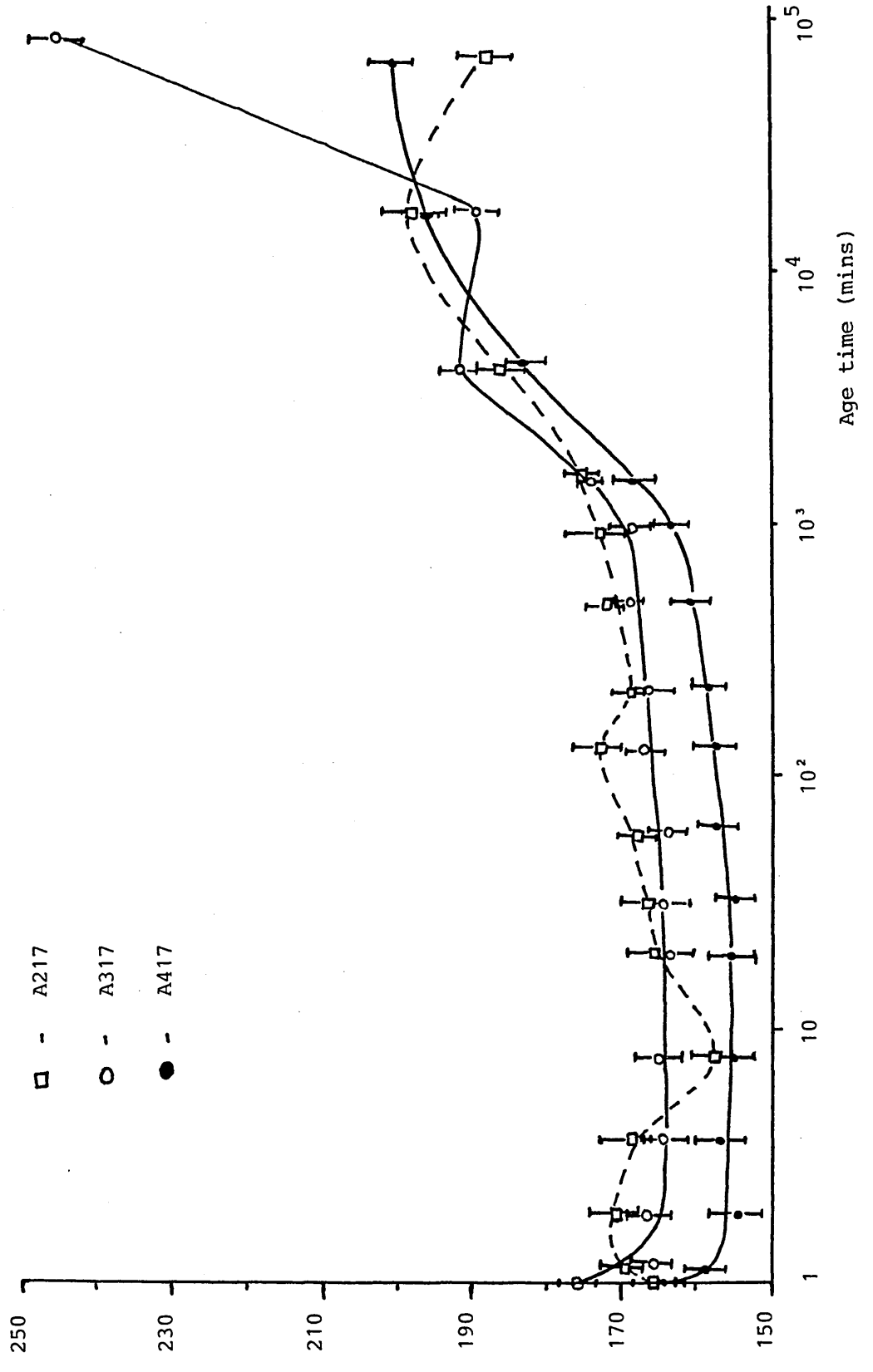
Hardness
Hv30
250
230
210
190
170
150
1
10
10^2
10^3
10^4
10^5
Age time (mins)
□ - A217
○ - A317
● - A417

FIGURE 139

Charpy Impact Transition Curves of Alloy A217 Showing the Effects of Aging at 450°C and 525°C After Previously Quench and Temper Treatments.

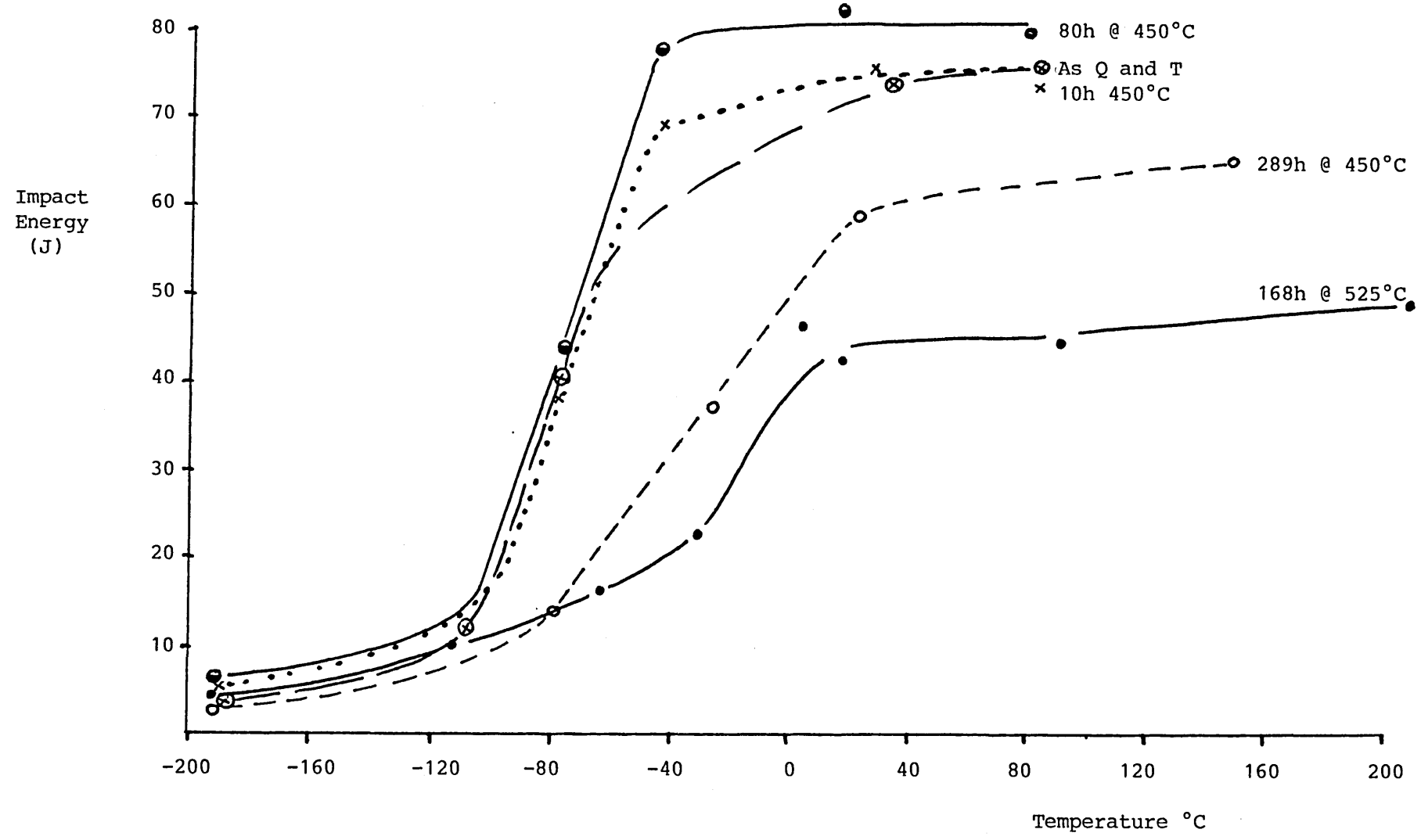
Impact Energy (J)
80
70
60
50
40
30
20
10
-200
-160
-120
-80
-40
0
40
80
120
160
200
Temperature °C
80h @ 450°C
As Q and T
10h 450°C
289h @ 450°C
168h @ 525°C

FIGURE 140

Charpy Impact Transition Curves of Alloy A317 Showing the Effect of Aging at 450°C and 525°C After Initially Quenching and Tempering.

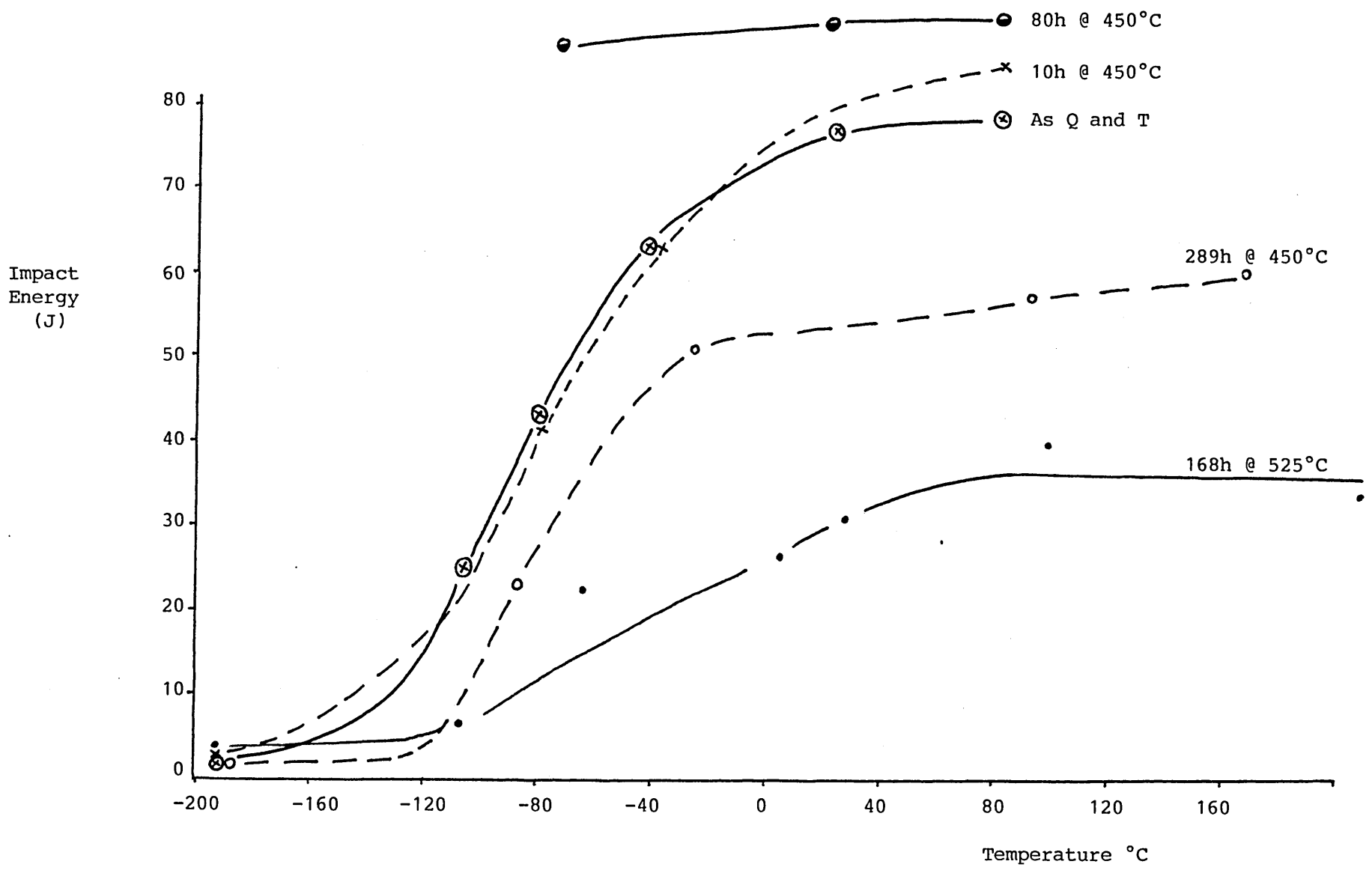
80h @ 450°C
10h @ 450°C
As Q and T
289h @ 450°C
168h @ 525°C
Impact Energy (J)
80
70
60
50
40
30
20
10
0
-200
-160
-120
-80
-40
0
40
80
120
160
Temperature °C

FIGURE 141

Charpy Impact Curves for Alloy A417 Showing Effects of Aging at 450°C and 525°C After Firstly Quenching and Tempering.

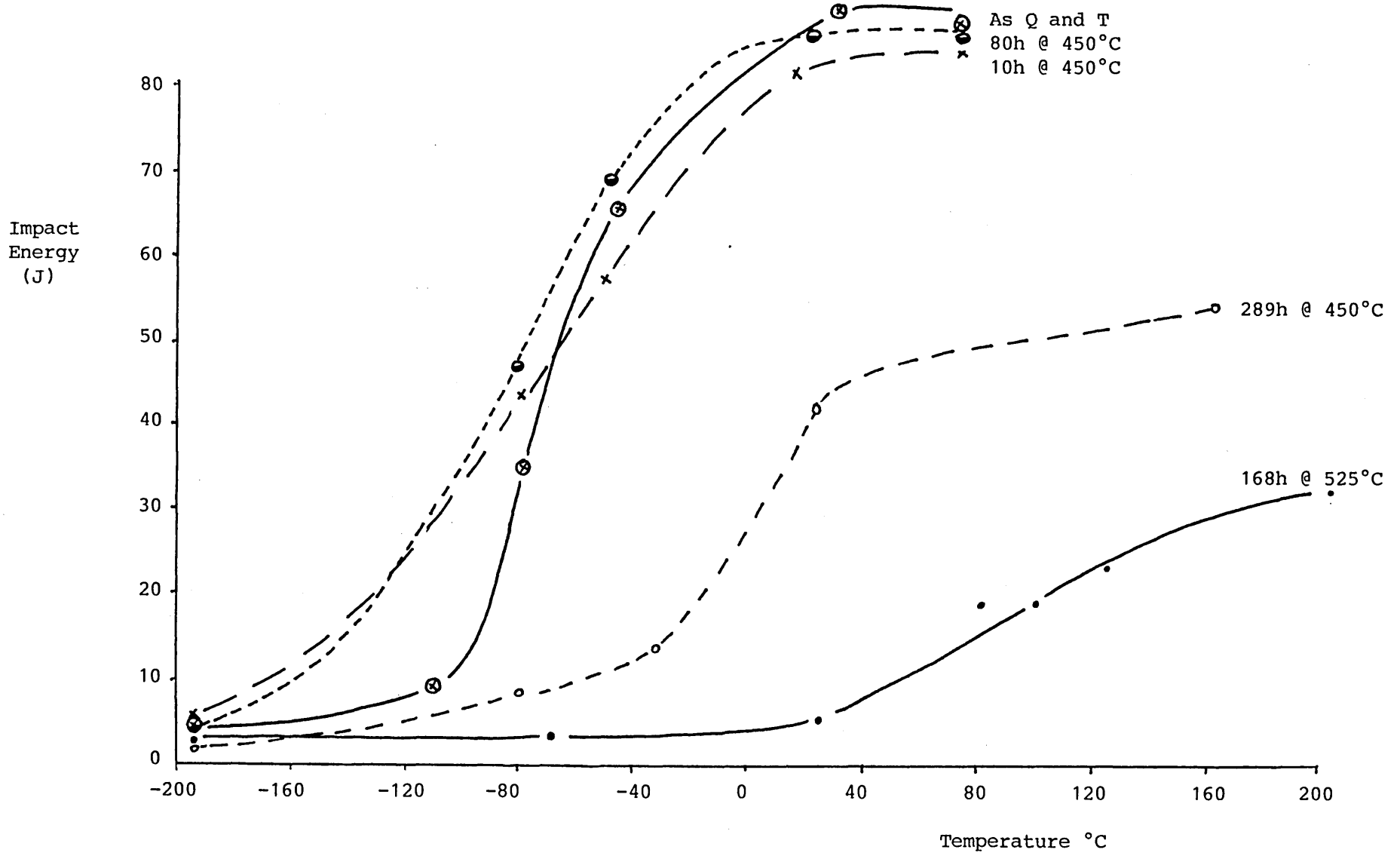
As Q and T
80h @ 450°C
10h @ 450°C
289h @ 450°C
168h @ 525°C
Impact Energy (J)
Temperature °C
80
70
60
50
40
30
20
10
0
-200
-160
-120
-80
-40
0
40
80
120
160
200

FIGURE 142

Charpy Fractographs Showing Brittle and Ductile Fracture Mode of Alloy A217 after Aging at 450°C for 10 Hours.

BRITTLE X463

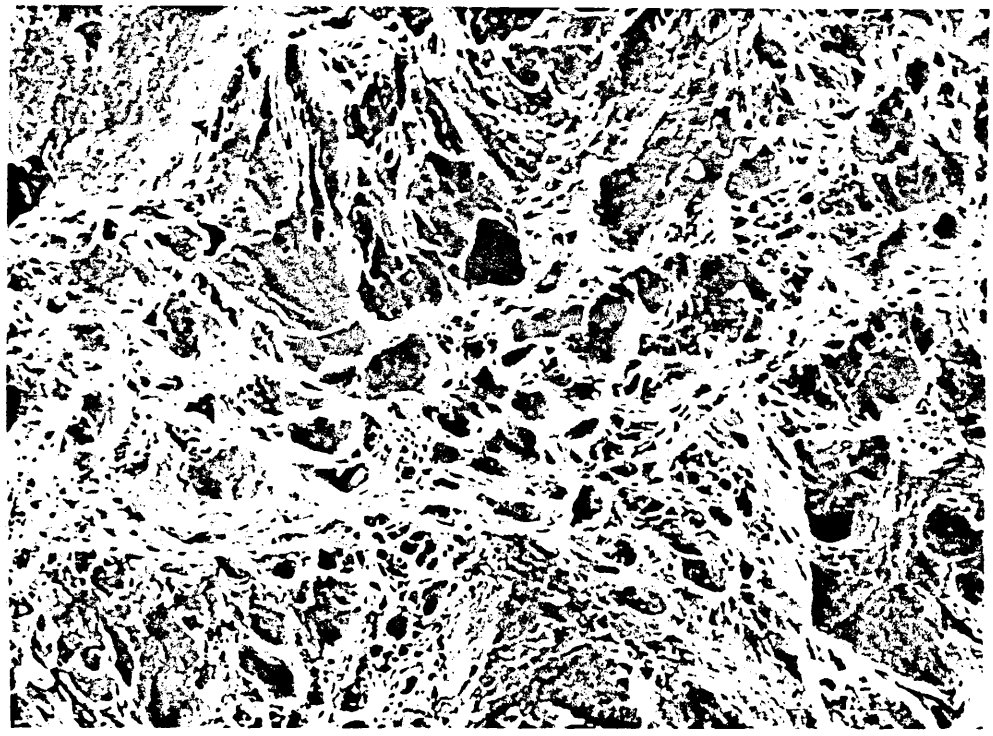

DUCTILE X463

FIGURE 143

Charpy Fractographs of Alloy A217 from Above and Below the Ductile to Brittle Transition Temperature After Aging for 168 Hours at 525°C.

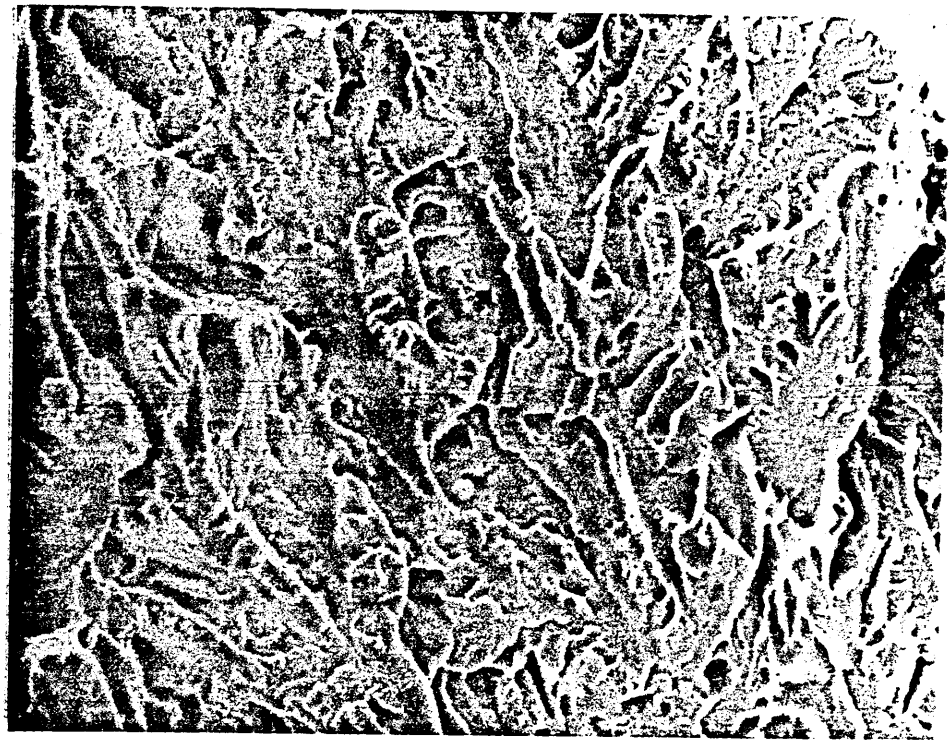

BRITTLE X880

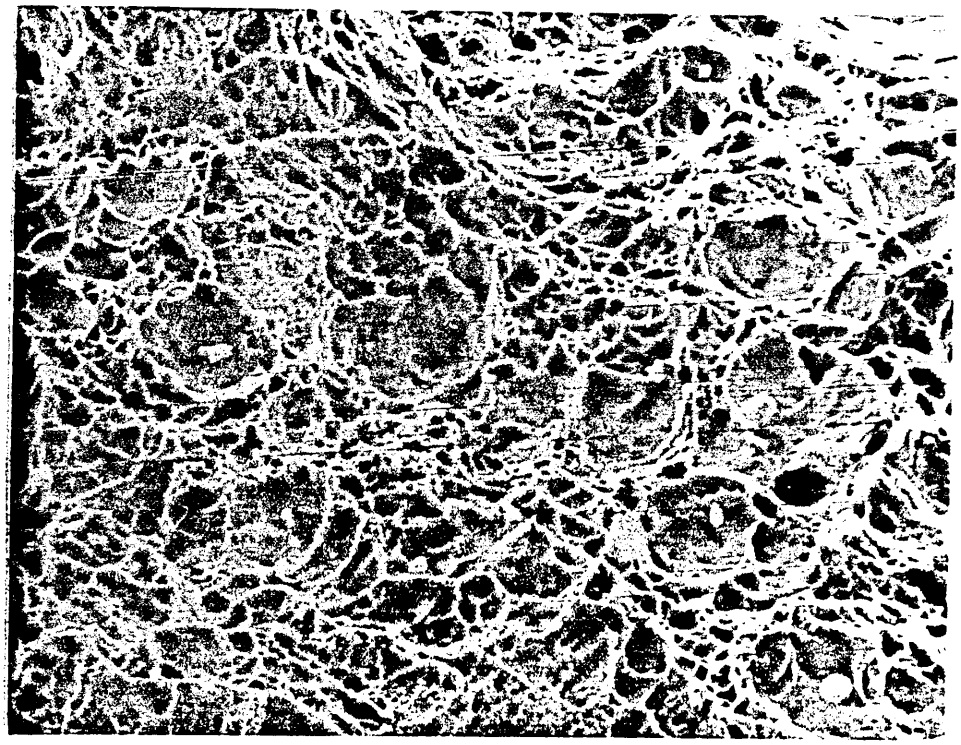

DUCTILE X880

FIGURE 144

Charpy Fractographs of Alloy A317 from Above and Below the Impact Transition Temperature After an Aging Treatment at 450°C for 10 Hours.

BRITTLE X556

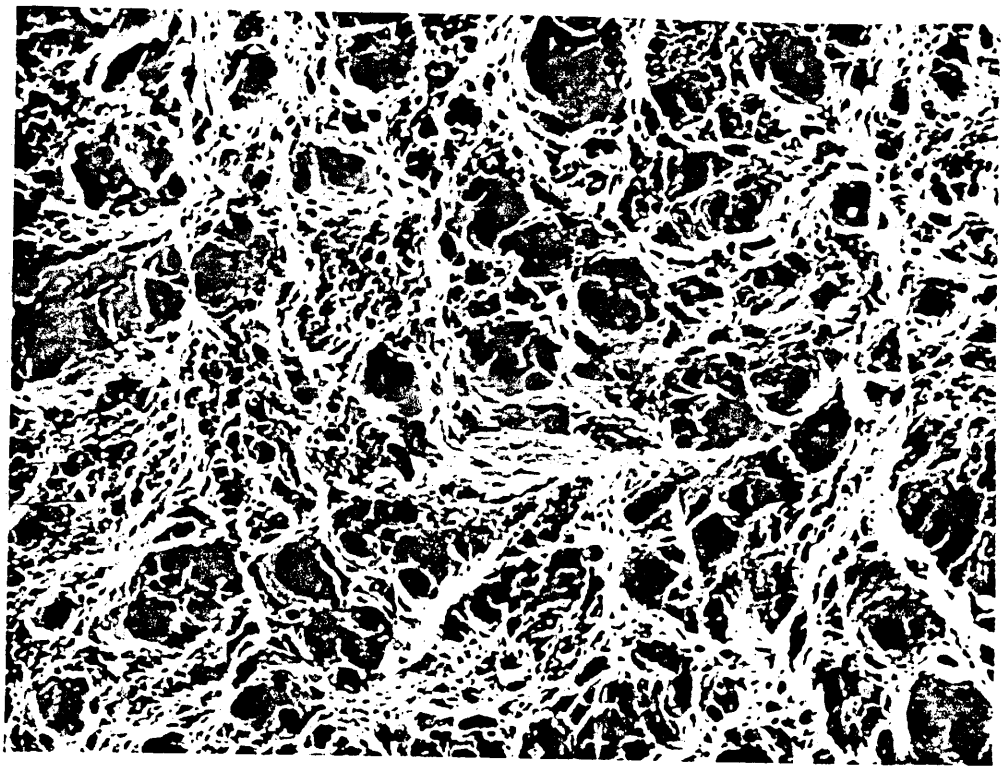

DUCTILE X556

FIGURE 145

Charpy Impact Fractographs of Alloy A317 from Below the Ductile to Brittle Transition Temperature After Aging at 525°C for 168 Hours.

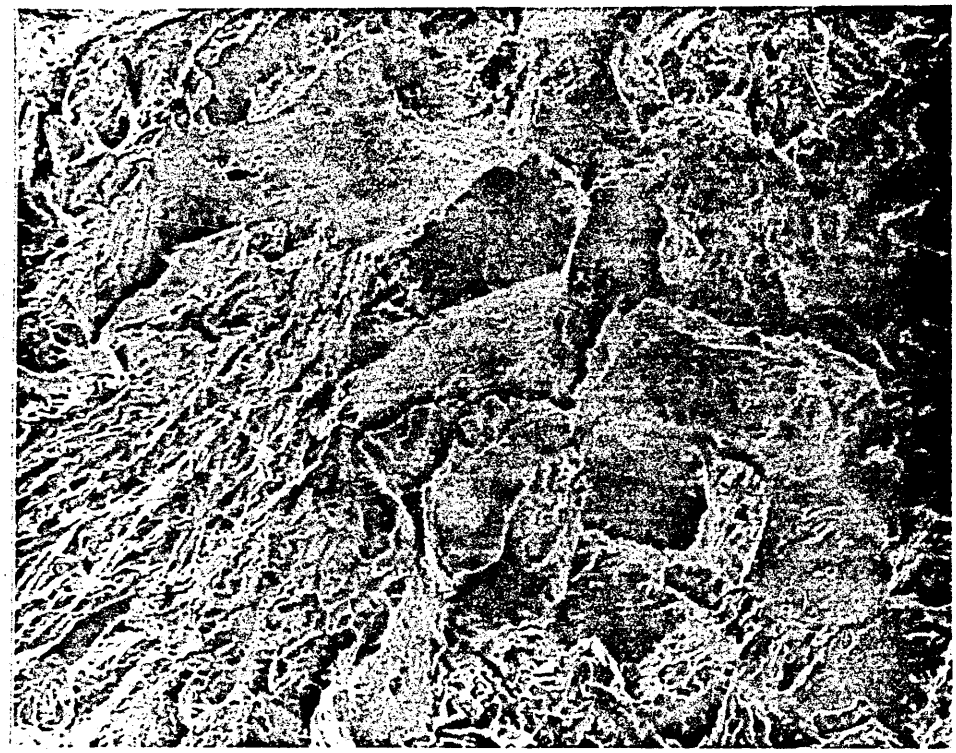

BRITTLE X220

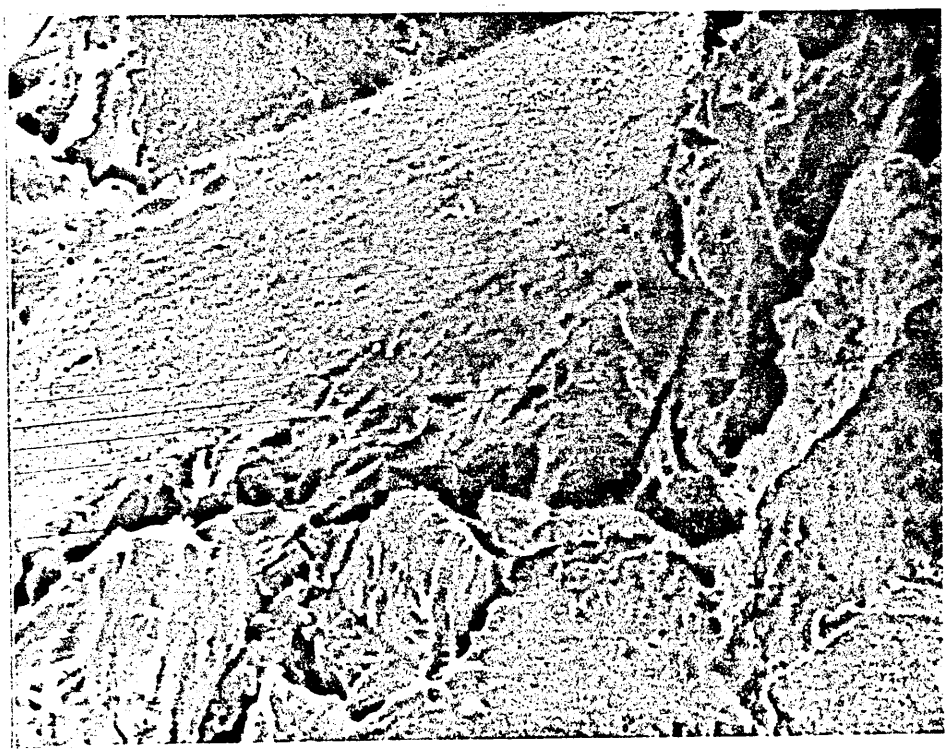

BRITTLE X880

FIGURE 146

Charpy Fractographs of Alloy A317 from Above the Ductile to Brittle Transition Temperature after Aging at 525°C for 168 Hours.

DUCTILE X440

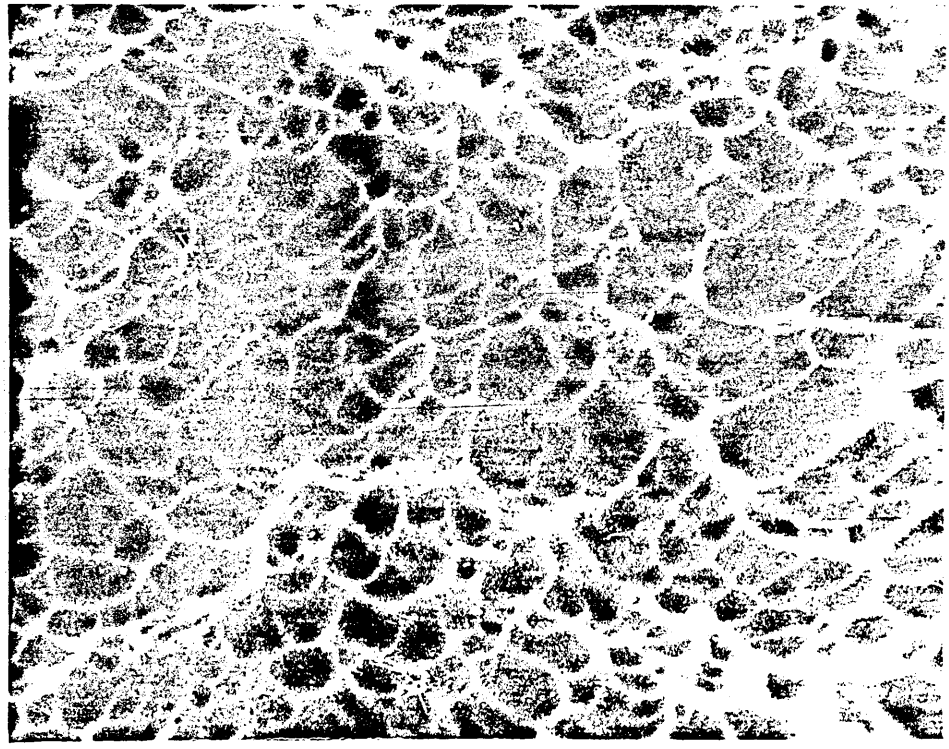

CLOSE UP OF "FLAT" AREA IN ABOVE X7037

FIGURE 147

Charpy Fractographs from Above and Below the Ductile to Brittle Transition Temperature for Alloy A417 after Aging for 10 Hours at 450°C.

BRITTLE X509

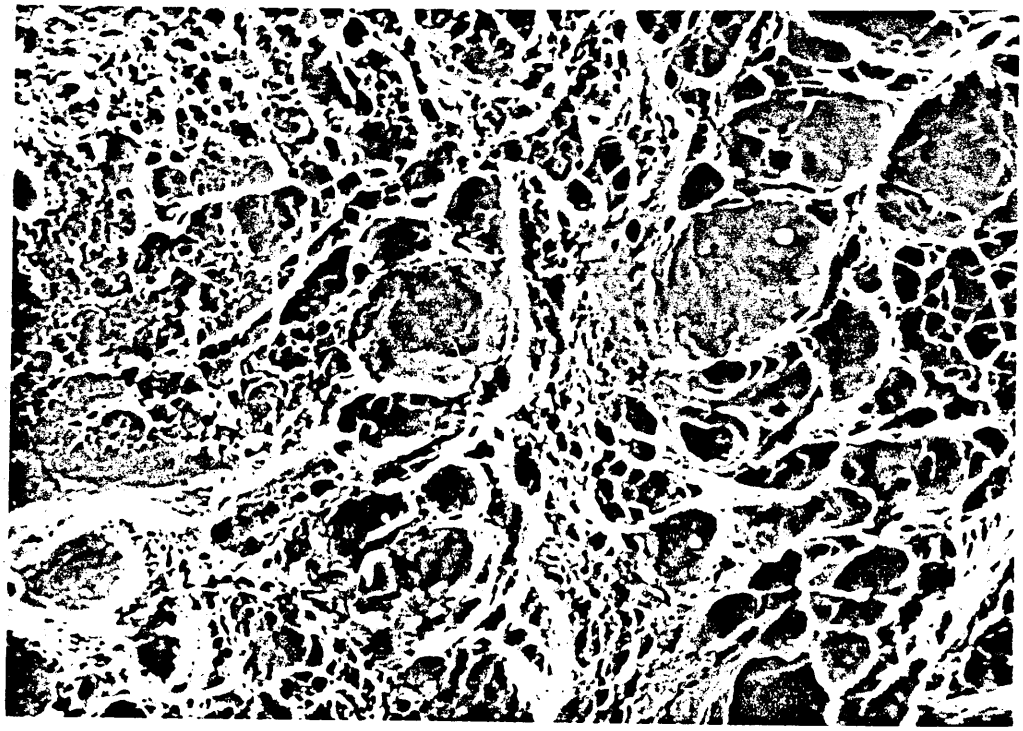

DUCTILE X1019

FIGURE 148

Charpy Fractographs from Below the Ductile to Brittle Transition Temperature for Alloy A417 after Aging at 525°C for 168 Hours.

BRITTLE X220

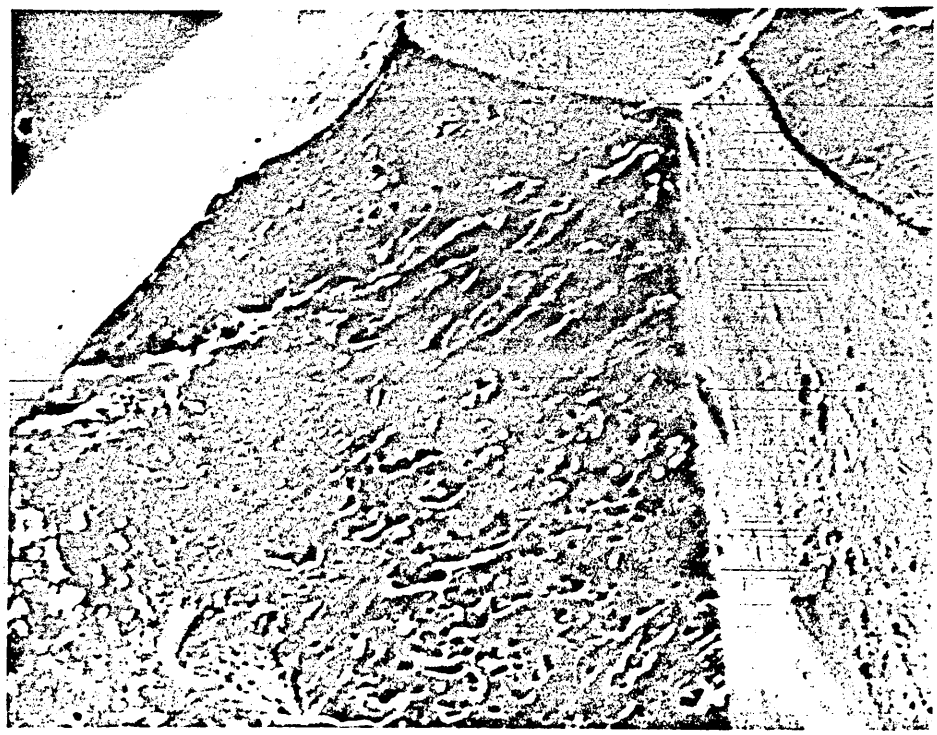

BRITTLE X880

FIGURE 149

Charpy Fractographs for Above and Below the Ductile to Brittle Transition Temperature from Alloy A417 after Aging at 525°C for 168 Hours.

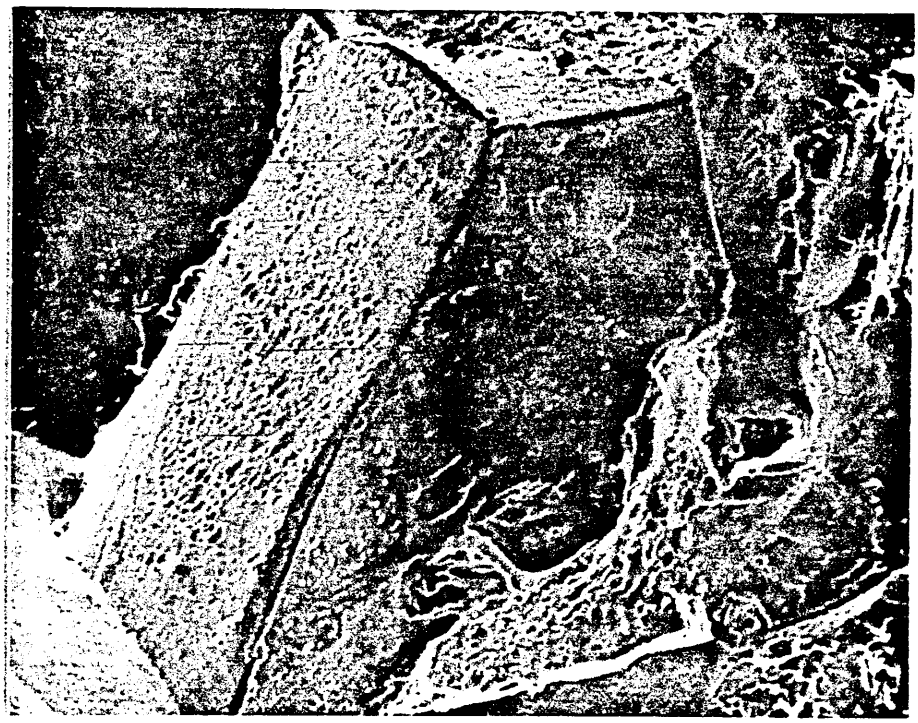

BRITTLE X190

DUCTILE X380

FIGURE 150

Micrographs Showing the Propogation of Cracks Along Prior Austenite Grain Boundaries Below the Intergranular Fracture Surface of Alloy K1526 after Aging at 525°C for 480 Hours.

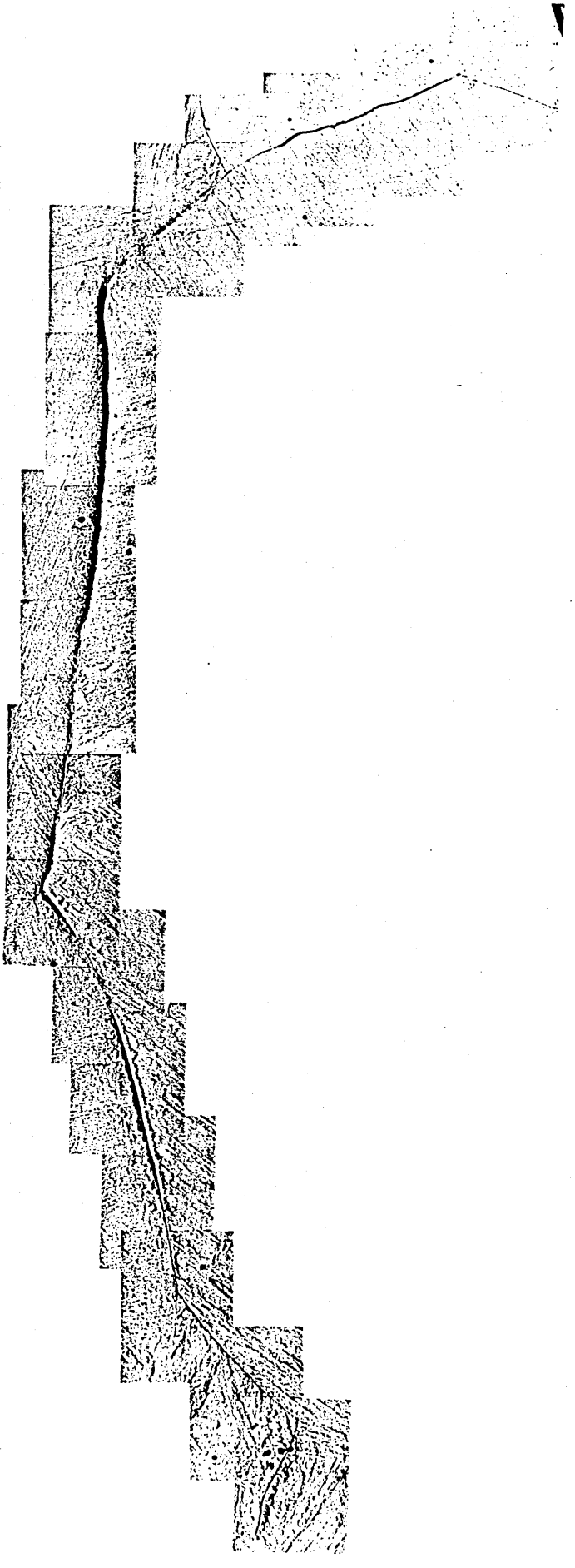

FIGURE 151 (a)

Interlath Fracture Shown on the Intergranular Facets of Alloy K1527 after Aging at 450°C for 193.5 Hours.

x433

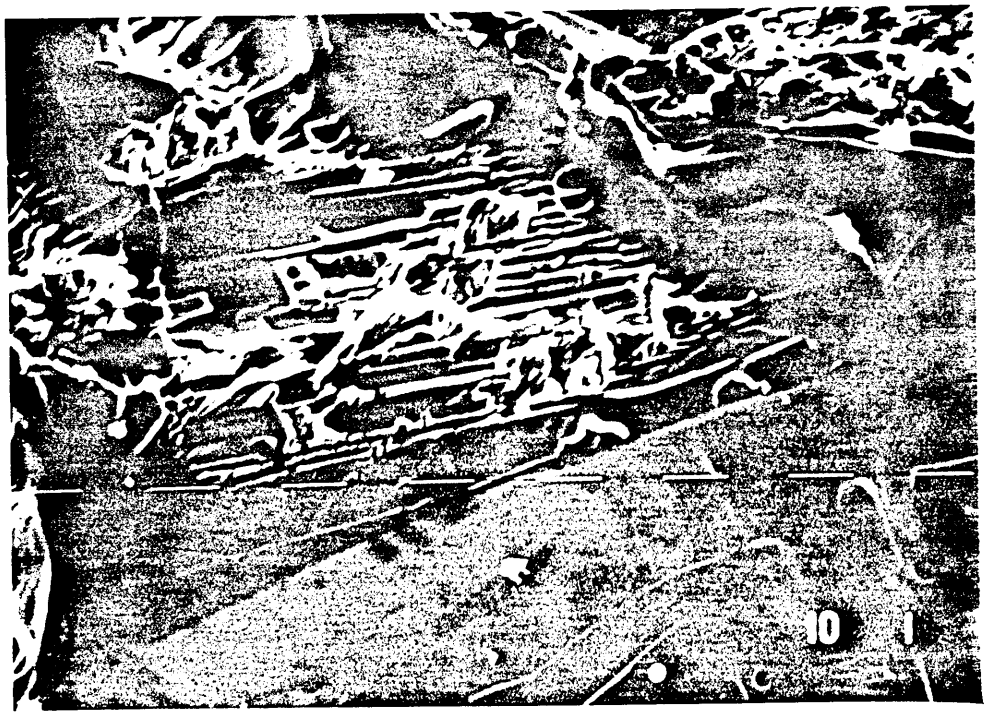

x900

FIGURE 151(b)

Interlath Fracture Shown on the Intergranular Facets of Alloy K1527 after Aging at 450°C for 193.5 Hours

x430

x850

FIGURE 152

Graph of $\frac{C_{bt} - C_{bo}}{C_{b\infty} - C_{bo}}$ Against $\sqrt{\text{time}}$ for Manganese in Alloy K1527 During Aging at 450°C.

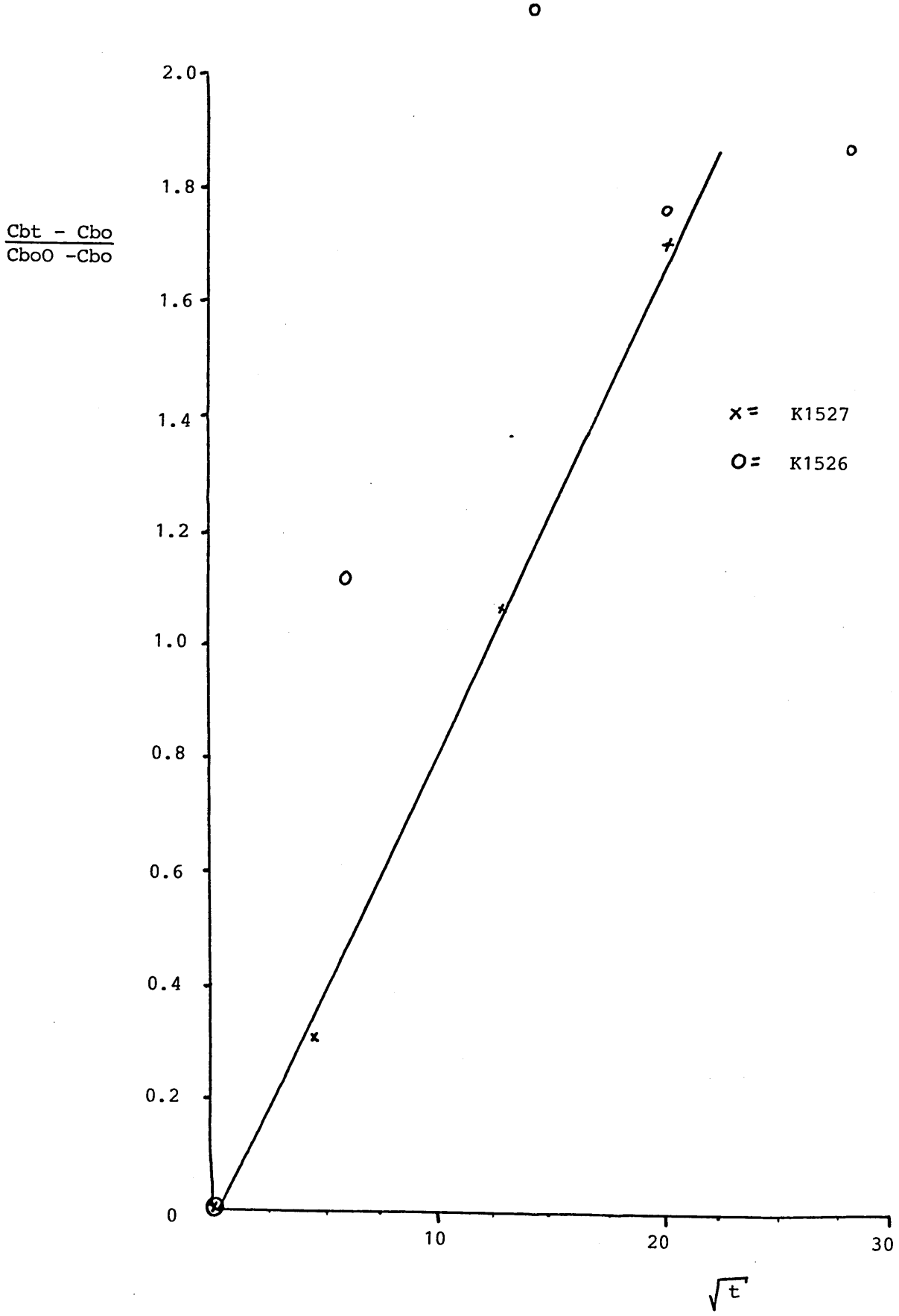
Cbt - Cbo
Cboo -Cbo
2.0
1.8
1.6
1.4
1.2
1.0
0.8
0.6
0.4
0.2
0
10
20
30
√t
x = K1527
O = K1526

FIGURE 153

Graph of Cbt vs $\sqrt{t}$ for Manganese and Molybdenum in Alloys K1526 and K1527 During Aging at 450°C.

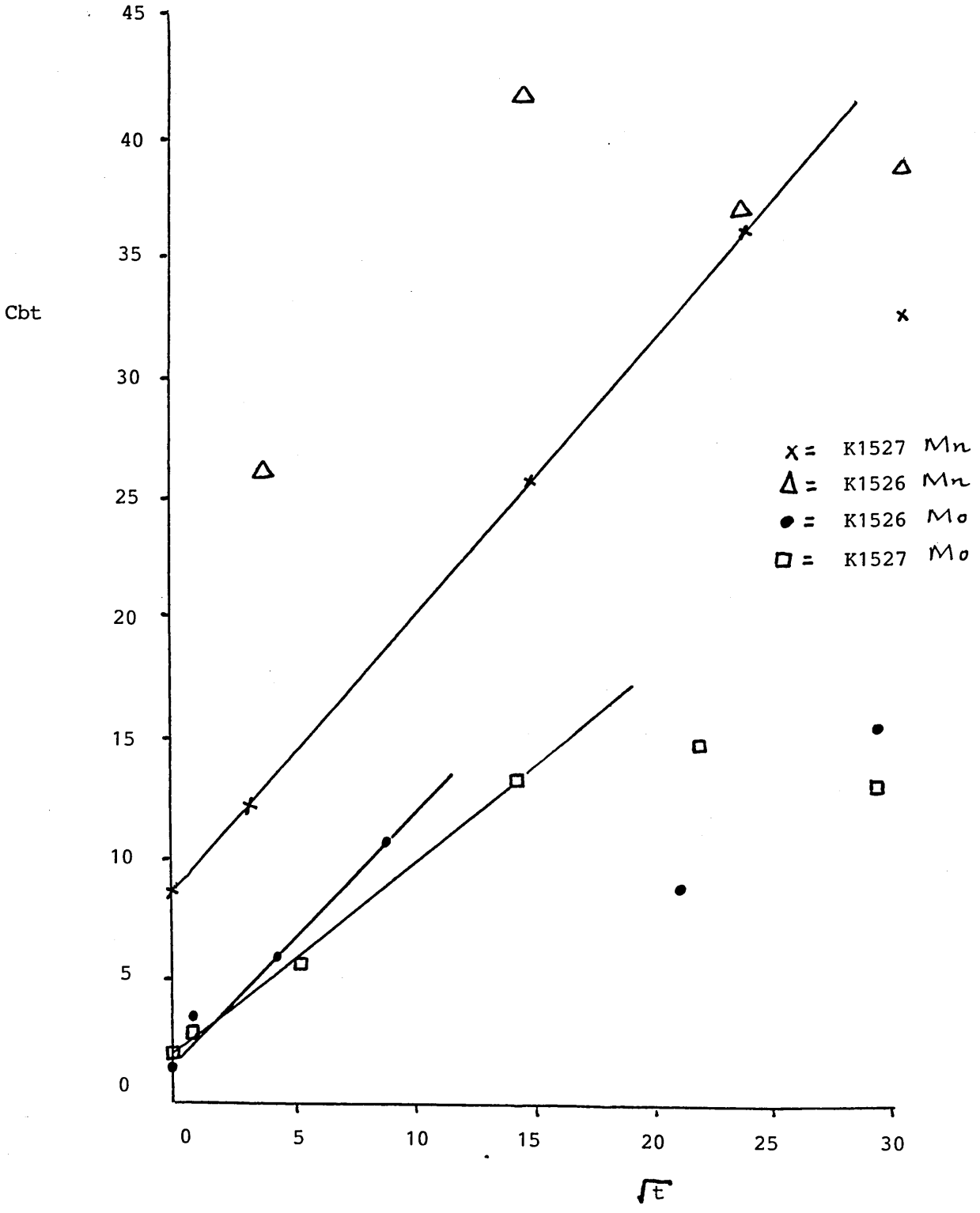
Cbt
45
40
35
30
25
20
15
10
5
0
0
5
10
15
20
25
30
√t
x = K1527 Mn
Δ = K1526 Mn
● = K1526 Mo
□ = K1527 Mo

APPENDIX

Tables of results used to formulate the graphs and not included in the results section.

HARDNESS DATA for K1526 & K1527 on aging at 450°C

(Ten impressions for each reading)

Prior heat treatment - Solution treatment for 1 hour at 1000°C + WQ

Aging Time (mins)	K1526		K1527	
	Hv30	σ	Hv30	σ
0	336	14.0	284	1.7
1	343	18.8	289	3.4
2	346	15.6	295	3.5
4	350	19.3	296	5.7
8	341	18.0	294	3.6
16	332	16.7	294	4.0
32	338	15.1	292	2.4
64	337	11.8	292	5.1
128	340	18.1	290	3.5
256	335	12.0	289	2.1
512	342	21.0	296	4.1
1024	340	15.3	305	3.2
2048	340	9.4	310	4.3
6256	350	11.5	340	5.2
8192	345	11.7	345	3.0
16384	339	4.8	401	2.9
22084	336	10.2	426	10.4
37579	321	13.5	442	22.0
123889	319	10.3	458	16.4
181800	308	6.3	484	12.4
3810600	307	5.2	409	4.2

σ = 90% Confidence Limits

HARDNESS DATA FOR K1526 & K1527 on aging at 525°C

(Ten impressions for each reading)

Prior heat treatment - 1 hour at 1000°C + WQ

Aging Time (mins)	K1526		K1527	
	Hv30	σ	Hv30	σ
0	337	4.8	277	2.7
1	335	7.2	289	4.3
2	338	8.5	290	5.1
4	331	8.4	279	2.9
8	329	7.6	282	4.4
16	336	8.5	283	2.8
32	329	8.4	279	3.2
64	322	9.0	271	4.3
128	312	8.5	264	2.9
256	305	7.1	270	4.7
512	270	4.1	274	6.3
1024	255	3.9	289	8.6
2048	254	5.0	310	8.7

HARDNESS DATA for alloys A217, A317, A417 on aging at 450°C and 525°C

(Ten impressions for each reading)

Aging Time (mins)	A217				A317				A417			
	450°C		525°C		450°C		525°C		450°C		525°C	
	Hv30	σ	Hv30	σ	Hv30	σ	Hv30	σ	Hv30	σ	Hv30	σ
0	164	3.2	164	3.2	175	2.1	175	2.1	163	2.1	163	2.1
1	169	2.5	158	4.6	165	1.5	172	2.8	158	4.3	158	1.3
2	170	2.5	157	4.9	166	2.4	171	2.5	154	2.1	159	3.5
4	167	2.1	157	4.2	164	2.0	172	2.6	156	2.1	158	2.1
8	159	3.7	155	3.6	164	4.8	169	2.9	154	2.9	156	2.3
16	166	2.1	160	5.5	163	3.3	169	2.4	154	2.3	161	2.4
32	167	4.1	157	6.8	164	2.1	170	1.4	154	1.8	160	2.6
60	169	1.7	157	5.0	164	1.8	170	3.5	159	4.3	159	2.9
120	172	3.2	158	5.1	168	2.2	174	2.3	158	2.0	162	3.5
240	168	2.5	157	4.5	167	1.3	171	3.2	159	3.5	160	1.0
480	172	2.1	158	5.3	170	3.7	169	3.6	161	2.3	159	1.6
960	173	5.0	157	5.9	170	3.3	172	1.9	165	1.8	161	2.0
1980	175	3.3	158	4.0	176	2.4	171	2.0	171	1.6	162	2.5
4710	188	4.4	156	5.0	198	3.5	174	3.2	186	3.1	158	1.7
14400	203	4.4	156	4.4	194	5.9	169	3.0	200	7.6	160	2.4
28800	191	4.2	153	4.7	243	4.8	170	2.8	206	5.1	157	1.8

CHARPY IMPACT DATA FOR ALLOYS A217, A317, A417

Heat Treatment - 1 hour at 1000°C + WQ

Temperature	Impact Energy (J)		
	A217	A317	A417
Liq. N_2	3	4	4
-80°C	4	9	5
-35°C	15	22	18
23°C	30	38	34
190°C	35	39	42

Heat Treatment - 1 hour at 1000°C + WQ followed by tempering at 650°C for 1 hour + WQ

Temperature	Impact Energy (J)		
	A217	A317	A417
Liq. N_2	3	2	3
-110°C	10	25	10
- 80°C	40	45	35
- 47°C	77	65	64
25°C	75	79	88
80°C	77	80	-

Heat Treatment - 1 hour at 1000°C + WQ, tempering for 1 hour at 650°C + WQ, aging for 10 hours at 450°C + WQ

Temperature	Impact Energy (J)		
	A217	A317	A417
-196°C	4	3	4
- 80°C	38	43	41
- 45°C	70	65	58
20°C	77	91	77
80°C	75	85	77

Heat Treatment - 1 hour at 1000°C + WQ, tempering for 1 hour at 650°C + WQ, aging 80 hours at 450°C + WQ

Temperature	Impact Energy (J)		
	A217	A317	A417
-196°C	4		3
- 80°C	45	84	47
- 45°C	78	-	69
20°C	85	90	82
80°C	83	90	80

Heat Treatment - 1 hour at 1000°C + WQ, tempering for 1 hour at 650°C + WQ, aging for 289 hours at 450°C + WQ

Temperature	Impact Energy (J)		
	A217	A317	A417
-196°C	1	1	1
- 80°C	15	22	9
- 34°C	40	52	13
21°C	76	66	43
98°C	-	60	-
165°C	70	66	56

Heat Treatment - 1 hour at 1000°C + WQ, tempering for 1 Hour
at 650°C + WQ, aging 168h at 525°C + WQ

Temperature	Impact Energy (J)		
	A217	A317	A417
-196°C	3	3	2
-105°C	10	7	-
- 65°C	16	23	4
- 30°C	22	-	-
5°C	50	27	-
27°C	45	34	8
80°C	-	-	22
100°C	47	47	22
127°C	-	-	28
166°C	-	-	66
210°C	54	40	35

Charpy Impact Test Data for Solution Treated Specimens of K1526

Heat Treatment	1300°C 1h WQ + 1000°C 1h WQ		1000°C 1h WQ		1300°C 1h WQ		1300°C 1h WQ +850°C 1h WQ	
	Temp °C	Energy (J)	Temp °C	Energy (J)	Temp °C	Energy (J)	Temp °C	Energy (J)
	-50	16	-48	19	-75	6	-80	4
	-15	18	-19	17.5	-26	6	20	4
	19	19	0	21.5	-20	20	37	25
	58	11	18	21.5	43	31	52	29
	59	38	48	34	70	42	100	33
	66	43	74	39	118	40	150	35
	83	48	100	43	177	39		
	105	42	152	43.5				
	152	42	172	39				

Charpy Impact Test Data for Solution Treated Specimens of K1527

Heat Treatment	1300°C 1h WQ + 1000°C 1h WQ		1000°C 1h WQ		1300°C 1h WQ		1300°C 1h WQ +850°C 1h WQ	
	Temp °C	Energy (J)	Temp °C	Energy (J)	Temp °C	Energy (J)	Temp °C	Energy (J)
	-50	6	-50	5.5	-75	2	-80	3
	-13	8	-21	11.0	-25	3	4	9
	20	20	0	9.5	20	7	20	21
	40	39	18	16.2	50	21	37	21
	58	59	34	7.0	70	44	150	38
	105	61	47	26.0	118	63		
			58	57.0	177	50		
			73	55.5				
			100	64.0				
			150	58.0				

Charpy Impact Data for Aged Alloys K1526 and K1527

K1526 Prior Solution Treatment 1hr. @ 1000°C + WQ

17hrs. @ 450°C		480hrs. @ 450°C		17hrs. @ 525°C		480hrs. @ 525°C	
Temp. °C	Energy (J)	Temp. °C	Energy (J)	Temp. °C	Energy (J)	Temp. °C	Energy (J)
-60	2	-80	1	-135	2	-80	17
23	3	23	2	- 37	3	-65	35
84	25	84	1	23	63	-37	42
142	51	142	51	84	70	23	52
256	54	260	53	187	75	84	53
320	55						

K1527 Prior Heat Treatment 1hr. @ 1000°C + WQ

17hrs. @ 450°C		480hrs. @ 450°C		17hrs. @ 525°C		480hrs. @ 525°C	
Temp. °C	Energy (J)	Temp. °C	Energy (J)	Temp. °C	Energy (J)	Temp. °C	Energy (J)
-135	3	23	5	-20	5	23	1
- 90	2	84	2	23	6	84	0
23	26	142	1	84	14	142	2
84	47	256	2	142	47	256	2
142	60	364	2	256	56		
256	63						

Relative Intensities of AES Peaks for Alloy K1527

As quenched (3 spectra)

	I	II	III
Mn	4.06	5.66	4.26
C	3.13	14.99	17.55
Mo	4.66	2.53	2.77
N	0.32	-	-
O	15.49	48.76	31.68

Aged for 30 mins at 450°C (2 spectra)

	I	II
Mn	5.10	5.4
C	7.89	16.79
Mo	4.62	4.57
N	0.54	-
O	33.43	35.67

Aged for 17 hours at 450°C (3 spectra)

	I	II	III
Mn	11.32	7.84	11.43
C	6.10	22.18	24.86
Mo	15.67	4.49	8.74
P?	2.41	-	1.44
N	2.67	0.9	
O	-	32.39	

Aged for 193.5 hours at 450°C (4 spectra)

	I	II	III	IV
Mn	14.31	15.72	17.08	14.35
C	23.15	30.45	25.55	23.98
Mo	15.85	16.94	16.71	11.89
P?	1.58	2.44	3.56	1.47
N	-	2.79	1.6	2.07

Aged for 480 hours at 450°C (4 spectra)

	I	II	III	IV
Mn	22.43	19.31	24.80	21.84
C	10.02	22.99	31.62	29.95
Mo	21.07	18.68	17.33	17.09
P?	2.61	1.55	1.54	6.95
N	-	1.96	1.94	-

Relative Intensities of AES Peaks for Alloy K1527

Aged for 858 hours at 450°C (3 spectra)

	I	II	III
Mn	18.9	20.36	20.36
C	6.78	23.72	30.86
Mo	15.39	16.07	15.86
P?	1.18	2.12	1.22
N	-	1.79	-

Relative Intensities of AES Peaks for Alloy K1526

As quenched (2 spectra)

	I	II
Mn	4.51	5.80
C	5.39	26.26
Mo	2.29	-
N	1.10	-

Aged for 30 minutes at 450°C (2 spectra)

	I	II
Mn	4.40	4.32
C	17.46	20.36
Mo	4.81	1.59
P?	0.25	-

Aged for 17 hours at 450°C (4 spectra)

	I	II	III	IV
Mn	16.06	16.68	18.71	11.15
C	22.29	27.68	37.66	26.95
Mo	7.48	6.33	7.81	2.96
P?	3.33	0.20	-	-
N	0.82	-	-	-

Aged for 193.5 hours at 450°C (6 spectra)

	I	II	III	IV	V	VI
Mn	31.98	30.4	9.06	23.38	25.40	21.03
Mo	18.80	15.17	3.96	9.77	12.02	7.66
C	17.47	27.74	16.16	28.86	32.97	65.79
P?	3.62	3.98	-	3.85	1.66	-
N	1.91	2.27	-	-	1.94	-
O	30.50	59.01	-	-	-	-

Aged for 480 hours at 450°C (5 spectra)

	I	II	III	VI	V
Mn	23.51	24.49	26.92	7.48	7.85
N	2.98	2.09	2.67	-	-
C	13.62	29.22	27.6	60.33	71.99
Mo	15.23	11.34	12.09	11.94	10.52
P?	-	1.74	0.76	2.14	2.11

Relative Intensities of AES Peaks for Alloy K1526

Aged for 858 hours at 450°C (3 spectra)

	I	II	III
Mn	19.01	23.3	16.42
Mo	19.76	18.38	9.17
P?	3.27	3.24	-
N	1.55	2.0	-
C	13.37	33.22	38.90

Prior austenite grain size of alloys K1526 and K1527

Austenitising Treatment	K1526 μm	K1527 μm
1000°C	62	50
1300 + 1000°C	132	54
1300°C	260	124

As quenched hardness of alloys K1526 and K1527

Austenitising Temperature (°C)	K1526 Hv30	K1527 Hv30
1000	336	284
1300 + 1000	321	282
1300	329	275
1300 + 850	336	332

Prior austenite grain size of alloys A217, A317 and A414 after solution treatment at 1000°C for 1hr. + WQ

A217	A317	A417
221 μm	457 μm	266 μm